Department of Applied Geology

Sources and Conditions for the Formation of Jurassic Post-Orogenic High-K Granites in the Western Guangdong Province, SE China

Hui-Qing Huang

This thesis is presented for the Degree of
Doctor of Philosophy
of
Curtin University

July 2012

Declaration

This thesis is produced from a jointly supervised PhD program under a bilateral agreement between the Curtin University, Western Australia and the Guangzhou Institute of Geochemistry, Chinese Academy of Sciences. According to that agreement, this thesis is to be sent to both institutions for the degree of Doctor of Philosophy. I have successfully passed the thesis examination and defence according to the Chinese Academy of Sciences regulations.

To the best of my knowledge and belief this thesis contains no material previously published by any other person except where due acknowledgement has been made. This thesis contains no material which has been accepted for the award of any other degree or diploma in any university.

Signature: _____

Huiqing Huang

Date: 9 July 2012

Table of contents

Table of figures

Acknowledgements

This thesis could not have been completed without the encouragement and support of the following individuals and organizations.

First of all, I'd like to sincerely thank my supervisors, Professor Xian-Hua Li and Professor Zheng-Xiang Li who offered me the great opportunity to undertake this study under their supervision and also to discover the Australian lifestyle. I thank them for their encouragement, patience and enlightening advices. Thanks also due to their efforts on improving my research papers and this thesis.

I am grateful to Dr. Wu-Xian Li for his instruction during my field trips and discussions on many geological problems. He has been very helpful during the entire period of my study. Mr Ji-Hua Tao is thanked for his assistance during a field trip.

I am also grateful to Professor Simon Wilde. He has been so nice and willing to discuss geological problems. He is very helpful in doing proofreading. I thank Dr. Katy Evans and Professor Ian Fitzsimons for their helpful discussions. Dr. Katy Evans also helped to do oxygen fugacity calculations.

Dr. Xiao-Long Huang is thanked for discussions and comments on an earlier version of this thesis.

I thank Professor Carlos Fernandez of the Universidad de Huelva, Spain, Professor William Collins of the University of Newcastle, Australia, Dr. Thomas W. Sisson of the US Geological Survey (USGS), Professor Bruce Chappell of the Wollongong University, Australia, and Dr. Hugh Smithies of the Geological Survey, Western Australia (GSWA) for their kind response to my emails and helpful discussions on many specific topics.

I am indebted to Ms Hua Tao, Yu-Ya Gao and Mr Wei Dan for their helps with the laboratory work. I would like to thank Ms Ying Liu, Guang-Qian Hu, Wen Zeng, Drs. Xiang-Lin Tu, Xi-Rong Liang, Jin-Long Ma, Yan-Bin Zhang, Yue-Heng

Yang, Qian Mao, Mr Lie-Wen Xie, Biao Song, Chao-Feng Li, Yu Liu, Guo-Qiang Tang and many other staffs for their helps and technical advices on laboratory work.

Thanks are also due to my many friends who made my life in the past years quite enjoyable. There are too many of them to list here. I would like to mention Ji-Bin Zhou, Chang-Shi Qi, Mei-Fang Ye, Xuan-Ce Wang, Jiang-Bo Lan, Liang Zou, Jin-Feng Sun, Ying Jia Teoh, Ying-Chao Liu, Jia-Wen Niu, Rob Madden, Fiona Mothersole, Erin Gray, Chong-Jin Pang, Kong-Yang Zhu, Yong-Jun Lv, Wei-Hua Yao and Li-Ping Liu.

Finally, I am very much indebted to my wife Lingling Huang, who has been patient and provided invaluable support and encouragement during the entire period of my PhD study. Also, I am grateful to my parents, my brother and sister for their understanding and love.

This project was financially supported by the Chinese Academy of Sciences (grants KZCX1-YW-15-2, KZCX-YW-128, KZCX2-YW-T004), the Ministry of Science and Technology (grant 2007CB411403), Australian Research Council (grant DP11010X799), and the Chinese National Natural Science Foundation (grant 40728002). My study at Curtin University was supported by the Curtin International Postgraduate Research Scholarship (CIPRS) and the Institute for Geoscience Research (TIGeR) Award.

Abstract

High-K granites have become volumetrically important since at least Proterozoic. Their study bears important implications to crustal and tectonic evolutions. Despite of intensive research, sources and conditions for the formation of high-K granites remain controversial, mainly resulted from the uncertainty regarding the magmatic evolution. Thus, to understand the origin of compositional variations in granite suites is fundamental for granite research.

Several petrogenetic models have been proposed to account for the mineralogical and chemical variations of granites, with each individual model bearing different implications to the origin of granitic magmas and the crustal evolution. In this study, Jurassic high-K granites in the western Guangdong Province of SE China are systematically studied for their geochronology, petrography, mineralogy, whole-rock geochemistry, whole-rock Sr-Nd isotope compositions, and in-situ zircon Hf-O isotopes. Their petrogenetic processes are then examined using these results as well as existing information for the exploration of sources and conditions for the extensive post-orogenic granitic magmatism in the Jurassic South China. Crustal evolution of the basement terranes in this region is also discussed.

Granites with features typical of A-type, I-type or S-type were formed during ~165−155 Ma in the study area. A-type granitic rocks from the Jiuyishan granite suite contain anhydrous ferromagnesian minerals fayalite and ferrosilite, implying low water activity and oxygen fugacity (fO_2<FMQ buffer) in their source rocks and high temperature for partial melting. Chemical and isotopic variations documented in the Jiuyishan A-type suite could be best explained using processes of fractional crystallization. Evolved radiogenic (whole-rock: I_{Sr} = 0.7151–0.7181, εNd(t) = -9.3 to -6.4; zircon: εHf(t) = -8.2 to -2.3) and high oxygen isotope compositions ($\delta^{18}O_{zircon}$ = 6.3‰−11.5‰) suggest that the Jiuyishan A-type granite was most likely derived from high temperature (>960 ºC) melting of granulitic metasedimentary rocks, with no or very limited contribution of mantle-derived materials.

Mineralogical, geochemical and isotopic results suggest that the Jiufeng granite as well as the Dadongshan granite was dominantly sourced from metasedimentary rocks (S-type), too, but at lower melting temperatures (~820 ºC). Different from the Jiuyishan A-type granite, chemical variations exhibited by the Jiufeng granite samples could not be a result of magma differentiation (with or without wall-rock assimilation), but were most likely inherited from the heterogeneous source region, with sporadic local magma mixing. Where the contribution of mantle-derived materials was significant, the rocks show mineralogical (e.g., hornblende-bearing) and geochemical (e.g., A/CNK <1) features similar to I-type granites.

Some other granites with typical I-type features have been intruded as stocks along the southern coastal area of the western Guangdong Province. They however show less ^{18}O and ^{87}Sr (but more ^{143}Nd and ^{176}Hf) enrichment than the Jiufeng I-type granite samples ($\delta^{18}O_{zircon}$: 6.3‰−7.9‰ vs. 7.5‰−8.8‰; I_{Sr}: 0.7057−0.7077 vs. 0.7125−0.7143). The granites, particularly those with high oxygen fugacities (fO_2 >NNO; e.g., the Gangwei and Lunshui), could have been generated by direct melting of high-K basaltic rocks. It is noted that even such granites contain contribution of supracrustal materials that were probably inherited from their source rocks.

Results obtained in the course of this research are consistent with those from experimental studies. Jurassic post-orogenic high-K granites in SE China are characterized by not only their high K_2O contents and K_2O/Na_2O ratios (>1), but also their enrichment in ^{18}O and ^{87}Sr. This work suggests that granites like these could be simply derived from dehydration melting of metasedimentary rocks, while those with high oxygen fugacities and mantle-like isotope compositions could also be generated by melting oxidized hydrous high-K basaltic-intermediate igneous rocks. Therefore, the seemingly well constructed mixing line exhibited by zircon Hf-O isotopes is most likely resulted from secular reworking of supracrustal materials by mantle-derived magmas to variable degrees, but not an instant result of magma mixing. In spite of

this, Nd isotope model ages of 2.0−1.2 Ga of these granites do not support the presence of a ubiquitous Meso- to Paleo-proterozoic crystalline basement in the study area.

A compilation of accurate and precise zircon U-Pb geochronological data shows that many magmatic flare-ups in the inland South China Block (SCB) postdate the Permian-Triassic orogeny, with the most intensive one in Jurassic occurring in a short period of time between 165 Ma and 150 Ma. Although coeval basaltic rocks are volumetrically minor and mantle-derived magmas do not contribute much to the geochemical and isotopic variations in granites at the present level of intrusion, it is believed that underplating and intrusion of mafic magmas into lower crust has acted as the major heat source for the granitic magmatism. The magmatism was most likely triggered by the upwelling of the asthenosphere related to the delamination of flat-subducted oceanic slab and thinning of subcontinental lithosphere.

Keywords: granite, geochronology, geochemistry, isotope, zircon, post-orogenic, flat-subduction, delamination, southeast China

Chapter 1: Introduction

1.1. Background

Granite is a kind of intrusive, felsic, igneous rock with medium- to coarse-grained texture. It is named according to the percentage of quartz, alkali feldspar and plagioclase on the QAPF diagram (Streckeisen, 1974), but is used in this study in a general sense to include all coarse-grained igneous rocks comprising feldspars and >20% norm quartz. Granites are ubiquitous in the Earth's continental crust and encompass a wide range of mineralogical, geochemical and isotopic compositions (e.g., Barbarin, 1999; Chappell and White, 1974; McCulloch and Chappell, 1982; Pearce et al., 1984). Estimations show that approximately 70% of the Earth's continental crust is composed of rocks with granitic composition (e.g., Hawkesworth and Kemp, 2006). Hence, granitic magmatism is critical for the growth and differentiation of the Earth's continental crust (Bonin, 2007).

High-K granites have become volumetrically important since Proterozoic (Clemens and Stevens, 2012; Roberts and Clemens, 1993), whereas low-K and Na-enriched TTG rocks are the main constituent of the Archaean continental crust (Martin and Moyen, 2002). There is no consensus as to how the compositional change of granitic magmatism is related to the transition in the Earth's dynamics. Though volumetrically significant, there is also no consensus, internationally, as to sources and conditions for the formation of high-K granitic rocks, particularly those showing I-type features (e.g., Clemens et al., 2011b; Roberts and Clemens, 1993; Sisson et al., 2005). For example, sources proposed for high-K granites vary from mantle peridotitic rocks influenced by crustal materials (e.g., Bonin et al., 1998; Dickinson, 1975) to metasedimentary rocks.

Controversies in terms of sources and conditions for granitic magmatism mainly arise from the uncertainty with respect to magmatic evolutions. Though it has been shown that granites with distinct compositions could originate from melting

different source rocks (Chappell and White, 1974), it is believed that compositional variations recorded in a granite suite are results of magmatic evolutions. Several petrogenetic models have been frequently used to interpret compositional variations observed in granite suites, those include restite-unmixing (Chappell et al., 1987; White and Chappell, 1977), magma mixing (Depaolo and Wasserburg, 1979; Gray, 1984), wall rock assimilation and fractional crystallization (AFC) (Depaolo, 1981), and peritectic assemblage entrainment (PAE) (Clemens and Stevens, 2012; Stevens et al., 2007), with each model bearing different implications to the origin of granitic magmas and evolution of continental crust (**Fig. 1.1**). For example, the restite-unmixing model suggests that granitic magmas are products of crustal melting and represent mixtures of melts and restites, so compositions of the most mafic samples in a granite suite approach that of the source rocks (e.g., Chappell et al., 1987; White and Chappell, 1977). Therefore, granite province may be used to define basement terranes (Chappell et al., 1988). Different from this model, granitic magmas in a mixing model represent mixtures of mafic and felsic magmas and imply crustal growth as well as differentiation (e.g., Gray, 1984; Griffin et al., 2002; Kemp et al., 2007). Most recently, it has been shown, however, that chemical variations exhibited by granite suites/plutons are probably primary, inherited from their source regions (Clemens et al., 2010), with peritectic assemblage entrainment (PAE) acting as the principal process for controlling variations of Ti, Mg, Fe, etc (e.g., Clemens et al., 2011a; Clemens and Stevens, 2012; Stevens et al., 2007).

To distinguish the various magmatic evolution processes and unravel the origin of compositional variations in granite bodies are fundamental in granite research, but turn out to be notoriously difficult (e.g., Chappell, 1996, 2004; Chappell et al., 1987; Clemens et al., 2010; Clemens and Stevens, 2012; Collins, 1998; Wall et al., 1987). This is largely due to the fact that whole-rock geochemical and isotopic compositions present a final picture only and do not preserve much information of magmatic evolution (Griffin et al., 2002). For example, linear geochemical variation of elements in granitic suites/bodies could be taken as

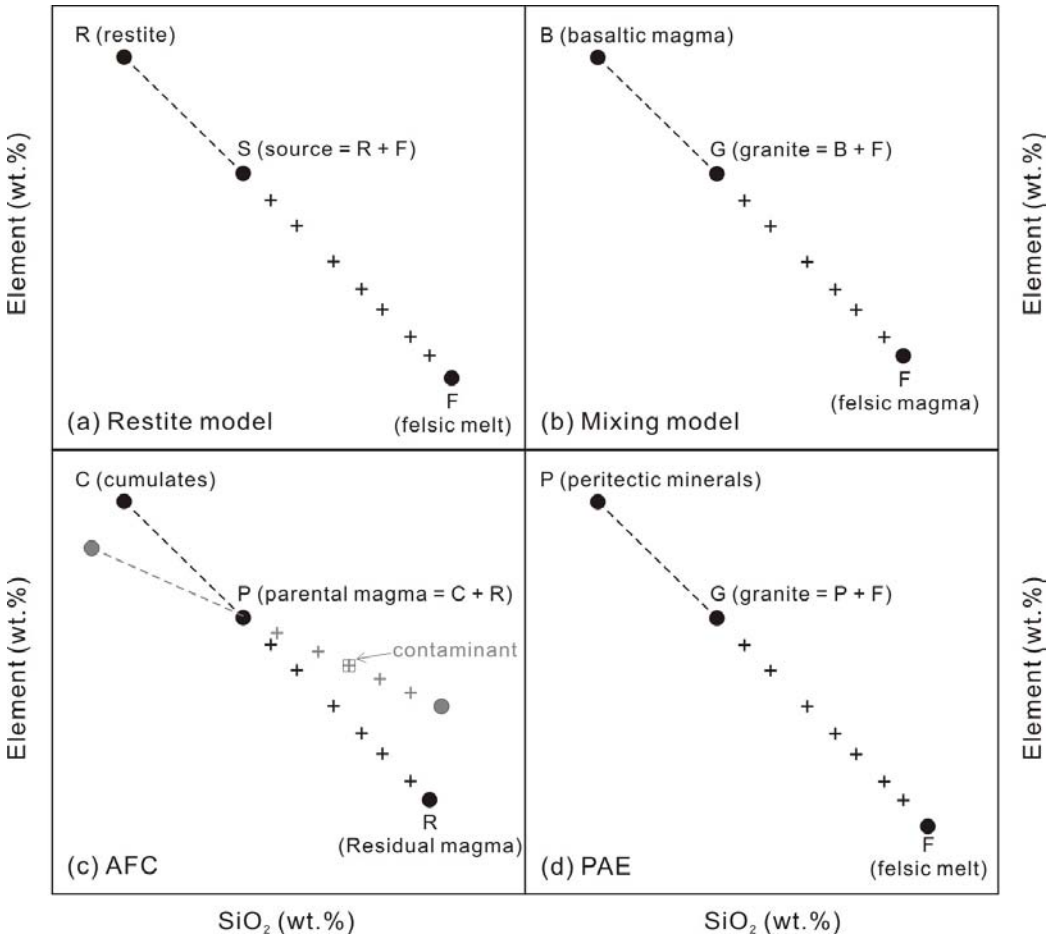

Figure 1.1 Chemical (and crustal evolution) implications of four petrogenetic models. (a) Restite model. Granites are composed of minimum melt and various amount of restite. (b) Mixing model. Granites are products of variable mixing between basaltic and felsic magmas. Chemical implication of a mixing model involving three components has been shown by Collins (1998). (c) Assimilation and fractional crystallization (AFC). The black symbols illustrate chemical variations that would be produced by fractional crystallization only, while the grey symbols represent variations that involve assimilation of wall-rock components (contaminants). It is noteworthy that the liquid line of ascent is usually mildly curved, but is simplified as straight line here. (d) Peritectic assemblage entrainment (PAE). This model is distinct from the restite unmixing model in that only certain element that enriched in peritectic minerals would show the linear variation patterns due to the entrainment of that particular mineral.

evidence for restite unmixing, fractional crystallization, and magma mixing as well (e.g., Collins, 1996; Gray, 1984; Wall et al., 1987; White and Chappell, 1977). Besides, there is usually a decoupling between chemical and isotope compositions. For example, the chemistry of some I-type granites is incompatible with the

contribution of high percentage (up to 50%) of sedimentary component that would be predicted using isotope compositions in a simple two-component mixing model (e.g., McCulloch and Chappell, 1982). The record of magmatic evolution, however, could have been documented within geochemical and isotopic stratigraphy of certain minerals, e.g. plagioclase, zircon, titanite, monazite. As analytical techniques develop, these minerals can now be analysed in fine scales and in-situ in particular; the records preserved have been revealed by recent studies that draw on several microanalytical innovations (e.g., Davidson and Tepley, 1997; Gregory et al., 2009; Griffin et al., 2002; Kemp et al., 2007; Vazquez and Reid, 2004; Waight et al., 2000).

Now, there is a rare opportunity to unravel the record of magma evolution and reveal sources and conditions for the formation of high-K granites using combined whole-rock analyses and micro-analyses (in-situ analyses in particular). In this study, the Jurassic post-orogenic high-K granites in the western Guangdong Province, southeastern China (SE China, **Fig. 1.2**) are investigated in details as an example. The study of the western Guangdong Jurassic high-K granites is not only significant for Mesozoic geology research, but also useful for the understanding of Precambrian tectonic evolution of the SCB and its paleogeographic reconstruction.

1.1.1. Intensive Jurassic granitic magmatism in the SCB

Jurassic (or early Yanshanian-aged in Chinese literature) granites are widespread in SE China, constituting an important feature of Mesozoic geology in the region (**Fig. 1.2**). They form part of a large Mesozoic magmatic province in the region and have an estimated outcrop area over 64,000 km^2 (Li et al., 2007b; Zhou et al., 2006), similar to that of the Paleozoic granites in the Lachlan Fold Belt (LFB), southeastern Australia (61,000 km^2, Chappell et al., 1988). Geochronological studies show that the Jurassic granites are products of several magmatic flare-ups that postdated the Permian-Triassic orogeny in the eastern South China Block (SCB) (Li and Li, 2007; Zhou et al., 2006) and were mainly generated in a short period of time of 165−155 Ma (Li et al., 2007b).

Many studies have been carried out on these granites in order to uncover their petrogenesis and geological significance (e.g., Chen et al., 2002; Chen et al., 2005; He et al., 2010; Huang et al., 2011; Jahn, 1974; Jahn et al., 1990; Jiang et al., 2009; Li, 2000; Li et al., 2003a; Li et al., 2009b; Li et al., 2007b; Li et al., 2007c; Wang et al., 2011a; Wang et al., 1989; Wang et al., 2003a; Xu et al., 1984; Xu et al., 2007; Zhao et al., 2011b; Zhou and Li, 2000; Zhou et al., 2006; Zhu, 1998). Studies show

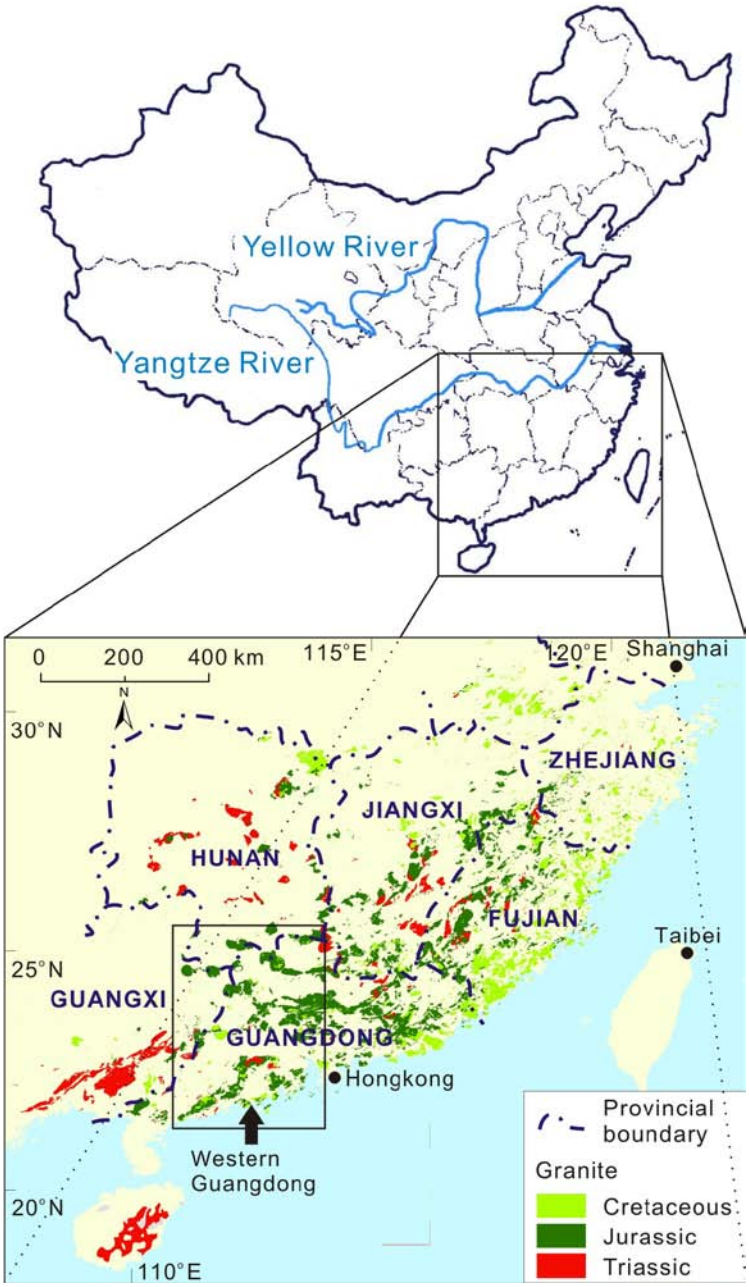

Figure 1.2 A geographical map of continental China, showing the distribution of Jurassic granites amongst the other Mesozoic granites in SE China.

that the widespread Jurassic granites in SE China vary in lithology from muscovite granite to two-mica granite to biotite granite to amphibole-bearing biotite granite. Some granites also contain anhydrous ferromagnesian minerals olivine and pyroxene (Fu et al., 2003a; Huang et al., 2011). Among these, biotite granites and two-mica

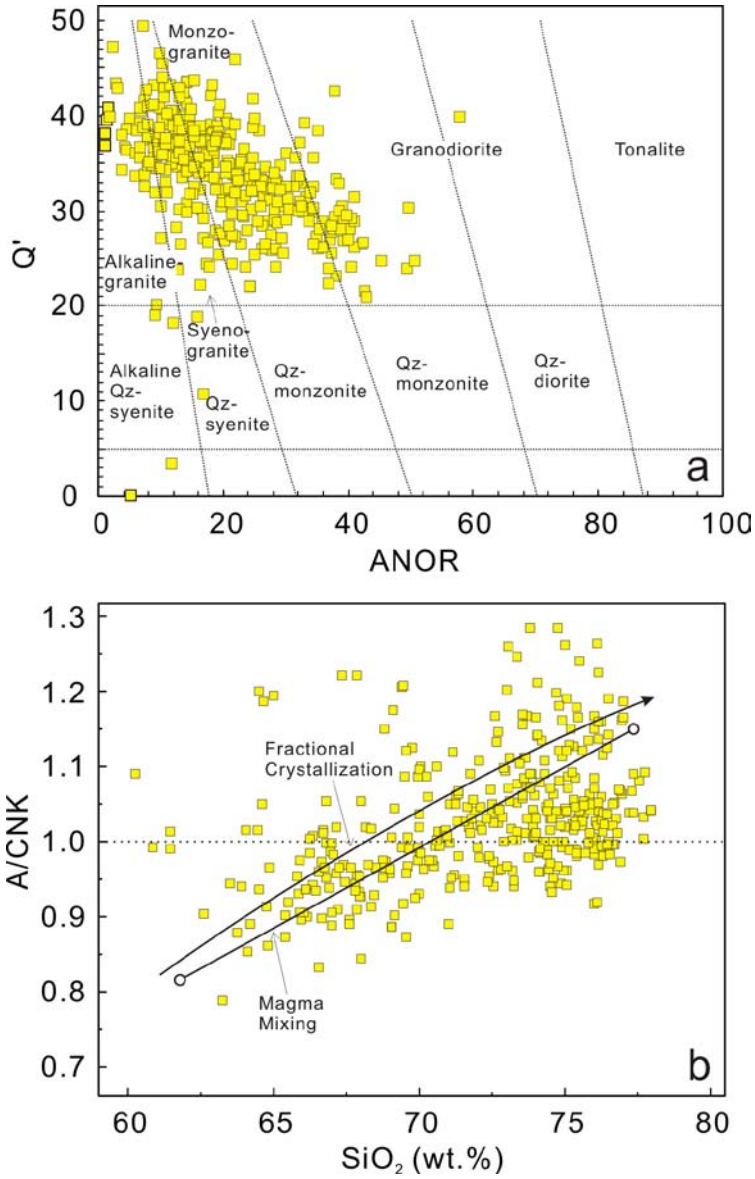

Figure 1.3 (a) Q' vs. ANOR normative composition diagram (Streckeisen and Le Maitre, 1979) for granite classification and (b) SiO_2−A/CNK diagram showing the aluminum saturation index of Jurassic granites in SE China (**Appendix Table 1**). The solid line with an arrow shows the interpreted A/CNK evolution trend when fractional crystallization predominates and the solid line with open circles at its ends illustrates the likely mixing trend of two end-members**.**

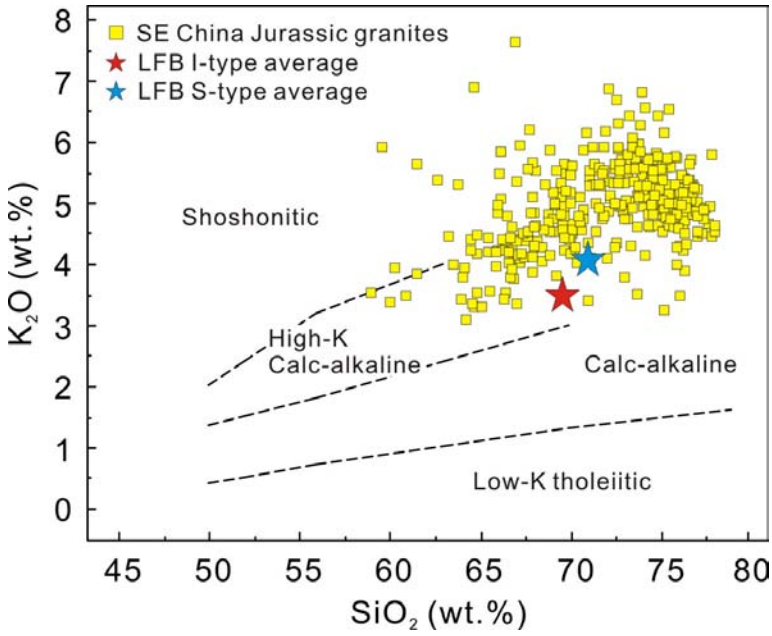

Figure 1.4 K_2O vs. SiO_2 geochemical plot showing K_2O compositions of Jurassic granites in SE China (**Appendix Table 1**). Dashed field boundary lines are after Peccerillo and Taylor (1976) and Rickwood (1989). The average compositions of I- and S-type granites in the Lachlan Fold Belt are also shown for comparison (Chappell and White, 1992).

granites dominate. As is shown in **Fig. 1.3a**, Jurassic granites in SE China are dominantly syenogranite and monzogranite, consistent with the result of previous QAPF classification by Jahn et al. (1990) and similar in composition to post-orogenic granite suite worldwide (Chen et al., 2002). Geochemical analyses show that they are transitional from metaluminous to strongly peraluminous (**Fig. 1.3b**). Particularly, these granites are characterized by their high SiO_2 and K_2O contents, ^{87}Sr- and ^{18}O-enriched whole-rock isotope compositions (Xu et al., 1984). Their K_2O concentration is even higher than that of S-type[1] granites in the LFB (**Fig. 1.4**). Taken together, some granites show features similar to A-type, I-type or S-type granites in the LFB, but most cannot be uniquely classified (e.g., Li et al., 2007b).

[1] The I- and S-type classification scheme was originally proposed by Chappell and White (1974), implying that granites are principally derived from melting of either **I**gneous or **S**edimentary rocks. A-type granite has been assigned to a group of granites with distinct characteristics (e.g., **A**nhydrous; Loiselle and Wones, 1979) and is widely accepted as a subgroup of I-type granite (e.g., Creaser et al., 1991). Extensive studies (including this study), however, have revealed a much more complex origin.

There is no consensus as to the material source of the Jurassic high-K granites in SE China. It has been suggested that they are transformation-type granites produced from melting of metasedimentary rocks (i.e. S-type) (e.g., Xu et al., 1984); on the other hand, these rocks are also considered as I-type derived from metaigneous rocks (e.g., Li et al., 2007a). In-situ zircon Hf and O isotope analyses, however, revealed reworking of old crustal components by mantle-derived materials in the genesis of some granites (e.g., Li et al., 2009b; Li et al., 2007b). Studies have also produced different results regarding the heat source and related geodynamic evolution process as for the Jurassic intensive granitic magmatism in the eastern SCB, with inferred models including microcontinental collision (Hsü et al., 1988; Jahn et al., 1990), Paleo-Pacific subduction (Zhou and Li, 2000), back-/intra-arc extension (e.g., Jiang et al., 2009; Jiang et al., 2006), continental rifting (e.g, Gilder et al., 1991; Li, 2000; Li et al., 2003a), delamination of flat-subducted slab (Li et al., 2007b; Li and Li, 2007), and post-orogenic lithospheric extension relative to continental collision (Chen et al., 2008).

1.1.2. Granite province and source terrane

The SCB is presently located in East Asia, adjoining the Pacific Ocean to the east and the South China Sea to the south (**Fig. 1.5**), but its Neoproterozoic geographic position remains controversial (see Li et al., 2008c for a detailed review). Knowledge of the relative geographic position of the SCB in Neoproterozoic is critical for the evolution of the supercontinent Rodinia. Li et al. (1995) proposed a "missing-link" model which positions the SCB between Australia-East Antarctica and Laurentia in the central Rodinia. Alternative positions have also been proposed (e.g., Jiang et al., 2003; Yu et al., 2008), but the missing-link model is the most compatible with global plate kinematics, paleomagnetism and orogenic histories (Li et al., 2008c). In particular, configuration in this model may explain age population of detrital grains from the clastic wedges in the Belt basin of the northwestern United States (Li et al., 2008d; Li et al., 2002b; Li et al., 1995).

Studies show that the SCB was formed through the amalgamation between the Yangtze Craton in the northwest and the Cathaysia Block in the southeast (present coordinates, **Fig. 1.6**) in Neoproterozoic time (Chen et al., 1991; Li et al., 2008a; Li et al., 2009a; Li et al., 2007d; Ye et al., 2007). As is shown in **Fig. 1.6a**, the southeastern part of the SCB, known as Cathaysia block, is interpreted to be part of the Proterozoic Laurentia in the missing-link model. It is implied that the Cathaysia block is/was once floored with Paleoproterozoic crystalline basement. Indeed, there are some Paleoproterozoic basement rocks exposed in the northeastern part of the Cathaysia block (**Fig. 1.6**). However, this block is now mostly covered with Neoproterozoic and Phanerozoic volcanic-sedimentary rocks. Numerous outcrops of Paleozoic and Mesozoic intrusive rocks also cover a wide area. Except a couple of outcrops of ~1.4 Ga granites and volcanic rocks in Hainan Island (number '4' in **Fig. 1.6b**), no other Precambrian crystalline rock has been identified in the whole southwestern part of the Cathaysia block yet. Due to this fact, the exact boundary

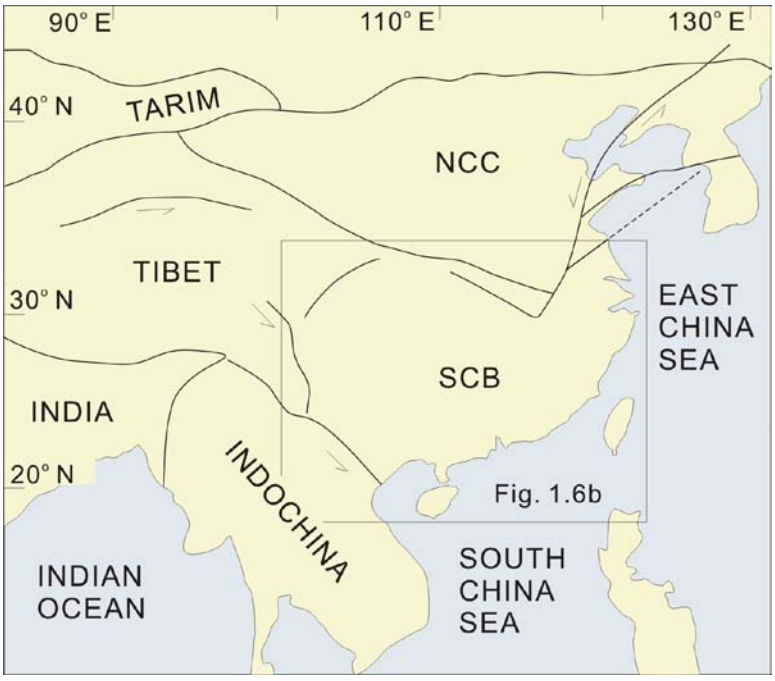

Figure 1.5 A sketch map showing major tectonic units in East Asia and the present geographical position of the South China Block. Symbols: NCC—North China Craton; SCB—South China Block.

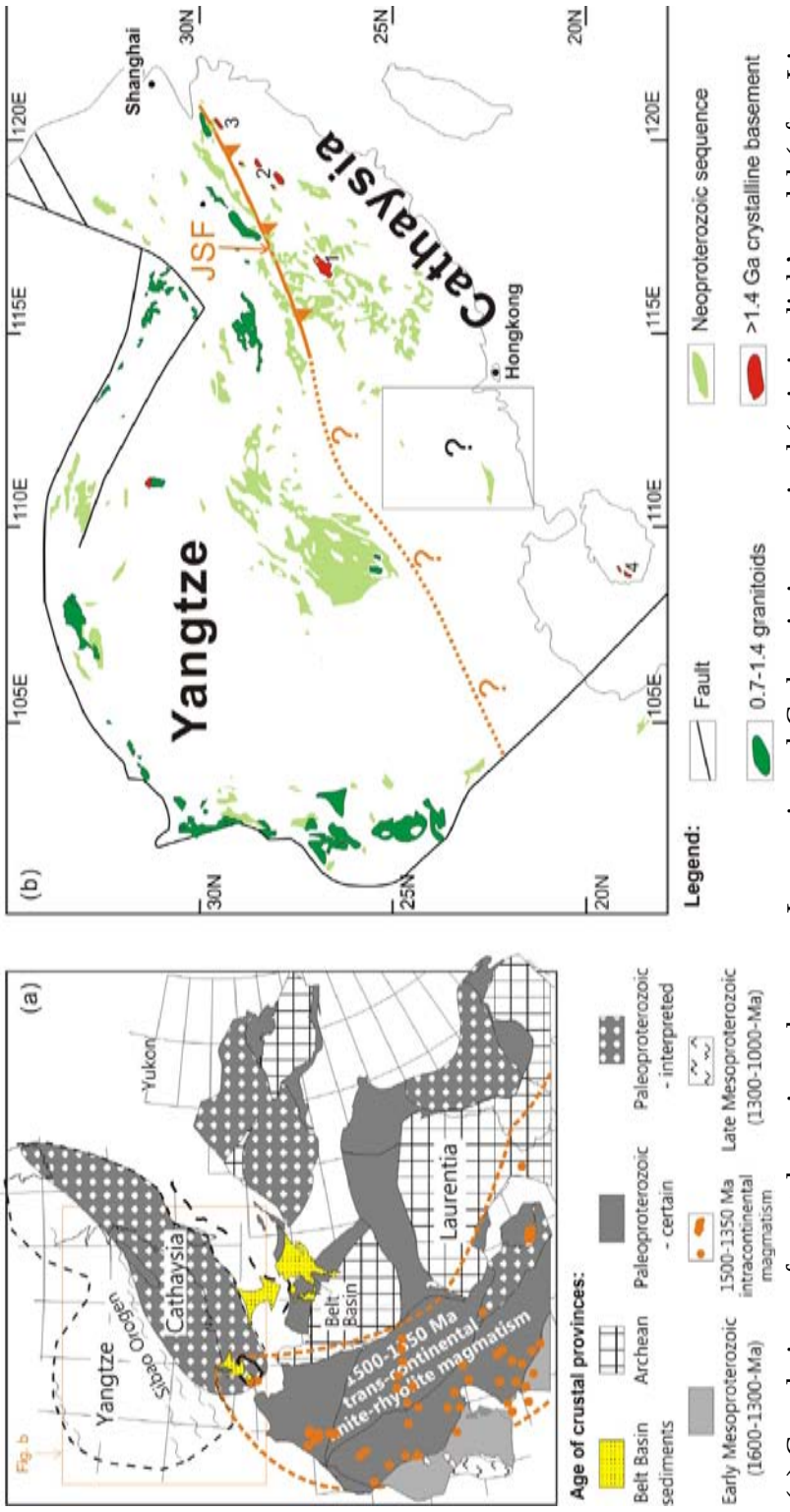

Figure 1.6 (a) Correlations of crustal provinces between Laurentia and Cathaysia in a revised 'missing-link' model (after Li et al., 2008d). Courtesy of Z. -X. Li. (b) Simplified geological map showing the distribution of Precambrian igneous and sedimentary rocks in SE China (after Li et al., 2003b; Li et al., 2002b). Symbols: 1. the Tianjingping amphibolites (Li, 1997); 2. the Badu complex and Danzhu granite (Li et al., 2011; Li and Li, 2007; Yu et al., 2009a); 3. the Chencai complex (Li et al., 2010e); 4. the Baoban complex and Shilu Group (Li et al., 2008d; Li et al., 2002b). JSF, the Jiangshan-Shaoxing Fault marks the probable boundary between the Yangtze and the Cathaysia. Courtesy of W. -X. Li.

between the Yangtze Craton and the Cathaysia block, particularly over its western half, remains unclear, either (**Fig. 1.6b**).

Most granites, particularly those with evolved radiogenic isotope compositions, come from the deep parts of the continental crust; they contain information about the nature of crust and represent probes into the source terrane (Chappell et al., 1988). Therefore, the study of the widely distributed Jurassic granites in the western Guangdong area is useful for revealing the nature of the crustal basement beneath and is potentially significant to the configuration and evolution of supercontinent Rodinia.

1.2. Objectives

The primary objective of this study is to identify material sources for the generation of various Jurassic high-K granites in the western Guangdong Province, SE China. This will be achieved primarily by integrating in-situ zircon Hf-O analyses with zircon U-Pb geochronology, petrography, mineralogy, whole-rock geochemistry and Sr-Nd isotope analyses. Based on these new data, on what degree a particular petrogenetic process operated in contributing to the chemical variations exhibited by granitic bodies will be evaluated on a case by case basis for each granite body. In the light of experimental studies, the integrated study should allow the nature of the magma sources to be determined.

The second objective of this study is to understand what the probable heat source was for the intensive Jurassic granitic magmatism and how the widespread granites could be generated in the context of tectonic evolution of the SCB. This will be achieved by an evaluation of temperatures for partial melting and an examination of existing geodynamic models.

1.3. Research methods

This thesis is based on field work and extensive laboratory studies.

1.3.1. Field work

A total of 45 days (for three field excursions) was spent in the field. Representative granitic plutons in the western Guangdong region have been surveyed and sampled. Samples collected in the field are fresh, undeformed/unmetamorphosed, varying from pale-grey to brick-red in colours. A total of 116 least-altered samples, encompassing a wide range of lithological phases, were selected from eight granitic plutons for petrological, whole-rock geochemical and isotopic studies. Samples for bulk-rock studies are generally ca. 10 × 10 × 10 cm^3 in sizes. For some samples, larger specimens of ca. 20 × 20 × 10 cm^3 in sizes were prepared for zircon extraction. All samples were located using the Global Positioning System with longitude and latitude values (**Appendix Table 2**).

1.3.2. Laboratory studies

Laboratory studies include thin-section preparation and examination, mineral examination by EPMA (Electron Microprobe), rock crushing, loss on ignition (LOI) determination, major element determination by XRF (X-Ray Fluorescence Spectrometer), wet-chemical analyses in ultra-clean laboratories, trace element determination by ICP-MS (Inductively Coupled Plasma Mass Spectrometry), Sr-Nd isotope determination by MC-ICP-MS (Multi-Collector Inductively Coupled Plasma Mass Spectrometry) and TIMS (Thermal Ionization Mass Spectrometry), cathodoluminescence (CL) imaging of zircons by SEM (Scanning Electron Microscopy), ion microprobe zircon U-Pb dating (SHRIMP II and Cameca IMS-1280 SIMS) and oxygen isotope analysis, and LA-MC-ICP-MS (MC-ICP-MS attached with a laser ablation system) zircon Hf isotope analysis. Detailed analytical procedures are given in Chapter 3.

- The crystallization age of granite samples will be determined by zircon U-Pb studies using SHRIMP II and Cameca IMS-1280 SIMS. Accurate and precise

age determination is important for initial isotope ratio calculation. The result not only provides constrains on the geochronological structure in granitic bodies, but also helps to understand the geological evolution of the SCB in Jurassic.

- Mineralogical and petrographical studies mean to identify rock type, to determine crystallization sequence and physio-chemical characteristics. The result contributes to the identification of the most probable source rocks.

- Variation of major and trace elements, Sr-Nd isotope ratios and in-situ zircon Hf-O isotopes help to determine on what degree a particular process operated in the course of magma evolution and how granitic magma were produced and segregated. In-situ zircon Hf-O isotopes are particularly useful in distinguishing crustal reworking from crustal growth.

1.4. Structure of the thesis

This thesis consists of seven chapters. They will be presented as follows:

Chapter 1 presents key background information and highlights scientific problems to be addressed in this thesis.

Chapter 2 introduces the geology of the SCB and the western Guangdong.

Chapter 3 details the analytical procedures.

Chapters 4, 5 and 6 present results, evaluate petrogenetic processes and speculate sources for the various types of rocks (including typical A-type and I-type granites) in the western Guangdong on a case by case basis.

Chapter 7 presents a comprehensive model for the genesis of the Jurassic high-K granites, discusses their implications to revealing crustal architecture and importance for paleographic reconstruction and tectonic evolution.

Chapter 2: Regional geology and sampling

(This chapter contains contents published in the following papers:

Huang, H.-Q., Li, X.-H., Li, W.-X., and Liu, Y., 2008, Age and origin of the Dadongshan granite from the Nanling Range: SHRIMP U-Pb zircon age, geochemistry and Sr-Nd-Hf isotopes: Geological Journal of China Universities, v. 14, no. 3, p. 317-333 (in Chinese with English abstract).

Huang, H.-Q., Li, X.-H., Li, W.-X., and Li, Z.-X., 2011, Formation of high $\delta^{18}O$ fayalite-bearing A-type granite by high-temperature melting of granulitic metasedimentary rocks, southern China: Geology, v. 39, p. 903-906.

Huang, H.-Q., Li, X.-H., Li, Z.-X., and Li, W.-X., Intraplate crustal remelting for the genesis of Jurassic high-K granites in the coastal region of the Guangdong Province, southeastern China: submitted to the Journal of Asain Earth Sciences.

All results and conclusions, otherwise acknowledged in these published/submitted papers, were made by myself under supervision.)

2.1. Introduction

The widespread (approximately ~64,000 km^2) Jurassic high-K granites in SE China were emplaced in a wide Mesozoic fold belt and its overlying basins in the eastern SCB. Levels of their intrusion remain largely unconstrained, but shallow levels in an extensional environment are favoured as they mostly show massive structure and remain undeformed (Zhou et al., 2006). At the present level of exposure, they are mostly intruded into Paleozoic sedimentary rocks. Some of them form complexes with early Mesozoic and/or early Paleozoic intrusive rocks (e.g., Fu et al., 2004b; Li, 1991; Xu et al., 2003), a few also form bimodal complexes with coeval gabbroic rocks (e.g., Xu et al., 2007; Yu et al., 2009b).

Regionally, the deformed early Paleozoic strata are ubiquitous. They have been strongly folded and metamorphosed to variable degrees, transitional from greenschist facies to amphibolite facies and in some instances granulite facies (e.g., Guangdong, 1988; Hunan, 1987; Wan et al., 2010; Wang et al., 2010b; Wang et al., 2007d). Deformation recorded by the late Paleozoic rocks is characterized by folding and thrusting with associated foliation and lineation (Wang et al., 2007b). Greenschist facies metamorphism is the most common for these rocks, while higher degree metamorphism may have also been developed for some (Fujian, 1985; Wang et al., 2005). Contact metamorphism is common where there is intrusion of granites, in age of both early Paleozoic and Mesozoic. Metamorphic aureoles vary from 200 m to 1500 m in width with sillimanite hornfels being the most common metamorphic rocks.

2.2. Tectonic context

The SCB is bounded by the Qinling-Dabie-Sulu orogenic belts produced by its collision with the North China Craton (NCC) to the north during the early Mesozoic (Ratschbacher et al., 2003); to the northwest and southwest, it is fault-bounded by the Longmenshan belt and the Ailaoshan-Red River shear zone, respectively (**Fig. 2.1**). As is shown in **Fig. 2.1**, SE China where the widespread Jurassic granites were emplaced is topographically high, covered with broad mountain ranges with many remanent basins on top, similar to the present day Basin-and-Range province in the western North American (Gilder et al., 1991). The topography is shaped from successive reworking of the SCB by a series of major tectonic events since its formation arguably through amalgamation of the Yangtze Craton and Cathaysia block in the early Neoproterozoic (**Fig. 2.2**). These major tectonic events include continental rifting in the Neoproterozoic, Wuyi-Yunkai orogeny in the early Paleozoic, Indosinian orogeny in the Permian and Triassic, and extension and rifting in the Jurassic.

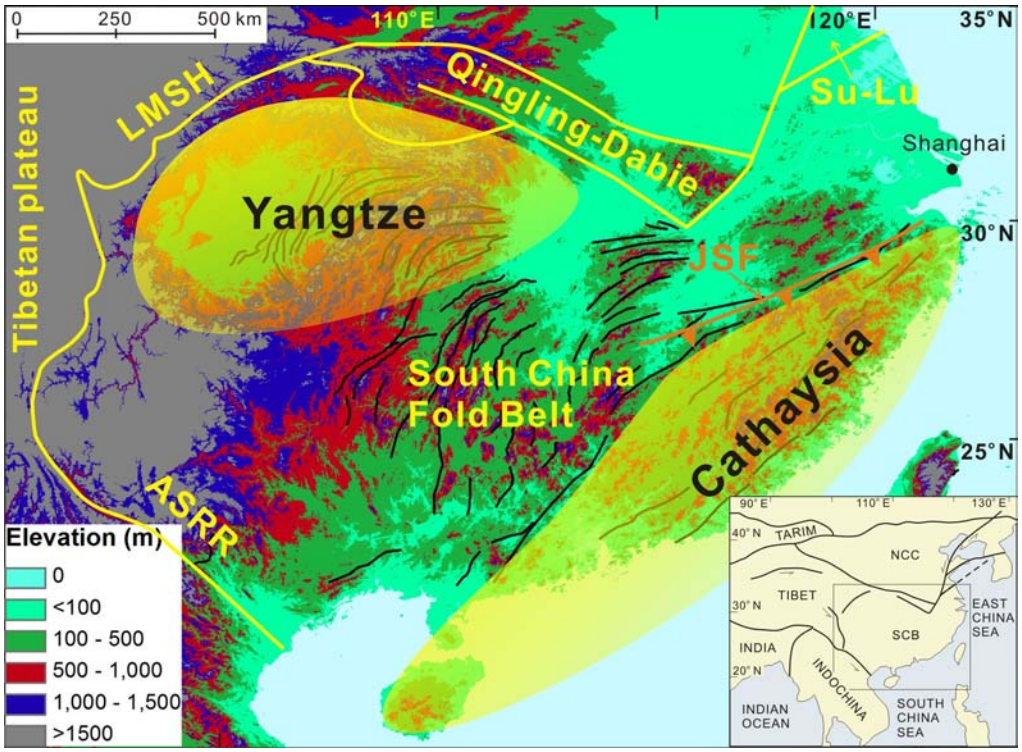

Figure 2.1 Digital topography of south China showing the major Mesozoic thrust faults and curvatures (solid black lines) (after Li and Li, 2007). Folded strata in the fold belt mainly exhibit northwest verging. Symbol: JSF—Jiangshan-Shaoxing Fault. The inset figure is a scale-down version of the **Fig. 1.5**.

2.2.1. Continental rifting in the Neoproterozoic

Sedimentary records (Liu and Xu, 1994) show that extensive deposition of volcanic rocks and sediments occurred around the Yangtze Craton and along northwest margin of the Cathaysia block in the Neoproterozoic (Li, 1998). Stratigraphical and facies analyses, together with geochronological studies, reveal that after a stage of initial bimodal and alkaline magmatism at ca. 860−850 Ma (e.g., Li et al., 2010b; Li et al., 2010c; Li et al., 2008b), at least four major episodes of magmatism occurred at ca. 825 Ma，ca. 800 Ma, ca. 780 Ma, and ca. 750 Ma, respectively (Li et al., 2003c). Voluminous basaltic rocks, as well as plutons and felsic volcanic rocks, were produced during that time (e.g., Li et al., 2002a; Li et al., 1999; Li et al., 2003c; Wang and Li, 2003; Wang et al., 2010a; Wang et al., 2009), marking an important stage of crustal growth. Geochemical analyses show that

basaltic rocks generated at this stage are dominantly tholeiitic in composition, with only a few being alkalic and calc-alkalic (Wang et al., 2009). The results, in conjunction with isotope studies, show that most basaltic rocks have geochemical and isotopic characteristics similar to OIB-type basalts, indicating that they were most likely produced from continental rifting, as compared with island-arc and syn-collisional orogenic environments (e.g., Li et al., 2005a; Li et al., 2008b; Li et al., 2003c). Considering the fact that high temperature komatiitic basalts were also produced (Wang et al., 2007a), the long-lived Neoproterozoic magmatism from 860 Ma to 750 Ma was most likely resulted from upwelling of a superplume (Li et al., 2010b), though alternative models, e.g. back-arc spreading (Zhao et al., 2011a), have also been proposed. Doming of the Rodinia superplume could also lead to the formation of continental rifts and breakup of the Rodinia (e.g., Li et al., 1999; Wang and Li, 2003). Some failed rifts, e.g. the Nanhua rift in the SCB (**Fig. 2.2**), were then

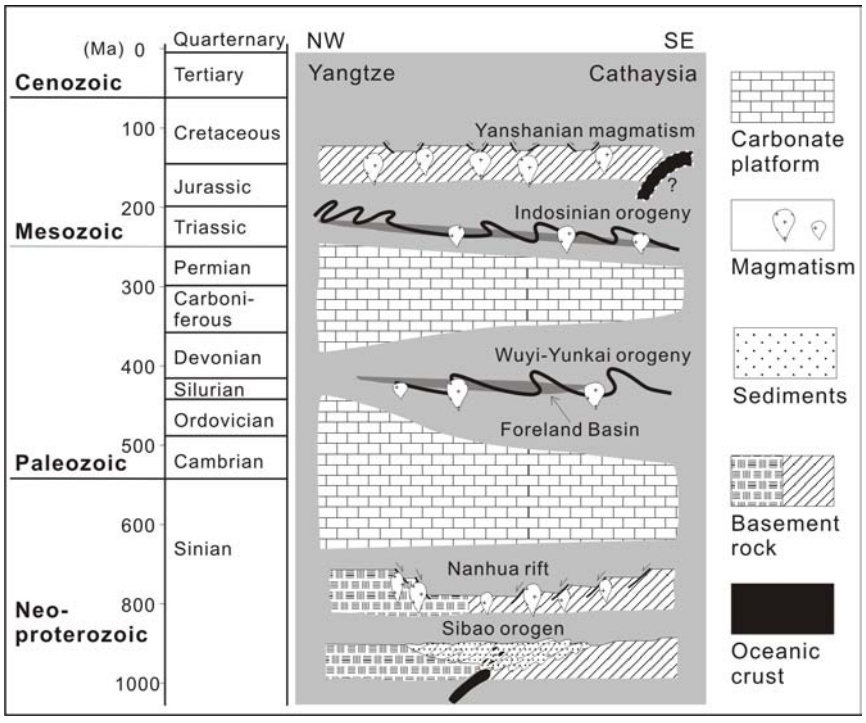

Figure 2.2 Schematic diagram demonstrating major Neoproterozoic and Phanerozoic tectonic events in the SCB (modified after Li, Z. X., 2009, A tectonic overview of the South China Block, p. 1-30).

filled with sediments (Wang and Li, 2003). A late Neoproterozoic marine transgression brought the whole region of the SCB to deep water to receive carbonate deposits (**Fig. 2.2**).

2.2.2. The Wuyi-Yunkai orogeny

After its formation and rifting in the Neoproterozoic, the SCB was subsequently reworked by the "Wuyi-Yunkai" orogeny in the early Paleozoic (**Fig. 2.2**). Clastic deposits resumed in the SCB in the Ordovician (Li et al., 2010e; Liu and Xu, 1994), indicating that retrogression might have started since then. Field studies have observed a regional angular unconformity between the upper Silurian/Devonian strata and their underlying deformed and folded strata that have been intruded by granites (e.g., Ren, 1991). The unconformity has long been interpreted to document an early Paleozoic orogenic event that led to the closure of a miogeosyncline/remanent oceanic basin (Shui, 1988).

Knowledge with respect to the tectonic regime and timing of the orogeny remains poor. It has been difficult to define the extent of magmatism and metamorphism due to the overprint of the Indosinian orogeny (**section 2.2.3**). Most recently, geochronological studies revealed that the Paleozoic magmatism and metamorphism peaked at 460−415Ma (e.g., Li et al., 2010e; Wan et al., 2010; Wan et al., 2007; Wang et al., 2007d; Yu et al., 2005). Petrological and tectonic analyses show that Paleozoic igneous and metamorphic rocks are dominantly exposed in the Wuyi and the Yunkai mountainous areas and the orogeny may extend from the Wuyi area in the northeast to the Yunkai area in the southwest with an extension of 2000 × 600 km^2 (**Fig. 2.3**). As a result, the orogeny was termed the Wuyi-Yunkai orogeny . Studies identified the Wuyi-Yunkai orogeny an intraplate orogenic event (Li et al., 2010e; Wang et al., 2010b), likely started with the Nanhua basin evolving into a foreland basin in the Ordovician and ended with its closure in the Silurian/Devonian (Li, 1998; Liu and Xu, 1994). During the closure of the basin, basement rocks and basin fills were metamorphosed to variable degrees from greenschist facies to

amphibolite and granulite facies (e.g., Li et al., 2010d; Yu et al., 2005), following a clockwise pressure-temperature (P-T-t) metamorphism path (Li et al., 2010d). Deformed metamorphic rocks in the orogenic belt were predominantly northwest-verging (Li et al., 2010d; Ren, 1991).

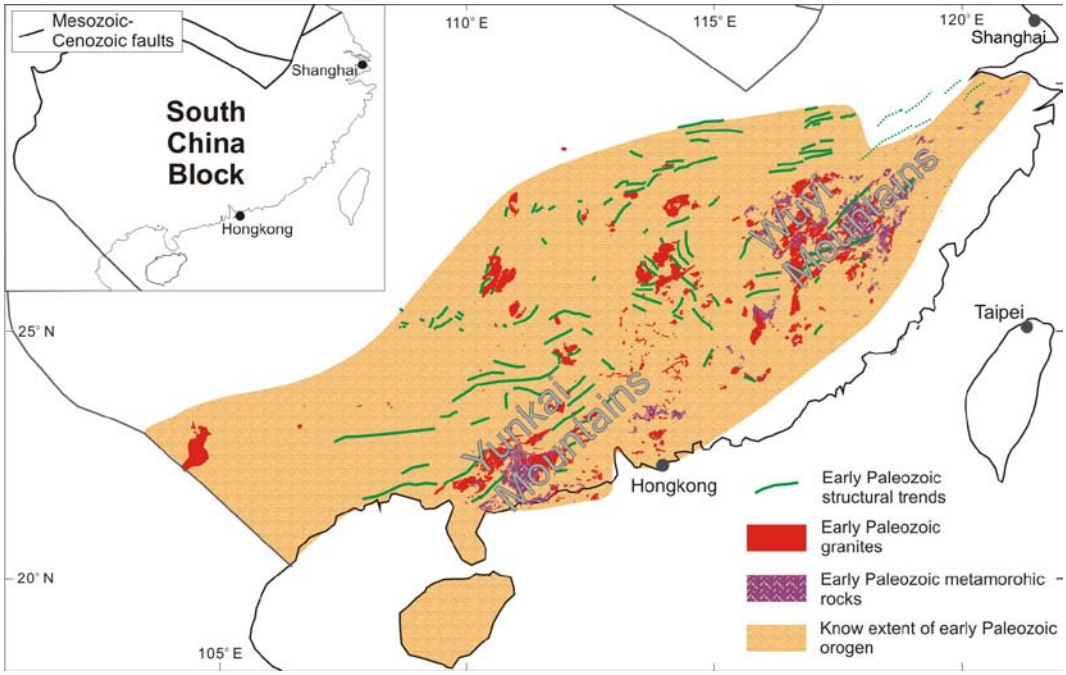

Figure 2.3 Simplified geologiclal map showing the regional extent of the early Paleozoic Wuyi-Yunkai orogeny (after Li et al., 2010e). Courtesy of Z. -X. Li.

2.2.3. The Indosinian orogeny

The early Mesozoic orogenic event in the SCB has been known as the "Indosinian" orogeny, a term borrowed from Indosinian thermotectonism in Vietnam, Indochina and used in a broad sense to encompass all late Paleozoic to early Mesozoic tectonic movements in East Asia (Carter and Clift, 2008; Cho et al., 2008). After the Wuyi-Yunkai orogeny, a late Paleozoic marine transgression occurred and the whole region of the SCB was mostly covered by platform carbonate (Li, 1998; Liu and Xu, 1994). This block became tectonically active again since the mid-Permian (**Fig. 2.2**). In the northeast (the present-day coordinates), initial collision between the SCB and the NCC possibly started at their eastern ends (Li, 1994; Yin and Nie, 1993; Zhao and Coe, 1987). The amalgamation of the two blocks

created the Qinling-Dabie-Sulu orogenic belt, well-known as one of the most typical ultrahigh-pressure metamorphic belts in the world (Xu et al., 1992). In the southwest, the coming of a mantle plume (the Emeishan mantle plume) caused the continent to dome and unroof (He et al., 2009; He et al., 2003). In the east, a >1300 km-wide north-easterly trending fold belt that covers much of the SCB was created (**Fig. 2.1**).

Sedimentary records show that coastal region of the South China platform was first uplifted in the mid-Permian, accompanied with a change of sedimentary facies from carbonates to clastic sediments in the region and to its northwest (Liu and Xu, 1994). Associated with the change, calc-alkalic magmatism was also produced, likely marking a transition of the platform into an active continental margin along the coastal area of the SCB (Cui and Li, 1983) and an early initiation of the Indosinian orogeny (Li et al., 2006; Li and Li, 2007). By the late Triassic, a broad fold belt had been developed, with associated magmatism and metamorphism (e.g., Wang et al., 2007b). Igneous rocks are predominantly peraluminous granites (e.g., Qi et al., 2007; Sun et al., 2005; Wang et al., 2007c). Some late Triassic metaluminous granites have also been found locally (e.g., Chen et al., 2007c). Time-space analyses revealed a migration of the orogeny into the continental interior during the early Mesozoic (Li and Li, 2007), consistent with an observed craton-ward fadeaway of the orogeny (Ren, 1984). Evolution of the orogeny and creation of north-easterly trending >1300 km-wide fold belt in the early Mesozoic, as well as subsequent intensive granitic magmatism in the late Mesozoic, could be well accounted for using a flat-slab subduction model (Li and Li, 2007), but are incompatible with pacific subduction model and terrain collision model as that proposed by Cui and Li (1983) and Hsü et al. (1988), respectively. Triassic thermal event recorded by metamorphic rocks in Vietnam was probably a result of tectonic reactivation; it does not lent support to a continental collision between the Indochina and the SCB (Carter and Clift, 2008).

2.2.4. Late Mesozoic extension and magmatism

After a ca. 10 Myr magmatic calm period from 205 Ma to 196 Ma at the last stage of the Indosinian orogeny (Yu et al., 2009b; Zhou et al., 2006), voluminous magmas were produced from magmatic flare-ups in the Jurassic and Cretaceous (Li et al., 2007b; Zhou et al., 2006). At the present level of exposure, the Early Jurassic igneous rocks are volumetrically minor and only found locally (e.g., Chen et al., 2005; Li et al., 2012; Li and Li, 2007; Yu et al., 2009b). Some are located nearly in the centre of the large magmatic province; a few have also been identified in the east coastal region (**Fig. 2.4**). Bimodal rocks and/or A-type granites are the major products of the earliest magmatism in the inland SE China, implying that the central South China Fold Belt was undergoing extension in the Early Jurassic (Li and Li, 2007; Zhu et al., 2010). The Middle to Late Jurassic igneous rocks, dominated by the ~165–155 Ma high-K granites, are voluminous and widespread in the broad inland region. They are dominantly biotite granites/monzogranites and are spatially associated with minor amounts of coeval basalts, gabbros and syenites (He et al., 2010; Li et al., 2003a; Li et al., 2004a; Wang et al., 2003b). Conversely, volcanic rocks outweigh intrusive rocks for the Cretaceous magmatism (Zhou et al., 2006). Cretaceous intrusive-volcanic rocks are volumetrically minor in the inland SE China. Overall, there is an ocean-ward shift of the late Mesozoic magmatism with the Cretaceous stage mostly concentrated along the coastal area (Li and Li, 2007; Wang et al., 2011a; Zhou and Li, 2000).

2.3. Jurassic high-K granites in the western Guangdong Province, SE China

As is shown in **Fig. 2.5**, the western Guangdong (and parts of the Hunan and Guangxi provinces) is mostly covered with Jurassic-Cretaceous granites and pre-Devonian and late Paleozoic strata. Although remains of Proterozoic and Archaean rocks (mostly zircon) have been frequently identified (e.g., Li et al., 1989; Wan et al., 2010; Xu et al., 2005; Yu et al., 2010a; Zheng et al., 2011), the oldest crystalline rocks in this region are the early Paleozoic granites and metamorphic

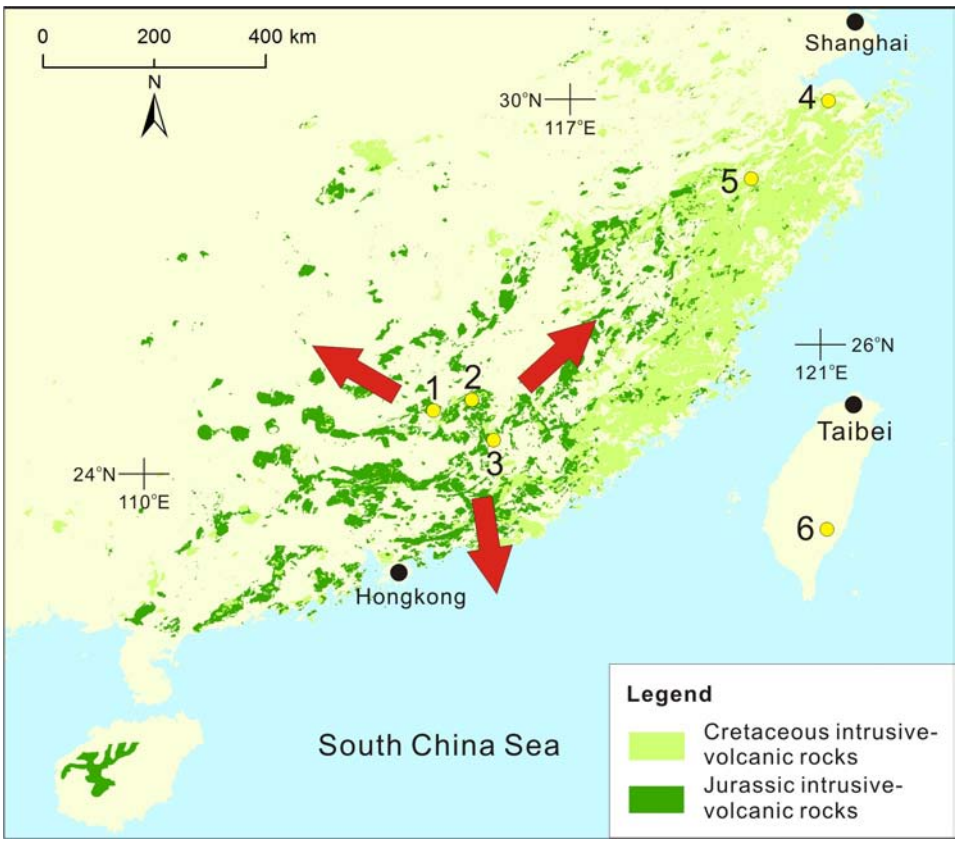

Figure 2.4 A simplified geological map showing the distribution of late Mesozoic magmatic rocks in SE China. 1—189 ± 2 Ma Taibei syenitic rocks (Chen et al., 2005); 2—189 ± 3 Ma Keshubei A-type granite (Li and Li, 2007); 3—ca. 195 Ma Dongken and Xialan complexes (Yu et al., 2009b; Yu et al., 2010b; Zhu et al., 2010); 4—~180 Ma Xiepu granite (Li et al., 2012); 5—180 ± 4 Ma Maorong volcanic (Chen et al., 2007b); 6—190 Ma Talun granite (Yui et al., 2009). Red arrows show the probable propagation directions of inland Jurassic magmatism (after Li and Li, 2007).

rocks with no Precambrian crystalline basement outcrop (e.g., Wan et al., 2010; Wang et al., 2007d).

2.3.1. The Jiuyishan fayalite-bearing granite

The Jiuyishan batholith (lat. 25º04' to 25º18' N; long. 111º55' to 112º30' E) is located in the northern part of the western Guangdong and extends to the southern Hunan Province. It was emplaced in folded pre-Mesozoic (mostly early Paleozoic) strata and has a total outcrop area of ~1,200 km^2. The batholith was considered a composite consisting of three individual bodies: the Jinjiling pluton, the Shaziling pluton and the Xishan intrusive-volcanic complex (**Fig. 2.6**). The Shaziling intrusion,

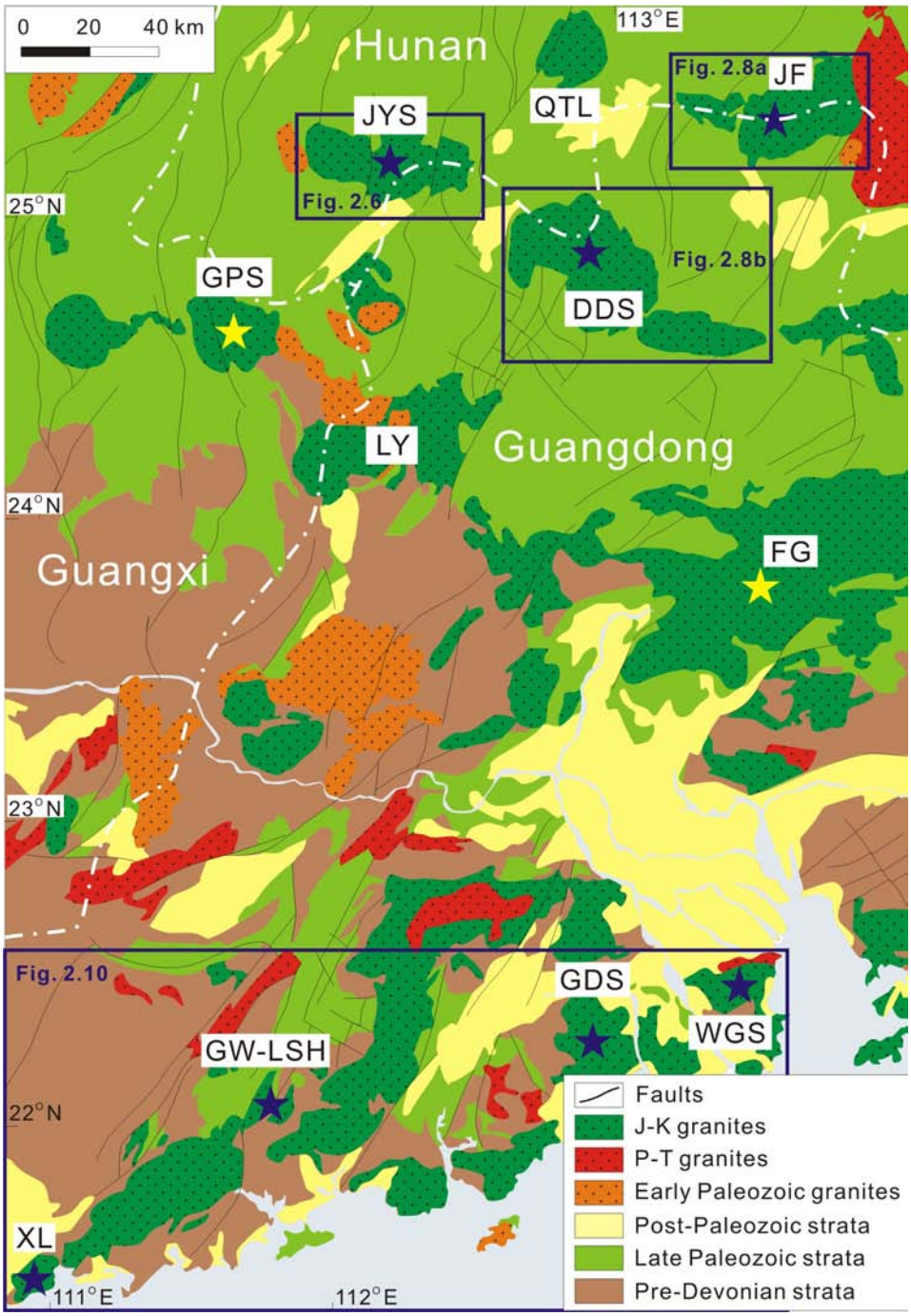

Figure 2.5 A simplified geological map showing the distribution of granites in the western Guangdong Province and adjacent areas (after Ma et al., 2002). Plutons highlighted with blue stars are targets of this study; those highlighted with yellow stars are additional granites that have been discussed. White dashdotted lines highlight the provincial boundaries. J-K—Jurassic and Cretaceous; P-T—Permian and Triassic. Symbols: GPS—Guposhan; JYS—Jiuyishan; QTL—Qitianling; JF—Jiufeng; DDS—Dadongshan; LY—Lianyang; FG—Fogang; XL—Xiaoliang; GW—Gangwei; LSH—Lunshui; GDS—Gudoushan; WGS—Wuguishan.

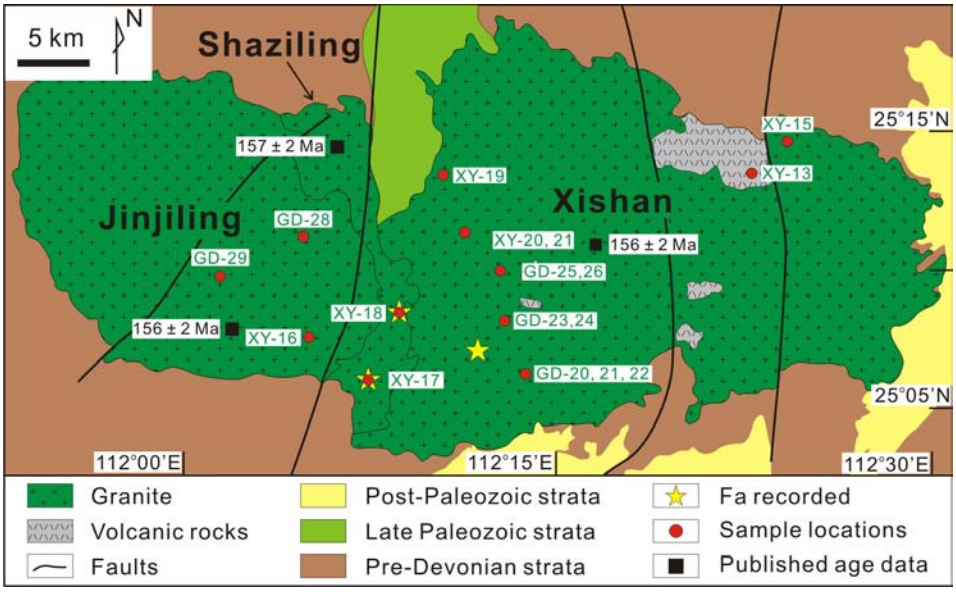

Figure 2.6 A simplified geological map showing the distribution of sampling localities in the Jiuyishan suite (modified from Huang et al. 2011). The published age data come from Fu et al. (2004b).

situated in between the other two, was suspected to be Triassic in age (Hunan, 1987). Geochronological studies (e.g., Chen et al., 1986; Fu et al., 2003b; Li et al., 1986; Zhang et al., 2001), however, show that granite bodies of the batholith all have Jurassic cooling ages (Rb-Sr isochrons). Recently, SHRIMP zircon U-Pb analyses (Fu et al., 2004b) confirmed that granites from every pluton are coeval and have identical crystallization ages of ~156 ± 2 Ma.

The Jiuyishan granitic rocks consist of coarse- to medium-grained granodiorite, medium- to fine-grained porphyritic granite and rhyolite porphyry (Hunan, 1987). Granites are usually pale-grey in colour with some being brick-red due to the appearance of red feldspars (**Fig. 2.7a**). Small dark enclaves occur occasionally in granite (**Fig. 2.7b**). Thirty nine samples in total, varying from rhyolite to coarse-grained amphibole-bearing biotite granite (see **Appendix Table 2** for details), have been used for this study.

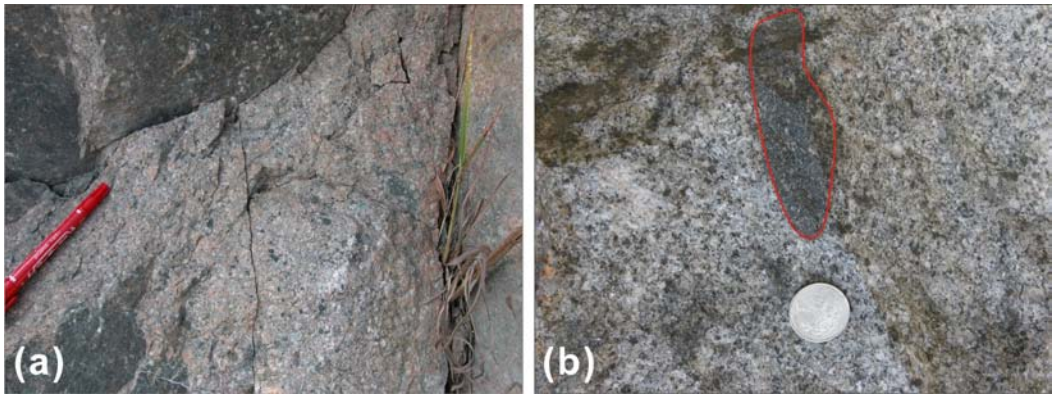

Figure 2.7 Photos of the Jiuyishan granites in the field showing red feldspars in (a) and a dark enclave in (b). The pen in (a) is about 12 centimeters in length; diameter of the coin in (b) is ~1.5 cm.

2.3.2. The Jiufeng granite suite

The Jiufeng suite (lat. 25º10' to 25º30' N; long. 113º10' to 114º00' E) is located ~100 km to the east of the Jiuyishan pluton (**Fig. 2.5**). It constitutes the southwestern part of a multi-stage magmatic complex and has an area of ~1000 km^2. Rocks of the Jiufeng pluton, crosscut by northeast-trending faults, dominantly intrude the pre-Devonian strata (**Fig. 2.8a**). Geochronological studies revealed that the Jiufeng granites are dominantly Jurassic in age, coexisting with Triassic peraluminous granites to the east and early Paleozoic granites to the northeast (Chen et al., 2007a; Li, 1991; Xu et al., 2005). Rocks of the Jiufeng pluton vary from medium- to fine-grained amphibole-bearing biotite granite, biotite monzogranite, two-mica granite and muscovite granite (**Fig. 2.9**), a rock association typical of the Early Yanshanian (i.e. Jurassic) Nanling Range granites (Li et al., 2007a). Twenty eight samples in total are used for analyses.

2.3.3. The Dadongshan granite

The Dadongshan batholith (lat. 24º30' to 25º10' N; long. 112º30' to 113º40' E) is located ~50 km to the southeast of the Jiuyishan pluton (**Fig. 2.5**). It has an area of over 1,400 km^2 and can be geographically subdivided into western and eastern parts (**Fig. 2.8b**). Both parts are dominantly composed of coarse-grained biotite K-feldspar

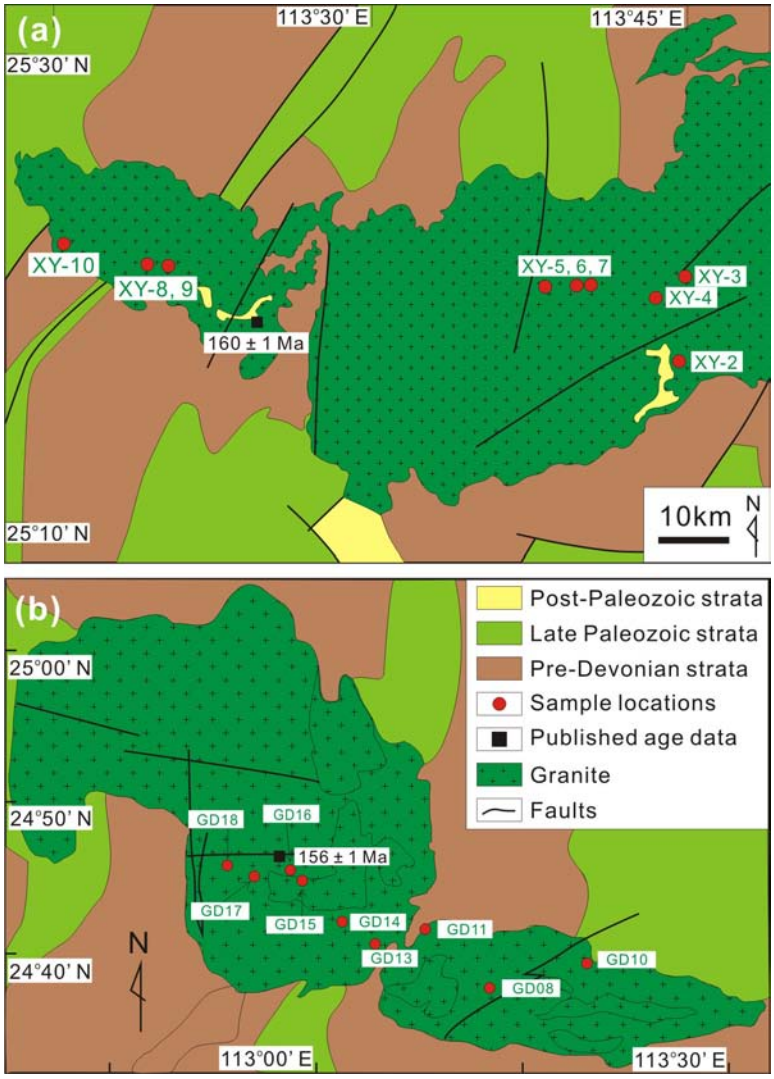

Figure 2.8 Simplified geological maps of (a) the Jiufeng pluton and (b) the Dadongshan batholith showing sample distributions. Published data in (a) and (b) are from Xu et al. (2005) and Zhang et al. (2003), respectively.

granites with subordinate two-mica granites, but as will be shown later in **Section 5.5.2.**, there is a ~10 Myr difference between the two parts. Granite rocks of the batholith are mostly composed of 40–45% K-feldspar, 20–25% plagioclase, ~30% quartz and ~4% biotite. Some may also contain minor amphibole (Guangdong, 1988; Zhang et al., 2003). Totally, twenty one samples have been analysed in this study.

2.3.4. Granites in the southern coastal region of the Guangdong Province

Late Mesozoic granites are widely distributed along the coastal region of the

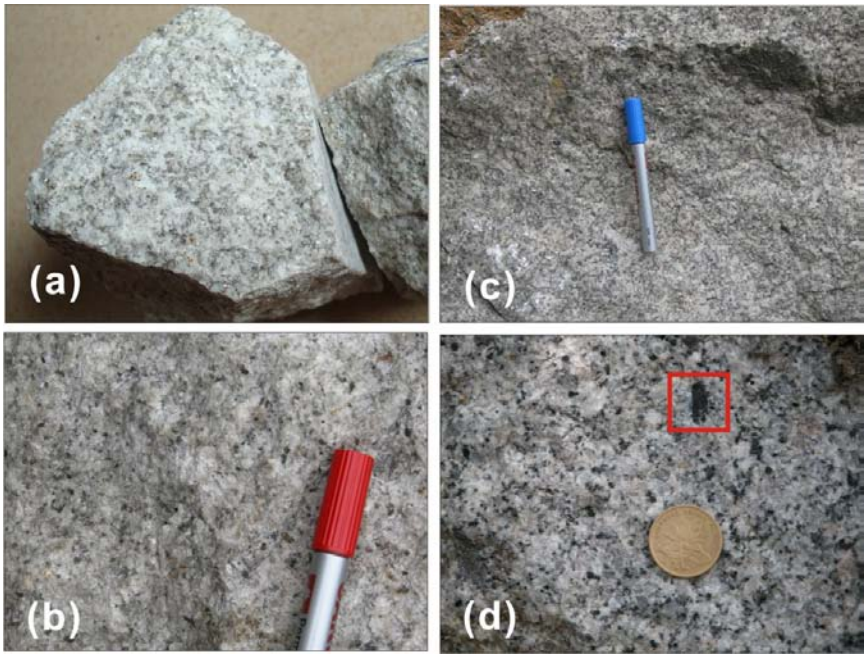

Figure 2.9 Granite rocks of the Jiufeng pluton showing (a) muscovite granite, (b) two-mica granite, (c) biotite granite and (d) hornblende-bearing granite. A large hornblende phenocryst is highlighted using a red square in (d). The pen in (c) is ~12 cm in length; a piece of coin in (d) is ~1.2 cm in diameter.

western Guangdong Province (**Fig. 2.5**). Most granites in this region were emplaced in the east into pre-Devonian strata (**Fig. 2.10**). These rocks usually form large plutons or batholiths, but amphibole is uncommon or totally absent in these rocks. They are mainly composed of biotite granite, similar to those widely exposed in the continental interior. Field observations found that some of these granites are spatially associated with volumetrically minor tourmaline-, muscovite- and garnet-bearing granites. In contrast, a few granites in this region intrude the Paleozoic strata to the southeast of the Wuchuan-Sihui fault (**Fig. 2.10**) and are associated in time and space with high-K, shoshonitic basaltic-intermediate rocks in the region (e.g., Li et al., 2000b; Li et al., 2000c; Wang et al., 2003). They occur as small plutons/stocks and commonly contain abundant amphibole. They show significant negative Nb-Ta-Ti anomalies in trace element distribution patterns (Li et al., 2001) and have been chemically classified as shoshonitic and high-potassium calc-alkalic granites (Li et al., 2000c). These rocks were likely generated in a different way from the other

high-K granites constituting large plutons.

Representative samples (**Appendix Table 2**) from the coastal region plutons have been collected for this study. Among those, five were collected from the Xiaoliang pluton, five from the Gangwei pluton, four from the Lunshui pluton, five from the Gudoushan pluton, and seven from the Wuguishan pluton (**Fig. 2.10**). Representative samples of each individual pluton were collected from an area smaller than 100 m in diameter.

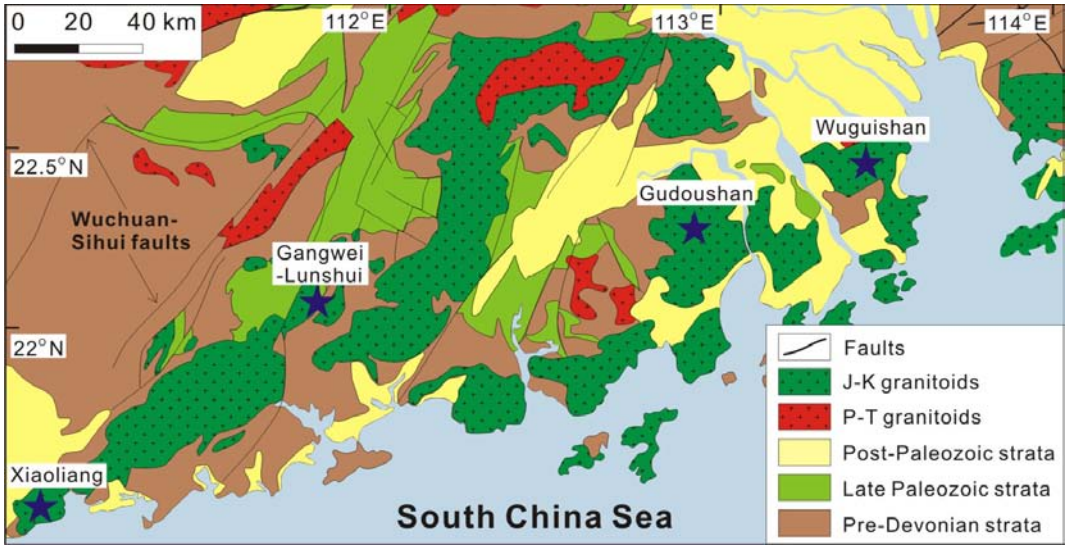

Figure 2.10 Geological map showing the distribution of Mesozoic granites along the southern coastal region of the western Guangdong Province, southeastern China. New geochronological results are shown in bold. J-K—Jurassic and Cretaceous; P-T—Permian and Triassic.

Chapter 3: Analytical procedures

3.1. Pretreatments

3.1.1. Whole-rocks

One hundred and fifteen fresh samples in total have been selected for this study (see **Appendix Table 2** for details) and among them eighty five samples have been thin-sectioned. Hand specimens were crushed into centimetre-scale grains using hammers. Fresh grains were hand-picked to avoid surface alteration and contamination and then cleaned using purified water before they were further ground to 200 meshes using a Vibratory Disc Mill RS 200 with grinding sets made of tungsten carbide.

Sample powders were dried at 105 ºC for two hours. To determine the loss on ignition, about 1 gram (precision is 0.0001 gram) powder of each sample was carefully weighed before and after being roasted at 900 ºC for two hours in a furnace. Half a gram (±0.0001, after LOI determination) of each sample was weighed and mixed with 4.5000 ± 0.0001 grams of lithium tetraborate. Well mixed powders were fused to produce glass discs for major element determination.

Sample powders, weighed ~50 mg each, were dissolved in pressured Teflon bombs using a mixed solution of HF + HNO_3. The solutions were dried and then re-dissolved with 2% HNO_3 for trace element measurements.

About 100 mg powder samples were digested in Teflon beakers using a mixed HF + HNO_3. Some samples were separated into halves and one half was spiked with ^{84}Sr and ^{87}Rb. Strontium and rare earth elements (REEs) fractions were separated using quartz columns with resin bed of AG50-8X, and Nd fractions were further separated from the rest of REEs by HDEHP-coated Kef columns. All procedure blanks are smaller than 100 pg for Sr and 10 pg for Nd.

3.1.2. Zircons

Zircon grains were extracted from rocks using standard density and magnetic separation techniques, mounted in epoxy mounts with zircon standards TEMORA 2, 91500 and MUD TANK, and then polished to expose their interior for analyses. Transmitted and reflected light micrographs were taken to document the interior and exterior structures of zircons using a camera attached to a Leica microscope. Cathodoluminescence (CL) images were produced using a LEO1450VP Secondary Electron Microprobe attached with a Mini CL to reveal the structures.

3.2. Mineral chemistry

Twenty-four thin sections were carbon-coated for mineral composition analyses. Electron microprobe studies of minerals were carried out using JEOL JXA-8100 Superprobes at either the Guangzhou Institute of Geochemistry, Chinese Academy of Sciences in Guangzhou (GIG) or the Institute of Geology and Geophysics, Chinese Academy of Sciences in Beijing (IGG). The electron beam was 1−2 μm and 5 μm in diameter at GIG and IGG, respectively, with accelerating voltage of 15 kV. Electron beam current of 20 nA and 10 nA were used at GIG and IGG, respectively. The peak counting time for Na is 7 seconds and for K is 8 seconds. Counting time for all other elements was set to 10 seconds. Well-characterized natural silicate minerals were used as standards for calibration. The data reduction was carried out using ZAF correction. All results of mineral chemistry are listed in **Appendix Tables 3−7**.

3.3. Whole-rock studies

Whole-rock studies include mineral chemical studies, major and trace elements and Sr-Nd isotopes.

3.3.1. Major elements

Glass discs made from melting dehydrated sample powders were analysed using a Rigaku RIX 2000 X-ray fluorescence spectrometry (XRF) at the GIG for major elements. Concentrations of elements were determined using calibration curves established by bivariate regression of data from 36 standard silicate samples encompassing a large range of compositions (Li et al., 2005b). Precision for the analytical results is typically 2−5%.

3.3.2. Trace elements

Trace elements were analysed either using a PerkinElmer Sciex ELAN 6000 quadrupole inductively-coupled plasma mass spectrometer (ICP-MS) at the GIG or using an Agilent 7500a quadrupole ICP-MS at the IGG on a solution basis. The procedure is much similar to that described by Li et al. (2000a). Counting signal drift was monitored by an internal standard Rh solution, whereas element concentrations of unknowns were calibrated using the concurrently processed standards. Standards chosen include BHVO-2, AGV-1, W-2, G-2, SY-4, MRG-1, SARM-4, GSR-1, GSR-3 and GSR-5. The precision is better than 5% for most trace elements (Liu et al., 1996). Major and trace elements are combined in **Appendix Table 8**.

3.3.3. Sr-Nd isotopes

Elements Sr and Nd were separated using conventional ion exchange procedures. The Sr isotope analyses were performed on either a Thermo-Fisher Triton thermal ionization mass spectrometry (TIMS) at the GIG or a Finnigan MAT-262 TIMS at the IGG. The Nd isotopes were analysed using either a micromass isoprobe multi-collector (MC-) ICP-MS at the GIG or a Finnigan MAT-262 TIMS at the IGG. The spectrometers were operated in a static multi-collector mode. The analytical procedures used for TIMS are similar to those described by Yang et al. (2004) and Chen et al. (2010), whereas those for MC-ICP-MS are the same as those detailed by Li et al. (2004b). The measured Sr and Nd isotope ratios were normalized to $^{86}Sr/^{88}Sr = 0.1194$ and $^{146}Nd/^{144}Nd = 0.7219$, respectively, to correct for mass fractionation. The reported Sr and Nd isotope ratios were then adjusted to the

standard NBS SRM 987 with $^{87}Sr/^{86}Sr$ = 0.710243 ± 14 (2σ) and the standard Shin Etsu JNdi-1 with $^{143}Nd/^{144}Nd$ = 0.512115 ± 7 (2σ) (or AMES with $^{143}Nd/^{144}Nd$ = 0.512147 ± 12 (2σ)), respectively. Results of whole-rock Sr-Nd isotope analyses are presented in **Appendix Table 9**.

3.4. In-situ zircon studies

In-situ zircon studies include U-Pb analyses and Hf-O isotope studies.

3.4.1. U-Pb geochronology

Most zircon U-Pb analyses were performed on a Cameca IMS-1280 ion microprobe at the IGG following procedures described by Li et al. (2009c). The mass resolution used to measure Pb/Pb and Pb/U isotopic ratios was ~5400 during the analyses. The O_2^- primary ion beam, with an intensity of ~8 nA, was accelerated at 13 kV. The elliptical spot is typically 20 × 25 μm in size. Positive secondary ions were extracted with a 10 kV potential. A single electron multiplier was used to measure the secondary ion beam intensities by peak jumping and each measurement consists of 7 cycles, sums up to ~12 minutes. Analyses of the standards 91500 and TEMORA 2 were interspersed with unknowns.

U-Th-Pb isotopic ratios and absolute abundances were determined relative to the standard zircon 91500 (Wiedenbeck et al., 1995). Measured Pb isotopic compositions were corrected for common Pb using a ^{204}Pb method. Corrections are sufficiently small to be insensitive to the choice of common Pb composition because the measured $^{206}Pb/^{204}Pb$ ratios are mostly higher than 10,000. In this study, the average of present-day crustal composition (Stacey and Kramers, 1975) was used for common Pb correction, assuming that the common Pb is largely surface contamination introduced during sample preparation.

A long-term uncertainty of 1.5% (1 RSD) for $^{206}Pb/^{238}U$ measurements of the standard zircon was propagated to the unknowns (Li et al., 2010a), although the

measured $^{206}Pb/^{238}U$ error in a specific session is generally around 1% (1 RSD) or less. Uncertainties on individual analyses in data table are reported at a 1σ level; mean ages for pooled U/Pb and Pb/Pb analyses are quoted with 95% confidence interval. Data reduction was carried out using a Isoplot/Ex v. 2.49 program (Ludwig, 2001).

Some zircon U-Pb analyses (the Dadongshan pluton) were conducted using a SHRIMP II ion microprobe at the Beijing SHRIMP centre. In this case, zircons were analysed following procedures similar to those described by Williams et al. (1996) and Williams (1998). Mass resolution for Pb/Pb and Pb/U was set to ~5000 during the analyses. The primary beam had a current of 5−8 nA and was about 25 μm in diameter. Analyses of standard zircons were interspersed with unknowns. U-Th-Pb ratios were determined relative to the TEMORA 2 standard with its $^{206}Pb/^{238}U$ = 0.06667 (= 416.78 ± 0.33 Ma; Black et al., 2004), whereas absolute abundances of U and Th were calibrated to the SL13 standard with its ^{238}U = 238 ppm. Measured Pb isotope ratios were corrected for common Pb using a ^{204}Pb method. The uncertainties on individual analyses are reported at 1σ level and the mean ages for pooled $^{206}Pb/^{238}U$ results are quoted at 95% confidence level. Data reduction was also carried out using the Isoplot/Ex v. 2.49 program (Ludwig, 2001).

All geochronological results can be found in **Appendix Table 10**.

3.4.2. Hafnium isotopes

In-situ zircon Hf isotope analyses were carried out at the IGG on a Neptune MC-ICP-MS equipped with a Geolas 193 nm excimer ArF laser-ablation system. The zircon grains previously dated were targeted wherever possible. The laser ablation pits for this study was ~50 μm or ~63 μm in diameter and the ablation time was 26 seconds for each analysis at a repetition rate of 6 Hz at 20 J/cm^2. The analytical procedures and calibration method were similar to those describe by Wu et al. (2006). During analyses, an isotopic ratio of $^{176}Yb/^{172}Yb$ = 0.5887 was applied to make correction for isotopic interference of ^{176}Yb on ^{176}Hf. But the isobaric interference of

^{176}Lu on ^{176}Hf was not corrected, because such interference is negligible due to the low ^{176}Lu/^{177}Hf ratio in zircon (normally <0.002； Wu et al., 2006a). The measured ^{176}Hf/^{177}Hf ratios were normalized to ^{179}Hf/^{177}Hf = 0.7325 using an exponential law for mass bias correction. Analyses of double standard zircons 91500 and FM0411 or Mud Tank and GJ-1 were interspersed with unknowns. The results of standard 91500 or Mud Tank were used for external correction. However, as the weighted average ^{176}Hf/^{177}Hf ratios of standard 91500 and Mud Tank analysed during the whole session are identical within analytical errors to their accepted values (0.282306 ± 8 and 0.282507 ± 6 for 91500 and Mud Tank, respectively; Woodhead and Hergt, 2005), no further external adjustment was made.

3.4.3. Oxygen isotopes

Zircon mounts were slightly polished after U-Pb and Hf isotope analyses and recoated with high purity gold. The same parts/rims for U-Pb and Hf isotope analyses were targeted for O isotopes. The oxygen isotope data were also acquired on the Cameca IMS-1280 ion microprobe at the IGG, using a ~2 nA Cs^+ primary ion beam (focused "Gaussian beam") accelerated at 10 kV. The analytical procedures were the same as those described by Li et al. (2010c). The spot size was about 20 μm in diameter. The field aperture was set to 5000 μm, and the transfer-optics magnification was adjusted to give a field of view of 125 μm (FA = 8000). Energy slit width was 30 eV, the mechanical position of the energy slit was tuned at the beginning of each session (5 eV gap, −500 digits with respect to the maximum). The entrance slit width is ~120 μm and exit slit width for multicollector Farady cups (FCs) for $^{16}O^-$ and $^{18}O^-$ is 50 0 μm (MRP = 2500). The magnetic field stability, as controlled by NMR (Nuclear Magnetic Resonance) probe, was better than 2.5 ppm over 16 h on mass 17 (Li et al., 2010c). Each analysis takes ~4.5 mins, consisting 2 mins of pre-sputtering, 1 min of automated centering of secondary ions and 80 secs (20 cycles) of data collection. Negative secondary ions $^{18}O^-$ and $^{16}O^-$ were extracted at a −10 kV potential and measured in multi-collector mode using two off-axis Faraday cups with intensity of $^{16}O^-$ typically at 1×10^9 cps.

Uncertainties on individual analyses are reported at 1σ level. Oxygen isotope ratios are expressed as delta notation $\delta^{18}O$, representing deviation of measured $^{18}O/^{16}O$ values from that of the Vienna Standard Mean Ocean Water ($(^{18}O/^{16}O)_{VSMOW}$ = 0.0020052) in parts per thousand: $(\delta^{18}O)_M = (\frac{(^{18}O/^{16}O)_M}{0.0020052} - 1) \times 1000$ (‰). The results are then corrected for instrumental mass fractionation factor (IMF), following the equation: $IMF = (\delta^{18}O_{measured} - \delta^{18}O_{accepted})_{standard} = (\delta^{18}O_{measured} - \delta^{18}O_{true})_{sample}$, using zircon standard TEMORA 2 with $\delta^{18}O_{VSMOW}$ = 8.20‰ (Black et al., 2004). The standard 91500 with $\delta^{18}O_{VSMOW}$ = 9.9‰ (Wiedenbeck et al., 2004) was measured as an unknown. Under the analytical conditions described above, the internal precision from one spot analysis is typically better than 0.2−0.3‰ for $^{18}O/^{16}O$ ratio.

For some samples (the Xiaoliang and Gangwei plutons), another method was applied for the IMF calibration. As can be seen in **Fig. 3.1**, the measured $\delta^{18}O$ for TEMORA 2 vary from 5.5‰ to 7.5‰ in a single session. The reported standard error is large, equals to 0.74‰ (1σ). As the measured $\delta^{18}O$ values of the standard fluctuate smoothly as time passes (**Fig. 3.1**), it could be expected that the measured $\delta^{18}O$ values of unknowns in this session also follow a similar variation pattern. Therefore,

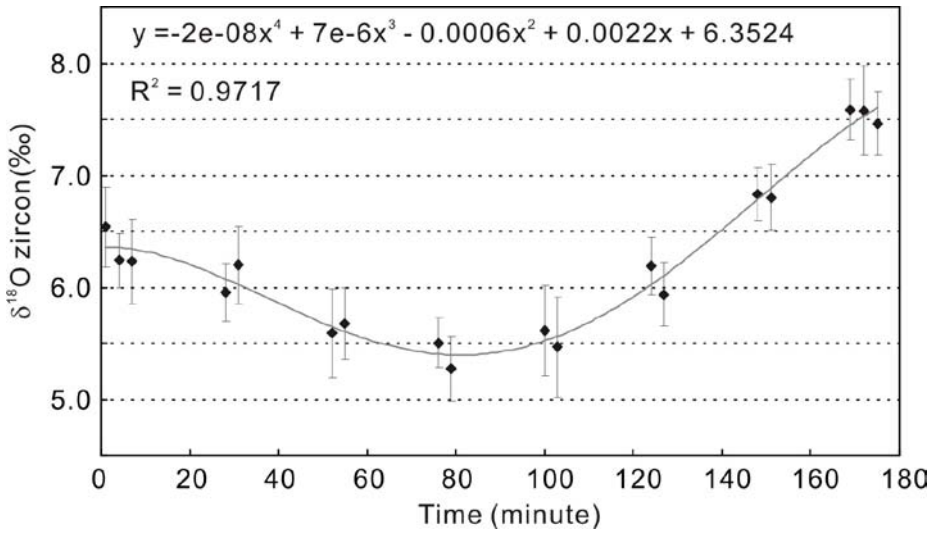

Figure 3.1 A fitted line for the variation of $\delta^{18}O$ of standard TEMORA 2 measured in a session. Error bars shown are 2σ.

using time as the only parameter, an equation can be fitted for the fluctuation and applied for IMF calculation through interpolation. Integrated Hf and O isotope results are presented in **Appendix Table 11** in a chronological sequence as the oxygen isotopes analysed.

Chapter 4: Formation of high $\delta^{18}O$ fayalite-bearing Jiuyishan A-type granite by high-temperature melting of granulitic metasedimentary rocks, southern China

(This chapter includes results published in a paper by **Huang, H.-Q., Li, X.-H., Li, W.-X., and Li, Z.-X., 2011, Formation of high $\delta^{18}O$ fayalite-bearing A-type granite by high-temperature melting of granulitic metasedimentary rocks, southern China: Geology, v. 39, p. 903-906.** All data, otherwise acknowledged in the published paper, were produced by myself under supervision. Results and conclusions were made through collaboration of myself with the three other authors.)

4.1. Introduction

Isotopic analyses of the Jiuyishan granite samples show that they are enriched in ^{87}Sr and ^{18}O (Chen et al., 1986; Fu et al., 2004a, 2005; Fu et al., 2003b; Jiang et al., 2009; Li et al., 1986; Zhang et al., 2001), with their initial $^{87}Sr/^{86}Sr$ ratios at 156 Ma higher than 0.717 (Fu et al., 2004a) and their whole-rock $\delta^{18}O$ higher than 10‰ (Li et al., 1986). Biotites in these rocks are characterized by their Fe-enriched feature (Zhang et al., 2001). For these features, they have been classified as S-type granites originated from melting of sedimentary rocks (e.g., Li et al., 1986; Zhang et al., 2001).

Conversely, the Jiuyishan granitic rocks also have many geochemical characteristics similar to typical A-type granites (Fu et al., 2004a, 2005; Jiang et al., 2009; Li et al., 2007a). As is shown in **Table 4.1**, their average compositions are comparable with those of typical A-type granites, but distinct from those of I-type granites in the LFB. They are high in K_2O but low in Al_2O_3, MgO, CaO and Na_2O; their Fe/(Fe + Mg), K_2O/Na_2O, and 10,000 × Ga/Al ratios are high; they are also

Table 4.1 Average compositions of Jiuyishan granitic rocks in the western Guangdong, SE China and A-type and I-type granites from Bega batholith in the LFB, SE Australia.

Sample	J1	A-type	I-type	J2	J3	A-type	I-type
Major elements (wt%)							
SiO_2	75.98	77.21	76.03	72.54	72.53	73.04	72.50
TiO_2	0.12	0.13	0.11	0.31	0.29	0.37	0.31
Al_2O_3	12.26	11.79	12.64	13.01	13.05	12.62	13.63
Fe_2O_3	2.19	0.36	0.46	3.43	3.21	1.63	0.7
FeO		0.85	0.7			1.51	1.65
MnO	0.04	0.03	0.03	0.05	0.05	0.08	0.06
MgO	0.13	0.04	0.24	0.37	0.35	0.33	0.72
CaO	0.61	0.39	0.80	1.22	1.18	0.96	2.32
Na_2O	2.92	3.08	3.43	2.62	2.65	3.70	3.09
K_2O	5.02	5.00	4.46	5.26	5.39	4.11	3.67
P_2O_5	0.04	0.02	0.02	0.11	0.11	0.08	0.08
LOI	0.45			0.79	0.97		
Total	99.72	98.99	99.00	99.54	99.61	98.60	98.91
A/CNK	1.08	1.05	1.06	1.07	1.06	1.03	1.03
K_2O/Na_2O	1.72	1.62	1.30	2.01	2.02	1.11	1.19
Fe*	0.93	0.97	0.82	0.89	0.89	0.90	0.76
Minor elements (ppm)							
Ga	20.9	20	14	21.9	22.9	21	15
Rb	496	242	212	356	369	167	160
Sr	24.7	43	67	79.3	76.0	148	165
Y	64.0	90	46	61.6	61.6	83	29
Zr	135	170	95	239	234	490	147
Nb	24.5	19	11	25.9	26.5	25	9
Ba	172	575	331	682	688	767	577
La	49.2	64	30	66.1	70.7	62	33
Ce	109	150	68	140	150	153	71
Th	36.8	26	25	35.7	39.4	21	20
U	11.8	6	6	9.09	10.8	5	4
10000×Ga/Al	3.2	3.2	2.1	3.2	3.3	3.1	2.1

J1, J2 and J3 are average compostions of the Jiuyishan granitic rocks calculated from data published by Fu et al. (2004a, 2005) and Jiang et al. (2009). J1 is the average of 10 samples with SiO_2 in the range 75.09−77.98 wt%; J2 is the average of 25 samples with SiO_2 in the range 66.20−75.00 wt%; J3 is the average of 10 samples with SiO_2 in the range 70.18−73.92 wt%. The data of A-type and I-type granites in the LFB are from Collins et al. (1982). LOI is an acronym for loss on ignition; A/CNK = molar $Al_2O_3/(CaO + Na_2O + K_2O)$; Fe* = $(FeO + Fe_2O_3 \times 0.9)/(FeO + Fe_2O_3 \times 0.9 + MgO)$.

enriched in high field strength elements (HFSE, e.g., Zr, Nb, Y) and rare earth elements (REE, e.g., Ce) (**Table 4.1**). Anhydrous ferromagnesian minerals, fayalite and ferrosillite, have been reported for some rocks from the Jiuyishan batholith (Fu et al., 2003a). The formation of these minerals imply low water activity (fH_2O), low oxygen fugacity (fO_2) and likely high temperature characteristics of the magma (Barker et al., 1975). The anhydrous and high temperature features of the magma are in contrast to their derivation from normal metasedimentary rocks (S-type), because such S-type magmas are typically hydrous and have low magmatic temperature (Chappell et al., 2004).

Internationally, similar ^{18}O-enriched granites with typical A-type features have been reported and interpreted as products derived from magma mixing (e.g., Steinitz et al., 2009; Trumbull et al., 2004). Yet, a convincing petrogenetic interpretation of the Jiuyishan granitic rocks was not possible on the basis of existing data due to the fact that ancillary information on petrology and geochemistry for those samples analysed for their whole-rock oxygen isotopes was not available. There was no description of the method applied for oxygen isotope analyses, either. Therefore, further study is required to test whether the ^{18}O-enriched feature is primary and to unravel magmatic processes for the generation of the Jiuyishan batholith. A comprehensive study integrating petrological, geochemical and isotopic studies has been carried out and the results are presented below.

4.2. Analytical results

4.2.1. Petrography and mineralogy

Thin section examination shows that the Jiuyishan granitic rocks are commonly porphyritic in texture (**Figs. 4.1a−b**) with a total volume of phenocryst estimated to be higher than 40%. Plagioclase and quartz are the main phenocrysts in all samples, whereas K-feldspar only becomes common in well-crystallized samples.

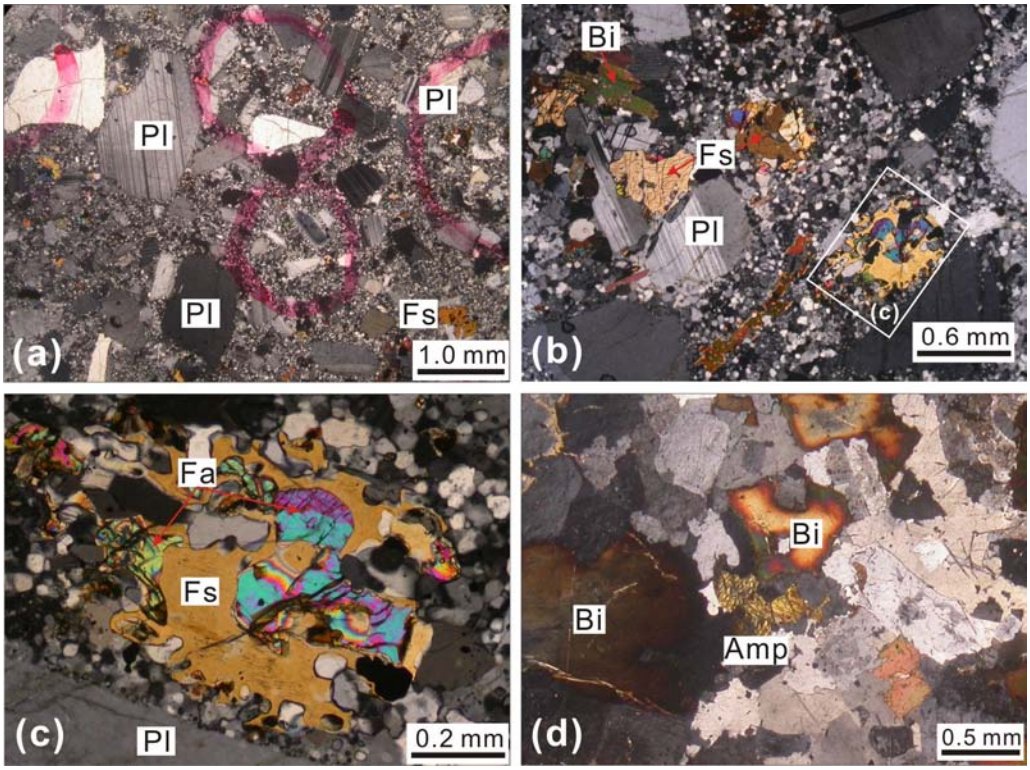

Figure 4.1 Thin section photomicrographs showing microstructures and mineral assemblages of the Jiuyishan granitic rocks. Pl: plagioclase; Fs: ferrosilite; Fa: fayalite; Bi: biotite; Amp: amphibole.

Many olivine and orthopyroxene phenocrysts present in some porphyritic samples, as well as in dark enclaves, with the former sometimes enveloped by the latter (**Figs. 4.1b−c**). Amphibole is rare and occurs as interstitial mineral only in a few well-crystallized samples (**Fig. 4.1d**). Biotite is the most common ferromagnesian mineral, mostly presents either as poikilitic phenocryst or otherwise interstitial mineral. Some are also found to rim orthopyroxene. Thin section examination allows the establishment of a general crystallization sequence from olivine and orthopyroxene, to plagioclase and quartz, and then to biotite, amphibole and K-feldspar.

Chemical compositions of minerals (**Appendix Tables 3−7**) have been examined using an electron microprobe at the GIG. Plagioclases analysed show large variation of An numbers, extending from 44.6 to 23.7 mol% and can be classified as

andesine and oligoclase, whereas K-feldspars studied are exclusively sanidine with Or varying between 80.1 and 88.3 (**Appendix Table 3; Fig. 4.2**). Overall, plagioclase phenocrysts in porphyritic rocks have lower SiO_2 contents and higher An numbers than plagioclases in well-crystallized samples. This seems to record the chemical changes of magma as it evolved.

Analyses of ferromagnesian minerals reveal that all of them (including olivine, pyroxene, biotite and amphibole) are relatively enriched in Fe (mainly occurs as Fe^{2+}) over Mg. The chemical results of olivine (**Appendix Table 4**) and orthopyroxene (**Appendix Table 5**) show that they are fayalite and ferrosilite with $Fe^{\#}$ (= molar [Fe/(Mg + Fe)]) of 0.88–0.92 and 0.72−0.76, respectively. The rare amphiboles are calcic and have chemical compositions similar to ferro-edenite (**Fig. 4.3**). As Fe-enriched amphiboles like these have Fe/(Fe + Mg) higher than 0.65 (**Appendix Table 6**) and were likely crystallized from low fO_2 magmas, their compositions are unsuitable for estimating pressures using a Al-in-amphibole barometer (Anderson and Smith, 1995). The biotites have $Fe^{\#}$ between 0.63 and 0.76 and are chemically close to annite (**Fig. 4.4**). It is interesting to note that biotites generated earlier (in porphyritic granites) are more F-enriched (~1 wt%) than biotites crystallized late (<0.2 wt%; **Appendix Table 7**). The results imply that F-enrichment in biotite is likely a primary feature inherited from source.

4.2.2. Zircon U-Pb geochronology

The analyses were carried out using a Cameca IMS-1280 ion microprobe housed at the IGG. Zircons extracted from all five samples are euhedral and are mostly transparent and colourless. In terms of size, most of the zircons have similar width of ~100 μm, but have variable width to length ratios from 1:2 to 1:5. All zircons studied are pristine magmatic zircons showing well-developed oscillatory zoning as revealed by CL images (**Figs. 4.5a−e**). No definite zircon cores were observed. Zircon fractions free of inclusions and cracks have been targeted and the results are presented in **Appendix Table 10**.

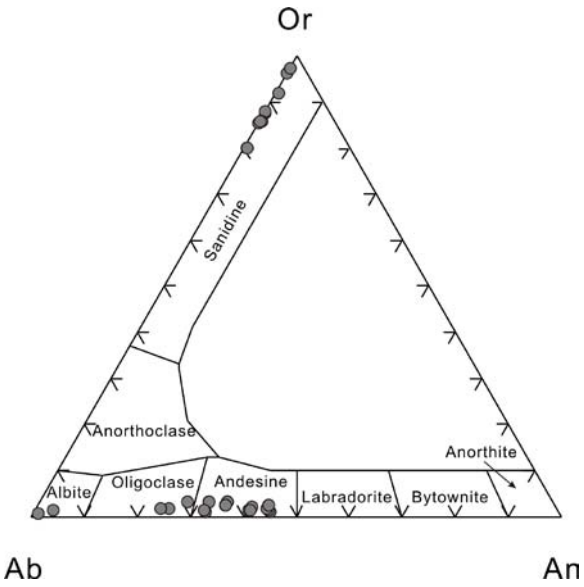

Figure 4.2 Composition of feldspars in the Jiuyishan granitic rocks.

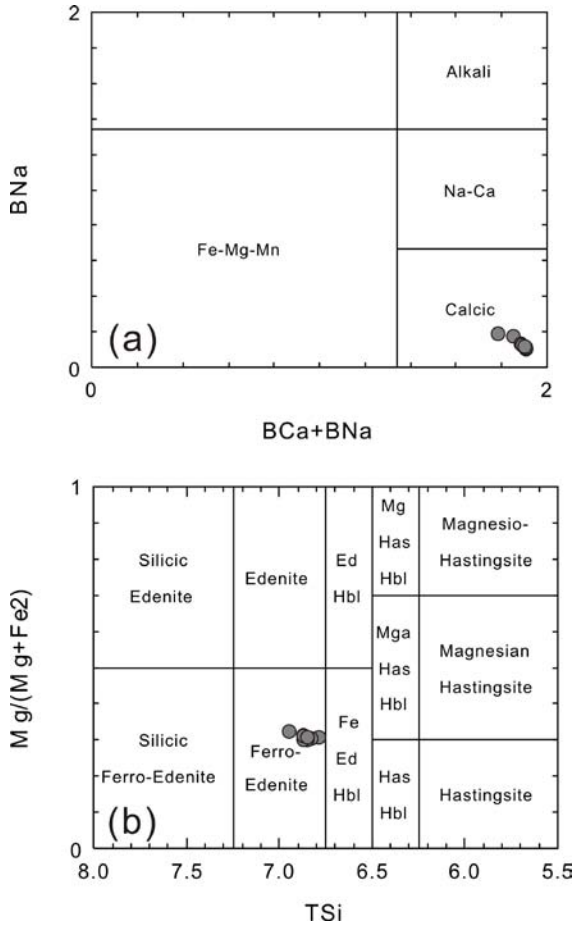

Figure 4.3 Composition of amphiboles in an equigranular granodiorite (Hawthorne, 1981).

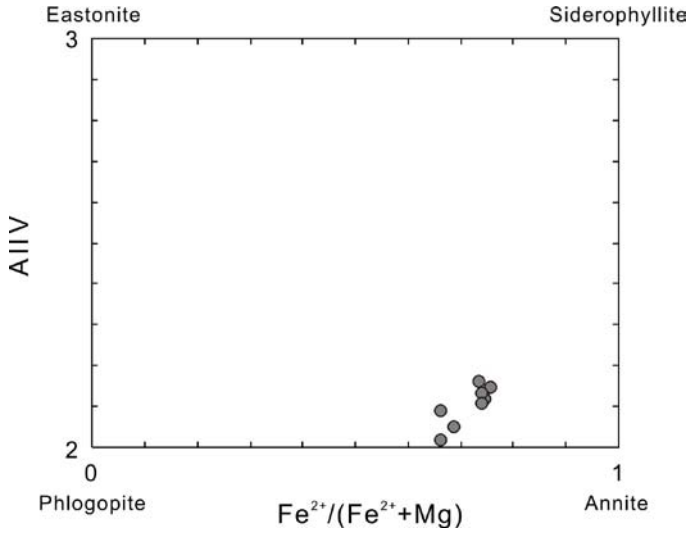

Figure 4.4 Chemical classification of biotites.

GD23-1 (lat. 25°08'53"N, long. 112°13'07"E):

Sixteen analyses of 16 zircon grains were performed for this sample. The results show relatively large variations of Th and U concentrations, which vary from 69 to 190 ppm and from 138 to 1053 ppm, respectively. The corresponding Th/U ratios vary from 0.73 to very low at 0.09. All analyses have very low common lead (f_{206} < 0.30%) and are concordant (**Fig. 4.5a**). Sixteen analyses give a weighted mean $^{206}Pb/^{238}U$ age of 154.3 ± 1.2 Ma (MSWD[2] = 0.91), the same as the concordia age (**Fig. 4.5a**).

XY20-1 (lat. 25°13'09"N, long. 112°10'59"E):

Sixteen analyses of 16 grains from this porphyritic granite sample gave low Th (66−177 ppm) and U (118−227 ppm) concentrations and limited variation of Th/U ratios from 0.52 to 0.82. All analyses are concordant (**Fig. 4.5b**) and have very low common lead (f_{206} < 0.19%). The Concordia age of 153.7 ± 1.3 Ma (MSWD = 0.94) is identical to the weighted mean $^{206}Pb/^{238}U$ age of 153.8 ± 1.2 Ma (MSWD = 1.15) of all analyses.

[2] MSWD stands for mean square weighted deviation.

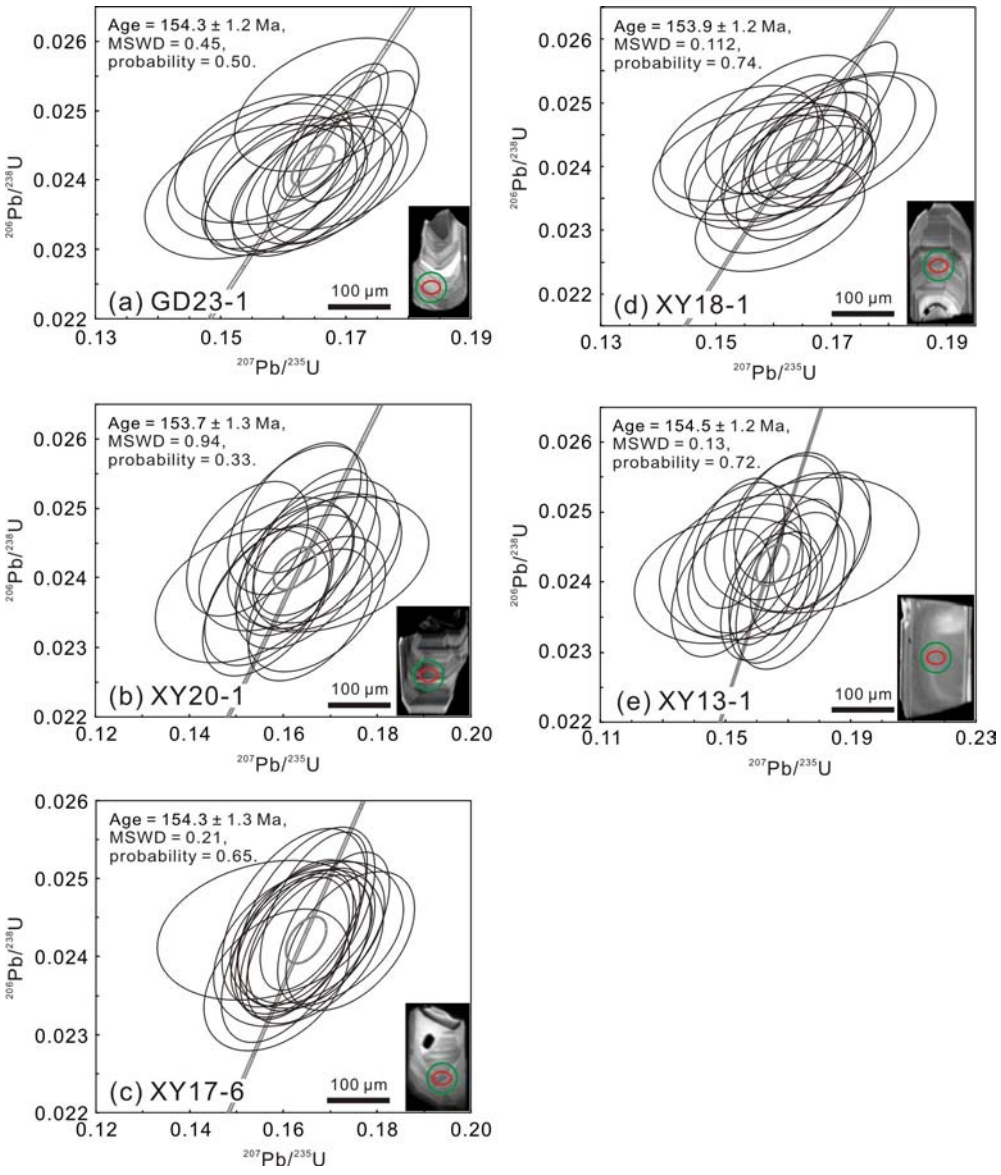

Figure 4.5 Zircon U-Pb Concordia diagrams showing chronological result of samples (a) GD23-1, (b) XY20-1, (c) XY17-6, (d) XY18-1, and (e) XY13-1 of the Jiuyishan granite suite. The numbers shown on top left of each diagram are Concordia ages. Representative CL images are shown at the bottom right of each diagram. Red ellipses highlight the SIMS analytical spots for U-Pb and O isotopes. Green circles show the LA-MC-ICP-MS analytical spots for Lu-Hf isotopes.

XY17-6 (lat. 25°06'02"N, long. 112°07'19"E):

This sample is a coarse-grained granodiorite that has the least evolved chemical compositions (low in SiO_2, but high in Fe_2O_3 and MgO). Sixteen analyses

of 16 zircons reveal low and homogeneous Th and U concentrations that range from 61 to 168 ppm and from 100 to 246 ppm, respectively. Their Th/U ratios vary from 0.47 to 1.00 and the common lead is very low with f_{206} < 0.21%. All analyses are concordant (**Fig. 4.5c**), giving a weighted mean $^{206}Pb/^{238}U$ age of 154.3 ± 1.2 Ma (MSWD = 0.29).

XY18-1 (lat. 25°08'32"N, long. 112°08'45"E):

The sample is dark in colour. It has porphyritic texture containing some fayalite and ferrosilite phenocrysts. Seventeen analyses on 17 grains were conducted and the results show variation of Th and U concentrations from 68 to 271 ppm and from 114 to 745 ppm, respectively. The ratios of Th to U have limited variation from 0.31 to 0.88. All zircons analysed have very low common lead (f_{206} < 0.22%). All analyses are concordant (**Fig. 4.5d**). These analyses give a Concordia age of 153.9 ± 1.2 Ma (MSWD = 0.112), identical to the weighted mean age of 153.9 ± 1.2 Ma (MSWD = 1.03) of all analyses.

XY13-1 (lat. 25°13'41"N, long. 112°23'13"E):

Seventeen analyses of 17 zircons from this volcanic sample were performed. Zircons analysed have low Th and U contents which vary from 12 to 161 ppm and from 24 to 261 ppm, respectively. The ratios of Th to U vary between 0.36 and 0.84. The common Pb for all analyses are low with f_{206} < 0.96% and many of them are undetectable (Table 4.9). All analyses give concordant results that are identical with each other within errors (**Fig. 4.5e**). All analyses yield a weighted mean $^{206}Pb/^{238}U$ age of 154.5 ± 1.2 Ma (MSWD = 0.87), the same as the Concordia age of 154.5 ± 1.2 Ma (MSWD = 0.13).

Results show that five samples varying from volcanic, subvolcanic to intrusive facies have similar crystallization ages of 154 ± 1 Ma (**Figs. 2.5 and 2.6**). The apparent age, though similar to, is slightly younger than previously published data (156−157 Ma, Fu et al. 2004b). A review of the published data finds that some

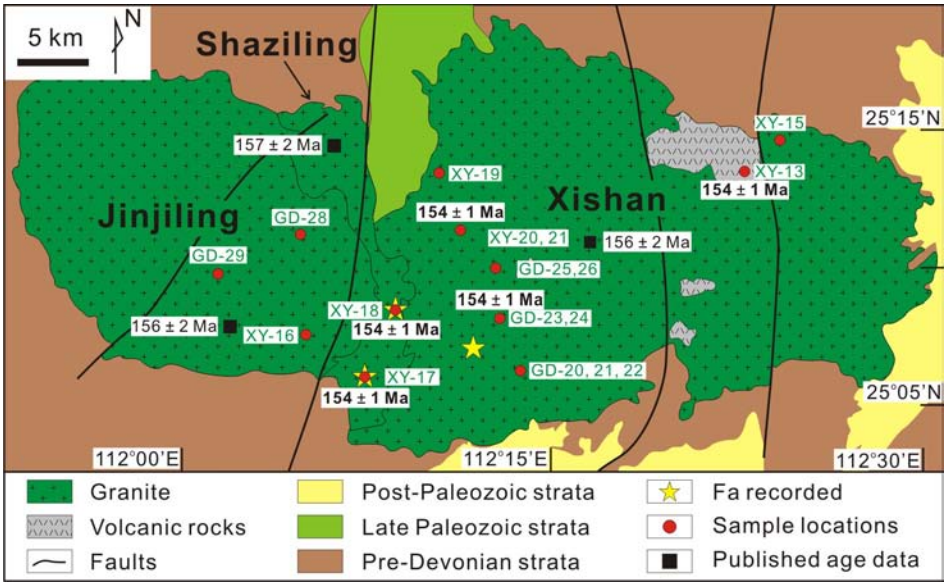

Figure 4.6 Simplified geological map showing the distribution of volcanic and intrusive rocks in the Jiuyishan suite (modified from Huang et al. 2011). The published age data come from Fu et al. (2004b).

analyses have high common lead (f_{206} up to 16%) and correspond to higher apparent age values. Therefore, new results of ~154 Ma from this study give the best estimation, suggesting that rocks constituting the Jiuyishan batholith are coeval (**Fig. 4.6**) and likely comagmatic.

4.2.3. Whole-rock geochemistry

Thirty-nine samples in total, including 6 volcanic samples, were analysed for their major elements at the GIG using XRF and for their trace elements at the IGG using quadrupole ICP-MS. New results are presented in **Appendix Table 8**. The samples studied show a wide compositional range with their SiO_2 contents varying from 64.1 to 76.5 wt%. As SiO_2 increase, most major elements of the Jiuyishan granitic rocks vary roughly in a linear fashion (**Fig. 4.7**): contents of Al_2O_3, CaO, TiO_2, $Fe_2O_3^T$, MgO, MnO, and P_2O_5 decrease (**Figs. 4.7a, b, and 4.7f–j**), whereas that of K_2O increases (**Fig. 4.7d**). Distinctively, the content of Na_2O remains largely unchanged as SiO_2 increases (**Fig. 4.7c**). Contents of CaO and Na_2O for some samples, dominantly volcanic rocks, vary anomalously to low values (**Figs. 4.7b and**

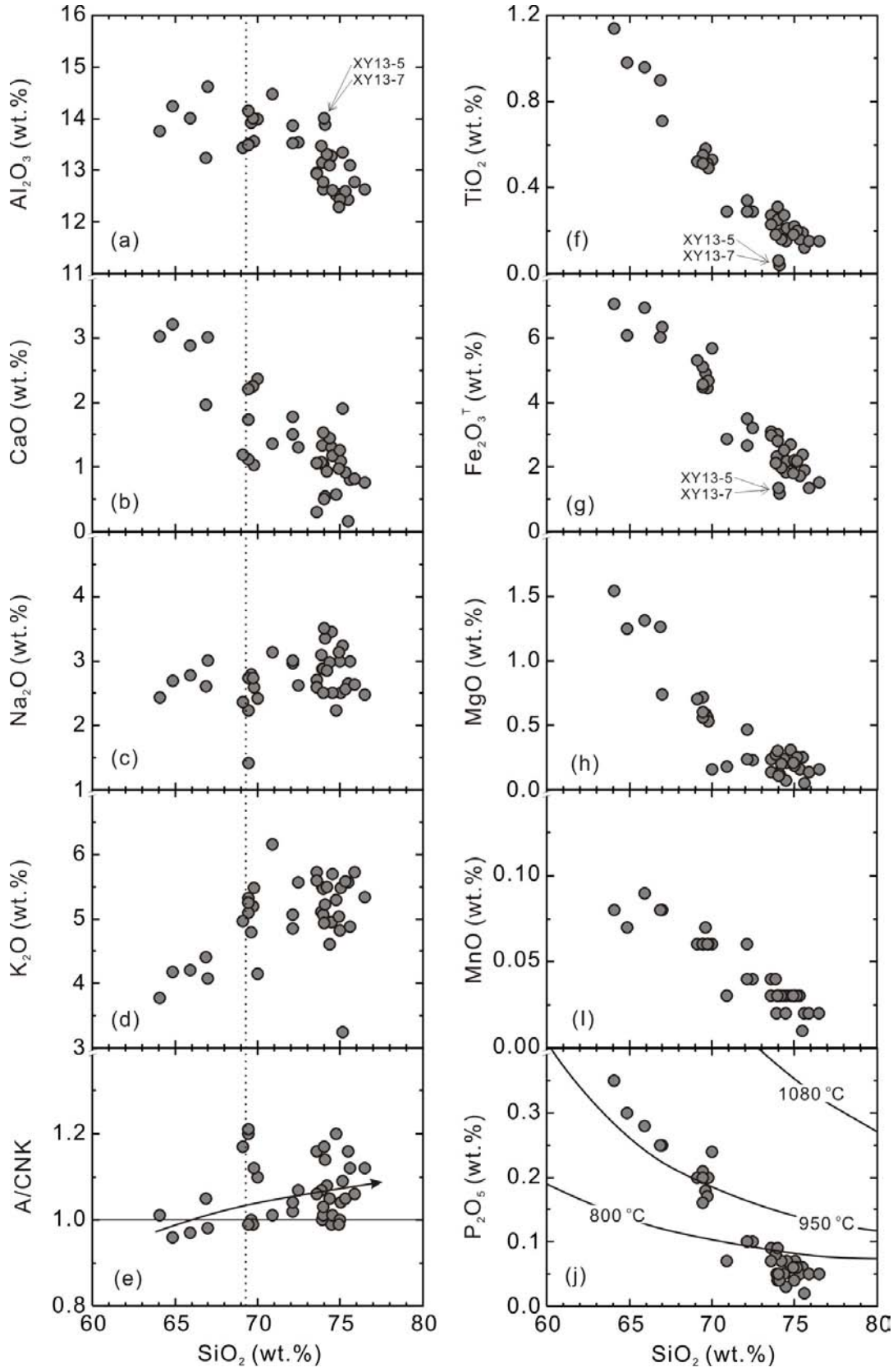

Figure 4.7 Harker diagrams showing chemical variations of the Jiuyishan granitic rocks. Contours in figure (j) are after Watson and Harrison (1984).

c), probably as a result of weathering. The anomalies cause a significant increase in A/CNK for these samples (**Fig. 4.7e**).

Comparatively, contents of trace elements show larger variations, but also vary in a linear fashion with increasing SiO_2 (e.g., **Fig. 4.8**). In particular, contents of Zr and Ba first increase with increasing SiO_2 but then decrease as SiO_2 increase further after ~70 wt.% SiO_2 (**Figs. 4.8c and d**). Such a geochemical variation pattern probably presents the most convincing evidence for fractional crystallization (Chappell, 1996). Noticeably, while elements define coherent variation trends in general, they show various degrees of scatter (**Figs. 4.7 and 4.8**).

The Chondrite-normalized rare earth elements (REE) variation patterns (**Fig. 4.9a**) of the Jiuyishan granitic rocks invariably show LREE (light REE) enrichments and Eu negative anomalies. The Eu negative anomaly appears to increase with increasing SiO_2 (**Fig. 4.9a**). In the ocean ridge granite-normalized variation diagram

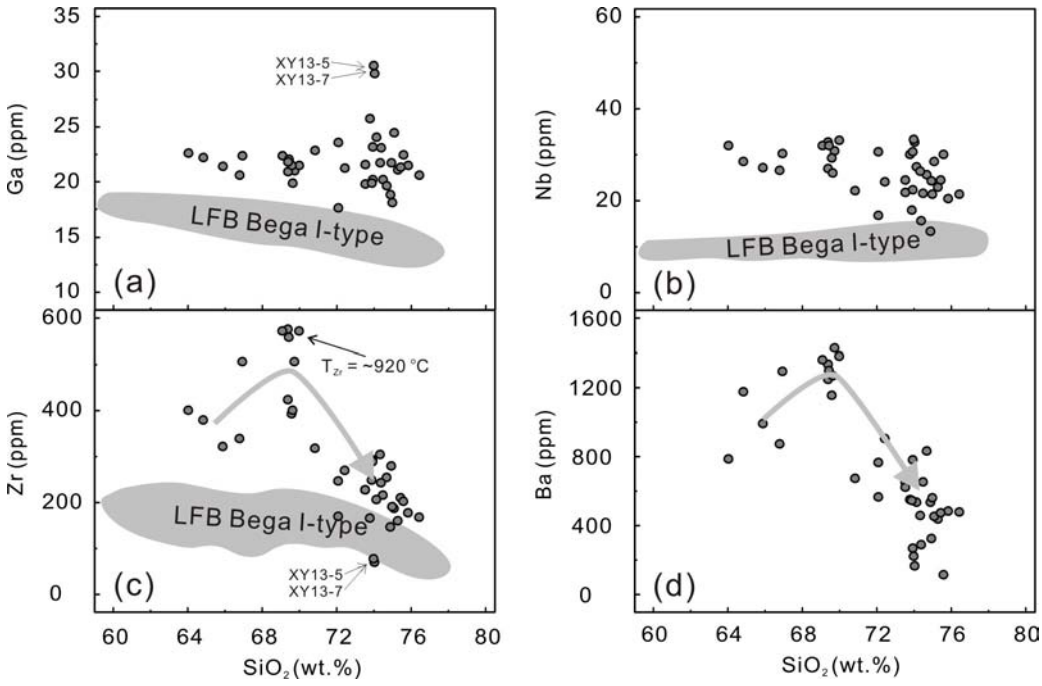

Figure 4.8 Trace element variation diagrams for Ga (a), Nb (b), Zr (c), and Ba (d) with increasing SiO_2. The fields for the LFB Bega I-type granites are modified from Collins et al. (1982).

(**Fig. 4.9b**), all the samples show coherent patterns with strong enrichment in large ion lithophile elements (LILE), but depletion in high field strength elements (HFSE). K_2O, Ba, Nb(Ta), and Zr(Hf) show negative anomalies relative to their neighbouring elements in the normalized trace elements variation pattern. Similar to Eu, degrees of anomaly for these elements also increase with increasing SiO_2. Two volcanic samples (XY13-5 and XY13-7) show distinctive REE and trace element variation patterns. Their REE distribution patterns demonstrate significant tetrad effect[3] ($TE_{1,3}$ = 1.14 and 1.13; **Fig. 4.9**). Besides, their Al_2O_3, Ga are higher (**Figs. 4.7a and 4.8a**), whereas their TiO_2, $Fe_2O_3^T$ and Zr are lower (**Figs. 4.7f, 4.7g, and 4.8c**) than the rest with similar SiO_2. These features were likely resulted from hydrothermal reactions that have commonly been proposed to account for REE tetrad effects and non-CHARAC (charge-and-radius-controlled) trace element behaviours (e.g., Jahn et al., 2001; Zhao et al., 2002).

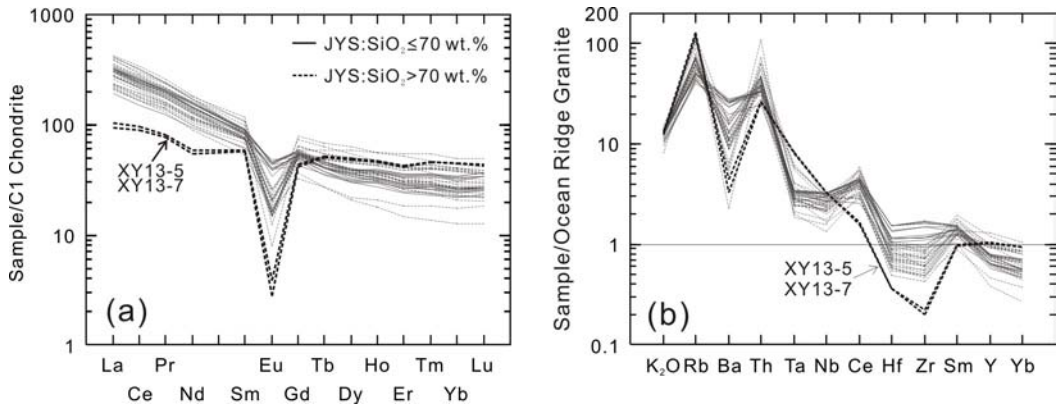

Figure 4.9 (a) C1 Chondrite-normalized rare earth elements (REE) distribution patterns; (b) ocean ridge granite-normalized major and trace elements distribution patterns. Normalization data are from Sun and McDonough (1989) and Pearce et al. (1984).

4.2.4. Whole-rock Sr-Nd isotopes

Strontium and Nd isotope compositions were determined using a Triton TIMS

[3] refers to the subdivision of the 15 rare earth elements into four groups in a chondrite-normalized distribution pattern. A brief definition of the tetrad effect can be found in Jahn, B. M. et al. (2001).

and a micromass isoprobe MC-ICP-MS, respectively, at the GIG. Only those samples with Rb/Sr ratios lower than two, for which the errors of I_{Sr} can be limited to lower than 0.001, were selected for bulk-rock Sr-Nd isotope studies. Rubidium, Sr, Sm and Nd contents determined by ICP-MS are employed for initial $^{87}Sr/^{86}Sr$ and $^{143}Nd/^{144}Nd$ calculations at t = 154 Ma. The results (**Appendix Table 9**) show that all samples have evolved isotope compositions with their initial $^{87}Sr/^{86}Sr$ ratios ranging from 0.7151 to 0.7181. Their εNd(t) values mostly vary from −7.4 to −6.4 (**Fig. 4.10**), corresponding to two-stage Nd model ages of 1.55 Ga to 1.46 Ga. Two samples have lower εNd(t) values of −8.4 and −9.3 (**Fig. 4.10**), with their relevant two-stage Nd model ages being 1.62 Ga and 1.70 Ga, respectively. The results are consistent with data published by Fu et al. (2004a, 2005) and Jiang et al. (2009).

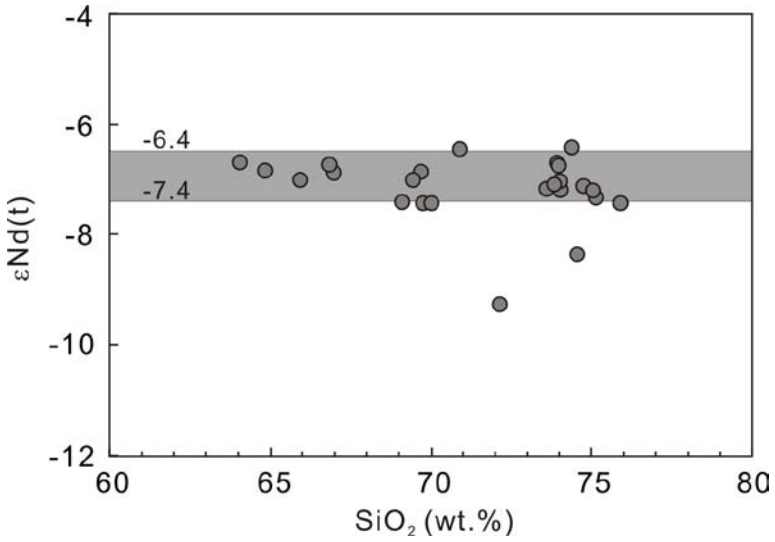

Figure 4.10 Variation of εNd(t) with increasing SiO_2.

4.2.5. In-situ zircon Hf and O isotope compositions

The zircons previously targeted for geochronological studies were further analysed in-situ for their Hf and O isotope compositions at the IGG using a LA-MC-ICP-MS and a Cameca IMS-1280 ion microprobe, respectively. The results are listed in **Appendix Table 11** in a chronological sequence as the oxygen isotopes analysed. The results show limited variation of $^{176}Hf/^{177}Hf$ from 0.282460 to

0.282569 and their corresponding crustal evolution model ages from 1.73Ga to 1.35 Ga. The initial εHf(t = 154 Ma) for all samples vary from −8.2 to −2.3. Individual samples have even smaller variation of εHf(t) values (<3.4ε units) and show unimodal distribution patterns (**Figs. 4.11a−e**). However, it is interesting to find a mild increase of εHf(t) from −7.0 for a volcanic sample to −4.6 for a well-crystallized intrusive sample (**Figs. 4.11a−e**).

The oxygen isotope compositions of all samples, expressed as $\delta^{18}O$, show restricted variation mostly from 8.0‰ to 10.1‰. There are two outliers, being 6.3‰ and 11.5‰. The results show that all zircons studied contain more heavy oxygen isotopes and apparently have much higher $\delta^{18}O$ than that of "mantle zircon", being ~5.3‰ (Cavosie et al., 2009; Grimes et al., 2011; Page et al., 2007; Valley et al., 1998). As pristine magmatic zircons are retentive of their primary oxygen isotope ratios (Peck et al., 2003; Valley et al., 1994; Zheng et al., 2004b), the results can be applied for the estimation of the primary oxygen isotope compositions of whole-rock, following the equation: $\Delta^{18}O$ (Zrc−WR) = $\delta^{18}O$ (Zrc) − $\delta^{18}O$ (WR) ≈ −0.0612 (wt.% SiO_2) + 2.5 (Valley et al., 2005). The estimated whole-rock $\delta^{18}O$ vary from 9.5‰ to 11.6‰ and are within the range of the data published by Li et al. (1986). The results are similar to those of typical S-type granites in the LFB, southeast Australia (e.g., O'Neil et al., 1977). Zircon $\delta^{18}O$ of individual sample also shows unimodal distribution and peak values for all samples are the same (**Figs. 4.11f−j**). No systematic correlation between oxygen and hafnium isotopes seems to exist (**Fig. 4.11**).

4.3. Discussion

4.3.1. Petrogenetic classification

The crystallization of fayalite indicates low fH_2O and low to moderate fO_2, features characteristic of A-type granite (Loiselle and Wones, 1979). Fayalite, as well

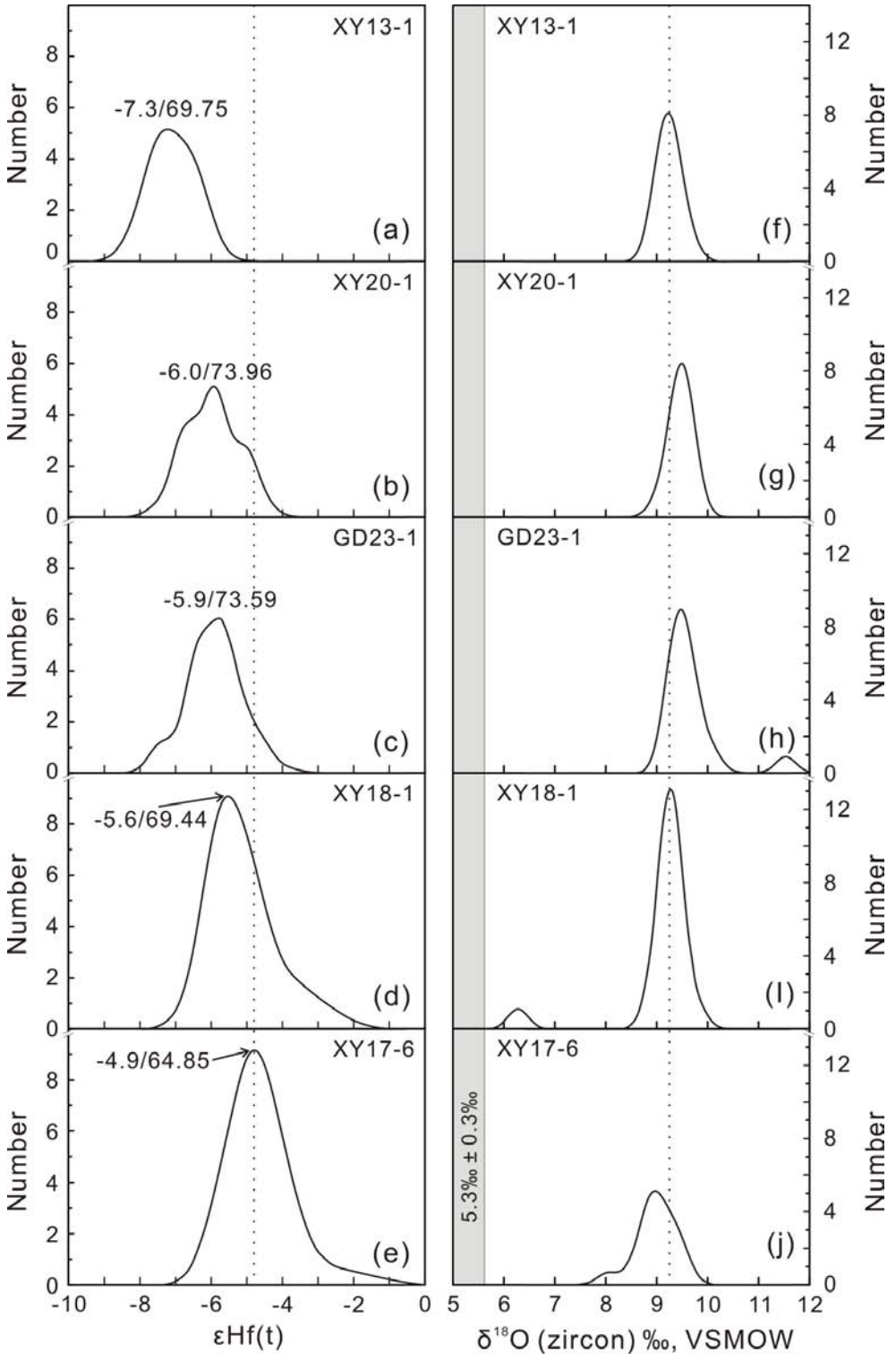

Figure 4.11 Probability density plots of zircon εHf(t) and $\delta^{18}O$ values for the Jiuyishan granitic rocks. Numbers in (a)−(e) show peak values of εHf(t) (on the left) and SiO_2 contents of each sample (on the right). The grey area in (f)−(j) shows the proposed range of $\delta^{18}O$ for "mantle zircon".

as ferrosilite, in the Jiuyishan granitic rocks was interpreted as ultramafic enclaves derived from the mantle (Fu et al., 2003a). However, its composition is distinct from regionally mantle-derived magnesian olivines that have been reported by Zheng et al. (2004a). Provided that this mineral is typically magmatic in origin (Fu et al., 2003a), it was likely originated from the magma. As has been pointed out earlier (**section 4.2.1.**), thin section examination finds that anhydrous fayalite was the earliest formed ferromagnesian mineral, amongst the others presented in the Jiuyishan granitic rocks. The early crystallization of fayalite and the subsequent crystallization of ferrosilite, Fe-enriched biotite and amphibole provide robust petrological evidence for the anhydrous nature of the parental magma. As no comagmatic magnetite has been identified to coexist with fayalite, it is reasonable to infer that the oxygen fugacity of the magma was originally lower than the fayalite-magnetite-quartz (FMQ) buffer. Therefore, the occurrence of fayalite reflects not only low water activity, but also low oxygen fugacity of the magma (Barker et al., 1975). For the anhydrous nature, the crystallization of fayalite may also imply high magma temperature. Indeed, estimations using apatite saturation thermometry and zircon saturation thermometry give a maximum magma temperature of ~960 °C (**Fig. 4.7j**) and minimum magma temperature of ~920 °C (**Fig. 4.8c**), respectively. On the other hand, the formation of high-F annite-rich biotite indicates that the parental magma probably had a high F concentration. These features are typical of A-type granitic magmatism.

Consistent with published data in **Table 4.1**, geochemical results of this study are also similar to that of A-type granite. The results show that the Jiuyishan granitic rocks are high in K_2O (~5 wt% at 70 wt% SiO_2), $Fe_2O_3^T$ and P_2O_5, but low in Al_2O_3, MgO, CaO and Na_2O. Therefore, their K/Na, (K + Na)/Al, and Fe/Mg ratios are relatively high. Besides, all samples are enriched in trace elements Ga, Zr, Nb, Y and REE (except Eu), distinct from I-type granite but similar to A-type granite (e.g., **Figs. 4.8a–c**). Geochemically, these granitic rocks can be classified as ferroan and calc-alkalic to alkali-calcic (**Fig. 4.12**) and diagnosed as A-type granite (**Fig. 4.13a**).

To conclude, the Jiuyishan granitic rocks have mineralogical and geochemical characteristics typical of A-type granite as defined by Loiselle and Wones (1979). However, it is also true that they have high whole-rock $\delta^{18}O$, varying from 9.5‰ to 11.6‰, whereupon they may be classified as S-type because ^{18}O-enrichment ($\delta^{18}O_{whole\text{-}rock} > 10‰$) is a feature most common for S-type granite (e.g., O'Neil and Chappell, 1977).

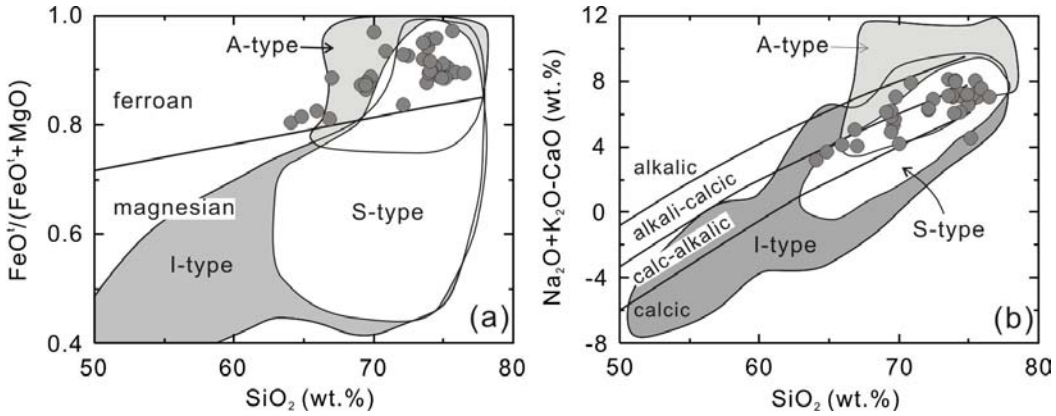

Figure 4.12 Geochemical classification diagrams showing that the Jiuyishan granitic rocks are (a) ferroan and (b) transitional between calc-alkalic and alkali-calcic. Fields for I-type, S-type and A-type granites are from Frost et al. (2001).

4.3.2. Genesis of the Jiuyishan batholith

Fayalite-bearing A-type granites, for their low water activity and low oxygen fugacity (fO_2<FMQ), could be derived through differentiation of tholeiitic magmas or alternatively from partial melting of primitive tholeiitic rocks (Frost and Frost, 1997). The high zircon $\delta^{18}O$ (mostly from 8.0‰ to 10.1‰), the evolved whole-rock Sr-Nd (I_{Sr} = 0.7151−0.7181, εNd(t) = -9.3 to -6.4), and the enriched zircon Hf (εHf(t) = -8.2 to -2.3) isotope compositions, however, suggest significant reworking of ancient supracrustal materials in the genesis of the Jiuyishan granitic rocks and rule out a complete tholeiitic connection. This is consistent with a geochemical classification of the Jiuyishan granitic rocks as A_2-type (**Fig. 4.13b**), which is interpreted to be derived from crustal source rocks that have gone through 'a cycle of

continent-continent collision or island-arc magmatism' (Eby, 1992). However, from the results it is not immediately clear if any mantle-derived materials contributed to the source as ^{18}O-enrichment in some A-type granites has been considered to result from assimilation or mixing of evolving magma with supracrustal component (e.g., Steinitz et al., 2009; Trumbull et al., 2004). A similar mixing scenario has also been invoked to explain the rise in zircon $\delta^{18}O$ of some typical I-type granites (e.g., Kemp et al., 2007). The mixing model alone does not explain the geochemical difference between I- and A-type granites. Besides, the mixing process possibly cannot yield A-type granites with low water and oxygen fugacities (Frost and Frost, 1997).

Several lines of evidence argue further against a magma mixing model. First, the whole-rock εNd(t) values of the Jiuyishan granitic rocks show limited variations as the SiO_2 content increases (**Fig. 4.10**). Anomalies of whole-rock isotope variation patterns may reflect sample source heterogeneity, or be merely a result of variant degrees of local assimilation upon intrusion/eruption. Second, samples studied here have rather homogeneous zircon Hf and O isotope compositions; every sample shows unimodal/quasi-unimodal distribution patterns of zircon εHf(t) and $\delta^{18}O$ (**Fig. 4.11**). While whole-rock compositions provide final pictures only, robust accessory

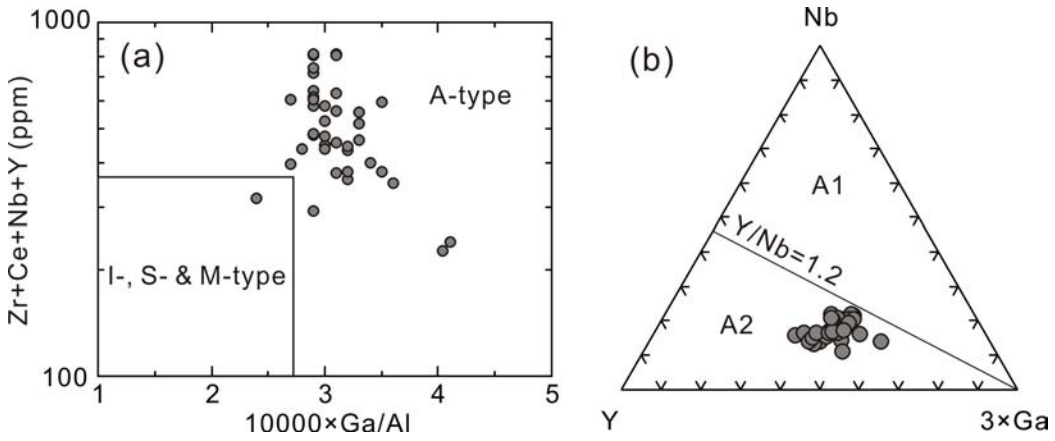

Figure 4.13 (a) Zr + Ce + Nb + Y vs. 10,000 × Ga/Al classification diagram, after Whalen et al. (1987); (b) Nb−Y−3×Ga diagram for the subdivision of A-type granites into A_1 and A_2 types, after Eby (1992).

mineral zircon could tape-record the magmatic evolution processes (Griffin et al., 2002). Therefore, records of magma mixing can be best retrieved by in-situ zircon Hf and O isotope studies (e.g., Kemp et al., 2007). The absence of correlation between Hf and O isotopes of the Jiuyishan granitic rocks lend little support for magma mixing. A mild increase of peak εHf(t) values from −7.3 to −4.9 (**Figs. 4.11a−e**) is not correlated with the change of SiO_2. Similar to the whole-rock Nd isotopes, it may also be a result of source heterogeneity or variable degrees of assimilation. Third, there is no field evidence for magma mixing, e.g., occurrence of mafic microgranular enclaves. Dark enclaves sampled in the field have chemical and isotopic compositions undistinguishable from their host rocks. Fourth, and most importantly, inflections of Zr and Ba as SiO_2 increase (**Figs. 4.8c−d**) point unambiguously to processes of fractional crystallization in controlling the chemical variation of the igneous suite (Chappell, 1996; Chappell et al., 1998). To summarize, fractional crystallization, possibly with variant degrees of local assimilation upon intrusion/eruption, instead of magma mixing, was the principal petrogenetic process for the chemical variations of the Jiuyishan granitic rocks.

With increasing SiO_2, the contents of CaO, TiO_2, $Fe_2O_3^T$, MgO, and P_2O_5 decrease sharply (**Figs. 4.7b, f−h, and j**), whilst the degree of negative anomalies of Eu, Ba, Nb, Zr increases in general (**Fig. 4.9**), demonstrating an advanced fractional crystallization. The marked decrease in Fe and Mg may result from separation of fayalite and ferrosilite. Fractionation of Ti-bearing phases, such as ilmenite and titanite that are common in felsic rocks, may result in a decrease in Ti−Nb−Ta. While titanite is stable under oxidized conditions, ilmenite tends to crystallize in more reduced environments (Wones, 1989). In this case, for the low oxygen fugacity of the Jiuyishan magma, ilmenite probably played a major role in Ti−Nb−Ta fractionation. The pronounced drop of P_2O_5 content was likely a result of apatite fractionation. The increasing degree of Eu negative anomalies could be a result of plagioclase and/or K-feldspar separation. The separation of K-feldspar may also lead to decrease of Ba. However, as can be seen in the Sr−Ba and Sr−Rb variation diagrams (**Fig. 4.14**), in

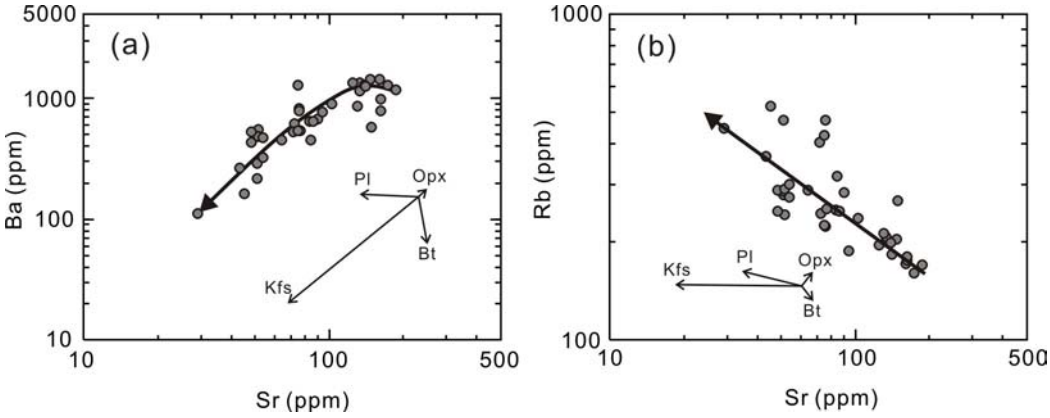

Figure 4.14 Log-log plots showing (a) Sr–Ba and (b) Sr–Rb variations of the Jiuyishan granitic rocks. Labeled vectors demonstrate the effects of fractionation of 10% each of orthopyroxene, plagioclase (An_{36}), K-feldspar (Or_{85}), and biotite (Clemens et al., 2010).

contrast to a sharp decrease of Sr, Ba and Rb increase instead at the early stage of magmatic evolution, likely resulted from separation of plagioclase and orthopyroxene, rather than K-feldspar. This process also explains a decrease of CaO, and is consistent with the conclusion that K-feldspar crystallized late, whereas plagioclase and orthopyroxene formed earlier. As the differentiation proceeds, both Sr and Ba decrease, while Rb keeps increasing till the last stage of magmatic evolution. This is likely a result of combined separation of biotite, plagioclase, and K-feldspar (**Fig. 4.14**). Overall, the Jiuyishan granitic rocks constitute a spectrum of rocks that are genetically linked through fractional crystallization.

The anomalously low contents of CaO and Na_2O in some samples (**Figs. 4.7b and c**) may be due to source heterogeneity or assimilation of wall rocks in the process of magmatic evolution as well. In both cases, systematic variations of the other elements are expected, yet not observed. Alternatively, the variations may have resulted from post-magmatic alteration of feldspars and biotite. In particular, the alteration of plagioclase to sericite, as has been observed in thin sections, may have led CaO and Na_2O to decrease. This explanation is consistent with variably higher LOI (> 1.24 wt% vs. < 0.34 wt%) of those samples.

To conclude, high $\delta^{18}O$ and evolved radiogenic isotope compositions of the Jiuyishan granitic rocks were most likely inherited from the source(s), indicating the source(s) to be supracrustal in origin. In terms of source interpretation, the Jiuyishan granitic rocks should be classified as S-type. Contribution of a mantle component, if any, must have been minor as the Jiuyishan granitic rocks show isotopic and geochemical compositions quite distinct from those of contemporaneous mantle-derived rocks in this region (**Figs. 4.15 and 4.16**). The low water activity and high temperature of the parental magma suggest that the supracrustal source must have been dehydrated and/or partially melt-depleted, being either granulitic metavolcanic rocks or metasedimentary rocks containing at least one F-enriched phase (Collins et al., 1982). Given that volcanic rocks can be oxidized easily after eruption, for example, as a result of hydrogen loss (Christie et al., 1986) or alteration (Benzerara et al., 2007), they are unlikely the source for generating the reduced Jiuyishan granitic rocks. In addition, restitic metavolcanic rocks may have mineralogy and geochemistry inappropriate for generating granites with typical A-type characteristics (Creaser et al., 1991). On the other hand, it has not previously

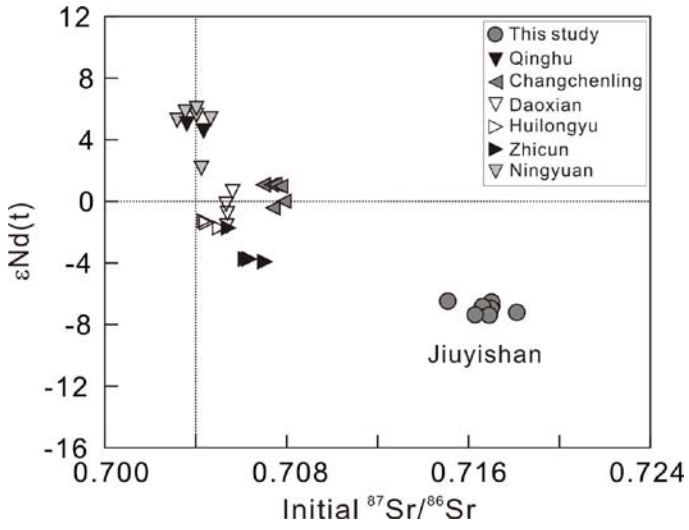

Figure 4.15 Plot of whole-rock Sr-Nd isotope compositions for the Jiuyishan granitic rocks as compared with coeval mantle-derived magmatic rocks in the region. The data shown for comparison are from Jiang et al. (2009), Li et al. (2004a) and Wang et al. (2003b).

been evaluated whether partial melting of metasedimentary rocks could produce reduced A-type granites. The process will be evaluated and an alternative model for the generation of A-type granite will be presented below.

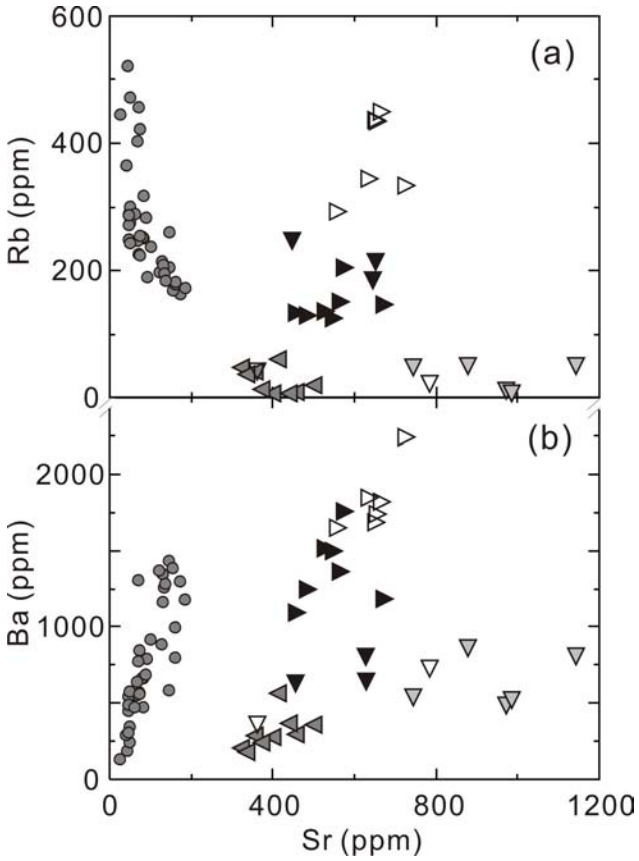

Figure 4.16 Plots of (a) Sr–Rb and (b) Sr–Ba showing distinct trace element variation trends of the Jiuyishan granitic rocks from coeval mantle-derived magmatic rocks in the region. Symbols and sources of the data are the same as in **Fig. 4.15**.

4.3.3. A-type granites generated from melting of granulitic metasedimentary rocks

A-type granites are typically low in Al_2O_3, MgO, CaO and Na_2O, but high in K_2O and FeO (total) contents (Collins et al., 1982; Loiselle and Wones, 1979). Except for Al_2O_3, sedimentary rocks intrinsically have these characteristics due to selective removal of MgO, CaO and Na_2O during weathering (e.g., Rudnick, 1995). Different from residual igneous sources, metasedimentary rocks more likely to

contain appropriate minerals and geochemical compositions required for A-type magmatism. A good example is the Ivrea Zone of Southern Alps, where granulite-facies metapelites (stronalites) contain quartz, K-feldspar, plagioclase, and subordinate biotite (Barboza and Bergantz, 2000; Bea and Montero, 1999). A similar mineral assemblage is present in migmatites, residue of greywackes which have lost ~20% melt, as in central Argentina (Otamendi and Douce, 2001). Such granulitic metapelites have been documented in the southeastern half of South China (Li et al., 2010d; Yu et al., 2005), where sedimentary rocks were brought to the lower crust during an early Paleozoic intraplate orogeny and experienced partial melting at ~440–420 Ma (Li et al., 2010d; Wang et al., 2010b; Wang et al., 2007d). Specifically, granulitic metasedimentary enclaves have been captured by some early Mesozoic cordierite-bearing S-type granites in this region (Zhao et al., 2010). High temperature melting of residual rocks with accessory phases (Collins et al., 1982) can account for the salient features of trace elements in the studied samples, e.g., enrichment in HFSE and REE. In addition, metasedimentary rocks may have similarly low fO_2 (Flood and Shaw, 1975) for producing fayalite granite.

Interpretation of the low Al_2O_3 contents in the Jiuyishan suite is not straightforward, as granitic rocks originating from sedimentary rocks are generally peraluminous (Chappell, 1999). Estimations reveal a maximum magma temperature of 960°C (**Fig. 4.7j**). In view of the low SiO_2 (~64 wt%) and high $Fe_2O_3^T$ (7.05 wt%), even higher temperature could be expected for the partial melting. The high temperature (>960°C) attained during partial melting may explain the low Al_2O_3 concentration. Several aluminous minerals, such as hercynite and cordierite, are abundant in high-temperature residual metapelites (e.g., Barboza et al., 1999; Vasquez et al., 2009). Their occurrence as restitic minerals could at least partly account for the low Al_2O_3 concentrations. Garnet could be another restitic mineral. But in the case of the Jiuyishan suite, with high Y (> 45 ppm) and relatively flat heavy REE pattern (**Fig. 4.9a**), garnet seems unlikely to be a major residual mineral, which may imply low pressure (<7 kbar; Patino Douce and Beard, 1996) for melting.

To conclude, some A-type granites can also be generated from melting of granulitic metasedimentary rocks at high temperature.

4.3.4. General implications for the origin of A-type granite

4.3.4.1. Sources

A-type granite is an unusual rock type with distinct mineralogical and geochemical characteristics (e.g., Collins et al., 1982; Loiselle and Wones, 1979; Whalen et al., 1987). Since the proposition of the rock type in 1979, there have been heated debates over its origin. Many A-type granite studies centred on discussing probable source rocks for the generation of distinctive geochemical characteristics (e.g., Collins et al., 1982; Creaser et al., 1991) as A-type was proposed at a time when chemical compositions of granites were arguably fingerprinting source compositions (Chappell and White, 1974; White and Chappell, 1977).

To identify source rocks is fundamental for understanding the genesis of granitic rocks and it remains a principal problem to be solved. When A-type granite was first proposed (Loiselle and Wones, 1979), the authors inferred that the granites could be generated either by interaction of alkali basalt with a residual source (Barker et al., 1975) or through fractionation of a basaltic melt without crustal contamination. Recognizing the distinct geochemistry of metaluminous A-type granites from spatially related I-type granites of the Bega batholith in the LFB, Collins et al. (1982) first proposed that partial melting of felsic granulitic rocks, restites of I- or S-type magmatism, may account for the origin of A-type granites. This model has the advantage of explaining distinctive trace element characteristics of A-type granites described there, e.g., high Zr, Nb, Ga, Y, and REE. An important implication of this model is that A-type granites may form at higher temperatures and have lower water contents than I-type granites (Collins et al., 1982). The idea has been supported by subsequent experimental studies on those A-type granites (Clemens et al., 1986).

The residual source model, however, has been challenged because residues left after the generation of I-type melts may be refractory and may not have appropriate mineral assemblage and chemical compositions to generate a second melt with typical A-type features (Creaser et al., 1991). For example, a residue would not contain quartz + plagioclase + K-feldspar, a mineral assemblage viewed as a must for the formation of A-type melts (Collins et al., 1982). Nor the melt produced from a residual source would have high Fe/Mg typical of A-type melts (Creaser et al., 1991). An alternative model involving partial melting of crustal igneous rocks of tonalitic and granodioritic compositions (Anderson, 1983) was accordingly favoured for the generation of metaluminous A-type granites similar to those studied by Collins et al. (1982). Based on the study of the Chaelundi complex in the LFB, Landenberger and Collins (1996) debated that a residual igneous source could be partially dehydrated and thus has higher solidi, but does not necessarily be refractory/melt-depleted. Since then, dehydrated quartzo-feldspathic rocks have been frequently proposed as sources for A-type magmatism (e.g., King et al., 2001). Meanwhile, evidences have also been presented to argue for the generation of some A-type granites from mantle through extreme fractionation of tholeiitic magma (e.g., Turner et al., 1992) or from mixing of mantle and infracrustal-derived magmas (e.g., Kerr and Fryer, 1993; Yang et al., 2006b).

To summarize, three main petrogenetic models have been proposed for A-type magmatism: (1) partial melting of quartzo-feldspathic crustal rocks; (2) extreme differentiation of basaltic magma; (3) mixing/assimilation of differentiating basaltic magma with crustal rocks. Source rocks invoked in these models are essentially igneous/infracrustal, in contrast to sedimentary/supracrustal. This is particularly true for fayalite granite, a member of the most iron-enriched and reduced A-type granites argued to have a tholeiite connection (e.g., Frost and Frost, 1997; Turner et al., 1992). Furthermore, a recent review by Bonin (2007) concluded that A-type granites are mostly mantle-derived because there is no convincing evidence from experimental studies or natural samples in support of the generation of such

melts solely from crust. Though oxygen isotope analyses reveal a contribution of supracrustal materials in the genesis of some A-type granites (e.g., Steinitz et al., 2009; Trumbull et al., 2004; Whalen et al., 1996), these rocks are in close association with mantle-derived rocks. Notably, no mantle-derived rocks or mafic microgranular enclaves are spatially related to the Jiuyishan granitic rocks. The Jiuyishan A-type granites therefore probably represent the first convincing example that A-type granite can be generated solely or at least dominantly from the reworking of old crustal materials.

In the light of this study, it can be suggested that A-type granites probably do not have a unique source, and may be generated in many different ways.

4.3.4.2. Intensive parameters

The apparently large variation of sources refutes a simple source connection for the origin of A-type granites. On the contrary, intensive parameters, such as low water activity and high temperature, have been widely acknowledged (e.g., Clemens et al., 1986; Collins et al., 1982; Creaser et al., 1991; Turner et al., 1992). These features are revealed by the mineralogy (e.g., fayalite) and geochemistry (e.g., high P_2O_5, Zr contents) of the Jiuyishan granitic rocks. Oxygen fugacity might be another intensive parameter of importance for the genesis of A-type granites (e.g., Dall'Agnol and de Oliveira, 2007; Frost and Frost, 1997). Many typical A-type granites have relatively low oxygen fugacities (e.g., Frost and Frost, 1997; Loiselle and Wones, 1979). Low oxygen fugacity may control the melting and differentiation processes and account for the Fe-enriched nature of most A-type granites (e.g., Frost and Frost, 2011), as seen in the ferroan Jiuyishan granitic rocks (**Fig. 4.12a**). “Oxidized A-type granites” have also been recognized (e.g., Dall'Agnol and de Oliveira, 2007; Wei et al., 2008), but these rocks, for example those described by Dall’Agnol and de Oliveira (2007), were crystallized from magmas with higher water contents (4.5−6.5 wt%; Dall’Agnol et al., 1999). Besides, they have chemical compositions somewhat transitional between reduced A-type granites and calc-alkalic I-type granites

(Dall'Agnol and de Oliveira, 2007). Strictly speaking, they are not typical A-type granites. Their relatively low Al_2O_3, CaO and high Fe/(Fe + Mg), TiO_2/MgO are probably a result of low pressure melting as has been examplified by Patino Douce (1997).

Pressure is another parameter considered important for the origin of A-type granites. It has been shown that melting of quartzo-feldspathic source rocks at low pressure (<4 kb), at which plagioclase and orthopyroxene are stable, may produce some features typical of A-type granites (Patiño Douce, 1997). This is in accord with the emplacement of A-type granites mostly in extensional tectonic environments (Patiño Douce, 1997). However, in the present study, although relatively low pressure (< 7 kbar) can be inferred from the enrichment of Y and flat HREE distribution pattern, it is not quantitative, nor is its significance in producing the A-type melts clear. The Jiuyishan intrusive-volcanic complex was apparently crystallized at low pressures with the mineral assemblage of plagioclase + orthopyroxene contributing to the early differentiation of the magma (**Fig. 4.14**), but the differentiation of plagioclase and orthopyroxene does not seem to have a vital impact in changing the already high Ga (**Fig. 4.8a**), low Al_2O_3 (**Fig. 4.7a**), and high TiO_2/MgO, etc. The effect of low pressure on generating A-type characters therefore appears to be limited. For those A-type granites of mantle origin, they were unlikely generated at pressures as low as <4 kb. On the contrary, the common alkalic to alkali-calcic nature of these rocks indicate that they might be crystallized at high pressures that favour a crystallization of clinopyroxene over plagioclase (Frost and Frost, 2011). This explains why some A-type granites, e.g., ~1.4 Ga Sherman granite in North America (Nyman et al., 1994), can also be produced in compressive environments.

To conclude, intensive parameters, such as low water activity, low oxygen fugacity and high temperature, have dominant impact over the geochemistry of source rocks for the generation of A-type granites.

4.4. Conclusions

Petrological and geochemical evidences indicate that the Jiuyishan A-type granitic rocks were produced at high temperature (> 960 °C) from anhydrous source rocks. Coupled geochemical and isotopic results reveal fractional crystallization as the controlling process in the evolution of the Jiuyishan granitic rocks. Therefore, the high zircon $\delta^{18}O$ (>8.0 ‰) and evolved radiogenic isotope compositions of these rocks directly image that of the source. Taken together, the reduced Jiuyishan granitic rocks were most likely originated from melting of granulitic metasedimentary rocks at high temperatures (> 960 °C).

Many petrogenetic models have been proposed for the generation of A-type granites. No unique source could possibly account for the origin of all A-type granites worldwide. Rather, intensive parameters like low water activity, low oxygen fugacity, and high temperature have been widely recognized and are critical factors for A-type magmatism. Low pressure, however, does not seem to have a direct impact on the genesis of A-type granites.

Chapter 5: Formation of high $\delta^{18}O$ hornblende-bearing granite by mixing of sedimentary-derived magma with minor mantle-derived magma? Examples of the Jiufeng and Dadongshan granites

(This chapter includes results published in a paper by **Huang, H.-Q., Li, X.-H., Li, W.-X., and Liu, Y., 2008, Age and origin of the Dadongshan granite from the Nanling Range: SHRIMP U-Pb zircon age, geochemistry and Sr-Nd-Hf isotopes: Geological Journal of China Universities, v. 14, no. 3, p. 317-333 (in Chinese with English abstract).** All data, otherwise acknowledged in the published paper, were produced by myself under supervision. Results and conclusions were made through collaboration of myself with the three other authors.)

5.1. Introduction

The Jiufeng granite samples vary from metaluminous to strongly peraluminous (A/CNK = 0.98−1.20). They have ^{18}O-enriched ($\delta^{18}O$ = ~10‰) whole-rock oxygen isotope compositions (Li, 1992). Their whole-rock Nd isotope compositions are enriched, corresponding to Paleoproterozoic depleted mantle model ages (Chen et al., 2007a; Li, 1992; Yin et al., 2010). Some of these features (e.g., occurrence of amphibole) are typical of I-type (e.g., Chen et al., 2007a), whereas many of the others (e.g., peraluminous, ^{18}O-enriched) are similar to S-type (Yin et al., 2010). The origin of these granites remains controversial despite many previous studies. In this study, for the first time, a comprehensive set of integrated mineralogical, geochemical and isotopic analyses was carried out to investigate the genesis of the Jiufeng granite. The origin of the Dadongshan granite is also a topic of debate (e.g., Huang et al., 2008; Ma et al., 2006; Zhang et al., 2003). For its similarity in petrology with the Jiufeng granite, genesis of the granite is examined

here together with the Jiufeng granite.

5.2. Analytical results

5.2.1. Petrography and mineralogy

Samples of the Jiufeng granite consist mainly of quartz (25−35%), plagioclase (30−40%), K-feldspar (25−40%), biotite (0−7%), amphibole (0−5%), and muscovite (0−7%). Accessory minerals include zircon, titanite (**Fig. 5.1a**), allanite, apatite, etc. Some plagioclases show well-developed oscillatory zonations (**Figs. 5.1b−c**). Amphibole does not distribute evenly in the rock and often occurs as aggregates with its pleochromatism varying from brown to brownish-green (**Fig. 5.1d**). Some tiny muscovites in the Jiufeng granite samples were produced from subsolidus alteration (**Fig. 5.1e**), but most of them commonly have clear end faces and cleavages (**Fig. 5.1f**), indicating that they are magmatic in origin. Samples of the Dadongshan granite pluton are composed of 40%−45% K-feldspar, 20%−25% plagioclase, 25%−30% quartz, and ~4% biotite. Titanite occurs as an accessory phase (**Fig. 5.1g**), but no amphibole has been identified. Thin-section examinations found that chloritization is common for biotite, whereas metasomatism of plagioclase produced secondary muscovite (**Figs. 5.1g −h**).

Feldspars and amphibole of the Jiufeng samples were examined for their chemical compositions using a JEOL JXA-8100 Superprobe at the IGG. The results are listed in **Appendix Table 3 and Table 6**. Plagioclase shows large variation of An number from 19.6 to 51.5, compositionally corresponding to oligoclase and labradorite, respectively (**Figure. 5.2**). In general, plagioclase phenocrysts that show oscillatory zonation are more Ca-enriched than the others. They have not reached compositional equilibrium with their felsic host rocks. They could either be restitic mineral of the residual source (White and Chappell, 1977) or be magmatic mineral crystallized from mafic magma and introduced into felsic magma through

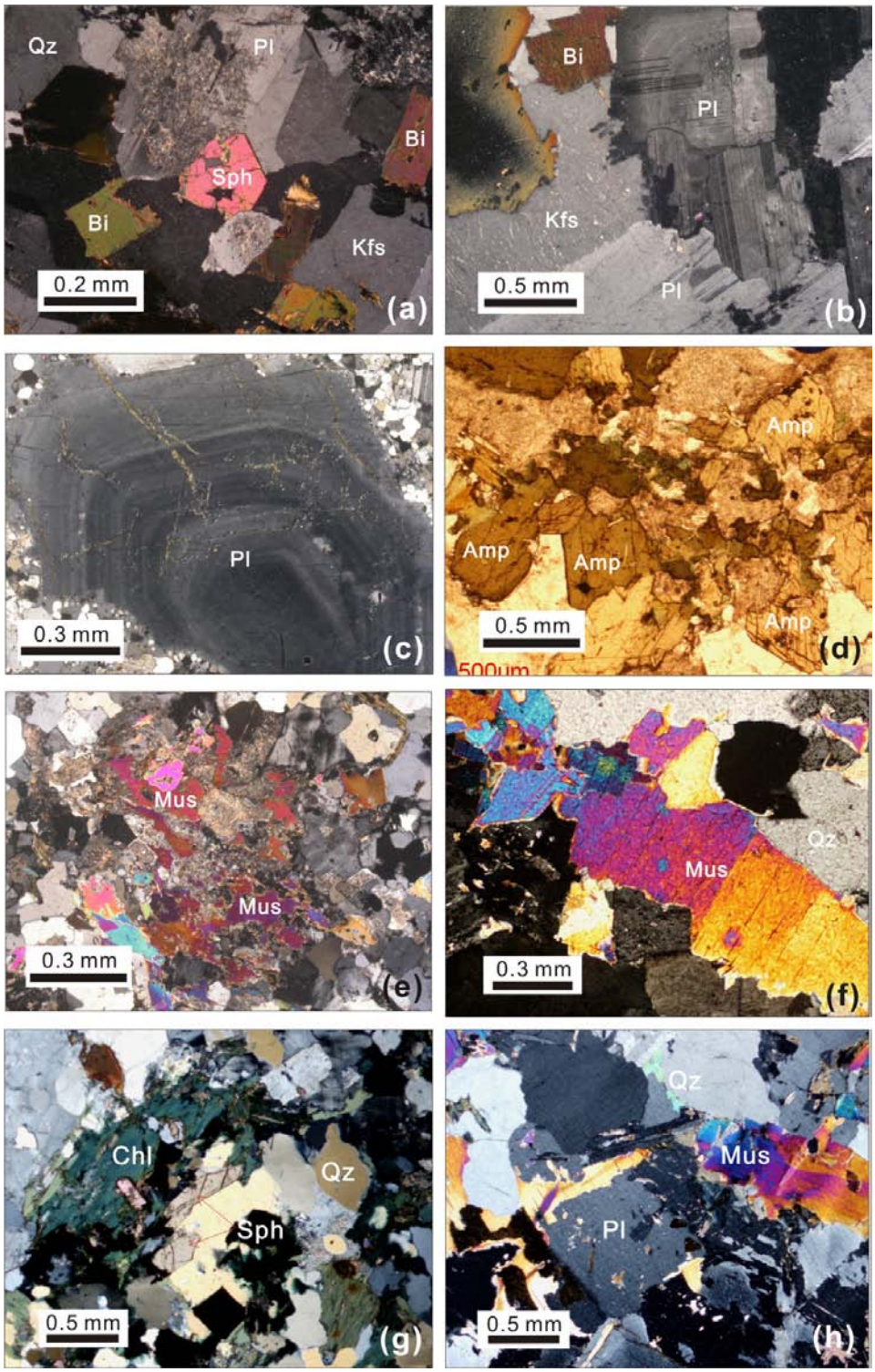

Figure 5.1 Photomicrographs showing mineral assemblages and structures of granites in the Jiufeng pluton [(a)−(f)] and Dadongshan batholith [(g) and (h)]. Photomicrograph d was taken under plain polarized light, whereas the rest were taken under cross polarized light.

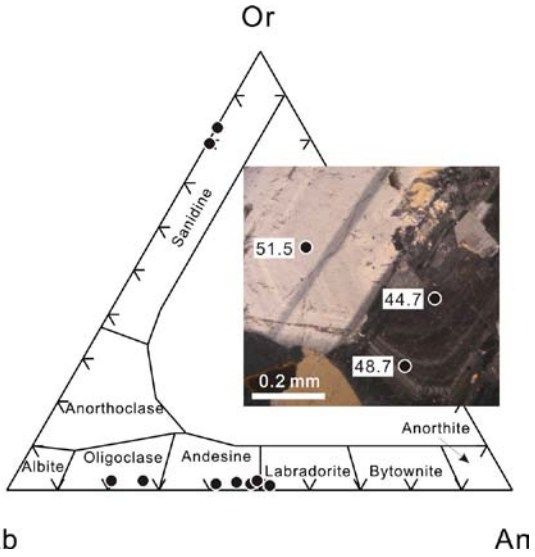

Figure 5.2 A classification diagram showing the composition of feldspars of the Jiufeng granites. Photomicrograph of a plagioclase shows twinning, magmatic zoning, and An number of spot analyses (cross polarized light).

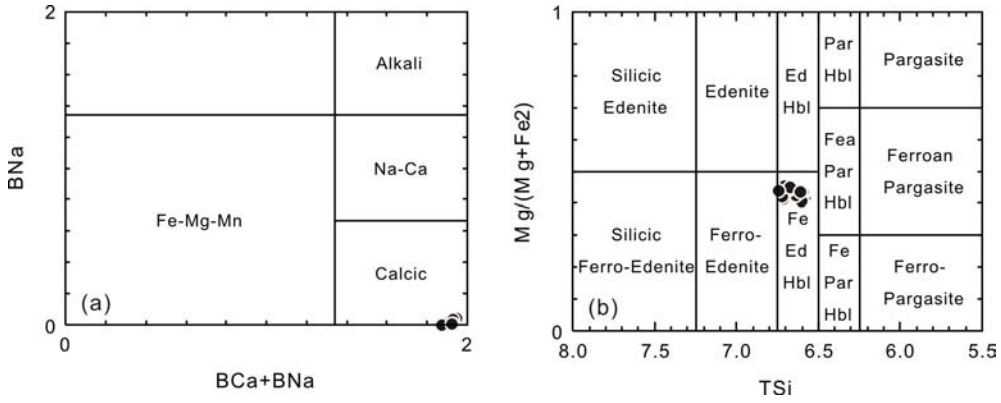

Figure 5.3 Composition of amphiboles of the Jiufeng hornblende-bearing biotite granite (Hawthorne, 1981).

mixing/mingling. Only two K-feldspars were measured for their chemical compositions and both are sanidine (~Or_{80}; **Fig. 5.2**). All amphibole phenocrysts analysed are calcic and iron-enriched and can be uniquely classified as ferro-edenitic hornblende (**Fig. 5.3**). It might be implied from the mineral assemblage (titanite + magnetite + quartz + amphibole) that the magma had relatively high oxygen fugacity (fO_2 >FMQ) (Wones, 1989). However, amphiboles commonly have very low

estimated Fe^{3+} contents (**Appendix Table 6**). Given the fact that no titanite is found to coexist with amphibole, it could be produced at a different stage of magmatic evolution from that for amphibole, implying that the magma likely had lower oxygen fugacities at the beginning.

5.2.2. Zircon U-Pb geochronology

To discuss the genetic relationships between the different granites of the Jiufeng pluton, five samples were selected from the pluton with lithologies varying from muscovite granite to amphibole-bearing biotite granite for an in-situ zircon U-Pb geochronological study. This was to make sure that all granites studied are coeval. Similarly, two samples were selected from the Dadongshan batholith. The analyses of the Jiufeng samples were conducted on a Cameca IMS-1280 ion microprobe hosted at the IGG. The two samples from the Dadongshan batholith were analysed for zircon U-Pb ages using a SHRIMP II ion microprobe hosted at the Beijing SHRIMP centre. The results, listed in **Appendix Table 10**, are summarized below.

Sample XY2-1 (lat. 25°17'04"N, long. 113°44'28"E):

Zircons from the coarse-grained biotite monzogranite are mostly idiomorphic, 100 μm in width, and have length to width ratios varying between 1:1 and 3:1. Some zircons show clear euhedral concentric zoning, whereas most of the others are dark in CL images (**Fig. 5.4**), indicative of their higher U concentrations.

Sixteen analyses were performed preferentially on 16 zircons with clear oscillatory zoning with additional five analyses performed on five zircons with dark CL images. Most zircons analysed have low common lead with $f_{206} < 0.42\%$; only four analyses give higher $f_{206} = \sim 1.5\%$. Analyses of the five zircons with dark CL images yield high U (4244–5819 ppm) and Th (629–1401 ppm) concentrations, while analyses of the others give invariably lower U (344–2361 ppm) and Th (161–865 ppm). Conversely, Th/U ratios of the five zircons are lower than the others

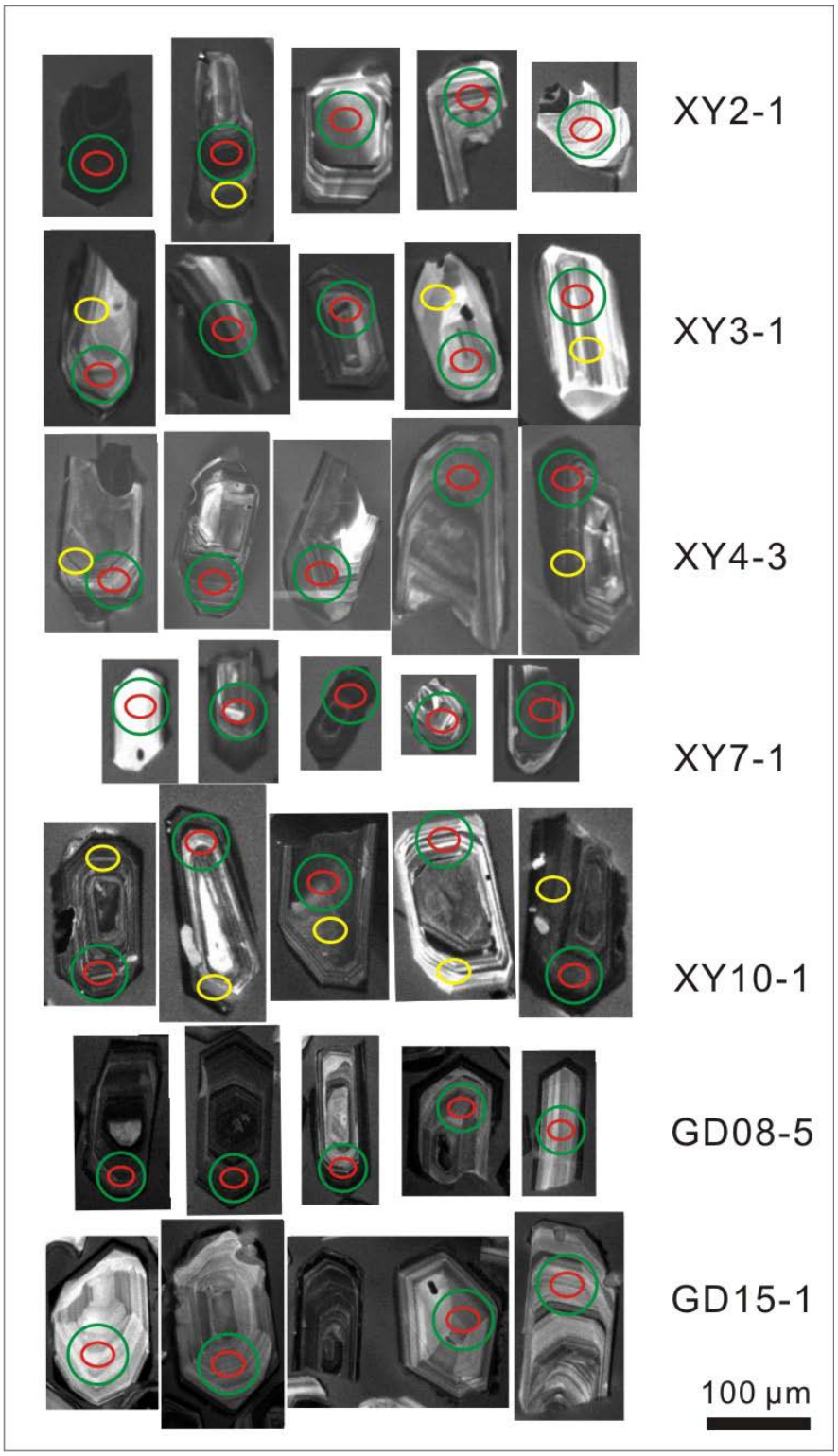

Figure 5.4 Representative CL images showing the internal structure of zircons of the Jiufeng and Dadongshan granites. Yellow ellipses show the spots for oxygen isotope analyses. Red ellipses and green circles highlight the spots for U-Pb and Hf isotope analyses, respectively. Where there is no yellow ellipse shown, red ellipses also represent the spots for O isotope analyses. There is no oxygen isotope analysis for samples GD08-5 and GD15-1.

(0.14–0.27 vs. 0.23–0.66). It has been shown that analyses of high U zircons commonly give higher apparent ages than their true values (Li et al., 2010a). In this study, the apparent $^{206}Pb/^{238}U$ age of the five high U zircons are clearly higher than the rest and are therefore excluded from age calculation. The sixteen analyses of the remaining 16 zircons give a weighted mean $^{206}Pb/^{238}U$ age of 159.7 ± 1.2 Ma (MSWD = 0.86), identical to a Concordia age of 159.7 ± 1.2 Ma (MSWD = 0.40) (**Fig. 5.5a**).

Sample XY3-1 (lat. 25°20'08"N, long. 113°44'51"E):

Zircons from the fine-grained two-mica granite are mostly euhedral and have similar sizes to those from the sample XY2-1. Under CL images, the zircons invariably show clear concentric zoning and thin dark rims (**Fig. 5.4**). Seventeen analyses on 17 zircons were performed for the sample. Fifteen analyses give Jurassic ages, whereas the other two analyses give much older $^{207}Pb/^{206}Pb$ ages of 964 Ma and 1275, indicative of their exotic origin, being either inherited zircons or xenocrysts captured upon intrusion. The fifteen analyses give a wide range of U (346–2407 ppm) and Th (86–1594 ppm) contents, but a relatively narrow range of Th/U ratios varying from 0.25 to 0.87. Except for one analysis which gives a common lead f_{206} of 1.96%, all the others are very low in f_{206} (< 0.19%). The weighted mean of all analyses gives a $^{206}Pb/^{238}U$ age of 158.6 ± 1.2 Ma (MSWD = 0.63), the same as the Concordia age of 158.5 ± 1.3 Ma (MSWD = 0.18) (**Fig. 5.5b**).

Sample XY4-3 (lat. 25°19'29"N, long. 113°42'50"E):

This is a fine-grained biotite granite sample. Zircons from the sample are euhedral, commonly 100 μm in width. Their length to width ratios vary from 3:2 to 3:1. Under CL images, zircons mostly show wide mantle concentric zonations and thin dark rims (**Fig. 5.4**). Some zircons may contain inherited cores, but the cores were not analysed. Sixteen analyses on 16 zircons give variable concentrations of U and Th (500–3039 ppm and 240–1268 ppm, respectively) and low Th/U ratios (0.09–0.56). They all have very low common lead contents with f_{206} being lower than

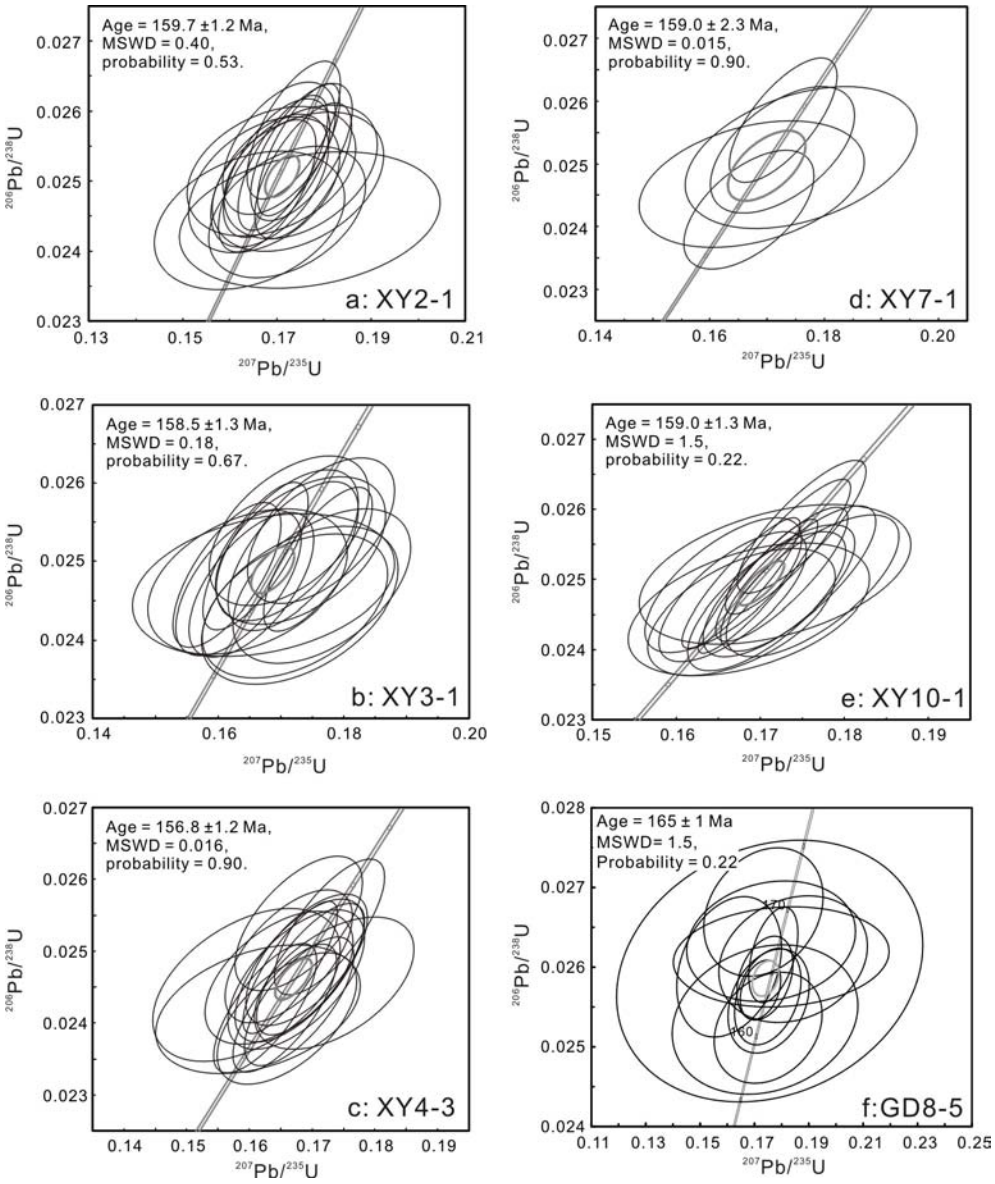

Figure 5.5 Zircon U-Pb Concordia diagrams showing chronological results of the Jiufeng and Dadongshan granites. Concordia ages are shown on the top left of each diagram.

0.41%. All analyses give a weighted mean age of 156.8 ± 1.2 Ma (MSWD = 1.06), the same as the Concordia age of 156.8 ± 1.2 Ma (MSWD = 0.016) (**Fig. 5.5c**).

Sample XY7-1 (lat. 25°19'57"N, long. 113°37'59"E):

Zircons from the fine-grained muscovite granite are mostly euhedral, and small in sizes. They are dominantly 30–50 μm in width and 50–100 μm in length.

Some zircons have bright CL images, but most of the others are very dark (**Fig. 5.4**). Fifteen analyses were performed on 15 zircon grains. The results indicate that only eight of those tested are magmatic; the rest are inherited or xenocrystic zircons and give Proterozoic and Paleozoic ages. The eight magmatic zircons have U contents of 176–4624 ppm and Th contents of 102–2357 ppm with their Th/U ratios varying between 0.30 and 1.48. Three zircons give higher U contents (> 3500 ppm) and apparent ages. They are therefore excluded from age calculation. The remaining five analyses have very low common lead with f_{206} being <0.32%. The weighted mean age of the five analyses is 159.0 ± 4.4 Ma (MSWD = 1.9), similar to a Concordia age of 159.0 ± 2.3 Ma (MSWD = 0.015) (**Fig. 5.5d**).

Sample XY10-1 (lat. 25°21'56"N, long. 113°15'09"E):

Zircons from the medium-grained amphibole-bearing biotite granite are idiomorphic, up to ~100 μm in width, and have length to width ratios of 1:1 to 3:1. CL images show that most zircons have well-developed concentric zoning (**Fig. 5.4**). Fourteen zircons in total were analysed for their U, Th and Pb isotopic compositions. Analyses show that U and Th contents of these zircons vary from 679 ppm to 2477 ppm and from 241 ppm to 857 ppm, respectively. Their Th/U ratios have a narrow range from 0.21 to 0.41. All but one analyses have low common lead compositions (f_{206} < 0.76%). The fourteen analyses give a weighted mean $^{206}Pb/^{238}U$ age of 158.9 ± 1.3 Ma (MSWD = 0.71), similar to a Concordia age of 159.0 ± 1.3 Ma (MSWD = 1.5) (**Fig. 5.5e**).

To summarize, geochronological studies of the five samples give ages varying from 157 Ma to 160 Ma. Although the mean age for sample XY4-3 is slightly younger, it is indistinguishable from the others within error. Results of this study are consistent with published zircon U-Pb data. Therefore, the average age of 159 Ma is taken as the best estimation of the crystallization age of the Jiufeng granites (**Fig. 5.6**).

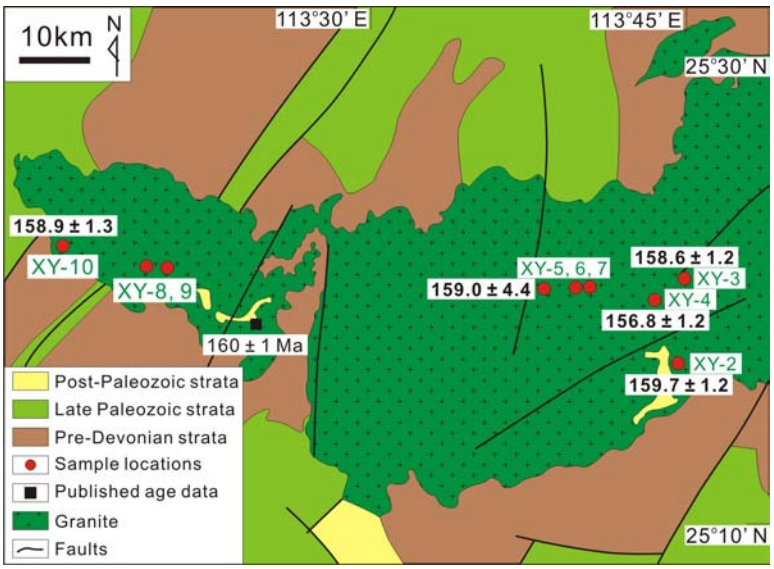

Figure 5.6 A simplified geological map showing the distribution of samples for geochronological studies.

Below are the results for the Dadongshan samples:

Sample GD08-5 (lat. 24°37'46"N, long. 113°13'38"E):

Zircons of this sample are mostly euhedral, varying from 100 μm to 200 μm in length, with their length to width ratios varying in the range of 4:1 to 3:2. They are mostly colourless, with a few being dark brown, likely a result of high U concentration. CL images show that all zircons have well-developed concentric rims and commonly contain small zircon cores (**Fig. 5.4**). Twenty one analyses were performed on 21 zircons and revealed variations of U and Th from 125 ppm to 4893 ppm and from 78 ppm to 3325 ppm, respectively. Correspondingly, their Th/U ratios vary from 0.13 to 0.85. One analysis gives a very high f_{206} of 7%, whereas the rest all have relatively low common lead (f_{206} < 1.9%). Among those analyses, two have apparent $^{206}Pb/^{238}U$ ages of 339.6 Ma and 204.8 Ma. After excluding four analyses with high U concentrations and three with distinct apparent ages are excluded, eleven analyses give a weighted mean $^{206}Pb/^{238}U$ age of 165 ± 1 Ma (MSWD = 1.03), identical to a Concordia age of 165 ± 1 Ma (MSWD = 1.5) (**Fig. 5.5f**).

Sample GD15-1 (lat. 24°45'11"N, long. 112°58'57"E):

Compared with the other sample, zircons of this sample are larger, but have lower length to width ratios. Their CL images are brighter, likely a result of lower U concentrations. Zircon cores are also common for this sample. Fifteen analyses on fifteen zircons give Th and U contents in the range of 101 ppm to 394 ppm and 188 ppm to 611 ppm, respectively. The Th/U ratios, correspondingly, vary from 0.46 to 0.88. All the analyses have common lead f_{206} lower than 1.67%. A probability density plot of $^{206}Pb/^{238}U$ ages reveals a multiple peak distribution pattern, with two major peaks at 158 Ma and 163 Ma (**Fig. 5.7**).

5.2.3. Whole-rock geochemistry

Twenty eight samples from the Jiufeng pluton have been studied for their major and trace elements (**Appendix Table 8**). The samples studied cover a wide range of SiO_2 contents (68.9 to 77.6 wt%). With increasing SiO_2, the contents of Al_2O_3, CaO, P_2O_5, TiO_2, $Fe_2O_3^T$, MgO, and MnO decrease in general, whereas that of Na_2O increases (**Fig. 5.8**). Interestingly, both K_2O and A/CNK appear to inflect as

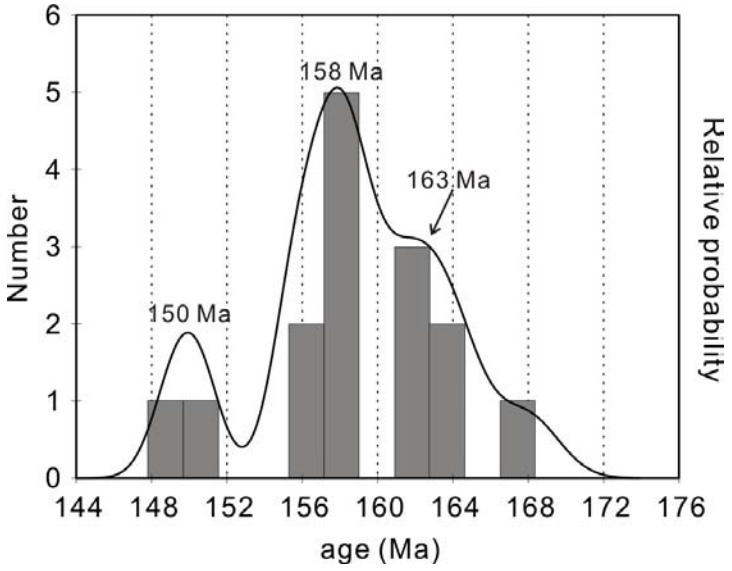

Figure 5.7 Probability of geochronological results of sample GD15-1 from the Dadongshan batholith. Numbers on some major peaks show the peak values.

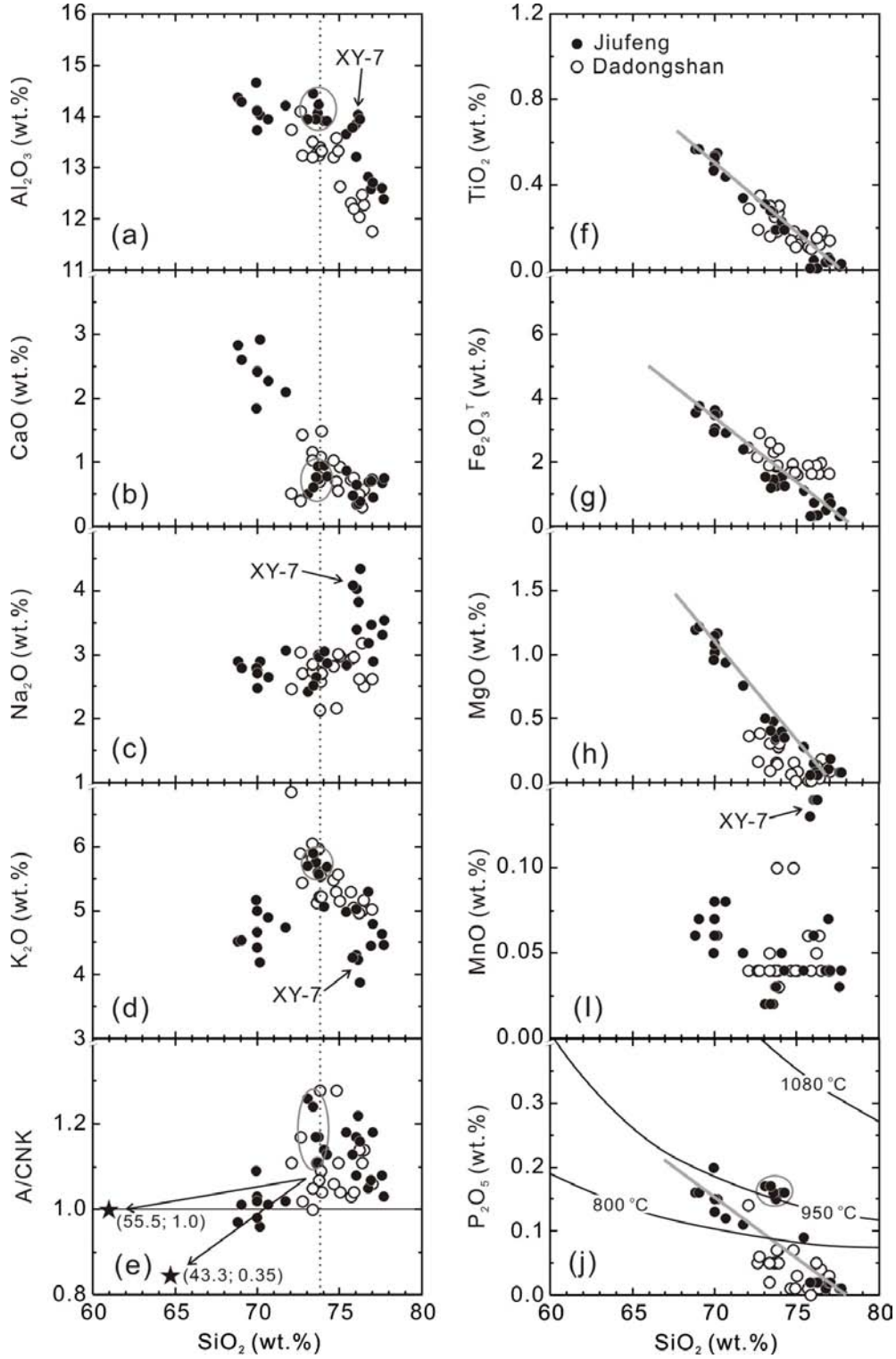

Figure 5.8 Harker diagrams showing the variation of major elements of the Jiufeng and Dadongshan granites. Solid grey lines are used to link the least and the most evolved samples of the Jiufeng pluton. A group of biotite granites with distinctive features is circled. Results of muscovite granites are identified. Stars with numbers in (e) represent the average (SiO_2; A/CNK) compositions of plagioclase (55.5; 1.0) and amphibole (43.3; 0.35). Arrows show the possible mixing trends. Contours in figure (j) are after Watson and Harrison (1984).

SiO_2 increases (**Figs. 5.8d–e**). A close examination, however, finds that only TiO_2, $Fe_2O_3^T$, and MgO show tight linear variation trends (**Figs. 5.8f–h**). Specifically, a group of biotite granites (XY-3 and XY-4) has prominently higher Al_2O_3, K_2O, P_2O_5, and lower CaO (**Figs. 5.8a, 5.8b, 5.8d and 5.8j**). Due to the high P_2O_5 contents, magma temperature estimations using the apatite saturation thermometry give values of ~950 ºC (**Fig. 5.8j**), much higher than results (~800 ºC) derived from zircon saturation thermometry (**Appendix Table 8**). For four muscovite granites (XY-7), they clearly have much higher Al_2O_3, Na_2O, MnO, and much lower K_2O than the others (**Figs. 5.8a, 5.8c, 5.8d and 5.8i**). These features are more evident in trace element variation diagrams in which samples of the Jiufeng pluton are distinctively plotted into four groups and show different variation patterns from those of the Jiuyishan A-type granites (**Figs. 5.9 and 5.10**). Granites of the Jiufeng pluton have relatively high Ga and Nb contents, transitional between typical A-types and I-types (**Figs. 5.11a and b**), but their Zr and Ba are much lower than those of the Jiuyishan A-type granites (**Figs. 5.11c and d**).

The Chondrite-normalized REE variation patterns (**Fig. 5.12a**) show that the Jiufeng granites invariably show enrichment in LREE and Eu negative anomalies (Eu* = 0.6–0.01). Fractionation between LREE and HREE is greater for less felsic samples.

The degrees of fractionation decrease, whereas the Eu negative anomalies increase as the granites get more felsic (with higher SiO_2). In the ocean ridge granite-normalized variation diagram (**Fig. 5.12b**), all the Jiufeng granites are enriched in LILE, and relatively depleted in HFSE. Elements K, Ba, Nb (Ta), and Zr (Hf) show strong negative anomalies relative to their neighbouring elements. Similar to Eu, the degrees of negative anomaly for these elements become higher as SiO_2 increases. Noticeably, the four muscovite granites showing distinctive major element features also demonstrate peculiar REE and trace element variation patterns (**Fig. 5.12**). Specifically, their REE patterns show prominent tetrad effects ($TE_{1,3}$ =1.16–1.18).

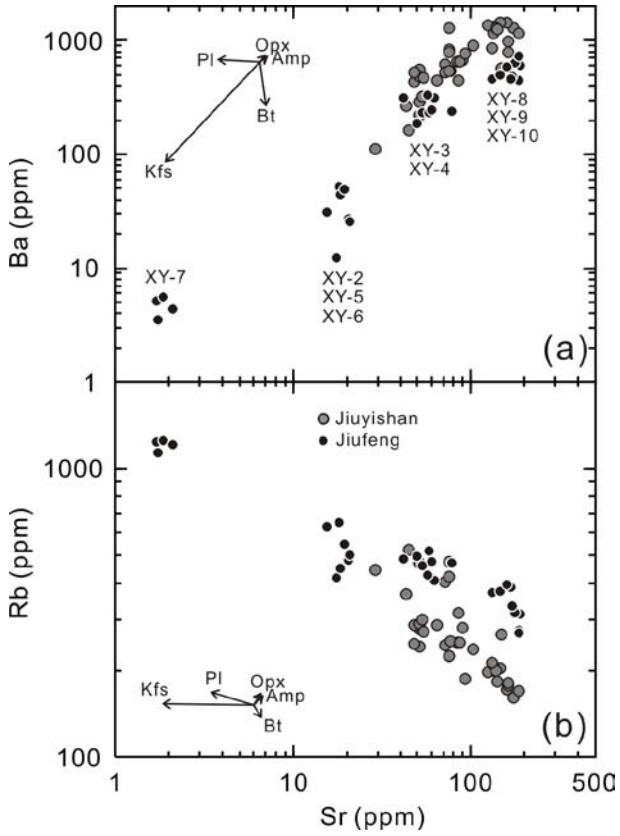

Figure 5.9 Log-log plots showing variations of (a) Ba vs. Sr and (b) Rb vs. Sr of the Jiufeng pluton (solid black circles), as compared with those of the Jiuyishan A-type granites (solid grey circles). Labeled vectors demonstrate the effects of fractionation of 10% each of orthopyroxene, amphibole, plagioclase (An_{36}), K-feldspar (Or_{85}), and biotite (Clemens et al., 2010; Janousek et al., 2004).

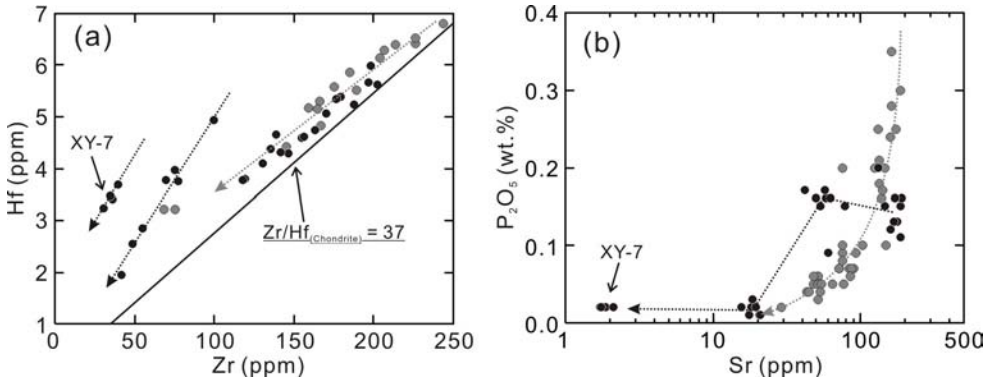

Figure 5.10 Geochemical plots showing distinct variation patterns of the Jiufeng granites, as compared with those of the Jiuyishan A-type granites. Symbols are the same as in **Fig. 5.9**. Dashed grey lines show the interpreted magmatic evolution trend of the Jiuyishan magma; dashed black lines show the possible evolution trend of the Jiufeng magmas.

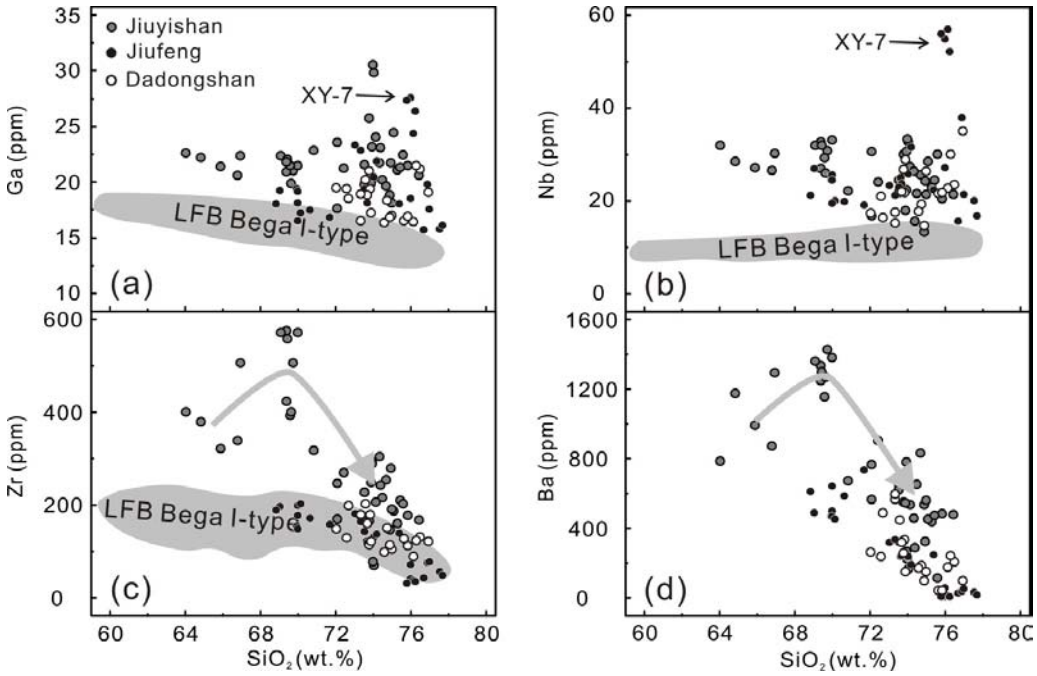

Figure 5.11 Trace element variation diagrams for Ga (a), Nb (b), Zr (c), and Ba (d). Results of the Jiuyishan A-type granites are shown for comparison. The fields for the LFB Bega I-type granites are modified from Collins et al. (1982).

Granites of the Dadongshan batholith show rather restricted SiO_2 variations of between ~72 wt% and 76.5 wt%. It has been shown that these granites have an almost complete overlap with high-Si samples from Fogang batholith, the largest batholith in the region (Huang et al., 2008). It can be seen in **Fig. 5.8** that most major elements decrease as SiO_2 increases. Na_2O does not show any clear variation trend (**Fig. 5.8c**). Overall, the Dadongshan granites are similar to the Jiufeng granites in both major and trace elements (**Figs. 5.8, 5.11 and 5.12**), but they have relatively higher $Fe_2O_3^T$ and lower MgO concentrations (**Figs. 5.8g and h**).

5.2.4. Whole-rock Sr-Nd isotope compositions

Twelve samples from the Jiufeng pluton were selected for whole-rock Nd isotope studies and among them, only those with Rb/Sr ratios lower than 2 were used for Sr isotope examinations. All the samples studied have highly evolved Sr-Nd isotope compositions (**Appendix Table 9**): the age corrected I_{Sr} vary from 0.7125 to

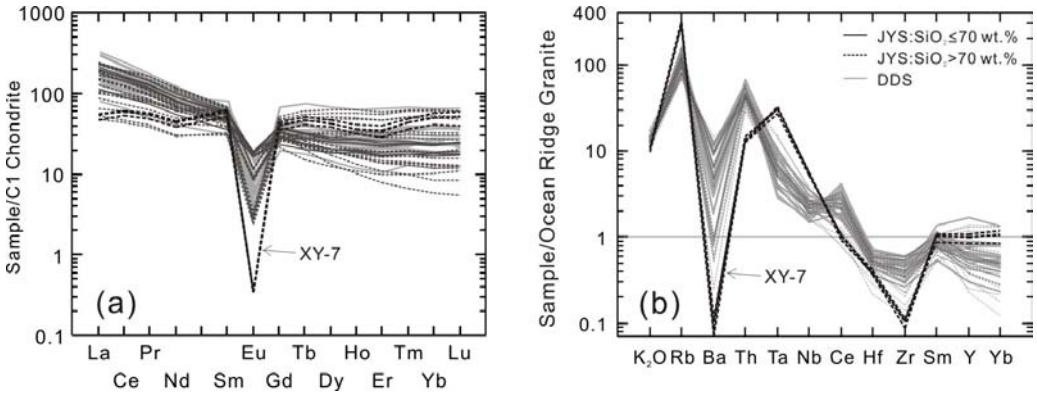

Figure 5.12 (a) C1 Chondrite-normalized rare earth elements (REE) distribution patterns; and (b) ocean ridge granite-normalized major and trace elements distribution patterns. Normalization values are from Sun and McDonough (1989) and Pearce et al. (1984).

0.7143 and are indistinguishable from each other within error; the $^{143}Nd/^{144}Nd$ vary from 0.511907 to 0.512148 with two-stage depleted mantle model ages ranging from 1.97 to 1.72 Ga. εNd (at 160 Ma) of the Jiufeng granites vary from -12.6 to -9.5, showing a rough negative correlation with SiO_2 (**Fig. 5.13**).

Eight samples from the Dadongshan batholith were analysed for their whole-rock Sr-Nd isotopes. Before the analyses, Rb-Sr system had been spiked with ^{84}Sr and ^{87}Rb. All samples studied also have enriched isotopic compositions (**Appendix table 9**), with their initial $^{87}Sr/^{86}Sr$ varying from 0.712 to 0.719 and their εNd(t) from -9.3 to -11.5. Correspondingly, their two stage Nd model ages range from 1.70 Ga to 1.89 Ga. As can be seen in **Fig. 5.13**, there is no correlation between εNd(t) and SiO_2.

5.2.5. In-situ zircon Hf and O isotope compositions

The zircons of the Jiufeng granites were also analysed for their Hf isotopes, but only part of them were examined for their O isotope compositions. The results are listed in sequence analysed **(Appendix Table 11)**. There is a relatively wide range of $^{176}Hf/^{177}Hf$ (0.282336 to 0.282508) and εHf(t = 160 Ma) (-12.0 to -6.3),

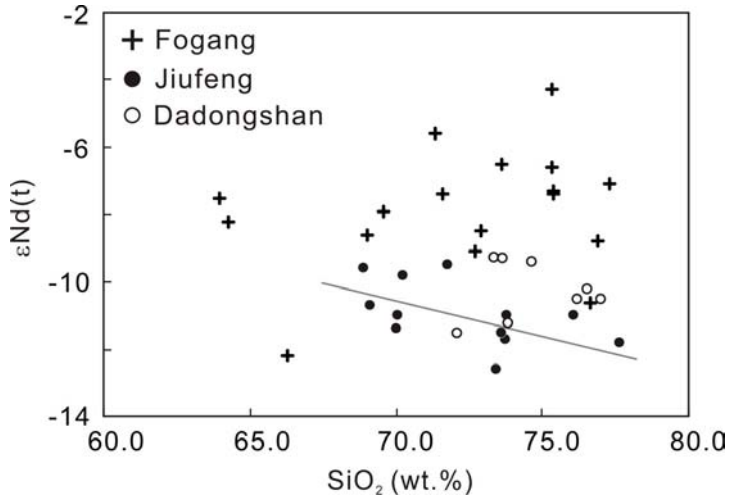

Figure 5.13 Variation of whole-rock εNd(t) with increasing SiO_2. Data of the Fogang batholith are from Li et al. (2007b)

corresponding to a variation of Hf crustal evolution ages from 1.97 Ga to 1.61 Ga. Probability density plots show that every sample has unimodal distribution of εHf(t) (**Figs. 5.14a–e**). There is a minor increase of peak εHf(t) values of about 1 ε unit with decreasing SiO_2, consistent with the variation of εNd(t).

Twenty oxygen isotope ratio analyses of sample XY10-1 give $\delta^{18}O$ values varying from 6.6‰ to 8.8‰. These results exhibit a multi-peak probability distribution pattern (**Fig. 5.14f**). This sample gives the highest εHf(t) and accordingly, the lowest $\delta^{18}O$. Eighteen zircons of sample XY4-3 were analysed. The results show a variation of $\delta^{18}O$ from 7.9‰ to 9.4‰. These results display a semi-unimodal distribution pattern (**Fig. 5.14g**). Fifteen analyses were made for sample XY3-1. The results are similar to that of sample XY4-3 with $\delta^{18}O$ varying from 8.0‰ to 9.3‰ and constituting a semi-unimodal probability density distribution pattern (**Fig. 5.15h**). Only nine analyses on nine zircons were conducted for sample XY2-1. The results show limited variations between 8.1‰ and 8.8‰ and exhibit a unimodal distribution pattern (**Fig. 5.14i**).

As discussed earlier, the oxygen isotope composition of pristine magmatic zircon can be used to estimate the primary oxygen isotope ratios of whole-rocks.

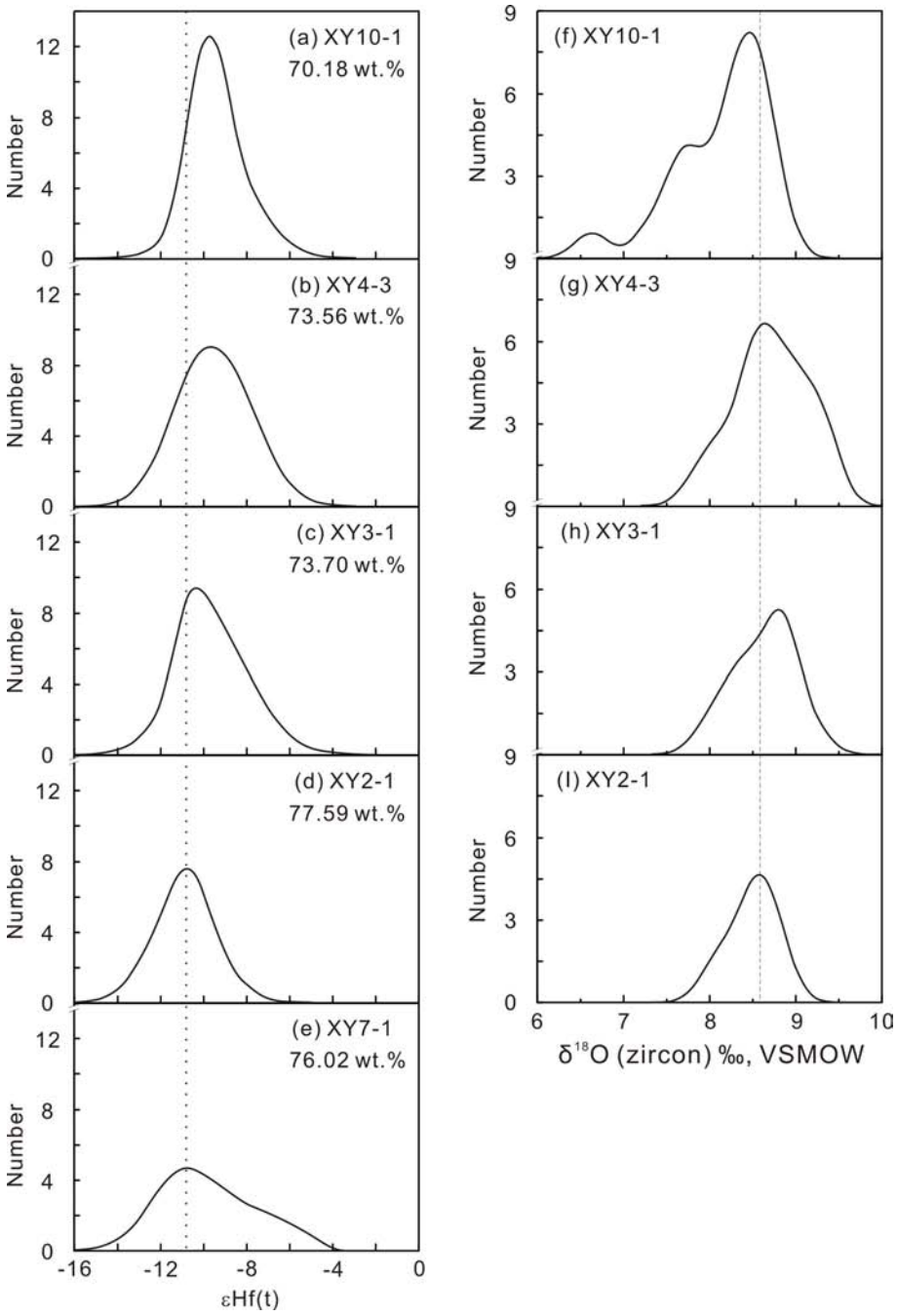

Figure 5.14 Probability distribution of zircon εHf(t) and $\delta^{18}O$ values for the Jiufeng granites. Numbers (top right) in (a)−(e) are SiO_2 concentrations of each sample.

Using the equation $\Delta^{18}O$ (Zrc−WR) = $\delta^{18}O$ (Zrc) − $\delta^{18}O$ (WR) ≈ −0.0612 (wt.% SiO_2) + 2.5 proposed by Valley et al. (2005), the estimated whole-rock $\delta^{18}O$ values vary from 8.5‰ to 11.3‰. The average is similar to the whole-rock data (~10‰) previously published by Li (1992).

Granites of the Dadongshan batholith were only analysed for their zircon Hf isotope compositions. Both samples studied show large variations of $^{176}Hf/^{177}Hf$. εHf(t) of one sample vary from -11.8 to -3.5 (at 165 Ma), whereas that of another vary from -10.2 to -4.9 (at 159 Ma). Both samples show bimodal probability distribution patterns (**Fig. 5.15**). Peak values of the two major peaks are -8 and -9.

5.3. Discussion

5.3.1. Petrogenetic classification: I-, S- or A-type?

The Jiufeng granites are lithologically complex. They contain amphibole-bearing biotite granite, biotite monzogranite, two-mica granite and muscovite leucogranite. These granites are coeval, as their crystallization ages are indistinguishable within error.

For the occurrence of characteristic mineral amphibole (as well as titanite), the metaluminous amphibole-bearing granites can be unambiguously classified as I-type following criteria proposed by Chappell and White (1974, 2001). The genetic classification of biotite granites (from both Jiufeng and Dadongshan), two-mica granites and muscovite leucogranites is somewhat more difficult (**Fig. 5.15**). Despite their high Ga, Nb, and Ga/Al contents (**Figs. 5.11 and 5.16**), the Jiufeng muscovite granites as well as some two-mica granites should not be classified as A-type for a number of reasons. The occurrence of primary muscovite (e.g., **Fig. 5.1d**) and relatively low Zr and Ce concentrations (e.g., **Fig. 5.11c**) of these rocks indicate that the magma was water-saturated and low in temperature. Although muscovite-bearing granites have mineralogical and geochemical features typical of S-type, many studies suggest that such granites in a pluton or suite could also result from magma differentiation of I-type magma and therefore should be classified as differentiated I-type (e.g., Li et al., 2007a; White et al., 1986). Given the fact that granitic magmas commonly have high viscosity (Clemens and Petford, 1999), high degrees of

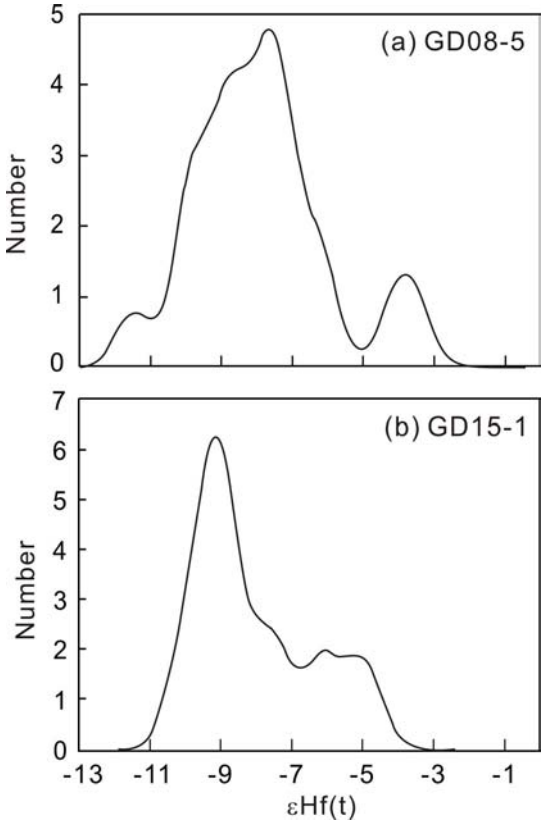

Figure 5.15 Probability distribution of zircon εHf(t) for the Dadongshan granites.

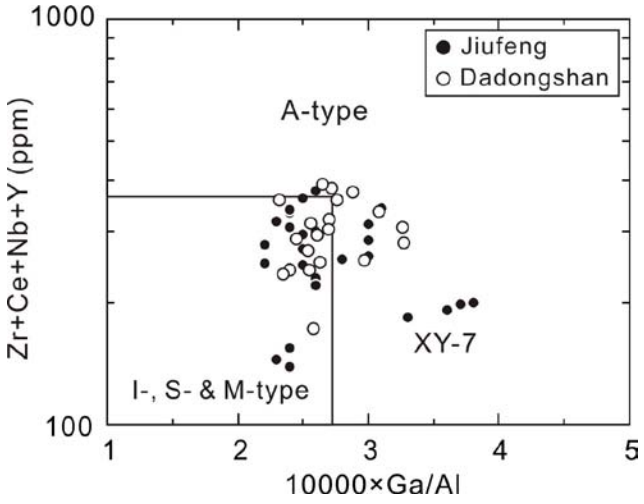

Figure 5.16 Zr + Ce + Nb + Y vs. 10,000 × Ga/Al classification diagram, after Whalen et al. (1987).

fractionation might be unrealistic (Clemens et al., 2010). In the case of the Jiufeng granite, while TiO_2, $Fe_2O_3^T$, and MgO show very well defined linear variation trends, most of the other elements do not (**Figs. 5.8 and 5.10**). The variation of Zr-Hf and Sr-P_2O_5 clearly show that the Jiufeng granites are distinct from the Jiuyishan granites, chemical variations of which were primarily controlled by fractional crystallization. In addition, the whole-rock isotope compositions of the Jiufeng granites also vary significantly with changing SiO_2 content (e.g., **Fig. 5.13**). Taken together, these features refute a differentiation model. In light of the ^{18}O-enriched oxygen isotope compositions, muscovite-bearing granites as well as biotite granites of the Jiufeng pluton should be classified as S-type.

Similar to granites of the Fogang batholith, biotite granites of the Dadongshan batholith were interpreted as fractionated I-types (Huang et al., 2008). Recent studies, however, revealed that some granites of the Fogang batholith were derived from reworking of sedimentary rocks by mantle-derived magma (Li et al., 2009b). An examination of whole-rock isotope compositions of the Fogang granites finds that their εNd(t) vary greatly and irregularly with increasing SiO_2 (**Fig. 5.13**), implying that their chemical variations were unlikely resulted from differentiation of a homogeneous parental magma. Similarly, the Dadongshan biotite granites could possibly be generated directly from melting, rather than being produced through extreme differentiation of a more primitive magma. Due to the similarities in their major and trace elements between the Dadongshan and the Jiufeng biotite granites, the former could also be classified as S-type.

5.3.2. Genesis of the Jiufeng and Dadongshan granites

The Jiufeng granites are heterogeneous in their chemistry and mineralogy. The amphibole-bearing biotite granites of the Jiufeng granites plot exclusively into the field of melts produced from amphibolites (**Fig. 5.17**). The result appears to match very well with them being classified as I-type. However, the model does not explain the occurrence of An-enriched (up to 50) plagioclase in these granites and

why these granites are ^{18}O-enriched ($\delta^{18}O_{Zrc}$ are mostly in the range of 8.0‰–9.4‰), overlap with that of S-type granites in the LFB, SE Australia (Kemp et al., 2008). It is proposed here that the formation of the Jiufeng amphibole-bearing biotite granites was likely a result of magma mixing/mingling, supported by the multiple peak distribution of the zircon oxygen isotope compositions (**Fig. 5.14f**). The addition of some mantle-derived materials to melts of supracrustal origin could produce a metaluminous magma. Amphibole could either be crystallized from the mixed

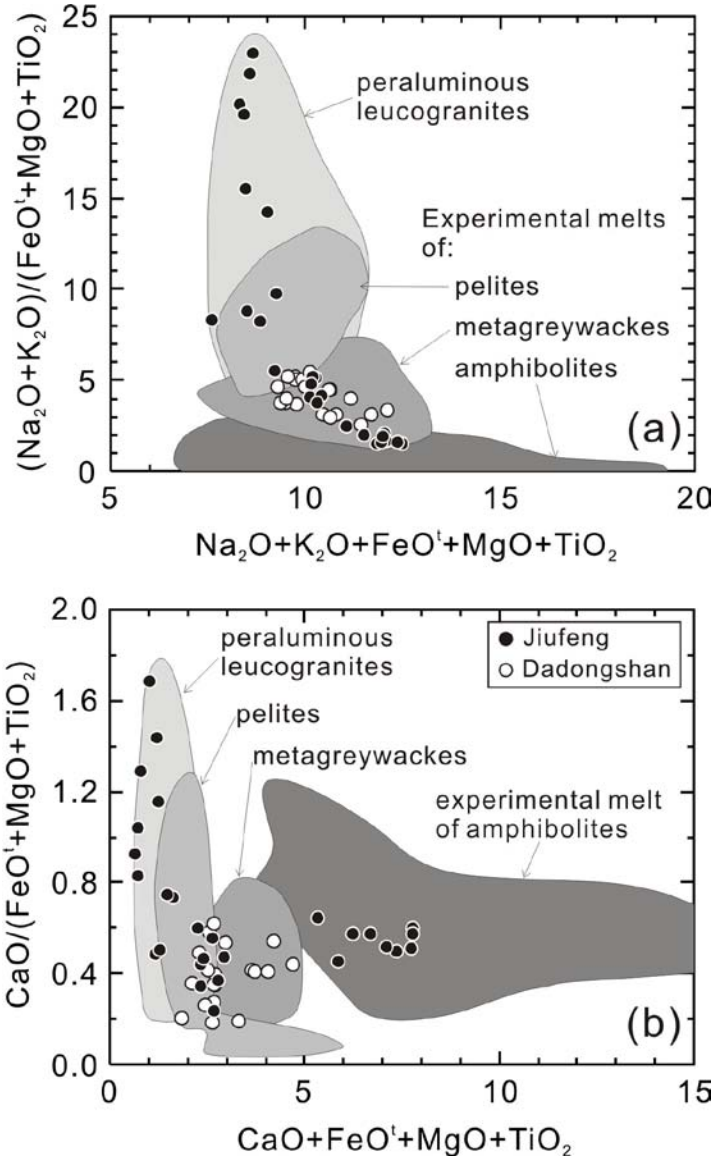

Figure 5.17 Major element compositions of the Jiufeng and the Dadongshan granites as compared with leocugranites and experimental melts. Modified from Jahn et al. (2001), after Patiño Douce (1999).

magma, or alternatively, be introduced from the mantle-derived basaltic magma. In any case, high Ca plagioclase was most likely captured from the basaltic magma, because the amphibole-bearing granite is too felsic (SiO_2 = ~69 wt%) to crystallize such plagioclase.

A mild decrease of εNd(t) with increasing SiO_2 (**Fig. 5.13**) might be further taken as evidence for a mixing/mingling origin of all Jiufeng granites. Principally, magma mixing/mingling would predict linear chemical variation trends (e.g., Collins, 1996). However, such variation pattern is only found for Ti, Fe, and Mg, while most of the others show non-linear variations (**Figs. 5.8 and 5.10**). Another petrogenetic process, most likely the PAE (**Fig. 1.1d**), seems to play a more significant role than the mixing/mingling process. The local occurrence of amphibole-bearing granites in the Jiufeng pluton and the similarity in isotope compositions between these rocks with the others suggest that the material contribution of mantle magma to the genesis of the Jiufeng granite could be minor at the present level of exposure.

Muscovite granites, two-mica granites and biotite granites of the Jiufeng pluton have major element compositions similar to peraluminous leucogranites, and experimental melts of pelites and metagreywackes (**Fig. 5.17**). The four muscovite-bearing granites studied have distinctive geochemical compositions. In particular, their REE distribution patterns show prominent tetrad effects (**Fig. 5.12a**), produced from hydrothermal reactions, indicating that the magma was enriched in water (e.g., Jahn et al., 2001; Zhao et al., 2002). Water enrichment in magma has been commonly interpreted to have resulted from magma differentiation. The abrupt changes of Ga, Nb, Na_2O, K_2O, etc for these muscovite granites (**Figs. 5.8 and 5.11**), however, lend little support for fractional crystallization. Magma crystallized to form the Jiufeng muscovite granites were most likely derived from melting of a water-saturated sedimentary source, and was originally water saturated. This proposition is not inconsistent with results of experimental studies, which showed that melts produced from partial melting of water-saturated sedimentary rocks are extremely enriched in Na_2O at the expense of K_2O (Patiño Douce, 1996; Patiño

Douce and Harris, 1998). Degassing of a water-enriched magma upon intruding into the lower crust would probably trigger hydrothermal reactions.

Different from muscovite granites, the biotite granites and some two-mica granites of the Jiufeng pluton contain more K_2O and P_2O_5 (**Figs. 5.8d and j**), but much less CaO and Na_2O (**Figs. 5.8b and c**). Magmas that crystallized to form these granites were more likely generated by dehydration (of biotite and muscovite) melting of meta-sedimentary rocks at higher temperatures (**Fig. 5.18**). Incongruent melting of biotite and muscovite would release K_2O to melts, e.g., Biotite + Quartz + Plagioclase = Garnet + Orthopyroxene + melt + Ilmenite ± K-feldspar (e.g., Stevens et al., 2007). The process would also release apatite therein to the melt. The enrichment in K_2O and the depletion in CaO and Na_2O of the biotite granites possibly image their source characteristics. The enrichment in P_2O_5, however, was probably a result of higher solubility of apatite in peraluminous melts (Bea et al., 1992; Wolf and London, 1994).

To summarize, granites of the Jiufeng pluton have different origins. They were crystallized from chemically heterogeneous magmas that had been produced

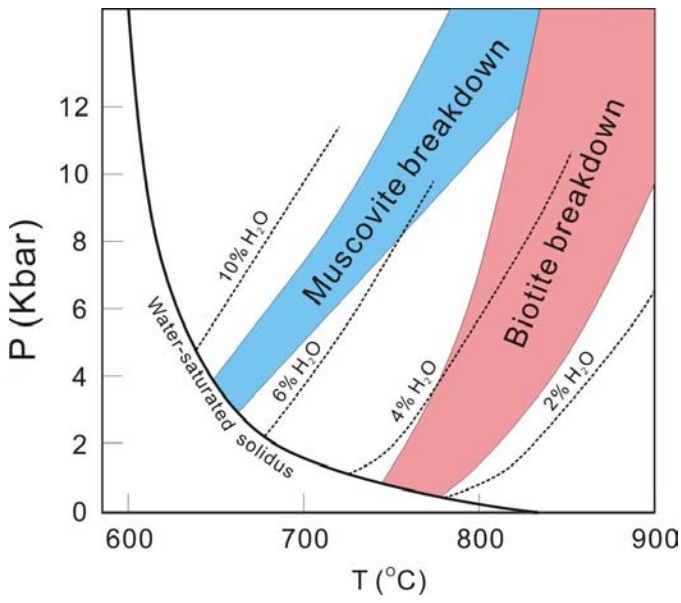

Figure 5.18 Phase diagram showing common partial melting reactions of metasedimentary rocks (Vielzeuf and Montel, 1994).

mainly from melting of various sedimentary rocks at diverse conditions. Local addition of mantle-derived materials to sedimentary melts could produce granites similar to I-types.

Similar to those of the Jiufeng pluton, the Dadongshan biotite granites also have major element compositions similar to melt of metagreywackes (**Fig. 5.17**) and have isotopic and chemical compositions distinct from coeval basaltic rocks in the region (**Figs. 5.19 and 5.20**). Although their bimodal distributions of zircon Hf isotopes (**Fig. 5.15**) signify the contribution of mantle-derived materials, they could be derived dominantly from melting of sedimentary rocks.

5.3.3. Implications

The above studies show that mineralogically and geochemically complex granites in a pluton may be derived from distinct sources. It has been suggested that S-type melts could be quickly extracted from their source regions soon after their generation (less than 100 years; Villaros et al., 2009), leaving little chance for them be homogenized. Usually it takes much longer time for granitic magmas to cool down in a magmatic chamber. It is uncertain whether the magma could be homogenized at this stage. The preservation of source heterogeneities in the Jiufeng granites suggests that hybridization and differentiation of granitic magmas probably operate in small scales only. The homogenization processes might be impeded by high viscosity of granitic magmas (Clemens and Petford, 1999). Alternatively, granitic magmas could be transported through dyke ascent (Petford et al., 2000). Geochronological studies have revealed that granites in a pluton could be formed in a very long time of up to 10 Ma (e.g., Coleman et al., 2004; Li et al., 2007b). The time range and field evidences for sheeting in granitic plutons (Clemens et al., 2010) support the construction of a granitic body through incremental assembly of magmatic batches (Clemens et al., 2010; Coleman et al., 2004). Incremental additions of granitic magmas into a granitic body would best explain the limited hybridization and the preservation of heterogeneities in granites. It is proposed here

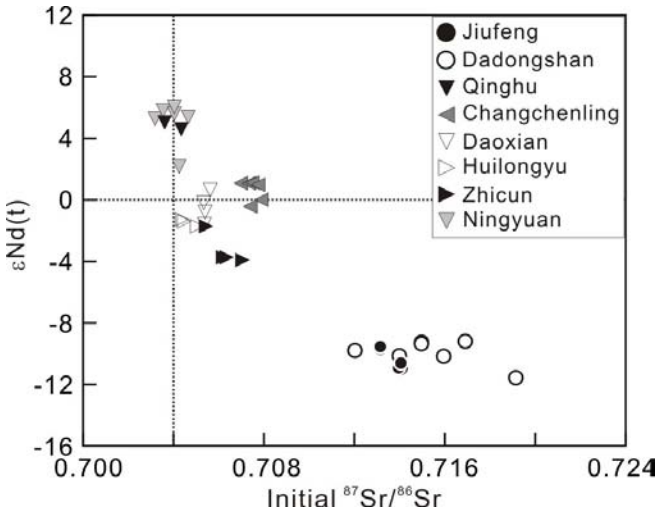

Figure 5.19 Whole-rock Sr-Nd isotope compositions. Those of basaltic rocks (triangles) are from Jiang et al. (2009), Li et al. (2004a) and Wang et al. (2003b).

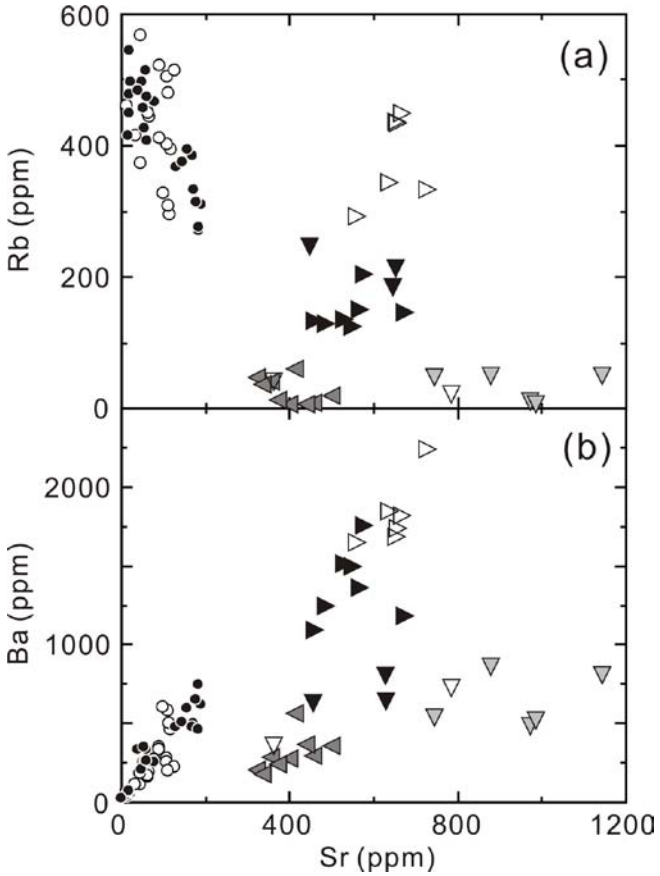

Figure 5.20 (a) Sr–Rb and (b) Sr–Ba showing trace element variations of the Jiufeng and the Dadongshan granites. Symbols and sources of data are the same as in the **Fig. 5.19**.

that the seemingly coeval granites in a pluton/suite (e.g., the Jiufeng granites) might also be emplaced at different stages even when they have indistinguishable crystallization ages.

Extra caution is also required when group granites into a suite for genetic classification purpose, because even granites within a single pluton might have completely different origins.

5.4. Conclusions

In the light of existing experimental results, intergrated petrological, mineralogical, geochemical, and isotopic studies show that both the Jiufeng and the Dadongshan granites were most likely derived from melting of heterogenesous metasedimentary rocks at ca. 159 Ma. Peritectic Assemblage Entranment process probably operated as the controlling petrogenetic process in the source region, whereas magma mixing/mingling process with secondary effect also operated locally. Chemical variations exhibited by granites studied in this chapter were mainly originated from the source region.

Chapter 6: Crustal remelting for the genesis of Jurassic high-K granites in the coastal region of the western Guangdong Province, SE China

(This chapter contain contents of a manuscript by **Huang, H.-Q., Li, X.-H., Li, Z.-X., and Li, W.-X., Intraplate crustal remelting for the genesis of Jurassic high-K granites in the coastal region of the western Guangdong Province, southeastern China.** The manuscript has been submitted to the Journal of Asian Earth Sciences for publication.)

6.1. Introduction

High-K granites are also widely distributed in the coastal region of the western Guangdong Province, but knowledge with respect to their genesis is poor. For example, geochronology of these rocks is poorly constrained, and both Jurassic and Cretaceous ages have previously been suggested (e.g., Sun, 2006). Two types of high-K granites in this region are investigated in details: one includes granite stocks/small plutons that are dominantly composed of amphibole-bearing rocks (Group A: Xiaoliang (~140 km^2), Gangwei (~110 km^2) and Lunshui (~60 km^2) plutons); the other includes large plutons/batholiths that are mainly composed of biotite granites (Group B: Gudoushan (~1500 km^2) and Wuguishan (~500 km^2) plutons). The aim is to reveal the difference in material sources for the genesis of the two types of granites and the differences in sources and conditions between these granites and those distributed inland SE China.

6.2. Analytical results

6.2.1. Mineralogy and petrology

Group A granites

Rocks from the Xiaoliang pluton vary from amphibole monzogranite to biotite K-feldspar granite. They are composed mainly of ~30%−35% plagioclase, ~25%−40% K-feldspar, ~15%−25% quartz, ~5%−8% biotite, ~4%−8% amphibole and contain minor amounts of zircon, apatite, titanite and allanite (Guangdong, 1988). K-feldspar in these rocks is enriched in normative Or composition (**Appendix Table 3; Fig. 6.1**). Thin section examinations show that amphiboles in these rocks vary in colour from yellowish-brown to dark green under a microscope (e.g., **Fig. 6.2**). Some biotite grains have been replaced by chlorite and contain large discrete crystals of apatite. Analyses show that both amphibole and biotite of the Xiaoliang pluton are Fe-enriched (**Appendix Tables 6 and 7**), and can be classified as ferro-edenitic hornblende and ferro-biotite (**Figs. 6.3a and 6.4**), respectively.

Rocks from the Gangwei and Lunshui plutons are dominantly amphibole granodiorite and quartz-monzonite. Geochemical and isotopic results show that the two plutons might be genetically linked and constitute a single pluton at depth (Li et al., 2000c). They are mainly composed of K-feldspar (~10%−25%), plagioclase

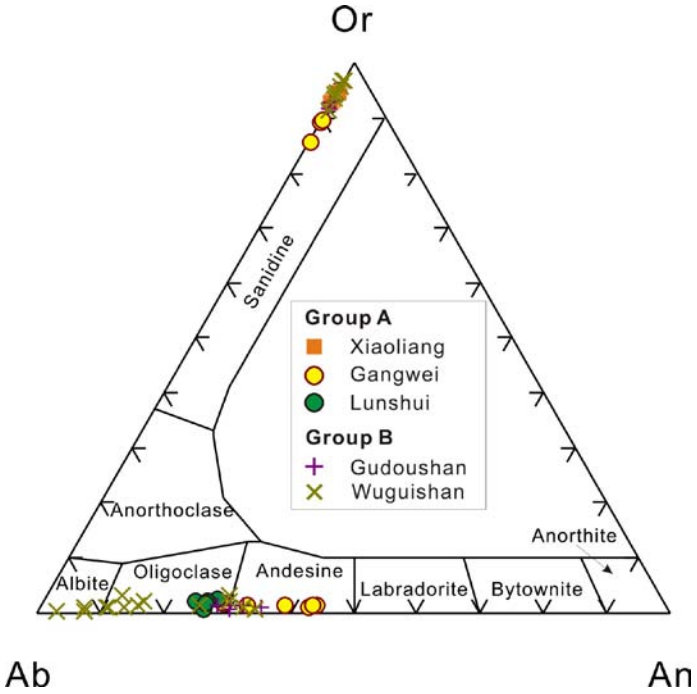

Figure 6.1 Classification diagram for feldspars.

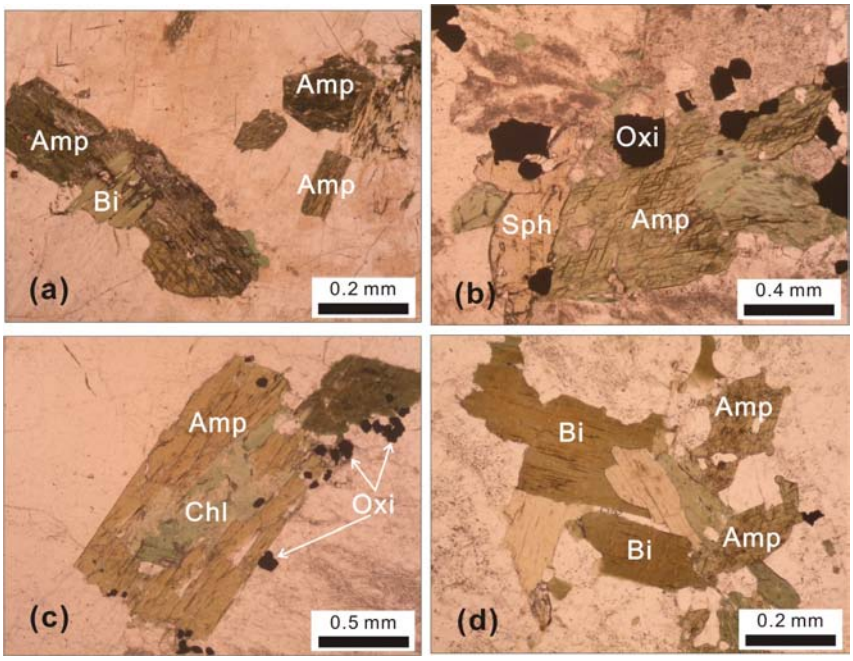

Figure 6.2 Thin-section photomicrographs (plain polarised light) showing amphiboles, biotites, chlorites and Fe-Ti oxides.

(~35%−50%), quartz (~15%−30%), amphibole (~10%−15%), biotite (~3%−5%) and titanite (~5%); accessory minerals include zircon, magnetite, and allanite (Guangdong, 1988). Plagioclase has relatively high An numbers, ranging from 24 to 44; K-feldspars are mostly sanidine with high percentage of orthoclase (**Fig. 6.1**). Plagioclase of the Gangwei pluton is more calcic than that of the Lunshui pluton. Amphiboles commonly coexist with titanite and Fe-Ti oxides (**Figs. 6.2b and 6.2c**). Both amphiboles and biotites of the Gangwei and Lunshui plutons are more magnesium-rich than those of the Xiaoliang pluton (**Figs. 6.3 and 6.4**). Amphiboles can be classified as actinolite, actinolitic hornblende and edenite (**Fig. 6.3**); biotites are plotted in the area for syntexis-type and have compositions similar to magnesio-biotite (**Fig. 6.4**). Mg-enriched amphiboles commonly crystallise at higher oxygen fugacities, and may thus be used for P-T estimations (Anderson and Smith, 1995). Physical-chemical conditions for the crystallization of magnesian amphiboles of the Gangwei and Lunshui plutons are estimated using a spreadsheet provided by Ridolfi et al. (2010). The results show that amphiboles of the Lunshui pluton were crystallised at 812−845 ºC and 1.4−1.7 kbar from an oxidised (ΔNNO = 0.1−0.4)

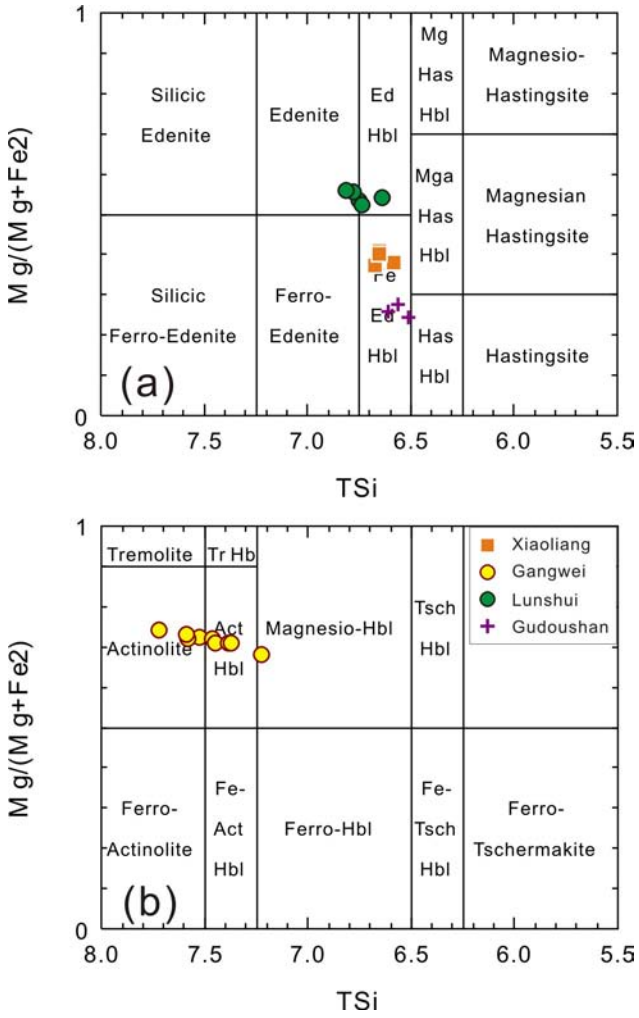

Figure 6.3 Classification diagrams for calcic group amphiboles (Hawthorne, 1981). a: ANa + AK > 0.5; Ti < 0.5; Fe3 > AlVI; b: ANa + AK < 0.5; Ti < 0.5.

magma (**Appendix Table 12**). Temperature and pressure estimations for the Gangwei amphiboles are lower than that for the Lunshui pluton and plot outside the reliable range as suggested by Ridolfi et al. (2010). They are therefore considered invalid, and expected true values should be similar to those of the Lunshui samples.

Group B granites

The Gudoushan pluton comprises mostly of biotite granites. Locally, there are also some amphibole-bearing biotite granites and tourmaline-bearing granites. Rocks of the Gudoushan pluton are composed of ~40%−45% K-feldspar, ~20%−30% plagioclase, ~20%−35% quartz, ~5% biotite and 0−3% amphibole and minor amount

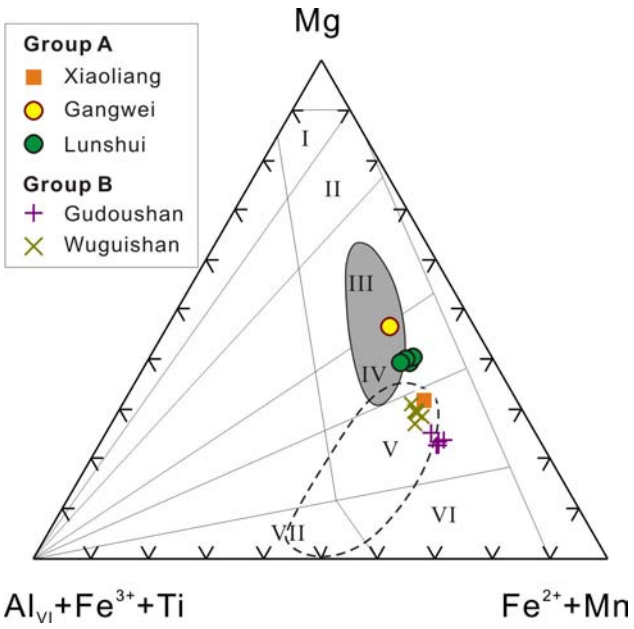

Figure 6.4 Classification diagram for biotites (Foster, 1960). The grey and dashed line fields are modified from Xu et al. (1984), representing compositions of biotites from syntexis-type granites and transformation-type granites, respectively. I – phlogopite; II – iron-phlogopite; III – eastonite; IV – magnesiobiotite; V – ferri-biotite; VI – annite (siderophyllite); VII – alumino-mica.

of titanite and muscovite (Guangdong, 1988). Accessory minerals include zircon, apatite and Fe-Ti oxides. K-feldspar has restricted variation of normative Or from 92 to 95. Plagioclase varies from oligoclase to andesine in composition with An ranging from 29 to 36 (**Fig. 6.1**). Small amphiboles commonly coexist with biotites (**Fig. 6.2d**) and have compositions similar to ferro-edenitic hornblende (**Fig. 6.3**). Biotites are also enriched in Fe and can be classified as ferri-biotite (**Fig. 6.4**).

The Wuguishan pluton consists mainly of coarse-grained biotite granites with ~35%−40% K-feldspar, ~20%−25% plagioclase, ~30% quartz and ~5% biotite (Guangdong, 1988). K-feldspar has restricted variation of normative Or from 92 to 97, whereas plagioclase varies greatly in composition with An ranging from 5 to 32 (**Fig. 6.1**). No amphibole has been identified in the Wuguishan pluton. Accessory minerals such as allanite, zircon, Fe-Ti oxides and apatite can be seen in thin sections under a microscope. The biotites are enriched in iron and can also be classified as

ferro-biotite (**Fig. 6.4**). Biotites from group B granites are exclusively plotted in the field for transformation-type biotites (**Fig. 6.4**).

6.2.2. Zircon U-Pb geochronology

Four samples, one from each pluton, are examined for their crystallization ages. Results are shown in **Appendix Table 10** and **Fig. 6.5**, and are interpreted as below.

Sample GD47-1 (an amphibole-bearing K-feldspar granite from the Xiaoliang pluton, lat. 21°31'10"N, long. 110°59'14"E):

Zircons from this sample are mostly idiomorphic, commonly 100–150 μm in width with low aspect ratios (2:1 to 1:1). Most magmatic zircon rims show well-developed concentric zoning, with some containing small dark cores (e.g., **Fig. 6.5a**). It is uncertain whether the cores were inherited or comagmatic. Fifteen zircon grains were targeted on their magmatic domains. All analyses give low common lead (f_{206} < 0.49%), low U and Th contents (129–976 ppm and 58–475 ppm, respectively). Their Th/U ratios have a narrow range of 0.38 to 0.80. Two analyses give near concordant $t_{206/238}$ ages of 767 Ma and 789 Ma, amongst the others. CL images of these two zircons do not show core-rim structure. So, they are probably xenocrysts, implying that the magma might have been contaminated by wall-rocks. The remaining 13 analyses give a weighted mean $^{206}Pb/^{238}U$ age of 159.4 ± 1.3 Ma (MSWD = 0.82), identical within errors to the Concordia age of 159.3 ± 1.4 Ma (MSWD = 1.04) (**Fig. 6.5a**). Thus, sample GD47-1 from the Xiaoliang pluton was most likely crystallized at 159 ± 1 Ma.

Sample GD51-1 (a granodioritic sample from the Gangwei pluton, lat. 22°04'07"N, long. 111°45'07"E):

Zircons from the Gangwei pluton sample are euhedral, ranging from 100 μm to 400 μm in length, and have aspect ratios mostly between 1:1 and 4:1. Most zircons show clear concentric zoning under CL images (**Fig. 6.5b**). Fifteen analyses on 15

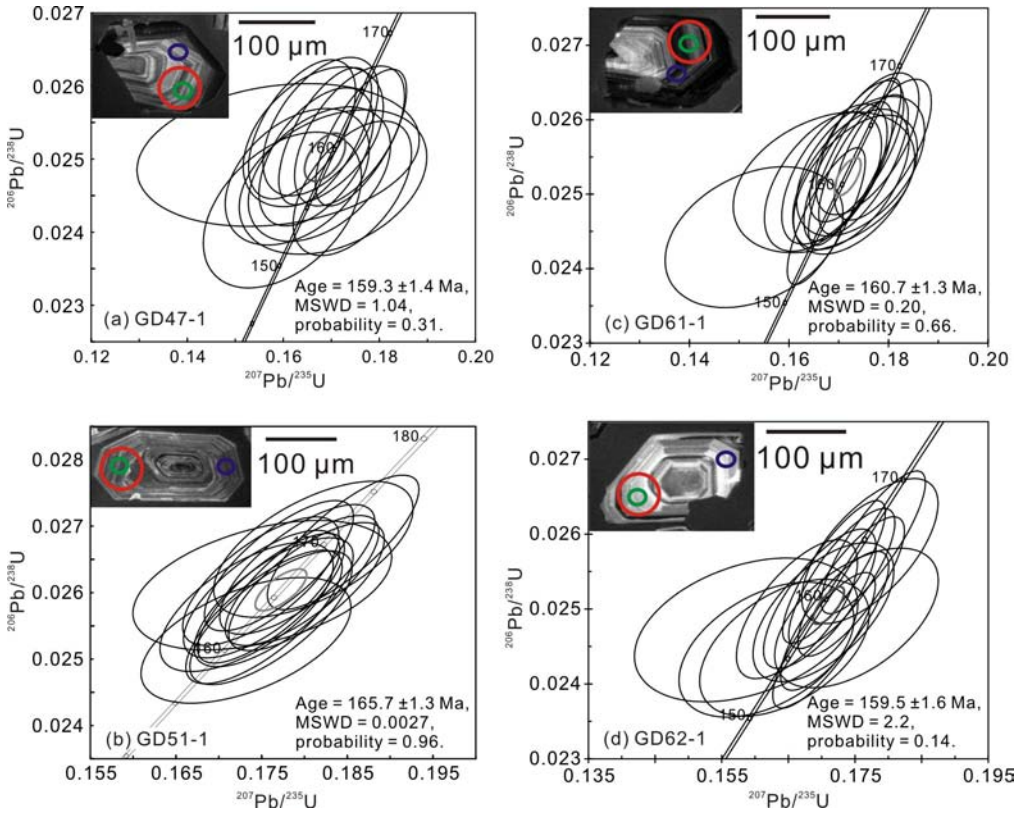

Figure 6.5 Zircon U-Pb Concordia diagrams showing chronological results of the Jurassic high-K granites in the coastal region. Representative CL images are shown at the top left corner of each diagram. Small green and blue ellipses indicate the SIMS analytical spots for U-Pb and O isotopes, respectively. Red circles show the LA-MC-ICP-MS analytical spots for Lu-Hf isotopes.

zircons were performed. These analyses give moderate U and Th contents, ranging from 293 ppm to 1379 ppm and 110 ppm to 957 ppm, respectively. Corresponding Th/U ratios have small variations (0.37 to 0.77). All analyses give common Pb compositions (f_{206}) lower than 0.22%. The measured Pb/U ratios are concordant and are indistinguishable within errors (**Fig. 6.5b**). The weighted mean $^{206}Pb/^{238}U$ age of the 15 analyses is 165.7 ± 1.3 Ma (MSWD = 0.96), the same as the Concordia age. The weighted mean age of 166 ± 1 Ma is interpreted as the crystallization age of the Gangwei pluton.

Sample GD61-1 (an amphibole-bearing biotite granite from the Gudoushan pluton, lat. 22°14'15"N, long. 112°55'06"E):

Zircons from the amphibole-bearing biotite granite are euhedral, varying greatly in length from <100 μm to >500 μm and aspect ratios from 1:1 to 6:1. Most zircons show well-developed concentric zoning and some appear to have core-rim structure under CL images (**Fig. 6.5c**). Fourteen analyses were made on 14 zircons which had been well characterised by microphotographs and CL images. Those zircons analysed show large variations in U, Th, and Th/U (125–1174 ppm, 87–457 ppm, and 0.15–1.28, respectively). They have low common lead with f_{206} value <0.51%. The measured Pb/U ratios are indistinguishable within analytical errors. The weighted mean $^{206}Pb/^{238}U$ age of the 14 analyses is 160.7 ± 1.3 Ma (MSWD = 0.77), identical to the Concordia age (**Fig. 6.5c**). It is interpreted that 161 ± 1 Ma gives the best estimation of the crystallization age of the Gudoushan pluton.

Sample GD62-1 (a biotite granite from the Wuguishan pluton, lat. 22°29'53"N, long. 113°19'17"E):

Zircons from the biotite granite sample are mostly idiomorphic. They vary in lengths from ~100 μm to 300 μm and have aspect ratios between 1:1 and 4:1. It is clear under CL images that a few zircons contain cores, but most zircons show well-developed concentric zoning and do not show core-rim structure (**Fig. 6.5d**).

Fourteen analyses were conducted on 14 zircon grains. The analyses showed large variations in U and Th, from 145 ppm to 1632 ppm and 104 ppm to 835 ppm, respectively. Correspondingly, their Th/U ratios range from 0.37 to 0.76. All analyses give low common lead (f_{206} < 0.51%). The measured Pb/U ratios are concordant within errors (**Fig. 6.5d**). The weighted mean $^{206}Pb/^{238}U$ age of 14 analyses is 159.5 ± 1.6 (MSWD = 1.4), the same as the Concordia age. Thus, 160 ± 2 Ma gives the best estimation of the crystallization age of the Wuguishan pluton.

Overall, geochronological results show that many granites along the coastal region are broadly coeval. They were generated in a short period of time between 166 Ma and 159 Ma. The result of the Gangwei pluton is slightly older than previously published biotite K-Ar age of 156 ± 2 Ma (Yu et al., 1998) and Rb-Sr

mineral isochron age of 154 ± 1 Ma (Li et al., 2000c). These data allow an estimation of cooling rate of >50 ºC/Ma from >900 ºC for the closure of U-Pb system in zircon (Lee et al., 1997) to ~300−400 ºC for the closure of Rb-Sr system in biotite (Jenkin et al., 2001). Such a fast cooling rate coincides with the shallow depth (~5 km) of emplacement of the Gangwei-Lunshui pluton by aforementioned hornblende geobarometer estimates.

6.2.3. Whole-rock geochemistry

A total of 26 samples have been analysed for their major and trace element compositions (**Appendix Table 8**). Their major elements show large compositional variations. Except $Fe_2O_3^T$ and P_2O_5, most major elements do not show coherent linear variation trends (**Fig. 6.6**). For example, CaO contents of the Gangwei pluton decrease with increasing SiO_2, whereas those of the Xiaoliang pluton show a reverse trend (**Fig. 6.6b**). Conversely, while K_2O concentrations of the Gangwei pluton increase as SiO_2 increases, those of the Xiaoliang pluton show a reverse trend (**Fig. 6.6d**). Geochemically, these plutons vary greatly from alkalic to calc-alkalic (**Fig. 6.7**). However, variations of trace elements are more regular. There is a constant mild increase in Nb and Y and decrease in Zr and Ga as SiO_2 increases (**Fig. 6.8**).

As can be seen from **Fig. 6.6**, the group A granites have lower SiO_2 (64 wt%−72 wt%) than those of group B (70 wt%−76 wt%). The difference between the two groups is also evident in the Sr-Rb and Sr-Ba plots in which samples of the group A plutons plot closer to coeval basaltic rocks in the region than those of group B plutons (**Fig. 6.9**). In the Chondrite-normalised REE variation diagram (**Figs. 6.10a and 6.10b**), both groups show enrichment in LREE over HREE. Nonetheless, differences in the degrees of differentiation of LREE from HREE and the degrees of Eu anomalies between the two groups are evident. Group A granites show highly differentiated REE ($[La/Yb]_N$ = 8.3–31.5) pattern and weak Eu negative anomalies (Eu* = 0.55−0.96). By comparison, group B granites have less differentiated REE ($[La/Yb]_N$ = 2.1−12.8) and stronger Eu negative anomalies (Eu* = 0.09−0.59).

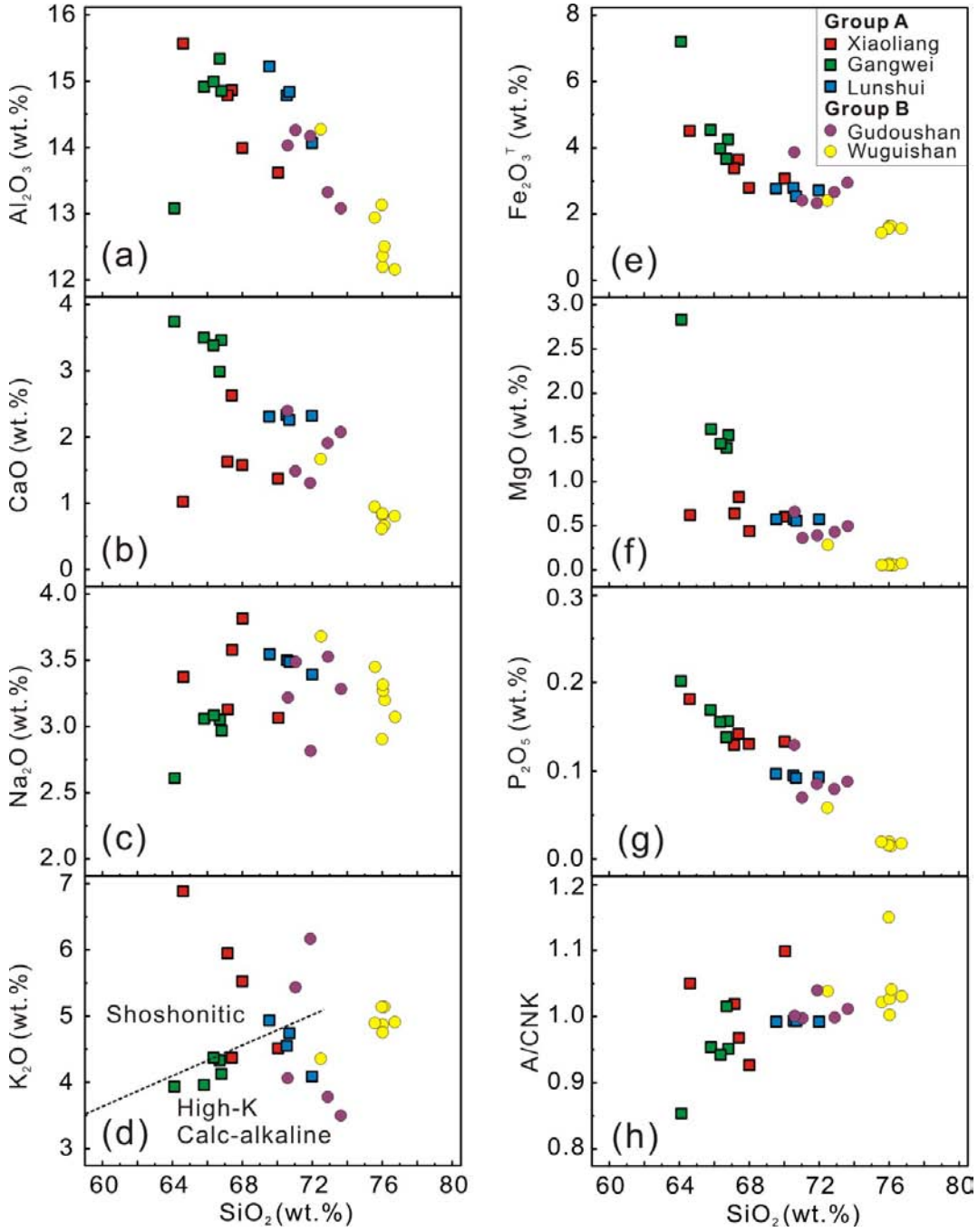

Figure 6.6 Major element compositions (a–g) and the calculated A/CNK values (h) showing chemical variations of the Jurassic high-K granites in the coastal region. The dashed line in (d) is after Peccerillo and Taylor (1976).

Difference between the two groups is also evident in the primitive mantle-normalised trace element distribution patterns (**Figs. 6.10c and 6.10d**). All samples from the group A plutons invariably show depletion in Ba, Nb, Ta, P, and Ti and enrichment in Rb, Th, K, Zr, and Hf (**Figs. 6.10c**). Samples of group B plutons, although exhibiting

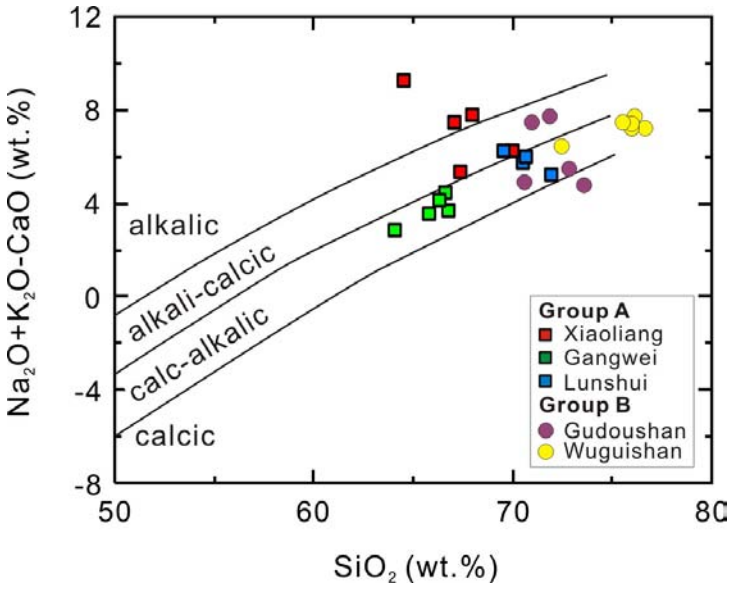

Figure 6.7 Chemical classification diagram (Frost et al., 2001) showing compositional variations of the high-K granites in the southern coastal region of the Guangdong Province.

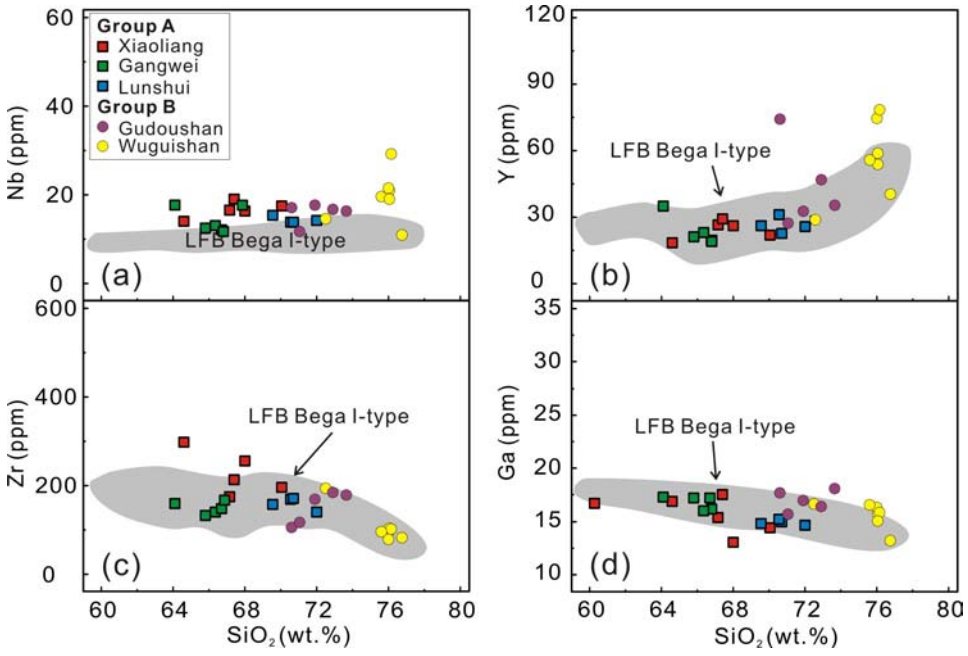

Figure 6.8 Trace element variation diagrams for Nb (a), Y (b), Zr (c), and Ga (d) with increasing SiO_2. The fields for the LFB Bega I-type granites are modified from Collins et al. (1982).

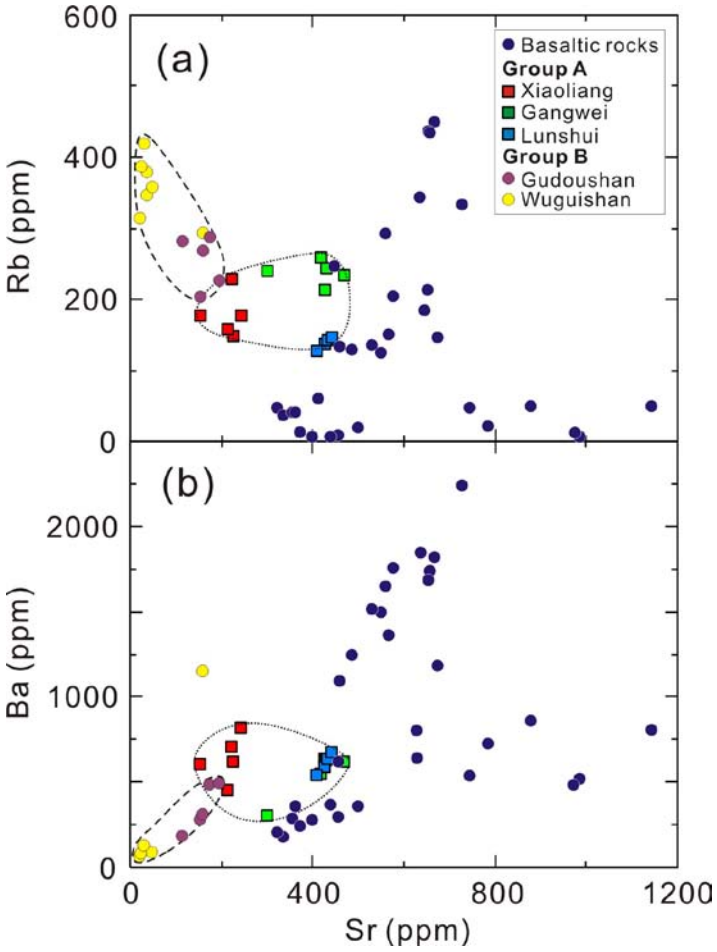

Figure 6.9 Variations of Rb (a) and Ba (b) versus Sr for the studied high-K granites, as compared with spatially related coeval basaltic rocks. Data for basaltic rock are from Jiang et al. (2009), Li et al. (2004a) and Wang et al. (2003b).

similar differentiation patterns, their Ta, Zr, and Hf negative anomalies are less significant, whereas their degrees of enrichment in Rb and U and depletion in Ba, Sr, P, and Ti are more enhanced (**Figs. 6.10d**).

6.2.4. Whole-rock Sr-Nd isotope compositions

Six samples from group A plutons were analysed for their whole-rock Sr-Nd isotope compositions (**Appendix Table 9**). They have evolved radiogenic isotope compositions with initial $^{87}Sr/^{86}Sr$ (0.7057−0.7077) and $^{143}Nd/^{144}Nd$ (0.512101−0.512272), corresponding to εNd(t = 160 Ma) values of -6.46 to -3.13. Their two-stage depleted-mantle model ages (T_{2DM}) are in the range of 1.47−1.20 Ga.

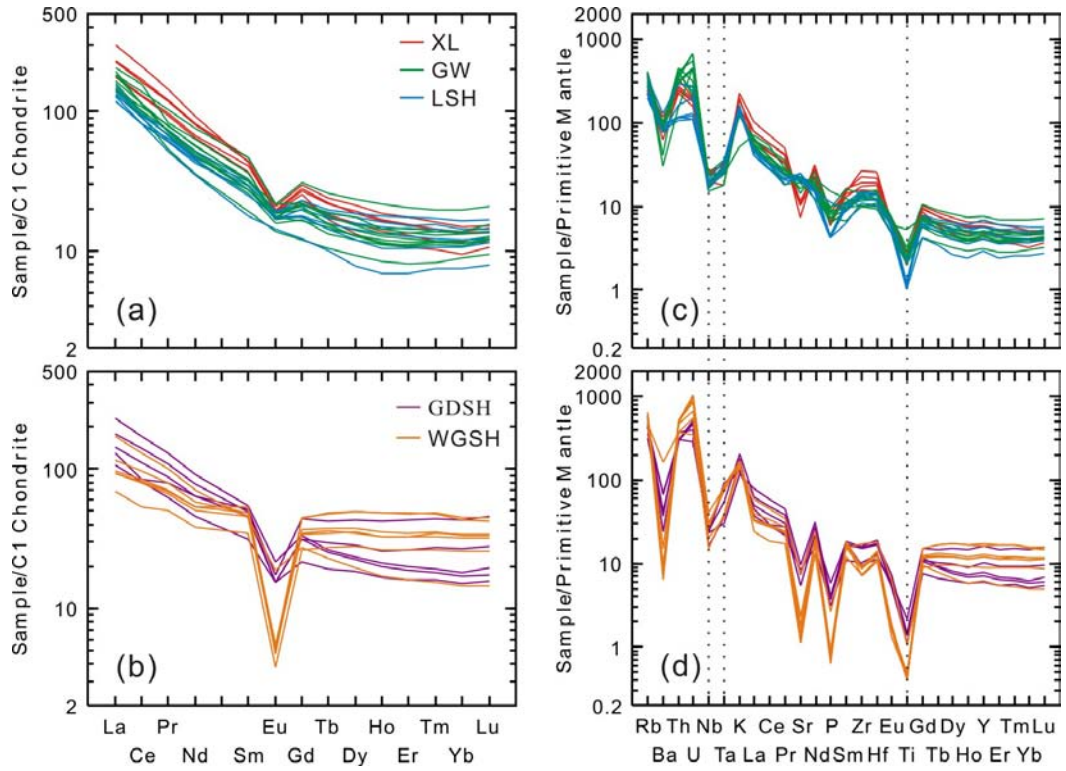

Figure 6.10 C1 Chondrite-normalised rare earth elements (REE) distribution patterns (a)−(b) and Primitive Mantle-normalised major and trace elements distribution patterns (c)−(d). Normalization data from Sun and McDonough (1989).

As can be seen in **Fig. 6.11**, Sr-Nd isotope compositions of group A are less evolved than the dominant coeval granites, and approach those of coeval basaltic rocks in the region (**Fig. 6.11**).

6.2.5. In-situ zircon Hf-O isotopes

Those zircons targeted for their U-Pb compositions and some extra magmatic zircons showing well-developed oscillatory zonings were analysed for their Hf and O isotope ratios. The analyses were performed in three sessions (**Appendix Table 11**).

Session one:

Eighteen zircons of the sample GD47-1 from the Xiaoliang pluton have been analysed. Results show that zircons have heterogeneous Hf and O isotope

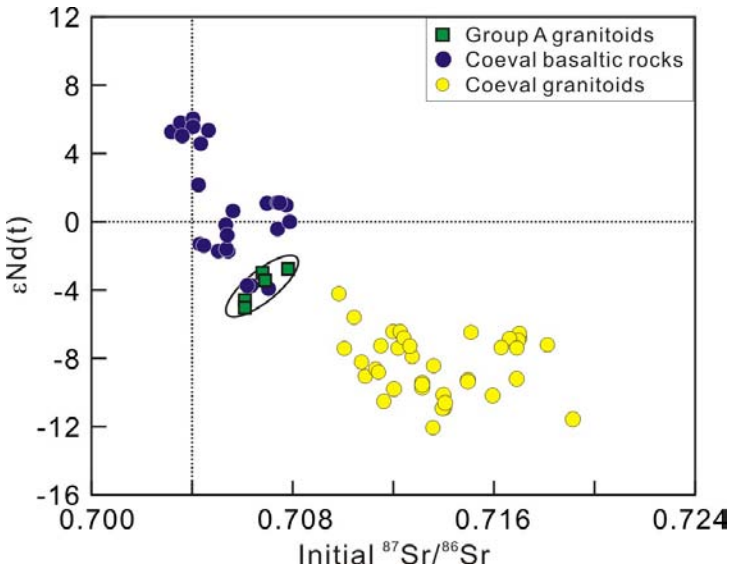

Figure 6.11 Whole-rock Sr-Nd isotope compositions for the Jurassic high-K granites emplaced in the coastal area. Data for coeval granites (data from Huang et al., 2011; Li et al., 2007; Xu et al., 2007) and basaltic rocks are shown for comparison. Basaltic rock data are from Jiang et al. (2009), Li et al. (2004a) and Wang et al. (2003b).

compositions. The measured $^{176}Hf/^{177}Hf$ ratios vary from 0.282508 to 0.282641, corresponding to εHf(t = 160 Ma) ranging from -5.9 to -1.2 and two-stage Hf depleted-mantle model ages (T_{DM}^{C}) (using a Lu/Hf value = 0.015 for the average continental crust) of 1.59-1.29 Ga. The zircon oxygen isotopes ($\delta^{18}O_{zircon}$) range from 6.8‰ to 7.9‰.

For sample GD51-1 from the Gangwei pluton, 18 analyses were performed on 18 zircons for Hf isotope compositions and twenty-three analyses on 19 zircons for O isotope ratios. There are some random duplicate analyses on some zircon grains to check the O isotopic homogeneity of these zircons and the reproducibility of analyses in this session (session 1). The measured $^{176}Hf/^{177}Hf$ ratios vary slightly from 0.282613 to 0.281672, corresponding to εHf(t = 160 Ma) values from -2.2 to -0.2 and T_{DM}^{C} ages from 1.35 Ga to 1.22 Ga. The oxygen isotope compositions show relatively large variation with $\delta^{18}O_{zircon}$ ranging from 6.3‰ to 7.4‰.

Session two:

In this session, 11 analyses for both Hf and O were conducted on 11 zircons of sample GD61-1 from the Gudoushan batholith. The $^{176}Hf/^{177}Hf$ vary from 0.282397 to 0.282514, corresponding to the variations of εHf(t = 160 Ma) values from -9.9 to -5.9 and T_{DM}^{C} ages from 1.84 to 1.58 Ga. The $\delta^{18}O_{zircon}$ show large variations from 6.6‰ to 9.0‰.

Session three:

Seventeen zircons of sample GD62-1 from the Wuguishan pluton were analysed. Their $^{176}Hf/^{177}Hf$ ratios vary from 0.282356 to 0.282481, corresponding to εHf(t = 160 Ma) values from -11.4 to -7.0 and T_{DM}^{C} ages from 1.93 Ga to 1.65 Ga. Zircon $\delta^{18}O$ values vary from 7.0‰ to 8.2‰.

Two analyses of sample GD61-1 give relatively high εHf(t) and low $\delta^{18}O_{zircon}$, constituting a minor peak in addition to a major one in probability distributions; all of the other samples show unimodal patterns for both εHf(t) and $\delta^{18}O_{zircon}$ (**Fig. 6.12**). There is no clear co-variation between εHf(t) and $\delta^{18}O_{zircon}$ for any individual sample, implying that magma mixing was not a primary mechanism for the genesis of these rocks. However, as can be seen in **Fig. 6.12**, peak values of εHf(t) and $\delta^{18}O$ for four samples vary significantly. Sample with the highest εHf(t) has the lowest $\delta^{18}O_{zircon}$, and vice versa. Therefore, results of the four samples appear to exhibit a coherent variation trend in a $\delta^{18}O_{zircon}$ vs. εHf(t) plot (**Fig. 6.13**). The estimated whole-rock $\delta^{18}O_{WR}$ vary from ~8.5‰ for the Gangwei pluton to 9.8‰ for the Gudoushan pluton, using the equation of $\delta^{18}O_{zircon} - \delta^{18}O_{WR} \approx -0.0612(wt.\%SiO_2) + 2.5$ (Valley et al., 2005).

6.3. Discussions

6.3.1. Petrogenetic classification

All of the studied Jurassic granites have high K_2O (~3.5−7 wt%) and relatively low CaO (~0.6−3.8 wt%), Na_2O (~2.6−3.8 wt%). In particular, the

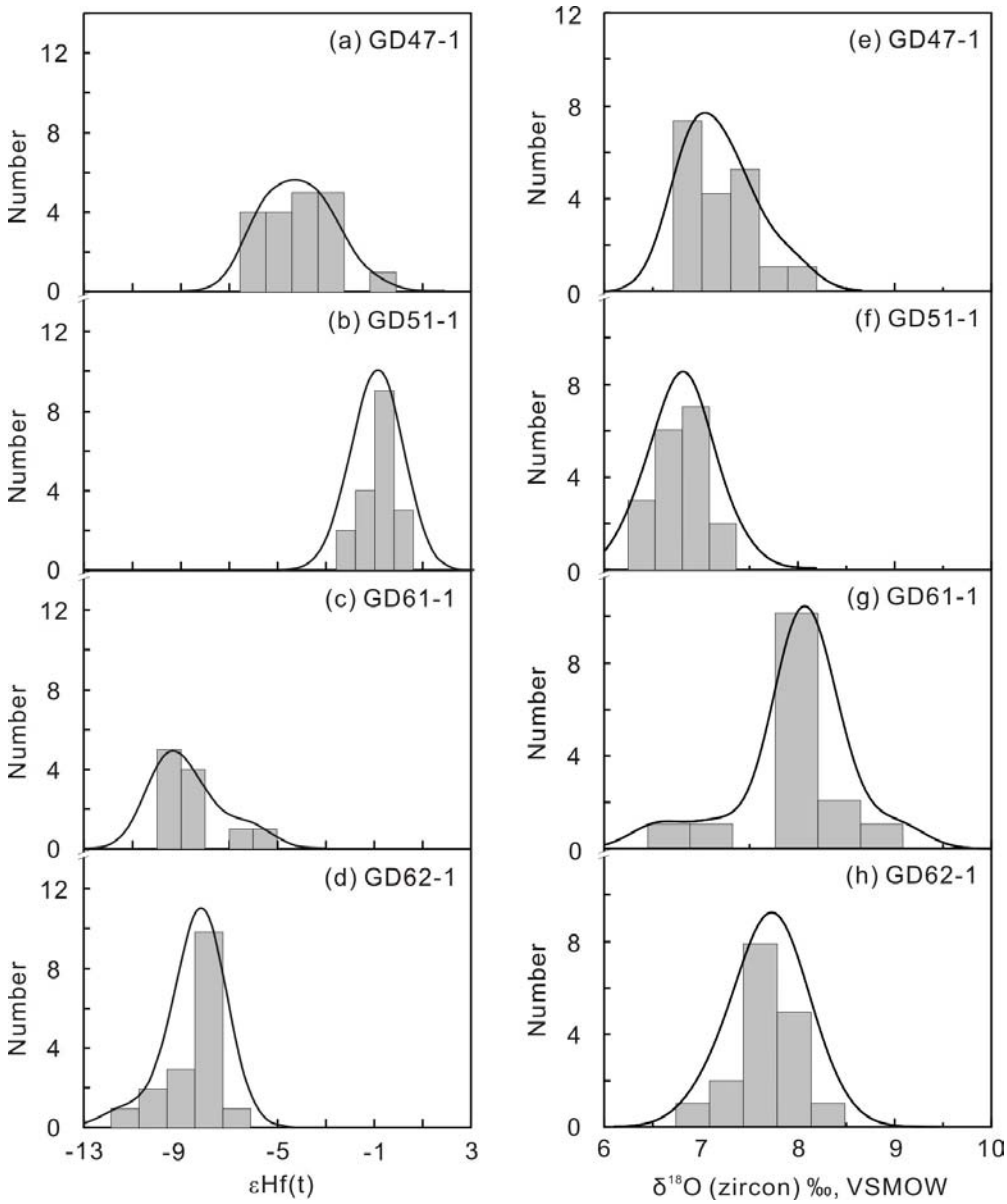

Figure 6.12 Probability density distribution of zircon εHf(t) and $\delta^{18}O$ values.

Xiaoliang granites have very high K_2O (up to 7 wt%), but relatively low CaO. These features are more akin to S-type than I-type granites in the LFB. However, group A granites commonly contain amphibole. Besides, they vary from metaluminous to slightly peraluminous, and show an increase of A/CNK from 0.85 to 1.03 as SiO_2 increases (**Fig. 6.6h**). These features are characteristic of I-type granites because typical I-types in the LFB contain amphibole and are metaluminous with A/CNK <1.0, whereas S-type granites do not contain amphibole and are typically peraluminous with A/CNK >1.05 (Chappell, 1999). This is further supported by the

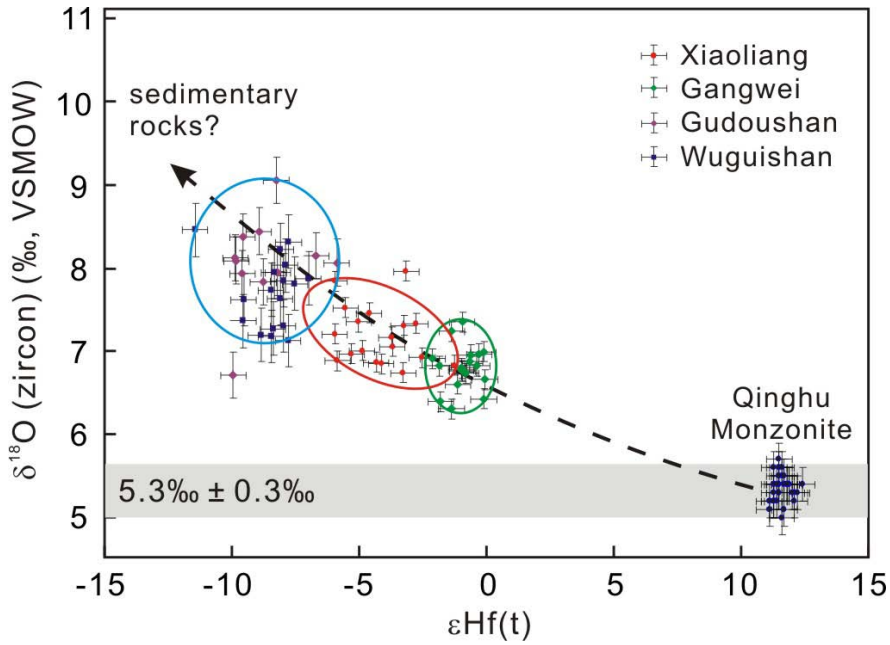

Figure 6.13 Plot of $\delta^{18}O$ vs. εHf(t) for high-K granites in the coastal region. Data of the Qinghu Monzonite are from (Li et al., 2009b).

similarities in trace element compositions between these granites and typical I-type granites in the LFB (**Fig. 6.8**). Therefore, the group A granites can be unambiguously classified as I-types using diagnostic criteria proposed by Chappell and White (1974, 2001). Distinctively, the group B granites have unusual to absence of amphibole. They are mostly weakly peraluminous, with A/CNK = 1.00 to 1.05. Thus, the group B granitic rocks show features somewhat transitional between typical I-types and S-types.

6.3.2. Petrogenesis

It can be seen from **Fig. 6.13** that group B granites contain more supracrustal composition than those of group A. The variations in whole-rock Sr-Nd isotopes and zircon Hf-O isotope compositions (**Figs. 6.11 and 6.13**) might be explained using an AFC model, in which the metaluminous group A granites (SiO_2 = 64−72 wt%; $\delta^{18}O_{zircon}$ = 6.3‰−7.9‰; zircon εHf(t) = -5.9 to -0.2) differentiated, with input of supracrustal components, to give rise to the peraluminous, chemically evolved group B granites (SiO_2 = 70−76 wt%; $\delta^{18}O_{zircon}$ = 6.6‰−9.0‰; zircon εHf(t) = -11.4 to

-5.9). However, geochemical variations in major and trace elements (**Figs. 6.6 and 6.9**) refute the model in general. These granites vary in compositions from shoshonitic to high-K calc-alkaline (**Fig. 6.6d**), and from alkalic to calc-alkalic (**Fig. 6.7**). Because comagmatic igneous suites typically show tight variation trends in a particular field in these diagrams (Frost et al., 2001; Roberts and Clemens, 1993), the loose compositional variations suggest that these rocks probably do not have the same origin.

Again, because co-magmatic igneous suites would usually evolve in a particular field in SiO_2-K_2O and SiO_2-MALI binary variation diagrams (Frost et al., 2001; Roberts and Clemens, 1993), the Xiaoliang I-type granites most probably have a shoshonitic protolith for their very high K_2O contents (**Fig. 6.6d**). These granites could either be derived from melting of shoshonitic meta-igneous rocks or be produced through extreme differentiation of potassium rich mafic magmas. In either way, the very low CaO and mildly high $\delta^{18}O_{zircon}$ of the granites can be easily accounted for. Many shoshonitic rocks have low CaO and relatively high $Fe_2O_3^T$ (e.g., Huang et al., 2010) and such rocks of Jurassic age did occur in the study area (e.g., Li et al., 2000c; Wang et al., 2003b). Shoshonitic magmas were derived from small degree partial melting of metasomatised mantle sources (e.g., Chung et al., 2001; Turner et al., 1996; Xu et al., 2001) with enriched ^{18}O as a result of addition of fluids, sediments, and/or melts from subducted oceanic slab. Rocks originated from a metasomatised mantle could inherit the ^{18}O-enriched feature and thus have relatively high $\delta^{18}O_{zircon}$ than primitive mantle values (~5.3‰; Eiler, 2001). As evidenced by the occurrence of old xenocrystic zircons, the magmas could also have been contaminated by wall-rocks upon intrusion, a process that might further contribute to the elevation of whole-rock $\delta^{18}O$ and chemical variations within the pluton.

Similarly, the Gangwei and Lunshui high-K calc-alkaline I-type granites were probably derived from melting of hydrous high-K, calc-alkaline, mafic to intermediate igneous rocks. Experimental studies show that melting of such protoliths at oxygen fugacities below the NNO (Ni-NiO buffer) would produce

magmas with moderate K_2O and low K_2O/Na_2O (< 1), whereas magmas generated at higher oxygen fugacities well above the NNO would usually have higher K_2O and high K_2O/Na_2O (> 1) (e.g., Carroll and Wyllie, 1990; Sisson et al., 2005). Taking the high K_2O and high K_2O/Na_2O ratios into consideration, the Gangwei and Lunshui granites were most likely generated at high oxygen fugacities. This prediction is consistent with the high oxygen fugacities (ΔNNO = 0.1−0.4 for the Lunshui) estimated using amphiboles of these rocks.

The group B granites could be generated through differentiation of I-type magmas. However, I-type granites with geochemical and isotopic compositions parental to group B granites are unknown in this region. Besides, fractional crystallization probably could be an effective process for the generation of large volume granitic magmas (e.g., Clemens et al., 2010). Instead, as group B granites have chemical and isotopic compositions transitional between I-type and S-type, they could be a mixture of magmas derived from metaluminous infracrustal and old supracrustal rocks. Due to the absence of strong evidence for magma mixing, both the Gudoushan and Wuguishan granites were most likely derived from a source region where there was a physical mixture of I-type and S-type sources, similar to that proposed for some granites in the New England Batholith, eastern Australia (Shaw and Flood, 1981). The interpretation is consistent with the occurrence of voluminous biotite granites with volumetrically minor amphibole granites, tourmaline- and garnet-bearing granites. This is also consistent with the overall negative correlation between SiO_2 and P_2O_5 of these rocks (**Fig. 6.6**) which indicates that the parental magmas of the studied granitic rocks are metaluminous to weakly peraluminous (Chappell, 1999; Li et al., 2007a).

As only a few representative samples have been analysed, SiO_2 contents of each pluton show limited variations, making it difficult to evaluate the origin of the chemical variations. However, the apparently large variations of some major elements exhibited by samples collected from any individual pluton in an area as small as the <100 m in sampling area dimensions strongly suggest that the

compositions of the parental magmas were heterogeneous. The documented heterogeneities most probably exhibit primary or near-source features, which could be common for granites worldwide (e.g., Clemens et al., 2010).

The discussions above imply that variations of trace elements in the coastal Guangdong granites are mostly primary. Magma differentiation, if occurred, could also have contributed to the enrichment and depletion of certain trace elements such as Eu, Sr and Ba.

6.4. Conclusions

Two types of granites were emplaced nearly coeval 166−159 Ma. The group A granites, characterised by their common occurrence of amphibole (± titanite) and dominantly metaluminous feature could have been generated from melting of oxidised high-K basaltic rocks. The group B granites, emplaced to the east of group A granites, contain higher percentage of supracrustal materials than those of the group A. A simple assimilation and fractional crystallization (AFC) model for the genesis of these granites can be ruled out. Instead, the group B granites, with features transitional between typical I-type and S-type granites, were most likely formed in a region where there was physical juxtaposition between infracrustal metaluminous and supracrustal peraluminous source rocks. Thus, granites of both groups represent products of crustal reworking likely due to asthenosphere upwelling and/or underplating and intrusion of mafic magmas.

Chapter 7: The origin and tectonic implications of Jurassic high-K granites in the western Guangdong, SE China: A synthesis

7.1. Models for the genesis of high-K granites

Traditionally, felsic and intermediate rocks have been taken as differentiated products of mafic or ultramafic melts (or magmas), and were grouped with mafic igneous rocks into magmatic series. Potassium behaves incompatibly in mafic melts and tends to be enriched in residual magmas as fractional crystallization proceeds. Potassium is a major element in all kinds of igneous rocks. The variation in the abundance of K_2O is minor, but significant among the major elements (Peccerillo and Taylor, 1976). Thus, it can be used as an useful index for the process of differentiation (Roberts and Clemens, 1993). Following the proposed differentiation trends of K_2O, igneous rocks can be subdivided into four series, including tholeiitic series, (low-K) calc-alkaline series, high-K calc-alkaline series, and shoshonitic series (Peccerillo and Taylor, 1976; Rickwood, 1989). The subdivision is supported by experimental studies which show that hydrous partial melting of a given igneous rock would usually produce melts with K_2O and SiO_2 compositions plotted in the same field as the protolith (Roberts and Clemens, 1993).

Granites and rhyolites typically have high K_2O contents and K_2O/Na_2O ratios, and their generation have been a topic of ongoing debate (Sisson et al., 2005). Roberts and Clemens (1993) noted that high-K granites have became common in orogenic belts since the Proterozoic and have been dominantly discovered in continental arc and postcollisional settings (Pitcher, 1987). Sedimentary rocks are relatively enriched in K_2O and depleted in CaO and Na_2O than their igneous provenance due to weathering and sedimentation. When melted, these features could be inherited by their melt products (Chappell and White, 1974). As potassium is highly incompatible and melting of metasedimentary rocks involves breakdown of K-bearing minerals in many melting reactions (e.g., Stevens et al., 1995), granites produced from melting of metasedimentary rocks are typically potassium-enriched.

This has been confirmed by melting experiments which cover a wide range of sedimentary rock compositions and melting conditions. A recent compilation by Villaros (2010) shows that experimental melts produced from melting of sedimentary rocks are dominantly K_2O-enriched and high in K_2O/Na_2O ratios and SiO_2 contents (>70 wt%) (**Fig. 7.1**) although there is a significant increase in Na_2O and decrease in K_2O/Na_2O when melting occurred at the presence of additional fluids (e.g., Patiño Douce and Harris, 1998).

While there is little doubt that high-K, strongly peraluminous granites with evolved radiogenic isotopes and supracrustal-like stable isotope compositions originate dominantly from melting of metasedimentary rocks, the generation of potassium-rich metaluminous I-type granites has been in dispute (e.g., Clemens et al., 2011b; Roberts and Clemens, 1993). As a typical example, granites produced in the Peruvian coastal region (Andes) are K_2O rich and are mostly plotted in the high-K calc-alkaline field ('c' in **Fig. 7.1a**). Consequently, the generation of high-K calc-alkaline I-type granites has been frequently related to subduction processes, formed by firstly melting metasomatised peridotites in a mantle wedge to generate K_2O-enriched basaltic melts, which then differentiate and experience crustal contamination (e.g., Dickinson, 1975; Hildreth and Moorbath, 1988). Alternatively, such high-K granites could have been formed from melting of pre-existing crustal rocks as a result of underplating of mantle-derived mafic magmas into somewhat thinned crust, which may or may not have been thickened previously (Roberts and Clemens, 1993). Roberts and Clemens (1993) argued that high-K, calc-alkaline, I-type granites can be generated "only by partial melting of hydrous, calc-alkaline to high-K calc-alkaline, mafic to intermediate" metaigneous rocks in the crust with the probable melting reactions including Biotite + Quartz + Plagioclase = Orthopyroxene/Clinopyroxene + K-feldspars + melt and Hornblende = Plagioclase + Quartz + Clinopyroxene + melt. Indeed, experimental studies show that high-K granitic melts could have been directly produced from melting of hydrous

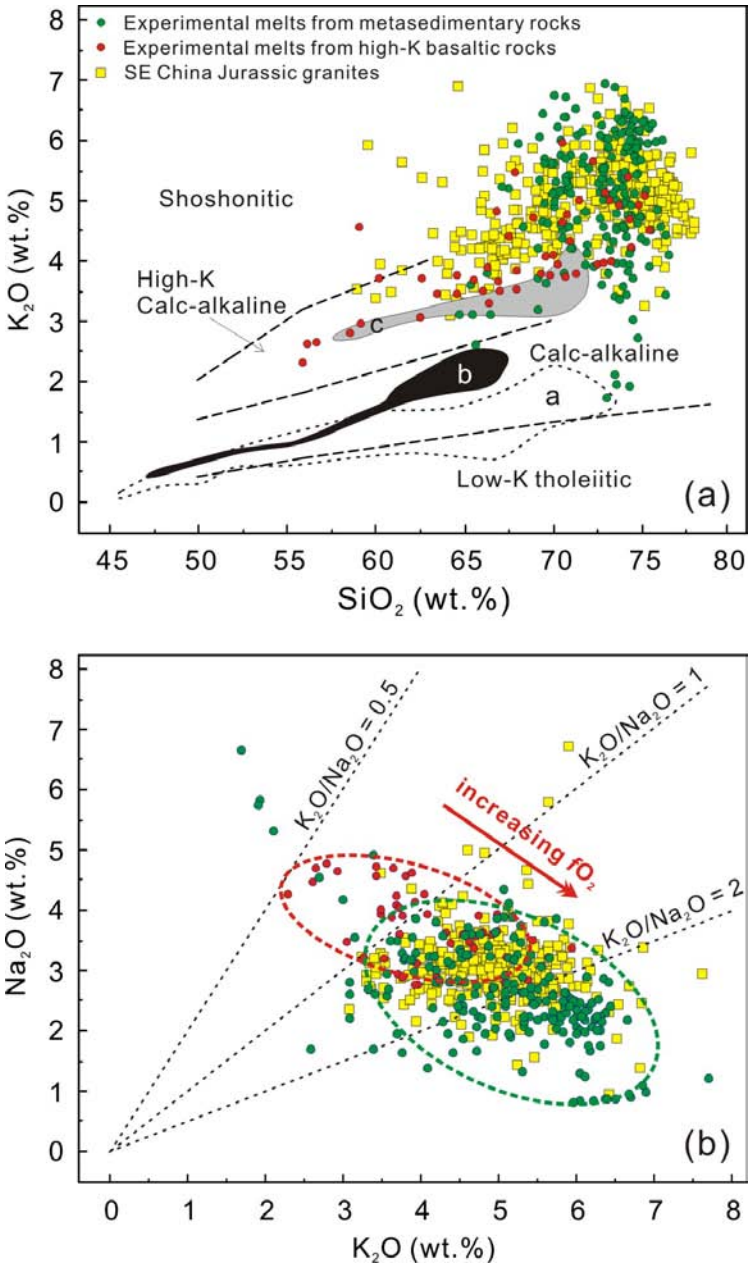

Figure 7.1 Geochemical plots of K_2O vs. SiO_2 (a) and Na_2O vs. K_2O (b) for the compositional comparison of Jurassic high-K granites in SE China (Appendix Table 1) with melts derived from melting of metasedimentary rocks (Villaros, 2010) and high-K basaltic rocks (Sisson et al., 2005). Field 'a', 'b', and 'c' in (a) are redrawn from Roberts and Clemens (1993), representing island arc magmatism in the New Britain, Papua New Guinea, composition of typical I-type granite in the LFB, and continental arc magmatism in the Peruvian coastal area, respectively. The vector in (b) shows the change of Na_2O and K_2O compositions of melts derived from high-K basaltic rocks as oxygen fugacities increase.

medium-to-high-K basaltic and intermediate rocks (e.g., Carroll and Wyllie, 1990; Sisson et al., 2005).

However, melts produced from melting of hydrous igneous rocks do not always have high K_2O/Na_2O ratios (Sisson et al., 2005). As can be seen from **Fig. 7.1a**, melts produced from melting of moderately hydrous, medium-to-high-K_2O basaltic rocks (K_2O = 1 wt%−2.3 wt% at 50 wt% SiO_2) are typically high in K_2O contents, but they have K_2O/Na_2O ratios varying between 0.53 and 1.90 (**Fig. 7.1b**). It is interesting to note that K_2O contents and K_2O/Na_2O ratios of the melts not only vary with the K_2O contents, but also with oxygen fugacities of the protoliths. Therefore, melts produced from hydrous, medium-to-high-K_2O basaltic rocks have both high K_2O contents and high K_2O/Na_2O ratios only if they are generated at high fO_2 (>NNO) (**Fig. 7.1**). Although it has been proposed that voluminous high-K granites (>5 wt% at 70 wt% SiO_2) could be produced from high-temperature melting of anhydrous tholeiitic rocks (Frost and Frost, 1997) and there are evidences that K_2O in some granitic melts could increase at the expense of Na_2O at decreasing water activities (e.g., Ebadi and Johannes, 1991), this proposition has not been tested yet by experimental studies.

Theoretically, melting of tonalitic–granodioritic rocks without the presence of additional aqueous fluids should yield melts with high K_2O and high K_2O/Na_2O ratios at high temperatures (Creaser et al., 1991). Melting experiments have been conducted on tonalitic-granodioritic rocks without added H_2O (e.g., Patiño Douce, 1997; Skjerlie and Johnston, 1992, 1993). Indeed, the results show that granitic melts produced in these studies typically have high K_2O and high K_2O/Na_2O ratios, even though various melting conditions were applied. However, melts produced in these studies are chemically similar to A-type granites, but distinct from common high-K calc-alkaline I-type granites in the LFB. In particular, significant amount of melts could be produced only at high temperatures (> 900 ºC). Therefore, anhydrous melting of tonalitic-granodioritic rocks may produce volumetrically minor amounts of high-temperature A-type like granites, but would not be favourable for the

formation of voluminous K_2O-enriched I-type granites.

To conclude, while high-K S-type granites could be produced simply from melting of metasedimentary rocks, voluminous high-K (calc-alkaline) I-type granites could be more easily generated from melting of basaltic rocks at high oxygen fugacities (> NNO; Sisson et al., 2005). Noteworthy is that, as exemplified by the Jindabyne I-type suite in SE Australia (Kemp et al., 2007) and the Fogang and the Jiufeng amphibole-bearing granites in SE China (Li et al., 2009b; Chapter 5 of this study), magma mixing could also have played a significant role in the genesis of some high-K I-type granites. Whether any high-K granite could be produced from extreme differentiation of mantle-derived magma/melt remains debated.

7.2. Formation of voluminous Jurassic high-K in the western Guangdong, SE China

Extensive Jurassic magmatism in SE China produced a variety of igneous rocks, ranging from mafic to felsic in composition. Among those, felsic intrusive rocks dominate and are mostly composed of biotite granite and two-mica granite. These rocks are spatially associated with sporadically distributed amphibole-bearing monzogranite, granodiorite, and muscovite granite. All these granites are enriched in K_2O and have high K_2O/Na_2O ratios (**Fig. 7.1**).

Early studies showed that Jurassic high-K granites in SE China are typically enriched in ^{87}Sr and ^{18}O (e.g., Wang et al., 1989; Xu et al., 1984). However, it had not been evaluated until recently whether the ^{18}O-enriched feature was primary for whole-rocks. Recent in-situ zircon oxygen isotope analyses of accurately dated magmatic zircons showed that ^{18}O-enrichment of Jurassic high-K granites is likely a primary magmatic feature, most probably resulted from reworking of supracrustal rocks by mantle-derived magmas (Li et al., 2009b). This study further examines the oxygen isotope compositions as a part of the detailed researches into the genesis of

the widespread Jurassic high-K granites. New results show that granites with A-, I- and S-type features all have whole-rock $\delta^{18}O$ higher than mantle values, signifying the contribution of supracrustal materials in their genesis (**Fig. 7.2**).

Systematic examinations show that some granites might have been derived dominantly from melting of metasedimentary source rocks with limited contribution of mantle-derived materials, e.g., the Jiuyishan A-type granite, the Jiufeng biotite granite, two-mica granite and muscovite granite (Chapters 4 and 5). The Jiufeng muscovite granites could be originated from a water- (or fluids-) saturated sedimentary source as suggested by their very high Na_2O (>4 wt%) and tetrad effect on REE distribution patterns, amongst many other features; but the others were more likely produced from metasedimentary rocks by dehydration melting of muscovite and/or biotite. This conclusion favours the proposition that reactions responsible for the creation of granitic magmas generally occur in the absence of excess fluids (Clemens and Watkins, 2001). Some granites may have been derived from magma mixing between S-type magmas and mantle-derived materials. When the contribution

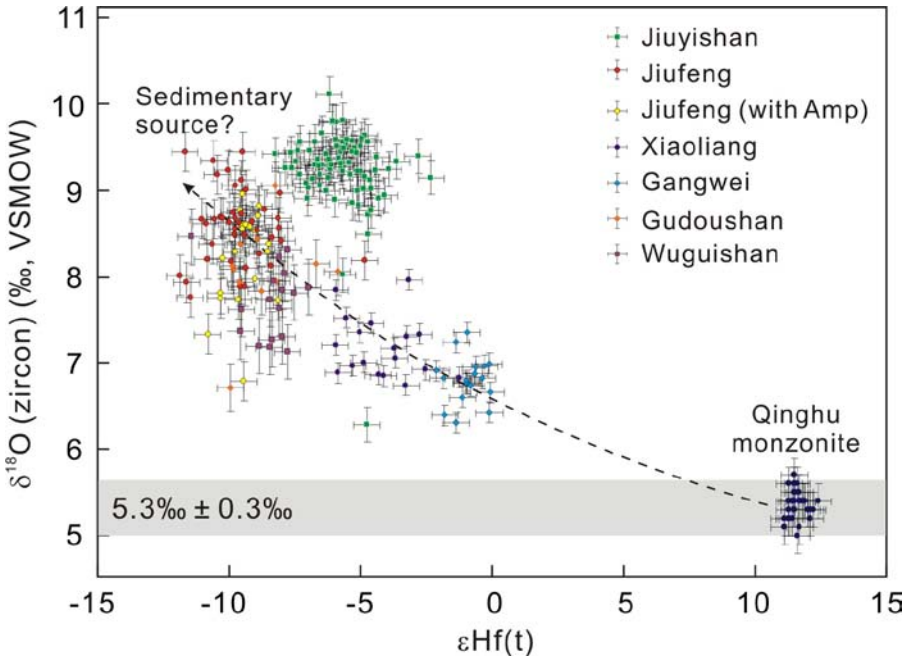

Figure 7.2 Plot of $\delta^{18}O$ vs. εHf(t) for granites. Data of the Qinghu Monzonite are from (Li et al., 2009b).

of the latter is significant, the mixed magma may crystallise to form granites with typical I-type features, e.g., the Jiufeng amphibole-bearing granites and possibly the Gudoushan amphibole-bearing granites. Some granites (e.g., the Xiaoliang, Gangwei and Lunshui granites) bearing typical I-type features, however, could have been derived simply from melting of igneous sources which were themselves K_2O- and ^{18}O-enriched (shoshonites and high-K basaltic rocks), likely inherited from their mantle source regions as a result of metasomatism. In this case, the reworking of supracrustal materials was involved at an earlier stage than the granitic magmatism.

From the results summarized above, it is clear that compositional variations of the widespread Jurassic high-K granites in SE China fingerprint heterogeneous basement compositions. Therefore, it is concluded that the first order control of the genesis of the various types of granites in the region was the composition of the source rocks, though processes like fractional crystallization, magma mixing/assimilation, alteration, etc, might have further contributed to the chemical variations.

In the light of experimental studies reviewed in the previous section, it is proposed here that the voluminous Jurassic high-K granites in the western Guangdong Province, SE China, were dominantly derived from melting of chemically heterogeneous sedimentary rocks. As can be seen from **Fig. 7.1**, there is a great overlap of melts produced from metasedimentary rocks with the high-K granites in the western Guangdong Province. Although there is also a significant overlap in the variation of K_2O vs. SiO_2 between the western Guangdong Jurassic high-K granites and melts derived from melting of high-K basaltic rocks, the latter have K_2O/Na_2O much lower than those of the former. Only those melts produced at increasing fO_2 have elevated K_2O/Na_2O ratios (**Fig. 7.1b**). The Gangwei and Lunshui granites have relatively high fO_2 (>NNO; **Appendix Table 12**). Their mineralogical, chemical and isotopic compositions favour their origination from melting of high-K basaltic rocks at high oxygen fugacities. Yet, lines of evidence reveal low oxygen fugacities for most of the western Guangdong Jurassic high-K granites. First,

analyses show that ferromagnesian minerals (e.g., biotite and amphibole) of the western Guangdong high-K granites are commonly enriched in Fe (e.g., Xu et al., 1984; this study). Estimations show that most Fe in these minerals occurs as Fe^{2+} (**Appendix Tables 6 and 7**), indicating that they were crystallized from reduced magmas. Second, high-K granites in the western Guangdong Province are closely associated with Sn-W deposits (e.g., Wang et al., 2011a; Zhu, 1998). Studies suggest that mineralization of Sn-W, as compared with Au-Cu, are closely related with reduced nature of the magma (e.g., Blevin and Chappell, 1992, 1995). Flood and Shaw (1975) suggested that probably due to the occurrence of graphite in sedimentary rocks, S-type granites commonly have oxygen fugacities lower than I-types. Therefore, the reduced nature of the widespread western Guangdong high-K granites further supports their origin from metasedimentary sources.

It is noteworthy that melts produced from melting of sedimentary rocks typically have high Si (SiO_2 >70 wt%) and low Fe + Mg (FeO^t + MgO <4 wt%) (e.g., Castro et al., 1999; Patiño Douce, 1999; Stevens et al., 2007). SiO_2 concentrations of the melts show minor changes even when the temperature for melting rises up to >1000 ºC (Patiño Douce, 1999). Therefore, lower Si and higher Fe + Mg in granites than crustal melts may imply entrainment of restites (White and Chappell, 1977), magma mixing (Patiño Douce, 1999), and/or entrainment of peritectic minerals (Stevens et al., 2007). As can be seen in **Figs. 7.1a and 7.3**, some high-K granites in the SE China have SiO_2 significantly lower and Fe + Mg notably higher than melts derived from sedimentary rocks. For example, the Jiufeng amphibole-bearing granites have SiO_2 similar to 69 wt%, but have high Fe + Mg. Due to their high Fe + Mg, they have been plotted in the field for experimental melts of amphibolite (**Fig. 5.17b**). The high Fe + Mg of the Jiufeng amphibole-bearing granites could be a result of magma mixing, a process arguably to be responsible for the genesis of these rocks (**Chapter 5**). Distinctively, the Jiuyishan A-type granites

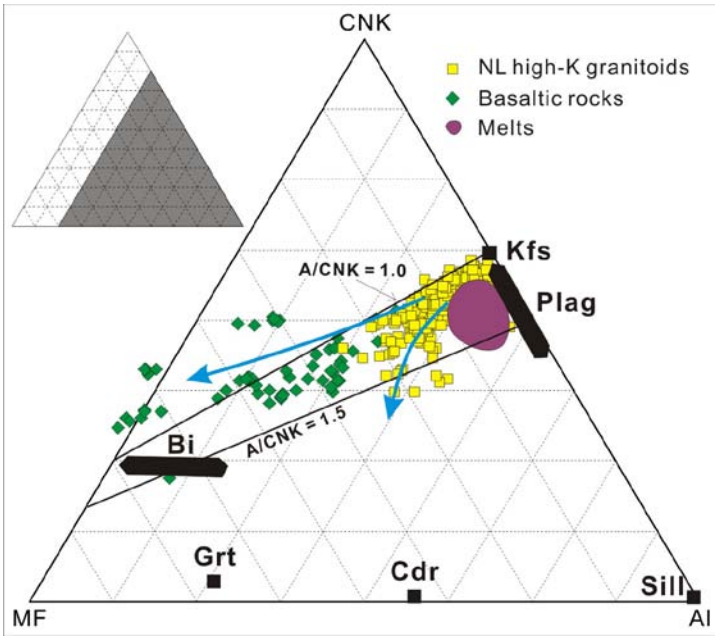

Figure 7.3 Ternary diagrams showing compositional differences between the SE China Jurassic high-K granitegranites and experimental melt. After Villaros (2010). Grt: garnet; Cdr: cordierite; Sill: sillimanite; Bi: biotite; Kfs: K-feldspar; Plag: plagioclase. Blue lines are used to delineate possible mixing trends of sedimentary melts with basaltic melts and restitic materials. CNK, MF, and Al stand for atomic Ca + Na + K, Mg + Fe, and Al per 100 g of rock, respectively.

have SiO_2 as low as 64 wt% and correspondingly FeO + MgO as high as ~7.8 wt%. There is little evidence for magma mixing for the genesis of these rocks. The liquidus temperature of granites with such a high Fe + Mg could be as high as 1100 ºC−1200 ºC (Castro et al., 2009; Fernandez et al., 2008), consistent with those estimated (> 960 ºC; **Chapter 4**). Nevertheless, to reach the temperature as high as 1200 ºC is considered unlikely at all crustal levels unless there was a mantle plume. So far, there has no geological record for a mantle plume in the Jurassic South China. Therefore, the primary magma of the Jiuyishan suite could contain some Fe- and/or Mg-enriched restites and/or peritectic crystals. As granitic magmas have relatively high viscosities, a complete separation of restitic and/or peritectic materials from granitic melts may be hardly achieved in the course of magma extraction, migration, and intrusion/eruption. Consequently, except the variations inherent of the granitic

magma sources, the increase of Fe + Mg in all western Guangdong high-K granites to higher values can be modelled generally using either magma mixing or entrainment of restites and/or peritectic minerals (**Fig. 7.3**).

7.3. Geological significance of the intensive Jurassic granitic magmatism in eastern South China Block

7.3.1. Basement components

A widely accepted concept regarding the evolution of the SCB is that it formed through the amalgamation between the Yangtze Craton in the northwest and the Cathaysia Block in the southeast, probably during the early-Neoproterozoic. Nevertheless, the precise position of the suture zone remains debated. There is no Precambrian crystalline basement outcrop in the western Guangdong Province. As granites originate from deep Earth, they have been frequently used as probes to gain insight into the inaccessible lower continental crust. The abundant western Guangdong Jurassic high-K granites commonly have evolved isotope compositions. Their whole-rock Nd isotope depleted mantle model ages vary from 1.9 Ga to 1.4 Ga and are mostly clustered at 1.8−1.7 Ga (e.g., Chen and Jahn, 1998; Li et al., 2007b; Ling et al., 2006; this study). Previous studies interpreted the western Guangdong high-K granites as I-types originated from melting of ~1.8 Ga juvenile basaltic protoliths, formation of which likely recorded an important crustal growth in the region (e.g., Li et al., 2007b). On the other hand, the granites have also been interpreted as S-types derived from melting of metasedimentary rocks in the middle-lower crustal level (e.g., Ling et al., 2006). In the latter case, whole-rock Nd model ages of the granites would represent the average ages of the components that make up the sedimentary sources, rather than those of the depositional ages of the sedimentary rocks (Collins, 1999).

Results of this study argue for a significant involvement of supracrustal rocks

for most of the Jurassic high-K granites. Whole-rock Nd two-stage depleted mantle model ages of these rocks vary dominantly from 1.9 Ga to 1.5 Ga (**Appendix Table 9**), but the isotopic results must not be interpreted to reveal a Paleoproterozoic basement source of these granites regardless whether the isotope compostions of the high-K granites accurately "image" that of their sources. Instead, they only reflect 'the average age of derivation of the source components' from the mantle (Collins, 1999). Therefore, the Nd model ages of granites studied here provide little insight into the formation age of the basement rocks.

Granites interpreted to be derived from melting of basaltic igneous rocks have younger Nd model ages, varying from 1.4 Ga to 1.1 Ga. Even in this case, the Nd model ages may not approximate the time when the medium-to-high-K basaltic rocks were generated from the mantle. This is due to the fact that their mantle source region had been metasomatized and/or contaminated; a large portion of Nd in these rocks may be contributed by supracrustal materials. As a result, Nd model ages of these basalt-derived high-K granites should predate the formation age of their source rocks.

To conclude, although the cores of the Yangtz and Cathaysia blocks may be composed of ~2.0−1.8 Ga (e.g., Li et al., 2011; Li, 1997; Ling et al., 2001; Wu et al., 2009; Yu et al., 2009a) and some Archaean rocks (Gao et al., 2011; Jiao et al., 2009; Qiu and Gao, 2000), the basement composition of the SCB in Mesozoic may be much more complex. In fact, the formation of the SCB and/or the closure of the Nanhua Rift basin at a later time may have created orogenic belts where the continental crust could be dominated by metasedimentary rocks metamorphosed to various degrees after delamination of old crystalline basement (**Fig. 7.4**). Indeed, sedimentary rocks may have been brought to middle and lower crust during the closure of the Nanhua Rift (Li et al., 2010e) and partially melted and metamorphosed in the early Paleozoic (e.g., Li et al., 2010e; Liu et al., 2010; Wan et al., 2007; Wang et al., 2007b; Wang et al., 2011b; Zeng et al., 2008). These rocks could form part of the basement of the SCB in the Mesozoic (**Fig. 7.4**).

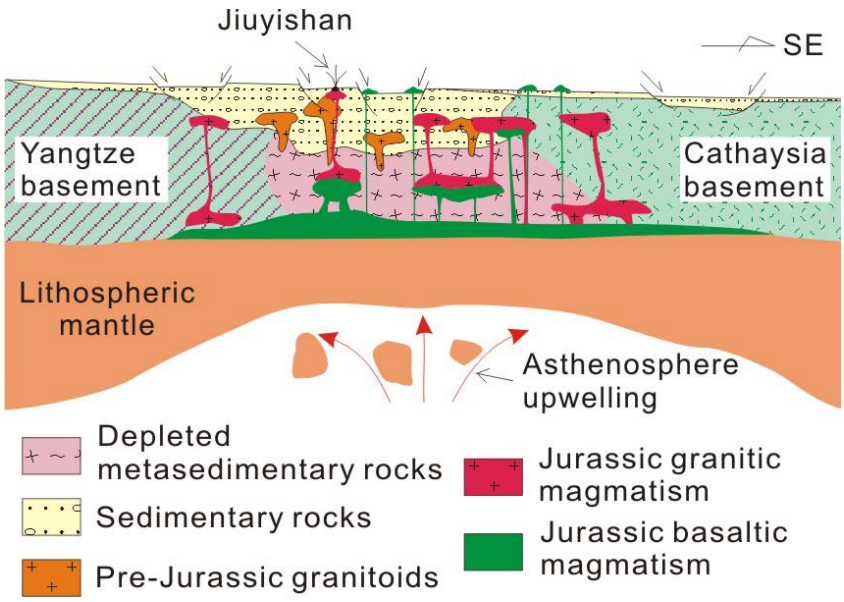

Figure 7.4 A cross section map showing the probable composition of the SCB basement. This also presents as a model for the genenration of high temperature Jiuyishan A-type granite and the other granites in this region. According to Li et al., (2010e), part of the crystaline basement could have been delaminated during the early Paleozoic Wuyi-Yunkai orogeny.

7.3.2. Tectonic implications

7.3.2.1. Heat source

The Jurassic high-K granites in SE China are widespread, constituting one of the largest magmatic provinces in the world. In collisional orogenic belt (e.g., the Himalaya), the generation of leucogranites may occur in the mid-lower crust (6−10 kbar), probably resulted from melting of metasedimentary rocks involving the dehydration reactions of muscovites at ~750−800 ºC (e.g., Patiño Douce and Harris, 1998). Although the western Guangdong Jurassic high-K granites are SiO_2-enriched, they are dominantly biotite granites. Such a feature is distinct from that of collisional zone granites where leucogranites dominate. This distinction may imply that granites in the western Guangdong Province were instead resulted from dehydration melting of biotite at higher melting temperatures (>800 ºC; **Fig. 5.18**), consistent with zircon saturation temperature estimations (**Appendix Table 8**).

Geochronological analyses confirm that Jurassic granites with an outcrop area

of ~64,000 km^2 in SE China were mostly (> 95%) generated between 165 Ma and 150 Ma (**Fig. 7.5**). It is proposed that a heat source external to the crust was required for the intensive granitic magmatism. Specifically, examinations reveal that the Jiuyishan A-type granite could have been generated at temperatures >960 ºC. The Jiuyishan A-type granite have high Y (>40 ppm) concentrations and flat Chondrite-normalized HREE distribution patterns (**Fig. 4.9**), indicating that garnet could not be a main residual phase. The results imply that the magma was produced at relatively low pressure (<7 kbar; e.g., Patiño Douce and Beard, 1996). The high temperature is unusual at all crustal levels and exceeds that could be achieved at ~7 kbar using a normal thermal gradient. Hence, as can be seen from **Fig. 7.4**, asthenosphere upwelling and underplating and/or intrusion of mafic magmas were required for such an intensive magmatism although geochemical and isotopic results reveal that the ca. 160 Ma granites were dominantly derived from remelting of old crustal rocks (e.g., Huang et al., 2011; Jiang et al., 2009; Li et al., 2007b; this study). Indeed, the Middle to Late Jurassic granites are associated in time and space with sporadically distributed basaltic rocks. Besides, a thick gabbroic layer (~4 km) has

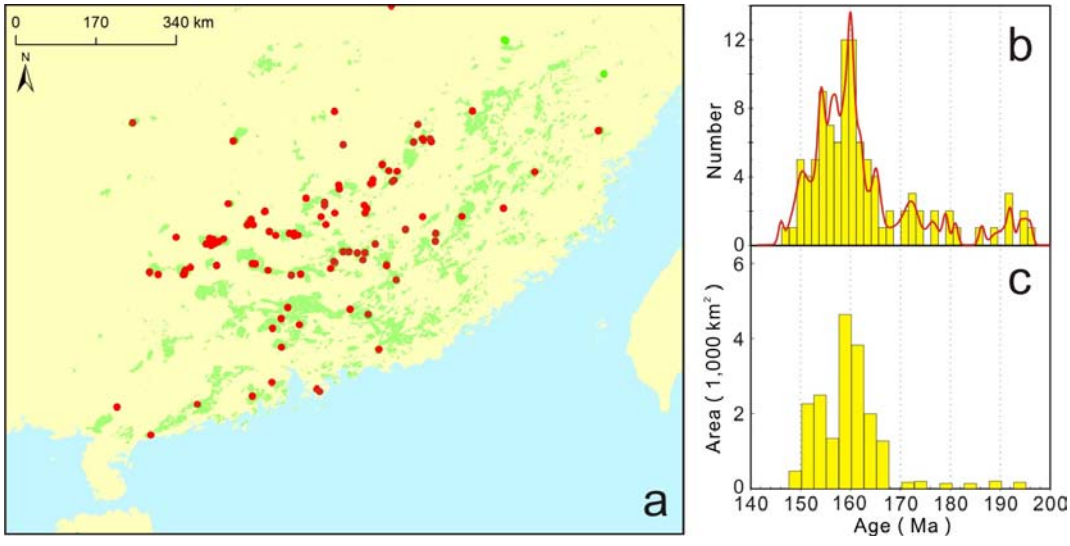

Figure 7.5 (a) A region map showing the distribution of Jurassic granitegranites (green polygons) in SE China. Each solid red point represents an individual geochronological analysis (zircon U-Pb age); (b) and (c) show the probability density distributions of geochronological results (Appendix Table 13) and outcrop areas.

been inferred to be present in the lower part of middle crust (~20 km) using geophysical results (Zhang et al., 2008). It is concluded that the intensive granitic magmatism in Jurassic South China probably signifies an important episode of crustal growth.

7.3.2.2. Geodynamics

Basaltic underplating in the region has variously been interpreted as a result of subduction in an continental arc setting (Zhou and Li, 2000), back-/intra-arc extension due to slab roll-back (Jiang et al., 2009; Jiang et al., 2006), lithospheric extension in an intraplate setting in response to delamination of a flat-subducted oceanic slab (Li et al., 2007b; Li and Li, 2007), and post-orogenic extension relative to continental collision (Chen et al., 2008). Chen et al. (2008) showed that inland basaltic rocks associated with the Jurassic granites are distinctively different in composition from arc basalts, consistent with their formation in an intraplate setting (Li et al., 2003a; Li et al., 2004a). Although some of them show characteristics of slab-induced melts and/or fluids (i.e., arc-like features) (e.g., Jiang et al., 2009), these basaltic rocks were dominantly derived from OIB-type mantle sources which remained largely unaffected by subduction liquids (e.g., He et al., 2010; Li et al., 2003a; Li et al., 2004a; Li et al., 2000b; Meng et al., 2012; Wang et al., 2004; Zhu et al., 2010). Despite the fact that granites from coastal region of the Guangdong Province are situated much closer to the proposed subduction trench in the Jurassic than those emplaced deeper in the continental interior (**Fig. 7.6**), they are spatially associated with coeval shoshonitic basaltic and syenitic intrusives that display intraplate affinities (Li et al., 2004a; Li et al., 2000b). Therefore, they were unlikely produced in an active subduction system. Instead, they were most likely produced intraplate (**Fig. 7.6b**). The arc-like features exhibited by some of these granites (i.e. group A granites described in Chapter 6), e.g., Nb and Ta depletions relative to Th and La (**Fig. 6.10c**), were probably inherited from their crustal source rocks rather

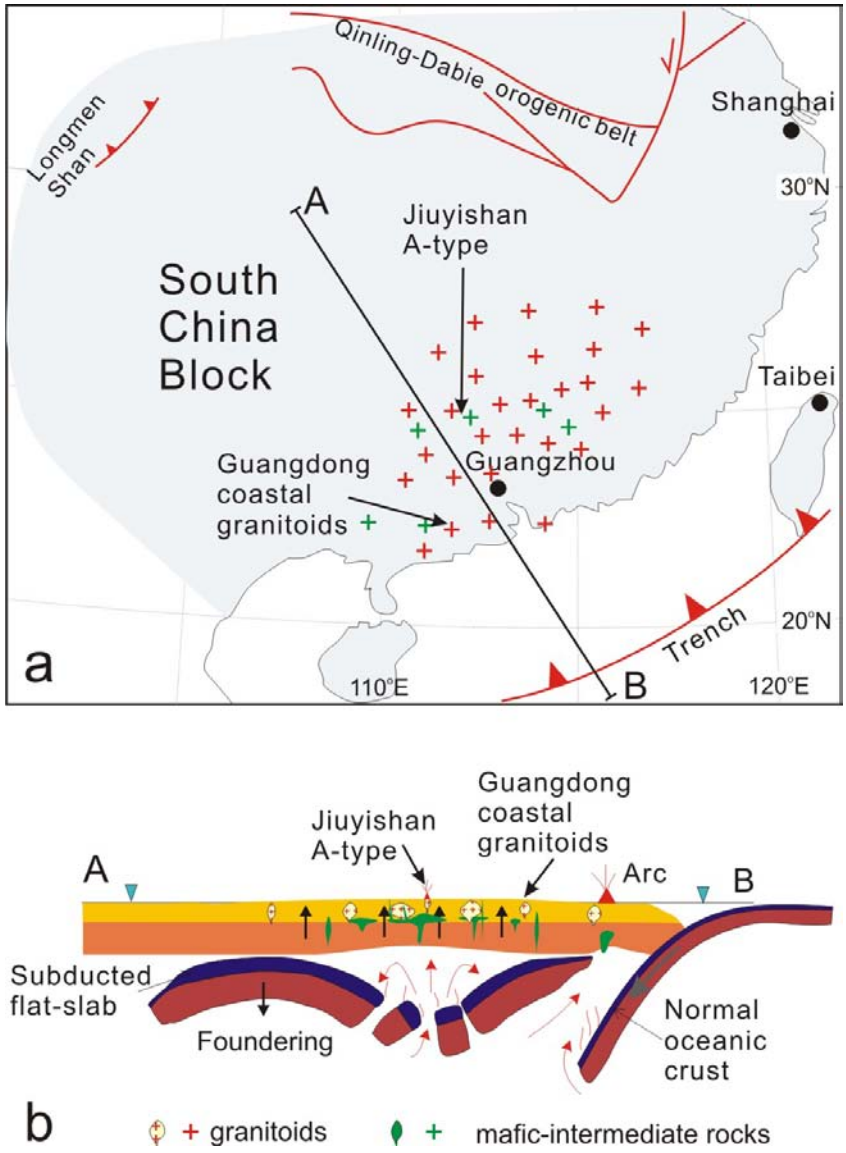

Figure 7.6 Geodynamic model for the generation of intraplate granites in SE China with the Jiuyishan A-type granite and granites in the western Guangdong coastal region being highlighted (modified after Huang et al., 2011; Li et al., 2012).

than being indicative of an active arc environment.

Most recently, Meng et al. (2012) showed that arc-like features in the late Mesozoic basaltic rocks become more prominent from the Early Jurassic to the mid- and Late-Jurassic, but diminished since then in the inland region of the SCB, whereas Late Cretaceous basalts in the coastal region show much stronger arc affinities. They

interpreted such secular compositional changes in the late Mesozoic basaltic rocks using the delamination of a previously flat-subducted slab between the Jurassic and the Early-Cretaceous, and the return to normal subduction during the Late Cretaceous (Li and Li, 2007). Such a model can also explain the formation of the large Jurassic intraplate magmatism in the region, where the delamination and foundering of the flat-slab induced substantial basaltic underplating, leading the formation of a large amount of high-K granites in an extensional environment, including those reported in this study (**Fig. 7.6**).

Appendix Table 1 Compiled geochemical data of the Jurassic high-K granites

Samples	SiO_2	TiO_2	Al_2O_3	Fe_2O_3t	MnO	MgO	CaO	Na_2O	K_2O	P_2O_5	LOI	Total	A/CNK
Yao Junming et al., Acta Petrologica Sinica (2005),21(3):688-696.													
H26	75.09	0.07	12.36	1.47	0.08	0.11	1.01	3.00	5.63	0.01	1.07	99.90	0.96
H34	74.97	0.05	12.89	0.74	0.05	0.16	1.29	3.34	5.15	0.01	1.08	99.74	0.96
H41	75.21	0.09	12.60	1.61	0.07	0.28	0.78	2.02	5.70	0.01	1.55	99.91	1.15
H43	74.54	0.09	12.24	1.76	0.10	0.16	1.39	2.89	5.24	0.01	1.31	99.73	0.94
H50	74.81	0.02	13.12	1.33	0.09	0.21	0.78	3.50	4.63	0.01	1.16	99.66	1.08
H51	75.07	0.02	13.30	0.53	0.04	0.24	1.04	3.06	5.37	0.01	1.36	100.04	1.04
H52	75.01	0.02	12.80	1.39	0.11	0.49	0.93	1.91	4.92	0.01	2.21	99.80	1.26
H53	73.25	0.05	12.46	0.66	0.13	0.34	2.62	0.93	6.42	0.01	2.99	99.87	0.94
H56	73.94	0.06	12.28	1.55	0.13	0.41	1.30	1.38	6.82	0.01	1.90	99.78	1.02
Jiang Xigen et al., Geotectonica Et Metallogenia (2006), 30(2): 206-219.													
C2	75.45	0.08	11.92	3.52	0.05	0.13	0.70	3.10	4.84	0.01	0.01	99.81	1.03
C1	77.39	0.11	11.11	2.52	0.04	0.19	0.51	2.42	4.91	0.02	0.60	99.82	1.09
C3	74.78	0.15	12.18	3.15	0.04	0.22	1.13	2.83	5.04	0.04	0.22	99.78	1.00
C7	73.99	0.16	12.34	3.97	0.05	0.25	0.86	2.79	5.09	0.06	0.23	99.79	1.06
C5	71.36	0.38	12.80	4.75	0.09	0.51	1.67	2.80	5.00	0.10	0.30	99.76	0.98
Wang Yuejun et al., Geochemical Journal (2003), 37: 427 - 448.													
TSD-1	66.58	0.41	15.86	3.20	0.06	1.30	4.06	2.94	4.01	0.13	1.82	100.37	0.96
TSD-2	65.52	0.48	15.70	3.80	0.06	1.39	4.47	3.12	3.54	0.17	1.92	100.17	0.92
TSD-4	67.20	0.42	14.97	2.94	0.06	1.11	3.93	3.02	4.02	0.16	2.12	99.95	0.91
TSD-9	65.42	0.49	15.84	3.72	0.02	1.39	4.61	3.18	4.20	0.19	1.04	100.10	0.87
JYT-3	68.16	0.42	14.36	3.14	0.08	1.09	2.90	2.50	4.37	0.16	2.88	100.06	1.02
JYT-10	66.85	0.45	14.86	3.79	0.10	1.33	3.37	2.86	3.75	0.17	2.59	100.12	1.00
TSX-1	67.18	0.45	15.26	3.63	0.09	2.19	3.66	2.96	4.08	0.14	0.98	100.62	0.96
TSX-5	66.18	0.45	15.70	3.84	0.09	1.58	4.20	3.21	4.21	0.15	0.70	100.31	0.90
TSX-6	67.02	0.47	15.26	3.94	0.09	1.86	4.47	3.12	3.34	0.15	1.10	100.82	0.90
TSX-7	64.78	0.48	15.99	4.20	0.04	1.81	4.61	3.23	3.52	0.17	1.30	100.13	0.91
JHT-2	66.67	0.50	15.14	4.03	0.09	1.46	3.69	2.89	3.79	0.19	1.68	100.13	0.97
JHT-8	65.87	0.53	15.02	4.10	0.09	1.62	3.84	2.81	4.20	0.20	1.89	100.17	0.93
JHT-13	66.76	0.45	15.14	3.65	0.09	1.36	3.59	3.01	3.91	0.17	1.98	100.11	0.96
BSH-1	66.58	0.37	14.39	2.52	0.13	1.14	4.65	2.62	4.20	0.18	3.25	100.03	0.83
BSH-2	65.40	0.41	14.61	3.25	0.05	2.23	3.75	2.81	4.42	0.14	3.18	100.25	0.90
BSH-3	68.01	0.36	13.67	2.74	0.11	1.29	3.68	2.75	4.61	0.17	2.52	99.91	0.84
BSH-4	64.46	0.45	14.68	3.58	0.04	2.76	2.89	2.82	4.22	0.15	3.72	99.77	1.02
BSH-5	68.80	0.43	13.73	2.89	0.08	1.55	2.33	2.83	4.81	0.15	2.40	100.00	0.97
BSH-6	64.50	0.48	15.12	4.08	0.06	3.06	3.57	2.99	4.39	0.16	2.04	100.45	0.94
BSH-7	63.28	0.44	15.19	2.89	0.10	2.21	5.96	2.22	4.44	0.15	3.78	100.66	0.79
SKS-1	60.26	0.78	17.00	5.58	0.06	3.39	4.30	2.14	3.94	0.41	2.68	100.54	1.09

SKS-3	60.00	0.81	17.51	5.69	0.05	3.29	2.98	2.67	3.36	0.35	3.40	100.11	1.30
SKS-5	64.67	0.68	15.91	5.18	0.04	2.34	2.77	2.92	3.30	0.38	1.85	100.04	1.19
SKS-6	65.05	0.70	15.68	4.74	0.05	2.59	2.73	2.80	3.30	0.38	2.05	100.07	1.19
SKS-7	60.88	0.77	16.28	5.11	0.06	3.01	4.27	2.98	3.48	0.37	2.54	99.75	0.99
SKS-8	64.53	0.70	15.67	5.20	0.05	2.59	2.73	2.72	3.35	0.38	2.17	100.09	1.20
SKS-9	61.48	0.74	16.43	4.69	0.07	3.05	4.22	2.90	3.84	0.36	1.82	99.60	0.99
Li Xianhua et al., International Geology Review (2003), 45: 898 - 921.													
GN28-1	74.29	0.18	12.65	2.37	0.03	0.17	0.78	3.66	4.82	0.10	0.95	100.01	1.00
GN28-6	74.84	0.19	12.45	1.88	0.02	0.27	0.80	2.65	4.89	0.04	1.50	99.53	1.12
GN30-2	76.65	0.09	11.89	1.63	0.02	0.04	0.47	3.12	5.27	0.01	0.81	100.00	1.02
GN30-4	75.54	0.09	12.21	1.60	0.02	0.04	0.50	3.20	5.11	0.01	0.99	99.31	1.04
GN31-3	71.07	0.44	13.51	3.72	0.05	0.45	1.10	2.97	5.53	0.08	1.00	99.93	1.05
GN33-1	71.30	0.29	13.77	2.73	0.02	0.24	0.98	3.20	5.62	0.05	1.03	99.21	1.05
GN34-2	76.00	0.09	11.92	1.67	0.02	0.05	0.55	2.91	4.94	0.00	0.99	99.14	1.07
GN34-5	76.52	0.09	12.12	2.06	0.01	0.10	0.15	2.50	5.38	0.02	1.05	99.99	1.19
GN34-7	76.11	0.10	12.14	1.83	0.03	0.06	0.55	3.04	5.44	0.02	0.68	99.98	1.02
GN34-8	74.74	0.11	13.02	1.81	0.02	0.06	0.48	3.25	5.81	0.02	0.61	99.94	1.04
GN34-12	76.67	0.09	11.46	1.64	0.02	0.04	0.41	2.86	5.03	0.01	1.02	99.25	1.05
Chen Peirong et al., Science in China Ser. D Earth Sciences (2005), 48 (7): 912 - 924.													
cpr04-1	71.06	0.17	13.63	2.61	0.03	0.16	0.80	4.42	5.38	0.11	1.44	99.81	0.94
cpr04-2	76.28	0.15	11.50	1.71	0.04	0.07	0.68	2.79	5.40	0.10	0.75	99.47	0.99
cpr05	74.87	0.18	11.96	2.39	0.04	0.25	1.16	3.20	4.90	0.09	0.69	99.73	0.94
cpr10-1	74.17	0.17	12.78	2.39	0.08	0.15	0.81	3.30	5.63	0.05	0.66	100.19	0.98
cpr11-1	73.10	0.24	12.96	2.78	0.09	0.15	0.58	3.07	5.55	0.07	0.85	99.44	1.07
Gu Chengyan et al., Acta Petrologica Et Mineralogica(2006), 25(2): 97-109.													
HS-4	74.62	0.18	12.86	1.86	0.03	0.19	1.26	3.31	5.35	0.00	0.34	100.00	0.95
HS-7	72.71	0.23	13.49	2.46	0.04	0.25	1.37	3.32	5.62	0.00	0.29	99.78	0.96
HS-9	74.14	0.19	13.17	2.06	0.03	0.19	1.09	3.15	5.72	0.00	0.33	100.07	0.99
HS-10	72.82	0.21	13.08	2.29	0.03	0.20	1.23	3.14	5.71	0.00	0.74	99.45	0.96
HS-13	73.24	0.23	13.15	2.41	0.03	0.22	1.26	3.27	5.56	0.00	0.43	99.80	0.96
HS-16	72.43	0.24	13.85	2.16	0.04	0.29	1.37	3.41	5.64	0.02	0.47	99.92	0.98
HS-26	74.17	0.25	12.84	2.20	0.05	0.38	1.40	3.24	5.10	0.03	0.53	100.19	0.96
HS-29	69.96	0.42	14.25	3.45	0.06	0.54	1.70	3.42	5.47	0.08	0.69	100.04	0.97
HS-33	73.21	0.35	12.75	3.18	0.05	0.34	1.19	3.13	5.02	0.04	0.44	99.70	1.00
HS-20	76.51	0.06	12.62	1.13	0.06	0.04	0.69	3.87	4.82	0.01	0.54	100.35	0.98
HS-25	76.04	0.07	12.67	1.04	0.03	0.10	0.76	3.55	5.24	0.00	0.69	100.19	0.98
HS-28	75.72	0.11	12.56	1.24	0.03	0.11	0.81	3.08	5.75	0.00	0.38	99.79	0.98
HS-31	76.35	0.08	12.59	1.17	0.03	0.07	0.93	3.93	4.33	0.00	0.34	99.82	0.98
HS34	76.18	0.08	12.86	1.57	0.06	0.13	0.41	3.24	4.64	0.00	0.69	99.86	1.16
HS36	75.99	0.08	12.66	1.23	0.03	0.09	0.60	3.66	5.07	0.00	0.50	99.91	1.00
LS4	74.49	0.20	12.54	1.94	0.03	0.22	1.20	3.33	4.95	0.00	0.39	99.29	0.96

LS6	69.04	0.42	14.50	3.29	0.07	0.62	1.74	3.88	5.17	0.15	0.53	99.41	0.96
LS7	70.05	0.42	13.84	3.22	0.07	0.72	1.67	4.21	4.54	0.14	1.42	100.30	0.93
LS9	74.44	0.18	12.87	1.94	0.03	0.26	1.01	3.29	5.41	0.00	0.55	99.98	0.98
LS10	72.57	0.18	13.88	2.02	0.03	0.20	0.94	3.75	5.91	0.00	0.45	99.93	0.97
LS11	71.20	0.34	14.16	2.90	0.05	0.43	1.65	3.70	5.30	0.05	0.40	100.18	0.96
GP1	75.07	0.27	11.73	2.65	0.04	0.33	1.30	3.16	4.52	0.01	0.29	99.37	0.94
GP6	73.05	0.31	12.68	2.86	0.05	0.39	1.39	3.13	5.03	0.03	0.67	99.59	0.97
GP13	74.12	0.28	12.22	2.95	0.06	0.31	1.48	3.38	4.15	0.02	0.41	99.38	0.96
GP5	76.05	0.10	12.18	0.92	0.03	0.14	1.18	3.38	5.17	0.00	0.59	99.74	0.92
GP8	76.01	0.07	12.64	1.39	0.03	0.21	0.79	4.61	3.48	0.00	0.71	99.94	0.99
GP11	76.31	0.09	12.41	1.44	0.04	0.10	0.64	3.62	4.74	0.02	0.74	100.15	1.01
GP16	76.17	0.11	12.23	1.82	0.05	0.10	0.81	3.22	5.41	0.00	0.47	100.39	0.97
LH1	74.80	0.08	12.63	1.57	0.03	0.11	0.99	3.56	5.01	0.00	0.43	99.21	0.97
LS15	75.26	0.10	12.83	1.64	0.03	0.21	0.88	3.32	5.08	0.00	0.51	99.86	1.02
Zhu Jinchu et al., Acta Petrologica Sinica (2005), 21(3): 665-676.													
HS402	74.52	0.18	12.19	2.22	0.07	0.12	1.24	2.99	4.99	0.00	0.87	99.39	0.97
GP47-1	68.55	0.48	14.25	3.43	0.06	0.65	1.74	3.57	5.29	0.16	0.98	99.16	0.97
GP33	62.60	0.65	16.43	5.64	0.12	0.85	2.61	4.66	5.36	0.22	0.83	99.97	0.90
GP61	76.28	0.15	12.07	2.06	0.04	0.11	0.91	3.28	4.71	0.03	0.62	100.26	0.99
GP6	76.73	0.07	12.34	1.21	0.03	0.07	0.81	3.24	5.16	0.00	0.43	100.09	1.00
GL1	73.37	0.24	13.02	1.76	0.05	0.58	0.91	3.11	4.92	0.05	0.83	98.84	1.08
DN4	67.06	0.48	14.36	3.70	0.07	1.40	2.82	3.05	4.15	0.13	2.56	99.78	0.98
GP22-1	68.81	0.31	14.49	3.04	0.06	0.43	1.60	3.51	5.85	0.08	0.57	98.75	0.97
NM42	59.56	1.50	14.38	7.64	0.13	3.68	5.70	3.02	4.00	0.30	0.48	100.39	0.73
NM53	57.83	1.60	14.14	8.29	0.12	4.19	6.11	2.97	3.58	0.33	0.70	99.86	0.71
NM56	58.27	1.60	14.29	7.94	0.12	3.94	6.03	3.00	3.92	0.32	0.59	100.02	0.71
NM47	60.30	1.45	14.73	7.70	0.15	3.25	5.21	3.27	4.08	0.32	0.19	100.65	0.76
NM46	60.11	1.46	14.46	8.01	0.16	3.33	5.18	3.20	4.12	0.33	0.81	101.17	0.76
NM48	62.72	1.10	14.52	6.61	0.14	1.79	3.81	2.94	4.12	0.26	0.98	98.99	0.90
NM49-1	61.98	1.36	14.46	7.09	0.13	2.52	4.63	3.01	4.11	0.29	0.73	100.31	0.81
NM63-1	62.66	1.22	14.33	6.35	0.10	2.48	4.52	2.93	4.16	0.26	0.60	99.61	0.82
NM68-1	62.64	1.26	15.02	7.00	0.11	1.84	3.63	3.54	4.33	0.31	0.56	100.24	0.88
NM44	66.27	0.82	13.60	4.50	0.07	1.25	4.36	2.79	4.35	0.17	1.74	99.92	0.79
TA102	65.59	0.76	14.39	5.03	0.10	0.85	2.35	3.38	5.62	0.14	0.64	98.85	0.90
TA301	65.91	0.82	14.49	5.39	0.12	0.89	2.38	3.37	5.78	0.15	0.65	99.95	0.90
TA302	62.88	1.08	15.07	6.32	0.13	1.42	3.44	3.53	4.80	0.23	0.62	99.52	0.87
Yang Ce et al., Geological Journal of China Universities (2006), 12(3): 310-318.													
GP10	69.88	0.54	14.18	3.98	0.08	0.76	2.13	4.08	4.41	0.22	0.66	100.92	0.92
GP11	69.96	0.38	14.12	3.03	0.05	0.48	1.53	3.38	5.46	0.10	1.06	99.55	0.99
GP12	67.89	0.37	14.71	2.70	0.07	0.49	1.65	3.82	5.65	0.14	0.70	98.19	0.96
GP40-1	71.05	0.33	13.19	3.23	0.06	0.46	2.23	3.09	5.26	0.11	1.16	100.17	0.89
GP23	61.95	0.69	16.63	5.98	0.14	0.91	2.53	4.23	6.04	0.25	0.41	99.76	0.92

GP27	59.62	1.33	15.50	7.65	0.16	1.82	3.67	2.80	4.88	0.46	1.11	99.00	0.94
GP30	63.08	0.72	15.38	4.88	0.10	1.07	2.54	4.11	4.90	0.26	1.57	98.61	0.92
GP31	62.58	0.97	15.23	5.62	0.10	1.53	3.21	4.03	4.71	0.39	1.05	99.42	0.87
GP47-3	59.74	1.17	15.69	7.79	0.15	1.66	3.39	4.29	4.74	0.48	0.55	99.65	0.85
GP7	74.03	0.29	12.78	2.78	0.06	0.36	1.29	2.68	5.22	0.09	0.68	100.26	1.03
GP8	73.15	0.19	13.76	1.77	0.04	0.31	0.94	3.40	5.77	0.06	0.71	100.10	1.02
GP9	72.59	0.13	14.19	1.45	0.03	0.15	0.86	3.33	6.29	0.03	0.60	99.65	1.02
GP63	75.84	0.23	11.87	2.77	0.05	0.17	1.07	3.43	3.99	0.05	0.56	100.03	1.00
Li Xianhua et al., Lithos (2007), 91(1-2): 186-204.													
2KSC1	75.02	0.11	12.61	1.43	0.07	0.13	0.77	3.33	5.08	0.01	0.93	99.49	1.02
2KSC2	76.25	0.09	12.22	1.43	0.07	0.10	0.76	3.19	4.86	0.00	0.30	99.27	1.03
2KSC3	76.69	0.08	12.32	1.30	0.05	0.10	0.77	3.51	4.82	0.03	0.16	99.83	0.99
2KSC4a	73.30	0.32	13.07	2.52	0.06	0.56	2.19	3.15	4.29	0.09	0.71	100.26	0.95
2KSC4b	76.94	0.12	12.03	1.35	0.03	0.18	1.03	2.95	5.21	0.04	0.28	100.16	0.97
2KSC75	72.71	0.18	13.46	2.44	0.05	0.22	0.76	3.29	5.64	0.05	0.95	99.75	1.04
2KSC76	69.01	0.58	14.18	3.88	0.07	0.83	2.43	3.16	4.73	0.19	0.69	99.75	0.96
2KSC78	75.40	0.11	12.34	1.85	0.03	0.10	0.93	3.14	5.29	0.03	0.50	99.72	0.98
2KSC79	71.58	0.37	13.51	3.46	0.07	0.43	1.50	2.68	5.58	0.09	0.70	99.97	1.03
2KSC79a	63.50	0.84	14.86	6.37	0.10	1.63	3.88	2.67	3.99	0.24	1.74	99.82	0.94
P1	64.24	0.62	14.41	6.23	0.11	2.99	4.95	2.35	3.08	0.21	1.51	100.70	0.89
P4	63.94	0.66	16.10	5.42	0.08	2.07	4.74	2.93	3.42	0.18	0.55	100.09	0.94
P9	66.26	0.76	15.14	5.01	0.07	1.27	3.06	3.08	4.39	0.22	0.49	99.75	0.98
MR28	69.56	0.47	13.76	4.51	0.05	0.74	1.27	3.01	4.64	0.14	1.92	100.07	1.12
MR42	75.35	0.11	12.33	1.87	0.06	0.12	0.86	3.30	4.77	0.01	0.41	99.19	1.01
2KF392	72.88	0.26	13.63	2.35	0.06	0.44	1.49	3.19	4.85	0.07	0.22	99.44	1.03
2KF393	72.33	0.24	13.98	2.48	0.06	0.40	1.47	3.14	5.31	0.09	0.50	100.00	1.03
2KF394	71.67	0.27	14.13	2.70	0.07	0.47	1.53	3.06	5.26	0.09	0.42	99.67	1.05
2KF395	71.86	0.29	14.30	2.64	0.07	0.52	1.59	3.35	4.77	0.10	0.29	99.78	1.05
2KF396	71.35	0.29	14.51	2.66	0.07	0.47	1.66	3.28	5.30	0.10	0.26	99.95	1.03
2KF397	73.12	0.32	13.85	2.94	0.08	0.51	1.66	3.05	4.73	0.09	0.23	100.58	1.05
2KF400	72.66	0.13	14.54	2.21	0.05	0.16	1.14	3.30	4.94	0.04	0.42	99.59	1.13
2KF401	73.63	0.14	13.74	2.33	0.06	0.17	1.25	3.31	4.59	0.05	0.37	99.64	1.08
2KF402	73.39	0.11	13.96	1.83	0.04	0.12	1.01	3.37	5.92	0.04	0.42	100.21	1.01
2KF403	75.33	0.13	13.55	2.03	0.05	0.14	0.95	2.94	5.06	0.05	0.44	100.67	1.13
2KF404	75.15	0.10	13.63	1.72	0.04	0.12	0.94	3.08	4.91	0.03	0.45	100.17	1.13
2KF405	74.31	0.16	13.70	2.34	0.06	0.19	1.18	3.17	4.63	0.05	0.44	100.23	1.11
2KG4.1	77.31	0.12	11.68	3.27	0.03	0.10	0.84	2.63	4.72	0.02	0.14	100.86	1.07
2KG4.2	75.38	0.12	12.18	2.40	0.03	0.09	0.89	2.86	5.13	0.01	0.26	99.35	1.03
2KG4.3	75.38	0.12	12.88	2.09	0.02	0.08	0.99	2.91	5.29	0.01	0.41	100.18	1.05
2KG4.4	72.93	0.33	13.69	3.46	0.06	0.49	1.30	3.04	4.72	0.09	0.61	100.72	1.10
Xu Xisheng et al., Science in China Series D-Earth Sciences (2007), 50(2): 209-220.													
FG33-2	68.27	0.58	14.25	4.73	0.07	0.90	2.74	3.10	4.27	0.16	0.95	100.02	0.97

FG22-1	66.72	0.65	15.06	5.23	0.08	1.44	3.12	2.58	4.60	0.21	0.61	100.30	1.01
FG34-2	67.46	0.63	14.64	4.60	0.11	0.98	2.92	3.47	4.12	0.16	0.66	99.75	0.95
FG9-1	68.39	0.64	14.59	5.16	0.07	0.94	2.83	2.95	4.03	0.18	0.53	100.31	1.02
FG15	69.18	0.42	14.76	3.55	0.07	0.85	2.38	3.46	3.81	0.10	1.41	99.99	1.04
FG2h	69.53	0.34	15.42	3.10	0.05	0.57	1.95	3.48	4.56	0.11	1.09	100.20	1.09
FG11-3	70.34	0.36	14.59	3.13	0.06	0.75	2.30	3.20	4.01	0.09	1.18	100.01	1.06
FG17-2	70.90	0.48	13.93	3.75	0.07	0.77	2.11	3.15	4.35	0.16	0.39	100.06	1.01
FG24-5	70.97	0.51	13.70	3.77	0.06	0.87	2.58	3.18	3.41	0.17	0.78	100.00	1.01
FG27	71.85	0.31	13.45	3.37	0.06	0.34	1.44	2.71	5.52	0.09	0.79	99.93	1.03
FG16	72.72	0.25	13.82	2.36	0.03	0.32	0.76	2.86	5.53	0.15	1.26	100.06	1.14
FG5-1	76.88	0.16	11.92	1.62	0.03	0.13	0.79	2.71	4.87	0.04	0.81	99.96	1.07
FG29-1	77.24	0.16	12.22	1.01	0.07	0.08	0.43	3.72	4.50	0.01	0.44	99.88	1.04
Fo3	75.26	0.11	12.93	1.88	0.06	0.22	0.63	3.38	4.76	0.05	0.81	100.09	1.09
Fo6er	61.46	0.25	18.33	4.93	0.30	0.22	1.38	5.77	5.64	0.05	1.61	99.94	1.01
Fo8	72.79	0.26	13.53	2.63	0.07	0.47	1.44	3.04	4.97	0.08	0.59	99.87	1.04
Fo10	67.84	0.47	14.61	4.25	0.08	1.17	3.52	2.83	4.11	0.15	0.94	99.97	0.94
Fo11	66.37	0.63	14.68	5.65	0.11	1.90	3.48	2.71	3.52	0.19	0.94	100.18	1.01
Fo12	66.28	0.60	15.44	4.83	0.10	1.34	3.68	3.03	3.43	0.19	0.89	99.81	1.00
Fo13	70.26	0.52	14.76	3.91	0.06	0.69	2.08	3.15	4.28	0.12	0.52	100.35	1.09
Deng Xiguang et al.,Acta Petrologica Et Mineralogica (2005), 24(2): 93-102.													
2ksc-10a	67.03	0.58	14.27	4.73	0.06	0.72	1.85	3.14	5.35	0.19	1.67	99.59	1.00
2ksc-10b	67.67	0.60	14.51	4.34	0.07	0.76	1.88	3.00	6.18	0.23	1.18	100.42	0.96
2ksc-10d	69.59	0.48	12.96	3.54	0.06	0.58	1.60	2.77	5.63	0.16	1.69	99.06	0.96
2ksc-10e	67.97	0.78	14.19	5.12	0.08	0.90	2.84	3.30	4.28	0.26	1.13	100.85	0.93
2ksc-12	66.48	0.72	14.33	4.95	0.07	0.85	2.50	3.42	4.77	0.24	1.02	99.35	0.93
2ksc-13	64.84	1.12	13.36	7.08	0.11	1.34	3.15	3.00	4.48	0.36	0.80	99.64	0.86
2ksc-14	74.57	0.24	12.00	2.06	0.03	0.25	1.31	2.84	5.37	0.09	0.25	99.01	0.93
2ksc-15	69.08	0.58	13.57	4.23	0.05	0.72	2.46	3.31	4.98	0.21	1.19	100.38	0.89
2ksc-16	69.19	0.64	13.85	4.32	0.07	0.75	2.35	3.12	5.52	0.21	0.74	100.76	0.90
2ksc-17	69.59	0.66	13.15	4.56	0.08	0.79	2.75	3.21	4.43	0.22	1.02	100.46	0.87
2ksc-18	67.63	0.58	13.47	4.41	0.07	0.56	2.26	2.99	5.56	0.21	2.96	100.70	0.90
2ksc-22a	70.55	0.45	13.88	3.39	0.05	0.52	2.02	3.15	5.08	0.12	0.84	100.05	0.97
2ksc-23	75.32	0.10	12.50	1.55	0.02	0.05	0.67	3.17	5.74	0.00	0.53	99.65	0.99
2ksc-24	76.59	0.13	11.78	1.40	0.02	0.09	0.66	2.82	5.70	0.01	0.56	99.76	0.98
2ksc-25	75.44	0.21	12.33	1.92	0.02	0.18	1.33	3.06	4.64	0.04	0.58	99.75	0.99
2ksc-26	72.41	0.45	13.36	3.39	0.05	0.43	1.83	3.22	4.99	0.11	0.74	100.98	0.95
2ksc-27a	66.14	0.69	14.81	4.39	0.07	0.86	2.34	3.21	5.83	0.21	1.54	100.09	0.93
2ksc-27b	65.95	0.94	13.77	6.03	0.09	1.21	2.81	3.07	4.84	0.28	1.27	100.26	0.89
2ksc-27c	67.25	0.81	14.03	5.06	0.08	0.95	2.81	2.99	4.17	0.26	1.26	99.67	0.96
Bai Daoyuan et al., Acta Petrologica Et Mineralogica (2005), 24(4): 255-272.													
C22	75.63	0.24	11.78	2.79	0.04	0.34	0.89	2.72	4.98	0.06	0.35	99.82	1.03
C41	75.38	0.15	11.80	3.44	0.04	0.15	0.61	3.07	4.99	0.02	0.12	99.77	1.02

C40	75.68	0.16	11.99	3.07	0.05	0.18	0.76	3.06	4.59	0.03	0.20	99.77	1.05
C43	73.75	0.21	12.36	3.62	0.05	0.24	1.13	2.97	5.27	0.04	0.15	99.79	0.98
C55	71.13	0.41	13.26	4.36	0.06	0.49	2.21	3.34	4.10	0.11	0.30	99.77	0.95
C24	71.57	0.48	12.90	3.94	0.06	0.60	1.77	2.82	5.29	0.13	0.20	99.76	0.95
C42	72.17	0.30	13.21	3.94	0.05	0.36	1.30	3.12	5.11	0.07	0.15	99.78	1.01
C21	67.89	0.61	13.74	5.55	0.08	0.66	2.45	3.14	5.09	0.21	0.30	99.72	0.91
C23	69.49	0.59	13.03	5.35	0.07	0.86	2.31	2.93	4.80	0.18	0.15	99.76	0.92
C48-1	67.96	0.75	13.47	5.57	0.08	0.95	2.52	2.87	4.84	0.24	0.50	99.75	0.93
C60	70.49	0.47	13.61	3.89	0.05	0.59	2.19	3.00	4.68	0.14	0.65	99.76	0.97
C47	68.38	0.73	13.17	5.78	0.09	1.07	2.81	2.86	4.26	0.23	0.40	99.78	0.91
C48-2	66.10	0.86	14.07	6.06	0.09	1.10	2.84	2.98	5.06	0.27	0.30	99.73	0.91
C54	65.92	0.82	14.32	5.65	0.09	1.08	3.01	3.02	4.97	0.25	0.58	99.71	0.91
Liu Yimao et al., Science in China Series D-Earth Sciences (2002), 32(supp):41-48.													
2kl-3	68.76	0.55	13.72	4.82	0.69	0.07	2.29	3.16	4.68	0.19	0.91	99.84	0.95
2kl-17	69.08	0.58	13.57	4.23	0.05	0.72	2.46	3.31	4.98	0.21	1.19	100.38	0.89
99-Q2	70.38	0.51	13.48	4.67	0.62	0.07	2.03	3.02	4.79	0.16	0.74	100.47	0.97
2kl-31	66.14	0.69	14.81	4.39	0.07	0.86	2.34	3.21	5.83	0.21	1.54	100.09	0.93
Zhu Jinchu et al., Geological Journal of China Universities (2005), 11(3):335-342.													
Zhu Jinchu et al., Geological review (2003), 49(3):245-252.													
QT87	68.49	0.76	13.47	4.70	0.07	0.99	2.61	2.96	4.54	0.19	0.65	99.43	0.93
QT99	70.08	0.50	14.14	3.54	0.06	0.69	1.92	2.93	5.61	0.15	0.45	100.07	0.98
QT100	68.01	0.75	13.68	4.91	0.08	0.90	1.61	3.30	4.29	0.23	1.84	99.60	1.05
QT-27	67.64	0.86	12.60	6.60	0.15	1.10	2.50	2.92	4.46	0.30	0.85	99.98	0.89
QT-29	67.01	0.88	13.06	6.32	0.16	1.22	2.58	3.22	4.37	0.33	1.12	100.27	0.89
QT-38	66.67	0.89	13.70	5.81	0.13	1.15	3.07	2.99	4.42	0.25	1.32	100.40	0.90
QT-31	63.80	1.05	13.80	7.60	0.19	1.44	2.96	2.80	5.29	0.36	1.13	100.42	0.88
Jiang Yaohui et al., Lithos (2009), 107(3-4): 185-204.													
TSL-1	66.00	0.47	15.97	4.04	0.09	1.30	0.90	1.55	5.47	0.20	3.33	99.32	1.58
TSL-2	68.08	0.46	15.35	3.78	0.07	1.62	0.96	1.88	4.62	0.18	2.96	99.93	1.56
TSL-3	67.39	0.43	15.46	3.95	0.09	1.48	1.96	2.58	4.50	0.17	1.56	99.59	1.22
TSL-4	67.60	0.44	15.30	4.08	0.08	1.50	1.09	2.10	4.52	0.17	2.74	99.63	1.48
TSL-5	58.93	0.85	18.24	6.08	0.14	2.33	2.95	2.53	3.52	0.28	3.71	99.53	1.37
TSL-6	67.87	0.41	15.13	3.98	0.09	1.45	2.26	2.51	3.86	0.16	1.68	99.41	1.22
TSL-7	68.83	0.41	14.83	3.83	0.09	1.43	2.26	2.61	4.14	0.16	1.33	99.92	1.15
JJL-1	76.99	0.13	12.17	1.47	0.03	0.15	0.21	2.99	4.79	0.03	0.68	99.65	1.16
JJL-2	74.06	0.13	13.64	1.65	0.07	0.14	0.09	2.43	6.54	0.03	0.94	99.73	1.21
JJL-3	74.53	0.15	12.91	1.70	0.03	0.14	0.89	3.44	4.82	0.04	0.84	99.49	1.03
JJL-4	73.82	0.14	13.23	1.66	0.07	0.20	0.78	2.55	6.27	0.04	0.98	99.74	1.07
JJL-5	77.98	0.13	11.20	1.56	0.04	0.15	0.61	2.88	4.53	0.03	0.74	99.87	1.04
JJL-6	73.57	0.16	13.47	1.85	0.04	0.26	0.91	3.05	5.54	0.04	1.18	100.08	1.06
JJL-8	76.51	0.17	11.83	1.81	0.03	0.18	0.81	2.63	5.63	0.04	0.23	99.89	1.00

JJL-9	74.37	0.24	12.51	2.25	0.04	0.32	1.28	2.69	5.31	0.07	0.47	99.54	1.00
XS-1	74.03	0.23	11.95	2.48	0.04	0.53	0.91	2.55	5.57	0.09	1.26	99.64	1.01
XS-2	74.31	0.22	12.54	2.39	0.03	0.47	0.49	2.69	5.70	0.07	0.90	99.81	1.09
XS-3	71.80	0.24	12.75	2.63	0.04	0.50	0.30	2.87	5.90	0.08	2.04	99.15	1.09
XS-5	73.83	0.22	12.63	2.58	0.04	0.31	0.81	2.29	5.83	0.08	1.32	99.94	1.09
XS-7	71.75	0.31	13.14	3.33	0.05	0.33	1.57	2.58	5.48	0.11	0.68	99.32	1.01
XS-8	75.09	0.11	12.82	1.74	0.04	0.15	0.49	3.11	5.04	0.06	0.69	99.32	1.12
XS-9	75.09	0.11	12.91	1.58	0.03	0.19	0.14	2.94	5.36	0.05	0.71	99.12	1.19
XS-10	74.83	0.19	12.75	2.08	0.04	0.23	0.37	2.37	5.75	0.06	0.81	99.47	1.18
XS-11	73.70	0.18	12.74	2.16	0.04	0.25	1.21	2.87	5.09	0.08	1.45	99.76	1.03
XS-12	74.59	0.16	12.73	2.14	0.05	0.18	1.19	2.73	5.24	0.07	0.85	99.94	1.03
Jiang Yaohui et al., Geological Magzine (2006),143(4): 457-474.													
JCT-29	74.49	0.12	12.81	1.58	0.04	0.14	1.11	2.65	5.39	0.03	1.14	99.37	1.05
SZY-19	74.87	0.11	12.60	1.64	0.04	0.17	1.16	2.82	5.23	0.03	1.18	99.73	1.02
SZY-1	75.86	0.05	12.67	1.08	0.03	0.12	0.90	3.49	4.80	0.01	0.50	99.45	1.01
SZY-20	75.92	0.05	12.41	1.33	0.03	0.15	0.85	3.24	4.57	0.01	1.08	99.60	1.05
SZY-9	74.62	0.01	13.55	0.26	0.01	0.09	0.88	4.02	5.12	0.01	0.96	99.51	1.00
JCT-15	72.57	0.25	13.47	1.37	0.04	0.37	1.95	3.06	5.33	0.07	0.98	99.36	0.94
JCT-27	74.17	0.12	12.73	1.63	0.04	0.15	1.09	3.17	5.28	0.03	0.99	99.23	0.99
SZY-18	72.42	0.31	13.29	2.41	0.04	0.40	1.80	2.94	4.99	0.08	1.06	99.59	0.98
SZY-21	71.56	0.27	13.84	1.97	0.04	0.44	2.51	2.91	4.92	0.07	1.34	99.76	0.94
Zhang Min et al., Geochemica (2003), 32(6): 529-539.													
1	77.71	0.18	11.12	1.39	0.03	0.20	0.73	2.68	4.94	0.03	0.93	99.94	1.00
2	76.26	0.15	12.66	1.30	0.04	0.10	0.84	3.39	4.49	0.03	0.56	99.82	1.06
3	75.65	0.19	12.49	1.47	0.05	0.18	0.85	3.04	4.98	0.06	1.14	100.10	1.05
4	76.39	0.16	12.41	1.41	0.06	0.09	0.72	3.28	5.02	0.03	0.67	100.24	1.02
5	76.33	0.16	12.53	1.32	0.04	0.07	0.88	3.14	4.91	0.03	0.71	100.12	1.04
6	77.37	0.15	12.03	1.33	0.04	0.08	0.72	3.03	4.89	0.02	0.57	100.23	1.04
7	74.93	0.21	13.13	1.73	0.04	0.25	0.49	2.69	5.54	0.07	1.09	100.17	1.16
8	74.51	0.27	12.58	2.01	0.04	0.32	0.94	2.48	5.52	0.08	1.26	100.01	1.07
9	77.97	0.09	11.84	0.71	0.03	0.00	0.52	3.30	4.62	0.02	0.85	99.95	1.04
10	75.72	0.13	13.56	0.99	0.02	0.08	0.11	2.02	5.29	0.02	1.84	99.78	1.47
11	77.02	0.11	12.96	0.72	0.03	0.08	0.16	3.62	4.52	0.03	0.62	99.87	1.16
Ma Tieqiu et al., Geochemica (2006), 35(4): 346-358.													
C24-4	75.18	0.11	12.42	2.40	0.00	0.10	0.82	2.70	6.13	0.01	0.24	100.11	0.99
C33	76.19	0.13	11.53	2.81	0.03	0.19	0.66	2.55	5.16	0.01	0.55	99.81	1.05
C36	76.14	0.12	11.47	2.53	0.03	0.10	1.24	2.64	5.45	0.02	0.14	99.88	0.92
C34	76.46	0.12	11.41	3.06	0.03	0.13	0.46	2.69	5.32	0.01	0.44	100.13	1.04
C37	75.40	0.20	11.93	2.85	0.04	0.18	1.03	2.95	5.00	0.03	0.29	99.90	0.98
C31	76.13	0.08	12.36	2.44	0.02	0.26	0.47	2.17	4.96	0.05	0.81	99.75	1.26
C32	76.49	0.16	11.33	2.92	0.03	0.14	0.61	2.71	5.38	0.01	0.27	100.05	0.99

DDS5	74.40	0.30	12.61	2.51	0.04	0.36	1.35	2.63	4.95	0.07	0.63	99.85	1.04
DDS4-2	75.51	0.05	14.01	1.01	0.08	0.03	0.14	3.60	4.74	0.05	0.77	99.99	1.24
GD08-1	72.39	0.42	12.70	4.02	0.08	0.33	1.12	4.11	4.28	0.08	0.62	100.15	0.95
GD8-4-1	67.98	0.62	14.76	3.99	0.05	0.51	1.27	4.98	4.60	0.10	0.78	99.45	0.95
GD8-4-2	67.82	0.65	14.90	3.65	0.06	0.57	1.43	4.94	4.83	0.09	0.80	99.54	0.93
D185	76.84	0.06	12.21	1.30	0.13	0.05	0.44	3.41	5.24	0.01	0.30	99.93	1.01

References: (Bai et al., 2005; Chen et al., 2005; Deng et al., 2005; Gu et al., 2006; Jiang et al., 2009; Jiang et al., 2006; Li et al., 2003a; Li et al., 2007b; Ma et al., 2006; Wang et al., 2003a; Xu et al., 2007; Yang et al., 2006a; Yao et al., 2005; Zhang et al., 2003; Zhu et al., 2003; Zhu et al., 2005a; Zhu et al., 2005b)

Appendix Table 2 List of samples studied

No.	Sample name	Lithology	GPS position	Thin section	In-situ zircon analyses
	Jiuyishan intrusive-volcanic complex				
1	XY13-1	Rhyolite	N25°13'41"; E112°23'13"	YES	YES
2	XY13-3	As above		YES	
3	XY13-4	As above		YES	
4	XY13-5	As above		YES	
5	XY13-6	As above		YES	
6	XY13-7	As above		YES	
7	XY15-1	Granite porphyry	N25°14'31"; E112°N25'42"	YES	
8	XY15-2	As above			
9	XY15-4	As above			
10	XY15-6	As above	N25°14'50"; E112°26'08"	YES	
11	XY16-1	Coarse-grained biotite K-feldspar granite	N25°08'19"; E112°07'41"	YES	
12	XY16-2	Coarse-grained biotite granite		YES	
13	XY17-1	Dark granite porphyry	N25°06'02"; E112°07'19"	YES	
14	XY17-4	Granodiorite (amphibole-bearing)		YES	
15	XY17-5	Granodiorite			
16	XY17-6	As above		YES	YES
17	XY18-1	Dark granite porphyry (fayalite-bearing)	N25°08'32"; E112°08'45"	YES	YES
18	XY18-4	As above			
19	XY19-1	Ignimbrite	N25°13'57"; E112°10'41"	YES	
20	XY19-2	As above		YES	
21	XY20-1	As above	N25°13'09"; E112°10'59"	YES	YES
22	XY21-1	Biotite granite	N25°12'13"; E112°11'20"	YES	
23	XY21-2	As above			
24	XY22-2	As above	N25°12'N25"; E112°11'05"	YES	
25	GD20-3	Quartz monzonite	25°06'02.5"; 112°13'25.2"	YES	
26	GD21-2	Biotite granite	25°07'11.3"; 112°13'05.0"		
27	GD22-1	Biotite quartz monzonite	25°08'31.6"; 112°13'03.5"	YES	
28	GD23-1	Biotite monzonite	25°08'52.8"; 112°13'07.4"	YES	YES
29	GD23-2	As above		YES	
30	GD24-2	Dark enclave		YES	
31	GD24-3	Biotite quartz monzonite		YES	
32	GD25-1	Biotite granite	25°11'10.5"; 112°12'05.0"		
33	GD26-1	Biotite quartz monzonite	25°12'23.3"; 112°11'03.6"		

34	GD26-2	As above		YES	
35	GD28-1	Biotite granite	25°11'17.5"; 112°05'15.2"	YES	
36	GD28-2	As above			
37	GD29-2	Coarse-grained biotite granite	25°08'37.1"; 112°04'54.5"	YES	
38	GD29-4	As above		YES	
39	GD29-6	Biotite granite	25°06'26.4"; 112°01'28.8"		
	Jiufeng pluton				
40	XY2-1	Coarse-grained biotite K-feldspar granite	N25°17'04"; E113°44'28"	YES	YES
41	XY2-2	As above		YES	
42	XY2-4	As above			
43	XY3-1	Two mica K-feldspar granite	N25°20'28"; E113°44'51"	YES	YES
44	XY3-3	As above			
45	XY3-6	As above			
46	XY3-7	As above		YES	
47	XY4-3	Fine-grained biotite K-feldspar granite	N25°19'29"; E113°42'50"	YES	YES
48	XY4-4	Fine-grained felsic dyke		YES	
49	XY4-5	Biotite granite			
50	XY4-7	As above		YES	
51	XY5-1	Biotite K-feldspar granite	N25°20'00"; E113°41'21"	YES	
52	XY5-3	As above			
53	XY6-1	As above	N25°19'56"; E113°39'52"	YES	
54	XY6-2	As above			
55	XY7-1	Fine-grained muscovite granite	N25°19'57"; E113°37'59"	YES	YES
56	XY7-2	As above			
57	XY7-3	As above			
58	XY7-4	As above		YES	
59	XY8-1	Biotite granite	N25°21'01"; E113°20'30"	YES	
60	XY9-1	Amphibole-bearing granite	N25°21'01"; E113°20'13"	YES	
61	XY9-3	As above		YES	
62	XY9-5	Amphibole-bearing biotite granite	N25°21'10"; E113°19'36"		
63	XY9-6	As above		YES	
64	XY9-9	As above	N25°21'01"; E113°18'57"		
65	XY10-1	As above	N25°21'56"; E113°15'09"	YES	YES
66	XY10-2	As above		YES	
67	XY10-3	As above		YES	
	Dadongshan pluton				

68	GD08-3	Coarse-grained biotite granite	24°37'46.0"; 113°13'38.0"	YES	
69	GD08-4	Fine-grained granitic enclave		YES	
70	GD08-5	Coarse-grained biotite granite		YES	YES
71	GD10-1	Biotite granite	24°39'18.2"; 113°18'46.0"	YES	
72	GD10-2	As above		YES	
73	GD10-3	As above		YES	
74	GD11-1	As above	24°41'41.8"; 113°07'03.6"	YES	
75	GD11-2	As above		YES	
77	GD13	As above	24°40'51.0"; 113°04'06.8"	YES	
78	GD14-1	Coarse-grained biotite K-feldspar granite	24°41'11.3"; 113°01'58.4"	YES	
79	GD14-2	As above		YES	
80	GD14-3	As above		YES	
81	GD15-1	As above	24°45'11.3"; 112°58'56.6"	YES	YES
82	GD15-2	As above		YES	
83	GD15-3	As above		YES	
84	GD16-2	As above	24°45'18.8"; 112°58'27.5"	YES	
85	GD16-3	As above		YES	
86	GD17-2	Fine-grained biotite granite	24°44'58.0"; 112°53'04.1"	YES	
87	GD17-3	As above		YES	
88	GD18-1	As above	24°45'28.8"; 112°53'43.2"	YES	
	Xiaoliang stock				
89	GD47-1	Amphibole-bearing biotite K-feldspar granite	21°31'10.4"; 110°59'13.6"	YES	YES
90	GD47-2	As above			
91	GD47-3	As above		YES	
92	GD47-4	As above			
93	GD47-5	As above		YES	
	Gangwei stock				
94	GD51-1	Quartz monzonite	22°04'07.3"; 111°45'07.2"	YES	YES
95	GD51-2	As above			
96	GD51-3	As above		YES	
97	GD51-4	As above		YES	
98	GD51-5	As above			
	Lunshui stock				
99	GD52-1	Amphibole-bearing granite	22°02'28.1"; 114°51'16.2"	YES	
100	GD52-2	As above			

101	GD52-3	As above		YES	
102	GD52-4	As above			
	Gudoushan pluton				
103	GD60-1	Biotite granite	22°14'43.0"; 112°53'34.5"	YES	
104	GD60-4	As above		YES	
105	GD61-1	As above	22°14'15.3"; 112°55'05.7"	YES	YES
106	GD61-3	As above		YES	
107	GD61-5	As above			
	Wuguishan pluton				
108	GD62-1	Coarse-grained biotite granite	22°29'53.3"; 113°19'16.8"	YES	YES
109	GD62-3	As above		YES	
110	GD63-1	Coarse-grained biotite K-feldspar granite	22°28'40.3"; 113°21'39.1"		
111	GD63-2	As above		YES	
112	GD63-4	As above			
113	GD63-7	Biotite granite		YES	
114	GD64-1	As above	22°28'22.1"; 113°21'19.3"	YES	
115	GD64-3	As above			

Appendix Table 3 Chemical compositions of feldspars

	Jiuyishan									
	Pl	Pl	Pl	Pl	Pl	Pl	Pl	Pl	Pl	Pl
Oxides (wt%)										
SiO_2	56.54	56.25	59.86	57.49	57.28	57.61	62.13	58.99	61.72	58.7
TiO_2	0.03	0.03	0.02	0.1	0.04	-	0.02	0.02	0.04	0.03
Al_2O_3	26.54	26.69	24.6	26.42	26	26.51	23.21	25.75	23.26	24.7
FeO	0.13	0.07	0.14	0.11	0.17	0.12	0.07	0.13	0.08	0.18
MnO	-	0.02	0.01	-	0.01	-	0.04	-	-	0.02
MgO	-	-	-	-	-	0.01	-	-	-	0
CaO	9.31	9.57	7.03	8.83	8.89	9.33	5.09	8.5	5.35	7.67
Na2O	6.48	6.52	7.93	6.95	6.87	6.31	8.87	6.79	8.66	7.37
K2O	0.32	0.23	0.19	0.24	0.36	0.17	0.3	0.21	0.33	0.57
Total	99.34	99.38	99.78	100.14	99.63	100.05	99.72	100.39	99.44	99.23
Cations per 32 oxygens										
Si	10.244	10.194	10.716	10.317	10.346	10.331	11.066	10.515	11.031	10.611
Al	5.664	5.695	5.186	5.584	5.53	5.598	4.869	5.405	4.896	5.258
Ti	0.003	0.003	0.003	0.013	0.005	0	0.003	0.003	0.005	0.004
Fe^{2+}	0.02	0.011	0.02	0.017	0.025	0.018	0.01	0.02	0.012	0.027
Mn	0	0.003	0.002	0	0.002	0	0.006	0	0	0.004
Mg	0	0	0	0	0	0.002	0	0	0	0
Ca	1.807	1.858	1.349	1.698	1.72	1.793	0.97	1.624	1.024	1.485
Na	2.275	2.292	2.753	2.417	2.407	2.193	3.063	2.347	3	2.582
K	0.074	0.054	0.043	0.055	0.084	0.038	0.068	0.048	0.075	0.131
Sum	20.087	20.11	20.072	20.101	20.119	19.973	20.055	19.962	20.043	20.102
Ab	54.7	54.5	66.4	58	57.2	54.5	74.7	58.4	73.2	61.5
An	43.5	44.2	32.5	40.7	40.8	44.6	23.7	40.4	25	35.4
Or	1.8	1.3	1	1.3	2	0.9	1.7	1.2	1.8	3.1

	Jiuyishan									
	Pl	Pl	Pl	Pl	Kfs	Kfs	Kfs	Kfs	Kfs	Kfs
Oxides (wt%)										
SiO_2	58.66	59.92	58.77	56.91	63.14	64.77	64.88	64.20	63.84	64.45
TiO_2	0.03	0.00	0.02	0.01	-	-	-	0.01	-	0.00
Al_2O_3	24.83	24.00	24.74	26.30	18.33	18.11	18.05	18.13	18.10	18.13
FeO	0.20	0.12	0.12	0.15	0.07	0.08	0.07	0.05	0.04	0.06
MnO	0.00	0.00	0.00	0.00	-	-	-	0.03	-	0.00
MgO	0.01	0.01	0.00	0.02	-	-	-	-	-	0.00
CaO	7.67	6.74	7.69	9.40	0.04	0.08	0.06	0.09	0.02	0.17
Na2O	7.33	7.59	7.45	6.46	1.57	1.40	1.64	1.60	1.39	2.32
K2O	0.58	0.53	0.46	0.43	14.99	15.98	15.00	15.47	16.03	14.73

Total	99.32	98.90	99.25	99.68	98.12	100.42	99.69	99.56	99.41	99.86
Cations per 32 oxygens										
Si	10.594	10.813	10.612	10.281	11.891	11.961	12.003	11.940	11.926	11.932
Al	5.281	5.100	5.261	5.595	4.066	3.939	3.931	3.970	3.981	3.954
Ti	0.005	0.000	0.003	0.001	0	0	0	0.001	0	0.001
Fe^{2+}	0.031	0.018	0.018	0.023	0.011	0.012	0.011	0.007	0.006	0.009
Mn	0	0	0	0	0	0	0	0.004	0	0
Mg	0.002	0.002	0.001	0.005	0	0	0	0	0	0
Ca	1.484	1.303	1.487	1.819	0.007	0.016	0.011	0.018	0.004	0.033
Na	2.565	2.657	2.610	2.262	0.573	0.502	0.586	0.576	0.502	0.832
K	0.134	0.121	0.106	0.098	3.601	3.765	3.540	3.670	3.819	3.480
Sum	20.096	20.014	20.098	20.084	20.149	20.195	20.082	20.186	20.238	20.241
Ab	61.3	65.1	62.1	54.1	13.7	11.7	14.2	13.5	11.6	19.1
An	35.5	31.9	35.4	43.5	0.2	0.4	0.3	0.4	0.1	0.8
Or	3.2	3.0	2.5	2.3	86.1	87.9	85.6	86.1	88.3	80.1

	Jiufeng								
	Pl	Pl	Pl	Pl	Pl	Pl	Pl	Kfs	Kfs
Oxides (wt%)									
SiO2	55.44	61.22	62.99	55.8	56.67	54.52	58.09	65.13	65.29
TiO2	0	0	0	0	0	0	0.04	0	0.05
Al2O3	27.18	23.54	22.01	27.65	26.53	27.61	25.78	17.91	18.27
FeO	0.24	0.19	0.14	0.19	0.26	0.19	0.19	0.09	0.04
MnO	0.01	0.03	0	0	0.01	0.05	0.01	0.01	0.02
MgO	0	0	0.03	0.01	0	0.03	0.01	0	0
BaO	0.05	0.05	0.1	0.09	0.03	0.1	0.03	0.02	0.05
CaO	9.86	5.53	4.08	9.96	9.01	10.68	8.33	0.04	0.11
Na2O	5.83	8.48	8.97	5.58	5.98	5.45	6.55	1.85	2.25
K2O	0.24	0.39	0.38	0.32	0.27	0.16	0.21	13.84	13.48
Total	98.85	99.43	98.7	99.6	98.76	98.79	99.24	98.89	99.56
Cations per 32 oxygens									
Si	10.106	10.964	11.297	10.084	10.297	9.97	10.475	12.068	12.012
Al	5.835	4.965	4.649	5.885	5.677	5.946	5.475	3.908	3.959
Ti	0	0	0	0	0	0	0.005	0	0.007
Fe2	0.037	0.028	0.021	0.029	0.04	0.029	0.029	0.014	0.006
Mn	0.002	0.005	0	0	0.002	0.008	0.002	0.002	0.003
Mg	0	0	0.008	0.003	0	0.008	0.003	0	0
Ba	0.004	0.004	0.007	0.006	0.002	0.007	0.002	0.001	0.004
Ca	1.926	1.061	0.784	1.929	1.754	2.093	1.609	0.008	0.022
Na	2.061	2.945	3.119	1.955	2.107	1.933	2.29	0.665	0.803
K	0.056	0.089	0.087	0.074	0.063	0.037	0.048	3.272	3.164
Cations	20.031	20.065	19.979	19.971	19.944	20.038	19.94	19.939	19.984

Ab	51	71.9	78.2	49.4	53.7	47.6	58	16.9	20.1
An	47.6	25.9	19.6	48.7	44.7	51.5	40.8	0.2	0.6
Or	1.4	2.2	2.2	1.9	1.6	0.9	1.2	82.9	79.3
			Xiaoliang				Gangwei		
	Kfs	Kfs	Kfs	Kfs	Kfs	Pl	Pl	Kfs	Kfs
Oxides (wt%)									
SiO2	64.29	64.99	64.63	64.81	64.09	56.97	56.82	64.42	64.89
TiO2	0.01	0.03	0.03	0	0.02	0	0	0.04	0.03
Al2O3	17.59	17.93	17.86	17.95	17.62	25.8	26.62	18.11	17.69
FeO	0.07	0.06	0.07	0.1	0.09	0.27	0.24	0.14	0.06
MnO	0	0	0.02	0	0.02	0	0.04	0	0
MgO	0	0.01	0.02	0	0.02	0	0	0	0
BaO	0.09	0.19	0.15	0.25	0.09	0	0.09	0.99	0.07
CaO	0.02	0.02	0.01	0.08	0.06	8.7	9.11	0.09	0.05
Na2O	0.56	0.72	0.78	0.68	1.16	6.37	6.33	1.51	1.1
K2O	15.81	15.41	15.72	15.69	14.93	0.18	0.23	14.31	15.02
Total	98.44	99.36	99.29	99.56	98.1	98.29	99.48	99.61	98.91
Cations per 32 oxygens									
Si	12.07	12.061	12.035	12.036	12.046	10.391	10.271	11.977	12.081
Al	3.889	3.919	3.917	3.926	3.9	5.542	5.667	3.965	3.878
Ti	0.001	0.004	0.004	0	0.003	0	0	0.006	0.004
Fe2	0.011	0.009	0.011	0.016	0.014	0.041	0.036	0.022	0.009
Mn	0	0	0.003	0	0.003	0	0.006	0	0
Mg	0	0.003	0.006	0	0.006	0	0	0	0
Ba	0.007	0.014	0.011	0.018	0.007	0	0.006	0.072	0.005
Ca	0.004	0.004	0.002	0.016	0.012	1.7	1.764	0.018	0.01
Na	0.204	0.259	0.282	0.245	0.423	2.253	2.219	0.544	0.397
K	3.787	3.648	3.734	3.717	3.58	0.042	0.053	3.394	3.567
Cations	19.98	19.935	20.016	19.992	20.001	19.969	20.028	20.07	19.956
Ab	5.1	6.6	7	6.2	10.5	56.4	55	13.8	10
An	0.1	0.1	0	0.4	0.3	42.6	43.7	0.5	0.3
Or	94.8	93.3	92.9	93.4	89.2	1.1	1.3	85.8	89.8
			Gangwei				Lunshui		
	Kfs	Pl	Pl	Pl	Kfs	Pl	Pl	Pl	Pl
Oxides (wt%)									
SiO2	64.29	60.64	59.56	56.79	64.36	61.68	60.78	61.61	62.06
TiO2	0.01	0.02	0	0	0.02	0	0.04	0	0.01
Al2O3	17.59	23.54	24.62	26.37	17.78	23.46	23.44	23.44	23.18
FeO	0.07	0.18	0.21	0.27	0.07	0.11	0.15	0.14	0.13
MnO	0	0.01	0	0	0	0	0	0	0
MgO	0	0.03	0	0.02	0	0.02	0	0.05	0

BaO	0.09	0.01	0.02	0.08	0	0	0	0	0
CaO	0.02	5.87	6.96	8.9	0.05	5.48	5.67	5.35	5.09
Na2O	0.56	7.96	7.8	6.39	0.53	8.53	8.09	8.19	8.71
K2O	15.81	0.3	0.23	0.23	15.8	0.1	0.43	0.32	0.39
Total	98.44	98.56	99.4	99.05	98.61	99.38	98.6	99.1	99.57
Cations per 32 oxygens									
Si	12.07	10.942	10.705	10.303	12.051	11.016	10.963	11.03	11.067
Al	3.889	5.002	5.211	5.634	3.921	4.934	4.979	4.942	4.868
Ti	0.001	0.003	0	0	0.003	0	0.005	0	0.001
Fe2	0.011	0.027	0.032	0.041	0.011	0.016	0.023	0.021	0.019
Mn	0	0.002	0	0	0	0	0	0	0
Mg	0	0.008	0	0.005	0	0.005	0	0.013	0
Ba	0.007	0.001	0.001	0.006	0	0	0	0	0
Ca	0.004	1.135	1.34	1.73	0.01	1.049	1.096	1.026	0.972
Na	0.204	2.785	2.718	2.248	0.192	2.954	2.829	2.843	3.012
K	3.787	0.069	0.053	0.053	3.774	0.023	0.099	0.073	0.089
Cations	19.98	19.975	20.061	20.026	19.962	19.997	19.994	19.948	20.028
Ab	5.1	69.8	66.1	55.8	4.8	73.4	70.3	72.1	74
An	0.1	28.5	32.6	42.9	0.3	26.1	27.2	26	23.9
Or	94.8	1.7	1.3	1.3	94.9	0.6	2.5	1.9	2.2

	Lunshui			Gudoushan					
	Kfs	Pl	Pl	Kfs	Kfs	Kfs	Kfs	Pl	Kfs
Oxides (wt%)									
SiO2	64.29	61.15	67.85	62.77	64.09	64.4	64.7	59.88	64.21
TiO2	0.01	0	0	0.03	0	0.04	0.01	0.01	0
Al2O3	17.59	23.28	18.78	19.12	17.92	17.93	17.55	24.69	17.95
FeO	0.07	0.17	0.02	0.56	0.2	0.05	0.04	0.09	0.07
MnO	0	0.02	0	0.07	0	0	0	0.01	0
MgO	0	0.02	0.01	0.28	0	0.02	0	0	0
BaO	0.09	0.02	0	0.23	0.05	0.09	0	0.07	0.23
CaO	0.02	5.43	0.11	0.05	0.02	0	0.01	6.81	0
Na2O	0.56	8.38	11.76	0.25	0.63	0.29	0.34	7.83	0.79
K2O	15.81	0.29	0.06	15.71	16.04	16.37	16.33	0.23	15.71
Total	98.44	98.76	98.59	99.07	98.95	99.19	98.98	99.62	98.96
Cations per 32 oxygens									
Si	12.07	11.006	12.027	11.761	11.998	12.021	12.088	10.73	12.008
Al	3.889	4.935	3.92	4.219	3.951	3.942	3.861	5.21	3.953
Ti	0.001	0	0	0.004	0	0.006	0.001	0.001	0
Fe2	0.011	0.026	0.003	0.088	0.031	0.008	0.006	0.013	0.011
Mn	0	0.003	0	0.011	0	0	0	0.002	0
Mg	0	0.005	0.003	0.078	0	0.006	0	0	0

Ba	0.007	0.001	0	0.017	0.004	0.007	0	0.005	0.017
Ca	0.004	1.047	0.021	0.01	0.004	0	0.002	1.307	0
Na	0.204	2.925	4.042	0.091	0.229	0.105	0.123	2.721	0.286
K	3.787	0.067	0.014	3.755	3.831	3.898	3.892	0.053	3.748
Cations	19.98	20.016	20.03	20.051	20.052	20	19.973	20.047	20.04
Ab	5.1	72.4	99.1	2.4	5.6	2.6	3.1	66.7	7.1
An	0.1	25.9	0.5	0.3	0.1	0	0	32	0
Or	94.8	1.7	0.3	97.4	94.3	97.4	96.9	1.3	92.9

				Gudoushan				Wuguishan	
	Kfs	Pl	Pl	Pl	Pl	Kfs	Pl	Kfs	Pl
Oxides (wt%)									
SiO2	64.29	60.54	59.83	60.37	60.2	63.81	60.62	64.33	59.04
TiO2	0.01	0.01	0	0.02	0	0.03	0.02	0	0
Al2O3	17.59	23.72	24.55	24.11	24.29	17.68	23.76	17.85	24.53
FeO	0.07	0.12	0.1	0.11	0.06	0.03	0.19	0.06	0.02
MnO	0	0	0	0.04	0.02	0	0	0	0
MgO	0	0	0	0.03	0.03	0.01	0	0	0
BaO	0.09	0.04	0.04	0	0	0.17	0	0	0
CaO	0.02	5.84	6.84	6.26	6.34	0.04	5.94	0.06	6.95
Na2O	0.56	8.25	7.87	8.08	8.09	0.91	7.74	0.69	7.3
K2O	15.81	0.27	0.22	0.24	0.09	15.53	0.53	15.69	0.11
Total	98.44	98.79	99.45	99.26	99.12	98.21	98.8	98.68	97.95
Cations per 32 oxygens									
Si	12.07	10.906	10.74	10.836	10.811	12.02	10.919	12.034	10.73
Al	3.889	5.032	5.19	5.097	5.137	3.922	5.04	3.932	5.25
Ti	0.001	0.001	0	0.003	0	0.004	0.003	0	0
Fe2	0.011	0.018	0.015	0.017	0.009	0.005	0.029	0.009	0.003
Mn	0	0	0	0.006	0.003	0	0	0	0
Mg	0	0	0	0.008	0.008	0.003	0	0	0
Ba	0.007	0.003	0.003	0	0	0.013	0	0	0
Ca	0.004	1.127	1.316	1.204	1.22	0.008	1.146	0.012	1.353
Na	0.204	2.882	2.739	2.812	2.817	0.332	2.703	0.25	2.572
K	3.787	0.062	0.05	0.055	0.021	3.732	0.122	3.744	0.026
Cations	19.98	20.034	20.056	20.038	20.026	20.052	19.962	19.981	19.934
Ab	5.1	70.8	66.7	69.1	69.4	8.2	68.1	6.2	65.1
An	0.1	27.7	32.1	29.6	30.1	0.2	28.9	0.3	34.2
Or	94.8	1.5	1.2	1.4	0.5	91.7	3.1	93.5	0.7

					Wuguishan				
	Kfs	Pl	Pl	Kfs	Pl	Kfs	Pl	Kfs	Pl
Oxides (wt%)									
SiO2	64.29	60.38	63.79	64.41	67.39	64.85	61.53	64.06	67.19

TiO2	0.01	0	0.01	0.01	0.02	0.01	0.05	0.01	0
Al2O3	17.59	24.12	21.56	17.62	19.96	17.84	23.39	17.83	19.56
FeO	0.07	0.19	0.05	0.07	0	0.09	0.11	0.02	0
MnO	0	0	0	0.02	0	0	0	0	0
MgO	0	0.04	0	0.01	0.02	0	0	0	0.03
BaO	0.09	0.06	0.08	0.06	0	0.01	0.02	0.02	0
CaO	0.02	6.2	3.38	0	1.55	0.04	5.25	0	0.67
Na2O	0.56	7.99	9.67	0.63	10.53	0.92	8.58	0.36	11.44
K2O	15.81	0.33	0.4	15.82	0.04	15.49	0.26	16.28	0.08
Total	98.44	99.31	98.94	98.65	99.51	99.25	99.19	98.58	98.97
Cations per 32 oxygens									
Si	12.07	10.838	11.401	12.066	11.846	12.053	11.018	12.027	11.886
Al	3.889	5.099	4.538	3.887	4.132	3.905	4.932	3.942	4.075
Ti	0.001	0	0.001	0.001	0.003	0.001	0.007	0.001	0
Fe2	0.011	0.029	0.007	0.011	0	0.014	0.016	0.003	0
Mn	0	0	0	0.003	0	0	0	0	0
Mg	0	0.011	0	0.003	0.005	0	0	0	0.008
Ba	0.007	0.004	0.006	0.004	0	0.001	0.001	0.001	0
Ca	0.004	1.192	0.647	0	0.292	0.008	1.007	0	0.127
Na	0.204	2.781	3.351	0.229	3.589	0.332	2.979	0.131	3.924
K	3.787	0.076	0.091	3.781	0.009	3.673	0.059	3.899	0.018
Cations	19.98	20.034	20.048	19.989	19.876	19.988	20.02	20.005	20.038
Ab	5.1	68.7	82	5.7	92.3	8.3	73.6	3.3	96.4
An	0.1	29.4	15.8	0	7.5	0.2	24.9	0	3.1
Or	94.8	1.9	2.2	94.3	0.2	91.5	1.5	96.7	0.4

	Wuguishan								
	Kfs	Kfs	Pl	Kfs	Pl	Pl	Pl	Kfs	Kfs
Oxides (wt%)									
SiO2	64.29	64.57	65.04	64.54	64.88	66.18	64.19	64.51	65.18
TiO2	0.01	0	0	0.02	0	0	0.01	0	0.04
Al2O3	17.59	17.77	21.03	17.7	21.02	20.13	21.22	18.03	21.15
FeO	0.07	0.06	0.08	0.01	0.11	0.01	0.05	0.07	0.05
MnO	0	0	0	0.01	0	0.02	0.01	0	0
MgO	0	0	0	0	0	0	0	0	0.01
BaO	0.09	0	0.03	0	0	0.01	0.08	0.02	0.03
CaO	0.02	0.02	2.27	0.03	2.56	1.52	2.78	0.01	2.22
Na2O	0.56	0.6	10.24	0.32	10.02	10.87	9.95	0.46	10.48
K2O	15.81	16.22	0.2	16.01	0.54	0.17	0.2	16.29	0.16
Total	98.44	99.24	98.89	98.64	99.13	98.91	98.49	99.39	99.32
Cations per 32 oxygens									
Si	12.07	12.044	11.571	12.078	11.539	11.748	11.491	12.012	11.554

Al	3.889	3.903	4.406	3.901	4.403	4.208	4.474	3.954	4.415
Ti	0.001	0	0	0.003	0	0	0.001	0	0.005
Fe2	0.011	0.009	0.012	0.002	0.016	0.001	0.007	0.011	0.007
Mn	0	0	0	0.002	0	0.003	0.002	0	0
Mg	0	0	0	0	0	0	0	0	0.003
Ba	0.007	0	0.002	0	0	0.001	0.006	0.001	0.002
Ca	0.004	0.004	0.433	0.006	0.488	0.289	0.533	0.002	0.422
Na	0.204	0.217	3.532	0.116	3.456	3.742	3.454	0.166	3.602
K	3.787	3.86	0.045	3.822	0.123	0.039	0.046	3.87	0.036
Cations	19.98	20.037	20.003	19.93	20.025	20.032	20.02	20.017	20.048
Ab	5.1	5.3	88.1	2.9	85	91.9	85.6	4.1	88.7
An	0.1	0.1	10.8	0.2	12	7.1	13.2	0	10.4
Or	94.8	94.6	1.1	96.9	3	1	1.1	95.8	0.9

Appendix Table 4 Chemical compositions of olivine

Mineral	Ol	Ol	Ol	Ol	Ol	Ol	Ol	Ol	Ol	Ol	Ol	Ol	Ol
						Oxides (wt%)							
SiO_2	30.81	30.79	30.83	30.85	30.46	31.26	31.19	30.71	29.90	30.57	31.01	31.09	30.95
TiO_2	0.00	0.01	-	-	0.05	0.02	0.00	0.07	0.10	0.05	0.02	0.02	0.00
Al_2O_3	-	0.00	-	-	-	0.00	0.00	0.00	0.03	0.00	0.00	0.02	0.01
FeO	63.55	64.42	64.60	63.34	65.45	62.61	62.78	63.60	62.90	62.87	63.69	64.17	64.70
MnO	0.99	0.97	1.11	0.97	1.27	1.15	1.13	1.14	1.17	1.15	1.21	1.29	1.51
MgO	4.33	4.06	4.07	4.03	3.47	4.79	4.74	3.75	3.53	3.83	4.27	3.48	3.19
CaO	-	-	-	-	-	0.00	0.00	0.00	0.00	0.01	0.00	0.00	0.02
Na_2O	-	0.03	0.08	-	0.03	0.02	0.03	0.01	0.06	0.02	0.04	0.00	0.04
K_2O	-	-	0.01	-	0.00	0.01	0.00	0.00	0.00	0.00	0.00	0.01	0.00
NiO	0.04	0.06	-	-	-	0.00	0.04	0.07	0.09	0.00	0.03	0.01	0.01
Total	99.72	100.33	100.69	99.20	100.74	99.85	99.91	99.35	97.77	98.50	100.26	100.09	100.43
Cations per 4 oxygens													
Si	1.009	1.006	1.005	1.016	0.998	1.016	1.015	1.012	1.005	1.015	1.010	1.017	1.014
Al	0	0	0	0	0	0	0	0	0.001	0	0	0.001	0
Ti	0	0	0	0	0.001	0	0	0.002	0.002	0.001	0	0.001	0
Fe2	1.741	1.760	1.760	1.744	1.793	1.702	1.708	1.753	1.769	1.745	1.735	1.756	1.772
Mn	0.028	0.027	0.030	0.027	0.035	0.032	0.031	0.032	0.033	0.032	0.034	0.036	0.042
Mg	0.212	0.198	0.197	0.198	0.17	0.232	0.230	0.184	0.177	0.190	0.207	0.170	0.156
Ca	0	0	0	0	0	0	0	0	0	0	0	0	0.001
Na	0	0.002	0.005	0	0.002	0.001	0.002	0.001	0.004	0.002	0.003	0	0.002
K	0	0	0	0	0	0	0	0	0	0	0	0.001	0
Ni	0.001	0.002	0	0	0	0	0.001	0.002	0.002	0	0.001	0	0
Cations	2.991	2.995	2.997	2.985	2.999	2.983	2.987	2.986	2.993	2.985	2.990	2.982	2.987
$Fe^{\#}$	0.89	0.90	0.90	0.90	0.91	0.88	0.88	0.91	0.91	0.90	0.89	0.91	0.92

Note: $Fe^{\#}$ = molar FeO/(FeO + MgO).

Appendix Table 5 Chemical compositions of pyroxene

Mineral	Fs	Fs	Fs	Fs	Fs	Fs	Fs	Fs	Fs
Oxides (wt%)									
SiO_2	47.39	47.85	47.95	48.03	45.03	48.66	47.39	47.89	48.18
TiO_2	0.20	0.24	0.21	0.13	0.17	0.15	0.29	0.10	0.25
$Al2O_3$	0.81	0.67	0.75	0.60	0.59	0.40	0.47	0.38	0.53
FeO	42.61	42.37	41.52	41.99	37.35	41.67	40.57	40.82	41.97
Fe_2O_3	-	-	-	-	-	-	-	-	-
Cr_2O_3	0.04	0.02	-	0.01	0.10	0.03	0.01	0.00	0.04
MnO	0.91	0.83	0.78	0.89	0.90	0.94	0.90	0.95	1.01
NiO	0.01	-	-	-	0.00	0.00	0.03	0.02	0.04
MgO	7.32	7.62	7.84	7.58	7.56	7.46	7.42	7.21	7.15
CaO	0.48	0.60	0.63	0.63	1.13	1.15	1.19	1.18	1.03
Na_2O	0.02	0.05	0.06	0.06	0.13	0.01	0.04	0.02	0.05
K_2O	0.02	0.00	0.02	0.01	0.02	0.00	0.00	0.00	0.01
Total	99.79	100.24	99.76	99.92	93.00	100.46	98.31	98.59	100.27
Cations per 6 oxygens									
TSi	1.966	1.972	1.979	1.984	1.986	2.001	1.989	2.007	1.989
TAl	0.034	0.028	0.021	0.016	0.014	0	0.011	0	0.011
TFe3	0	0	0	0	0	0	0	0	0
M1Al	0.006	0.004	0.016	0.014	0.017	0.019	0.012	0.019	0.015
M1Ti	0.006	0.007	0.006	0.004	0.006	0.005	0.009	0.003	0.008
M1Fe3	0.017	0.012	0	0	0	0	0	0	0
M1Fe2	0.517	0.508	0.495	0.515	0.477	0.518	0.513	0.527	0.535
M1Cr	0.001	0.001	0	0	0.004	0.001	0	0	0.001
M1Mg	0.452	0.468	0.483	0.467	0.497	0.457	0.465	0.451	0.440
M1Ni	0	0	0	0	0	0	0.001	0.001	0.001
M2Mg	0	0	0	0	0	0	0	0	0
M2Fe2	0.944	0.941	0.939	0.936	0.900	0.915	0.911	0.904	0.914
M2Mn	0.032	0.029	0.027	0.031	0.034	0.033	0.032	0.034	0.035
M2Ca	0.021	0.026	0.028	0.028	0.053	0.051	0.054	0.053	0.046
M2Na	0.001	0.004	0.005	0.005	0.011	0.001	0.004	0.002	0.004
M2K	0.001	0	0.001	0	0.001	0	0	0	0
Sum_cat	3.999	4.000	3.999	4.000	3.999	4.000	4.000	4.000	4.000
Wo	1.069	1.325	1.413	1.411	2.722	2.572	2.715	2.695	2.315
En	22.804	23.587	24.486	23.614	25.335	23.165	23.53	22.893	22.336
Fs	76.128	75.088	74.100	74.975	71.943	74.264	73.754	74.412	75.349

Appendix Table 6 Chemical compositions of amphibole

	Jiuyishan							
Oxides (wt%)								
SiO_2	42.98	43.55	43.62	44.05	43.92	43.65	44.15	45.23
TiO_2	1.72	1.44	1.57	1.48	1.53	1.50	1.44	1.01
Al_2O_3	7.68	7.47	7.43	7.26	7.35	7.38	7.13	6.30
FeO	24.64	25.12	25.38	25.34	25.45	25.10	26.00	27.37
Cr_2O_3	-	-	0.00	-	-	0.02	0.03	0.05
MnO	0.41	0.38	0.44	0.42	0.53	0.41	0.57	0.72
MgO	5.83	5.72	5.75	5.92	5.64	5.80	5.80	6.01
CaO	10.65	10.70	10.66	10.57	10.48	10.73	10.05	9.68
Na_2O	1.72	1.67	1.71	1.58	1.65	1.59	1.51	1.30
K_2O	1.00	0.97	0.91	0.86	0.92	0.92	0.86	0.69
F	0.11	0.08	0.07	0.22	-	0.12	0.13	0.04
Cl	0.09	0.07	0.03	0.03	-	-	0.03	0.08
Total	96.82	97.17	97.56	97.71	97.46	97.22	97.67	98.42
Cations per 23 oxygens								
TSi	6.598	6.666	6.646	6.711	6.702	6.678	6.743	6.868
TAl	1.389	1.334	1.333	1.289	1.298	1.322	1.257	1.126
TFe3	0.013	0	0.021	0	0	0	0	0.006
TTi	0	0	0	0	0	0	0	0
CAl	0	0.013	0	0.013	0.023	0.008	0.026	0
CCr	0	0	0	0	0	0.002	0.004	0.005
CFe3	1.323	1.295	1.323	1.237	1.233	1.255	1.176	1.144
CTi	0.198	0.166	0.179	0.169	0.175	0.173	0.166	0.116
CMg	1.335	1.306	1.306	1.344	1.283	1.324	1.319	1.361
CFe2	1.827	1.921	1.89	1.991	2.015	1.956	2.144	2.325
CMn	0.053	0.049	0.057	0.054	0.069	0.053	0.073	0.049
CCa	0.264	0.25	0.244	0.192	0.202	0.229	0.092	0
BMg	0	0	0	0	0	0	0	0
BFe2	0	0	0	0	0	0	0	0
BMn	0	0	0	0	0	0	0	0.043
BCa	1.488	1.505	1.495	1.534	1.512	1.53	1.552	1.574
BNa	0.512	0.495	0.505	0.466	0.488	0.47	0.448	0.383
ACa	0	0	0	0	0	0	0	0
ANa	0	0	0	0	0	0	0	0
AK	0.195	0.189	0.176	0.167	0.18	0.18	0.168	0.134
Sum_cat	15.195	15.189	15.176	15.167	15.18	15.18	15.168	15.134

	Jiufeng								
Oxides (wt%)									
SiO_2	43.32	43.52	43.03	43.23	43.06	42.85	42.95	43.19	43.47

TiO_2	1.58	1.58	1.75	1.41	1.58	1.62	1.73	1.56	1.37
Al_2O_3	8.36	8.98	9.15	9.06	9.16	9.15	8.97	9.00	8.48
FeO	19.28	20.31	20.79	20.43	20.61	20.26	21.09	20.46	20.84
Cr_2O_3	0.04	0.04	0.03	0.00	0.02	0.03	0.00	0.02	0.00
MnO	0.50	0.53	0.61	0.52	0.53	0.54	0.67	0.57	0.60
MgO	8.98	8.67	8.46	8.65	8.75	8.76	8.08	8.47	8.23
CaO	11.47	11.62	11.47	11.60	11.51	11.46	11.49	11.49	11.38
Na_2O	1.73	1.92	1.77	1.67	1.70	1.54	1.75	1.62	1.74
K_2O	1.32	1.43	1.43	1.44	1.42	1.39	1.41	1.41	1.25
Total	96.57	98.59	98.49	98.00	98.34	97.59	98.15	97.79	97.36
Cations per 23 oxygens									
TSi	6.704	6.629	6.561	6.606	6.555	6.557	6.59	6.618	6.702
TAl	1.296	1.371	1.439	1.394	1.445	1.443	1.41	1.382	1.298
TFe3	0	0	0	0	0	0	0	0	0
TTi	0	0	0	0	0	0	0	0	0
CAl	0.226	0.239	0.203	0.236	0.197	0.206	0.211	0.241	0.242
CCr	0.004	0.005	0.003	0	0.003	0.003	0	0.003	0
CFe3	0.093	0.102	0.186	0.164	0.237	0.262	0.152	0.165	0.15
CTi	0.184	0.181	0.201	0.162	0.181	0.186	0.2	0.18	0.159
CMg	2.071	1.969	1.922	1.971	1.984	1.997	1.849	1.934	1.891
CFe2	2.389	2.47	2.446	2.433	2.364	2.31	2.545	2.44	2.519
CMn	0.033	0.034	0.039	0.034	0.034	0.035	0.043	0.037	0.039
CCa	0	0	0	0	0	0	0	0	0
BMg	0	0	0	0	0	0	0	0	0
BFe2	0.013	0.014	0.019	0.013	0.023	0.021	0.008	0.016	0.017
BMn	0.033	0.034	0.04	0.034	0.034	0.035	0.044	0.037	0.039
BCa	1.901	1.896	1.874	1.9	1.877	1.879	1.889	1.886	1.879
BNa	0.053	0.056	0.067	0.054	0.066	0.064	0.059	0.061	0.065
ACa	0	0	0	0	0	0	0	0	0
ANa	0.466	0.511	0.455	0.442	0.437	0.393	0.461	0.42	0.455
AK	0.26	0.277	0.277	0.281	0.275	0.271	0.276	0.276	0.246
Sum_cat	15.727	15.789	15.733	15.723	15.712	15.664	15.737	15.696	15.701

	Jiufeng					Xiaoliang			
Oxides (wt%)									
SiO_2	43.68	44.06	43.55	43.79	43.05	42.37	43.11	42.78	43.42
TiO_2	1.59	1.36	1.65	1.38	1.63	1.79	1.72	1.54	1.47
Al_2O_3	8.41	8.06	8.65	8.23	8.93	8.79	8.49	8.85	8.77
FeO	20.29	21.39	19.71	20.13	20.23	22.75	22.72	22.03	22.23
Cr_2O_3	0.00	0.03	0.00	0.02	0.01	0.05	0.04	0.02	0.04
MnO	0.70	0.70	0.57	0.59	0.53	0.91	0.96	0.95	0.86
MgO	8.94	8.69	8.98	8.78	8.68	7.01	6.98	6.94	7.63
CaO	11.49	11.54	11.50	11.61	11.63	10.57	10.82	10.97	10.73
Na_2O	1.77	1.76	1.82	1.58	1.75	1.8	1.79	1.46	1.78

K_2O	1.36	1.24	1.25	1.29	1.40	1.22	1.18	1.24	1.25
Total	98.21	98.83	97.68	97.40	97.83	97.26	97.81	96.78	98.18
Cations per 23 oxygens									
TSi	6.658	6.687	6.662	6.723	6.597	6.586	6.67	6.665	6.652
TAl	1.342	1.313	1.338	1.277	1.403	1.414	1.33	1.335	1.348
TFe3	0	0	0	0	0	0	0	0	0
TTi	0	0	0	0	0	0	0	0	0
CAl	0.168	0.128	0.221	0.21	0.209	0.195	0.216	0.289	0.235
CCr	0	0.003	0	0.002	0.001	0.006	0.005	0.002	0.005
CFe3	0.177	0.245	0.132	0.133	0.135	0.328	0.248	0.226	0.32
CTi	0.182	0.155	0.19	0.16	0.188	0.209	0.2	0.18	0.169
CMg	2.031	1.966	2.047	2.009	1.983	1.624	1.61	1.612	1.743
CFe2	2.397	2.457	2.373	2.448	2.449	2.578	2.658	2.628	2.473
CMn	0.045	0.045	0.037	0.038	0.034	0.059	0.062	0.062	0.055
CCa	0	0	0	0	0	0	0	0	0
BMg	0	0	0	0	0	0	0	0	0
BFe2	0.012	0.013	0.017	0.004	0.008	0.052	0.033	0.016	0.056
BMn	0.045	0.045	0.037	0.038	0.034	0.06	0.063	0.063	0.056
BCa	1.877	1.876	1.885	1.91	1.909	1.76	1.794	1.831	1.761
BNa	0.065	0.066	0.061	0.048	0.049	0.127	0.11	0.09	0.127
ACa	0	0	0	0	0	0	0	0	0
ANa	0.458	0.451	0.479	0.421	0.47	0.415	0.427	0.351	0.402
AK	0.264	0.24	0.244	0.253	0.274	0.242	0.233	0.246	0.244
Sum_cat	15.721	15.692	15.723	15.675	15.744	15.657	15.66	15.598	15.646

Xiaoliang				Gangwei				
Oxides (wt%)								
SiO_2	43.57	52.13	51.6	52.29	50.81	49.14	50.52	52.21	53.43
TiO_2	1.79	0.3	0.43	0.17	0.53	0.77	0.57	0.25	0.12
Al_2O_3	8.9	3.48	3.66	3.27	4.12	5.5	4.22	3.11	2.29
FeO	22.24	12.7	12.84	12.55	12.79	13.65	13.19	12.23	11.67
Cr_2O_3	0	0	0.03	0.01	0	0.02	0	0	0.03
MnO	0.99	0.71	0.64	0.76	0.77	0.75	0.73	0.7	0.75
MgO	7.48	15.38	15.34	15.27	14.69	13.89	14.69	15.47	15.97
CaO	10.52	11.87	11.88	11.84	11.38	11.5	11.67	11.81	11.9
Na_2O	1.99	0.59	0.74	0.59	0.9	1.15	0.66	0.44	0.3
K_2O	1.23	0.23	0.31	0.21	0.38	0.53	0.38	0.24	0.16
Total	98.71	97.39	97.47	96.96	96.37	96.9	96.63	96.46	96.62
Cations per 23 oxygens									
TSi	6.653	7.524	7.462	7.581	7.452	7.229	7.386	7.59	7.723
TAl	1.347	0.476	0.538	0.419	0.548	0.771	0.614	0.41	0.277
TFe3	0	0	0	0	0	0	0	0	0
TTi	0	0	0	0	0	0	0	0	0

CAl	0.254	0.115	0.086	0.14	0.164	0.181	0.113	0.122	0.113
CCr	0	0	0.003	0.001	0	0.002	0	0	0.003
CFe3	0.303	0.266	0.26	0.235	0.256	0.248	0.301	0.249	0.223
CTi	0.206	0.033	0.047	0.019	0.058	0.085	0.063	0.027	0.013
CMg	1.703	3.309	3.307	3.301	3.212	3.046	3.202	3.353	3.441
CFe2	2.472	1.234	1.258	1.259	1.262	1.39	1.277	1.206	1.161
CMn	0.063	0.043	0.039	0.046	0.047	0.046	0.045	0.043	0.046
CCa	0	0	0	0	0	0	0	0	0
BMg	0	0	0	0	0	0	0	0	0
BFe2	0.066	0.033	0.035	0.028	0.051	0.041	0.035	0.032	0.027
BMn	0.065	0.044	0.039	0.047	0.048	0.047	0.045	0.043	0.046
BCa	1.721	1.836	1.841	1.839	1.788	1.813	1.828	1.839	1.843
BNa	0.148	0.082	0.085	0.082	0.113	0.1	0.092	0.062	0.042
ACa	0	0	0	0	0	0	0	0	0
ANa	0.441	0.083	0.123	0.083	0.143	0.228	0.096	0.062	0.042
AK	0.24	0.042	0.057	0.039	0.071	0.099	0.071	0.045	0.03
Sum_cat	15.681	15.12	15.18	15.119	15.214	15.328	15.166	15.083	15.03

	Gangwei			Lunshui			Gudoushan		
Oxides (wt%)									
SiO_2	50.16	44.88	44.08	44.56	44.94	45.46	40.7	41.76	41.32
TiO_2	0.58	1.37	1.71	1.25	1.37	1.3	1.49	1.3	1.1
Al_2O_3	4.48	8.06	8.52	8.09	7.97	7.97	9.5	9.3	9.34
FeO	12.97	18.43	17.95	18.72	17.62	17.69	25.5	25.23	25.12
Cr_2O_3	0.03	0.11	0.04	0	0	0	0.02	0.03	0.01
MnO	0.72	1.47	1.39	1.66	1.37	1.41	1.23	1.21	1.23
MgO	14.59	10.08	10.25	9.81	10.5	10.55	4.28	4.58	4.83
CaO	11.44	10.93	11.18	11.01	10.96	10.9	10.66	10.76	10.72
Na_2O	0.78	1.64	1.81	1.68	1.75	1.62	1.54	1.63	1.5
K_2O	0.41	1.03	1.01	1.03	0.94	0.93	1.41	1.27	1.36
Total	96.16	98	97.94	97.81	97.42	97.83	96.33	97.07	96.53
Cations per 23 oxygens									
TSi	7.371	6.75	6.641	6.733	6.778	6.812	6.511	6.609	6.56
TAl	0.629	1.25	1.359	1.267	1.222	1.188	1.489	1.391	1.44
TFe3	0	0	0	0	0	0	0	0	0
TTi	0	0	0	0	0	0	0	0	0
CAl	0.146	0.178	0.152	0.172	0.194	0.218	0.3	0.342	0.306
CCr	0.003	0.013	0.005	0	0	0	0.003	0.004	0.001
CFe3	0.295	0.358	0.31	0.353	0.321	0.351	0.265	0.227	0.321
CTi	0.064	0.155	0.194	0.142	0.155	0.147	0.179	0.155	0.131
CMg	3.196	2.26	2.302	2.21	2.361	2.357	1.021	1.08	1.143
CFe2	1.251	1.943	1.95	2.012	1.882	1.839	3.147	3.111	3.014
CMn	0.044	0.093	0.088	0.111	0.087	0.089	0.086	0.081	0.083
CCa	0	0	0	0	0	0	0	0	0

BMg	0	0	0	0	0	0	0	0	0
BFe2	0.048	0.017	0.002	0	0.019	0.027	0	0	0
BMn	0.045	0.094	0.089	0.102	0.088	0.09	0.081	0.082	0.083
BCa	1.801	1.761	1.805	1.782	1.771	1.75	1.827	1.824	1.823
BNa	0.106	0.127	0.104	0.116	0.122	0.133	0.092	0.094	0.094
ACa	0	0	0	0	0	0	0	0	0
ANa	0.116	0.351	0.425	0.376	0.39	0.338	0.386	0.407	0.368
AK	0.077	0.198	0.194	0.199	0.181	0.178	0.288	0.256	0.275
Sum_cat	15.193	15.549	15.619	15.575	15.571	15.516	15.673	15.663	15.643

Appendix Table 7 Chemical compositions of biotite

	Jiuyishan									
	Poikilitic texture					Interstitial mineral				
Oxides (wt%)										
SiO_2	35.96	36.3	34.64	34.7	35.34	35.02	34.8	35.14	34.85	34.58
TiO_2	4.13	2.96	2.98	3.52	3.44	3.48	2.98	4.6	3.63	2.94
Al_2O_3	12.6	13.36	12.86	13.14	13.13	13.29	13.44	13	13.33	13.28
Cr_2O_3	0.07	-	-	0.28	0.07	0	0.02	0.02	0.08	0.01
FeO	26.37	25.37	25.67	25.6	26.7	28.61	28.6	28.54	27.71	28.07
Fe_2O_3	-	-	-	-	-	-	-	-	-	-
MnO	0.08	0.13	0.15	0.13	0.14	0.3	0.33	0.29	0.31	0.18
MgO	6.4	8.22	7.31	7.36	6.84	5.58	5.46	5.12	5.44	5.53
BaO	-	-	-	-	-	-	-	-	-	-
CaO	0.03	0.03	-	-	-	-	-	-	-	-
Na_2O	0.19	0.11	0.08	0.1	0.14	0.1	0.08	0.12	0.11	0.12
K_2O	9.87	10.06	9.62	9.94	9.98	9.87	9.83	9.98	10.03	9.97
F	1.06	1.24	1.13	1.12	0.87	0.23	0.21	0.15	0.1	0.21
Total	96.99	98.03	94.73	96.25	97	96.47	95.84	97.1	95.69	95.04
Cations per 23 oxygens										
Si	5.964	5.928	5.893	5.817	5.877	5.85	5.862	5.838	5.856	5.872
AlIV	2.036	2.072	2.107	2.183	2.123	2.15	2.138	2.162	2.144	2.128
AlVI	0.425	0.498	0.468	0.412	0.449	0.464	0.528	0.382	0.493	0.528
Ti	0.515	0.364	0.381	0.443	0.43	0.437	0.378	0.574	0.459	0.376
Fe3	0	0	0	0	0	0	0	0	0	0
Fe2	3.658	3.466	3.652	3.589	3.714	3.998	4.028	3.966	3.894	3.987
Cr	0.009	0	0	0.038	0.009	0	0.003	0.003	0.011	0.001
Mn	0.011	0.017	0.022	0.018	0.019	0.042	0.047	0.041	0.045	0.026
Mg	1.583	2	1.855	1.84	1.695	1.389	1.37	1.268	1.362	1.401
Ba	0	0	0	0	0	0	0	0	0	0
Ca	0.005	0.005	0	0	0	0	0	0	0	0
Na	0.06	0.036	0.025	0.031	0.045	0.032	0.025	0.039	0.036	0.04
K	2.089	2.096	2.088	2.126	2.117	2.103	2.112	2.115	2.15	2.159
Cat	16.355	16.482	16.491	16.497	16.478	16.465	16.491	16.388	16.45	16.518
$Fe^{\#}$	0.7	0.63	0.66	0.66	0.69	0.74	0.75	0.76	0.74	0.74

	Jiuyishan	Xiaoliang		Gangwei	Lunshui				Gudoushan	
Oxides (wt%)										
SiO_2	34.88	36.36	36.72	37.07	36.74	36.89	37.35	36.91	35.71	35.76
TiO_2	4.16	3.17	3.58	3.57	3.31	3	3.42	2.64	2.17	3.3
Al_2O_3	13.29	13.65	13.6	13.76	13.5	13.66	13.69	14.22	17.36	13.88
Cr_2O_3	-	0.02	0	0.05	0.05	0.02	0.02	0	0	0.02

FeO	27.75	23.35	23.47	17.69	20.22	20.51	20.09	19.34	22.97	26.31
Fe_2O_3	-	-	-	-	-	-	-	-	-	-
MnO	0.25	0.57	0.56	0.68	1.24	1.32	1.14	1.22	0.39	0.77
MgO	5.61	8.23	8.23	12.41	10.25	10.77	10.64	10.28	7.28	6.09
BaO	-	0.09	0.1	0.34	0.11	0.06	0.09	0.09	0.08	0.1
CaO	-	0	0.05	0.04	0.14	0.03	0.03	0	0.37	0.04
Na_2O	0.14	0.07	0.04	0.14	0.07	0.14	0.1	0.13	0.12	0.03
K_2O	9.98	9.59	9.36	9.48	9.32	9.53	9.52	9.65	9.39	9.43
F	0.21	0.05	0.09	0.05	0	0	0.03	0.04	0	0.38
Total	96.31	95.15	95.8	95.28	94.95	95.93	96.12	94.52	95.84	96.11
Cations per 23 oxygens										
Si	5.822	5.967	5.975	5.916	5.958	5.931	5.968	5.986	5.771	5.921
AlIV	2.178	2.033	2.025	2.084	2.042	2.069	2.032	2.014	2.229	2.079
AlVI	0.434	0.605	0.581	0.502	0.536	0.517	0.544	0.702	1.075	0.627
Ti	0.522	0.391	0.438	0.429	0.404	0.363	0.411	0.322	0.264	0.411
Fe3	0	0	0	0	0	0	0	0	0	0
Fe2	3.873	3.205	3.194	2.361	2.742	2.757	2.684	2.623	3.105	3.643
Cr	0	0.003	0	0.006	0.006	0.003	0.003	0	0	0.003
Mn	0.035	0.079	0.077	0.092	0.17	0.18	0.154	0.168	0.053	0.108
Mg	1.396	2.013	1.996	2.952	2.478	2.581	2.534	2.485	1.754	1.503
Ba	0	0.006	0.006	0.021	0.007	0.004	0.006	0.006	0.005	0.006
Ca	0	0	0.009	0.007	0.024	0.005	0.005	0	0.064	0.007
Na	0.044	0.022	0.013	0.043	0.022	0.044	0.031	0.041	0.038	0.01
K	2.125	2.008	1.943	1.93	1.928	1.955	1.941	1.996	1.936	1.992
Cat	16.429	16.332	16.257	16.343	16.317	16.409	16.313	16.343	16.294	16.31
$Fe^{\#}$	0.74	0.61	0.62	0.44	0.53	0.52	0.51	0.51	0.64	0.71

	Gudoushan				Wuguishan					
Oxides (wt%)										
SiO_2	35.69	35.66	35.89	35.74	36.06	36.3	36.22	36.2	36.24	36.51
TiO_2	3.2	3.38	2.35	3.83	3.43	3.35	3.69	3.57	3.91	3.41
Al_2O_3	13.97	14.18	14.84	13.84	14.34	14.84	14.81	14.74	14.4	14.44
Cr_2O_3	0.02	0	0	0.07	0.01	0.05	0.02	0.07	0.02	0
FeO	25.48	25.51	24.96	25.72	23.75	22.42	23.25	23.31	22.96	23.15
Fe_2O_3	-	-	-	-	-	-	-	-	-	-
MnO	0.72	0.76	0.74	0.71	0.48	0.49	0.44	0.42	0.44	0.52
MgO	5.86	5.71	6.41	5.66	7.24	7.9	6.79	7.43	7.51	7.5
BaO	0.02	0.05	0.06	0.23	0	0.46	0.11	0.29	0.18	0.09
CaO	0.05	0.03	0.03	0.01	0.05	0	0.09	0	0.01	0.01
Na_2O	0.09	0.11	0.03	0.14	0.03	0	0.09	0	0.07	0.07
K_2O	9.41	9.43	9.32	9.44	9.59	9.57	9.51	9.6	9.66	9.65
F	0.34	0.23	0.39	0.26	0.47	0.51	0.16	0.47	0.56	0.75

Total	94.85	95.05	95.02	95.65	95.45	95.89	95.18	96.1	95.96	96.1
Cations per 23 oxygens										
Si	5.959	5.937	5.954	5.931	5.927	5.914	5.93	5.901	5.914	5.957
AlIV	2.041	2.063	2.046	2.069	2.073	2.086	2.07	2.099	2.086	2.043
AlVI	0.706	0.717	0.853	0.636	0.703	0.761	0.786	0.731	0.681	0.732
Ti	0.402	0.423	0.293	0.478	0.424	0.411	0.454	0.438	0.48	0.419
Fe3	0	0	0	0	0	0	0	0	0	0
Fe2	3.558	3.552	3.463	3.569	3.265	3.055	3.184	3.178	3.134	3.159
Cr	0.003	0	0	0.009	0.001	0.006	0.003	0.009	0.003	0
Mn	0.102	0.107	0.104	0.1	0.067	0.068	0.061	0.058	0.061	0.072
Mg	1.459	1.417	1.585	1.4	1.774	1.919	1.657	1.806	1.827	1.824
Ba	0.001	0.003	0.004	0.015	0	0.029	0.007	0.019	0.012	0.006
Ca	0.009	0.005	0.005	0.002	0.009	0	0.016	0	0.002	0.002
Na	0.029	0.036	0.01	0.045	0.01	0	0.029	0	0.022	0.022
K	2.004	2.003	1.972	1.998	2.011	1.989	1.986	1.996	2.011	2.009
Cat	16.273	16.263	16.289	16.252	16.264	16.238	16.183	16.235	16.233	16.245
$Fe^{\#}$	0.71	0.71	0.69	0.72	0.65	0.61	0.66	0.64	0.63	0.63

Note: Cat = Cation; $Fe^{\#}$ = mole FeO/(FeO + MgO).

Appendix Table 8 Whole-rock chemical compositions

	XY 13-1	XY 13-3	XY 13-4	XY 13-5	XY 13-6	XY 13-7	XY 15-1	XY 15-2	XY 15-4	XY 15-6
					Jiuyishan					
Major elements (wt%)										
SiO_2	69.75	69.43	69.10	74.08	69.45	74.02	75.31	75.88	76.47	74.53
TiO_2	0.49	0.55	0.52	0.04	0.51	0.06	0.16	0.15	0.15	0.21
Al_2O_3	13.57	13.51	13.43	13.88	13.49	14.02	12.59	12.78	12.64	12.61
Fe_2O_3t	4.66	5.12	5.31	1.19	4.55	1.35	1.72	1.36	1.52	2.18
MnO	0.06	0.06	0.06	0.03	0.06	0.03	0.03	0.02	0.02	0.03
MgO	0.53	0.72	0.70	0.12	0.60	0.11	0.16	0.14	0.16	0.21
CaO	1.03	1.12	1.19	0.55	1.74	0.50	0.92	0.82	0.76	1.18
Na_2O	2.59	2.23	2.37	3.35	1.42	3.51	2.57	2.64	2.48	2.51
K_2O	5.48	5.09	4.96	5.22	5.25	4.94	5.58	5.72	5.34	5.69
P_2O_5	0.20	0.21	0.20	0.04	0.20	0.05	0.05	0.05	0.05	0.07
LOI	1.24	1.77	1.77	0.99	2.69	0.99	0.58	0.39	0.39	0.56
Total	99.62	99.81	99.61	99.50	99.94	99.58	99.66	99.94	99.98	99.79
A/CNK	1.12	1.20	1.17	1.14	1.21	1.17	1.05	1.06	1.12	1.01
MALI	7.05	6.20	6.14	8.01	4.93	7.96	7.23	7.54	7.06	7.03
Fe*	0.89	0.86	0.87	0.90	0.87	0.91	0.91	0.89	0.89	0.90
Trace elements (ppm)										
Ga	20.9	20.8	22.3	29.7	22.0	30.5	21.0	21.4	20.5	20.1
Rb	203	200	196	523	225	472	288	289	273	249
Sr	147	133	125	45.0	74.8	51.0	48.0	51.6	53.9	86.0
Y	54.3	53.8	53.4	71.2	56.1	73.7	66.3	68.7	69.5	55.2
Zr	505	575	569	68.3	556	75.3	159	175	166	214
Nb	30.8	32.7	31.8	32.7	31.7	33.1	22.8	20.2	21.3	21.4
Ba	1424	1332	1357	162	1297	218	432	478	474	648
La	75.3	76.7	77.1	22.0	79.4	24.2	53.3	55.3	55.2	70.7
Ce	151	154	156	54.3	161	58.4	112	115	117	146
Pr	19.1	19.6	19.5	7.16	20.0	7.64	14.1	14.6	14.8	18.1
Nd	70.4	72.2	71.0	25.3	73.8	27.2	50.8	53.3	54.5	65.4
Sm	13.3	13.6	13.4	8.63	13.8	8.81	11.1	11.3	11.6	12.9
Eu	2.59	2.51	2.55	0.16	2.60	0.22	0.84	0.94	0.87	1.15
Gd	11.4	11.6	11.5	8.44	11.8	8.81	10.6	10.8	11.0	11.2
Tb	1.62	1.63	1.63	1.85	1.68	1.90	1.76	1.81	1.86	1.67
Dy	9.62	9.77	9.32	12.2	9.87	12.5	11.5	11.9	12.4	9.99
Ho	2.10	2.12	2.07	2.55	2.17	2.63	2.47	2.54	2.63	2.09
Er	5.59	5.67	5.48	6.74	5.80	6.99	6.63	6.80	7.00	5.40
Tm	0.87	0.88	0.86	1.15	0.91	1.17	1.02	1.03	1.07	0.81
Yb	5.52	5.51	5.23	7.48	5.74	7.55	6.32	6.44	6.76	4.87
Lu	0.86	0.86	0.85	1.08	0.93	1.09	0.89	0.91	0.93	0.71
Hf	12.4	13.8	13.7	3.22	13.6	3.21	5.17	5.58	5.31	6.39
Ta	2.35	2.41	2.28	5.72	2.36	5.63	2.16	2.07	2.02	1.97
Th	26.5	26.8	26.6	20.6	27.4	21.2	30.5	31.1	31.8	36.2
U	4.56	5.07	5.03	25.2	5.29	27.1	8.85	8.58	8.51	6.90
T_{Zr}	903	926	922	727	924	736	791	801	802	813
10^4*Ga/Al	2.9	2.9	3.1	4.0	3.1	4.1	3.2	3.2	3.1	3.0

	XY 19-1	XY 19-2	XY 20-1	XY 21-1	XY 21-2	XY 22-2	GD 20-3	GD 21-2	GD 22-1	GD 23-1
					Jiuyishan					
Major elements (wt%)										
SiO_2	75.12	74.17	73.96	66.85	74.93	73.83	75.49	74.73	73.57	73.59
TiO_2	0.20	0.16	0.31	0.90	0.18	0.18	0.19	0.20	0.27	0.23
Al_2O_3	13.34	13.31	12.77	13.25	12.30	13.47	12.43	12.52	12.96	12.93
Fe_2O_3t	2.17	1.98	2.82	6.01	1.82	2.13	2.37	2.70	3.10	3.00
MnO	0.03	0.03	0.03	0.08	0.03	0.04	0.01	0.03	0.03	0.04
MgO	0.25	0.20	0.30	1.26	0.21	0.27	0.25	0.31	0.24	0.14
CaO	1.91	0.93	1.53	1.96	0.97	1.07	0.16	0.58	0.31	1.06
Na_2O	3.23	2.85	2.50	2.60	3.14	3.10	2.65	2.24	2.70	2.59
K_2O	3.25	5.50	5.07	4.40	5.04	5.11	5.57	5.29	5.73	5.59
P_2O_5	0.06	0.07	0.09	0.25	0.06	0.08	0.06	0.06	0.09	0.07
LOI	0.88	0.57	0.64	2.29	1.22	0.83	0.69	1.20	0.86	0.64
Total	100.43	99.78	100.01	99.85	99.90	100.10	99.88	99.87	99.86	99.87
A/CNK	1.09	1.08	1.03	1.05	0.99	1.07	1.16	1.20	1.16	1.06
MALI	4.56	7.42	6.04	5.04	7.21	7.15	8.06	6.96	8.13	7.12
Fe*	0.89	0.90	0.90	0.81	0.89	0.88	0.90	0.89	0.92	0.95
Trace elements (ppm)										
Ga	24.4	24.0	20.1	20.5	18.8	25.6	18.1	21.5	19.6	21.5
Rb	317	403	187	212	248	423	242	279	223	250
Sr	84.6	71.2	93.6	131	48.3	75.0	51.3	51.1	75.5	83.1
Y	64.8	64.6	45.1	48.7	26.5	53.9	48.8	51.9	45.2	55.4
Zr	185	204	290	338	145	165	189	207	253	226
Nb	28.3	27.2	22.2	26.4	13.3	30.0	21.2	24.4	25.4	24.4
Ba	450	529	777	869	529	545	556	483	829	646
La	50.2	52.9	82.7	95.9	54.3	48.2	66.4	72.1	75.6	72.9
Ce	101	106	168	191	108	101	138	150	155	149
Pr	13.4	14.0	20.6	22.8	13.0	12.7	16.8	18.6	18.8	18.6
Nd	48.0	51.2	73.6	78.4	46.1	45.0	59.7	66.5	66.1	64.6
Sm	11.1	11.3	13.5	13.4	9.03	10.3	11.8	13.0	12.9	13.1
Eu	0.85	0.96	1.53	1.93	0.85	1.01	0.94	0.92	1.44	1.21
Gd	9.96	10.3	11.2	11.3	7.46	9.04	9.99	11.0	10.8	11.3
Tb	1.78	1.78	1.51	1.55	0.99	1.58	1.51	1.67	1.52	1.69
Dy	11.2	11.4	8.53	8.90	5.27	9.52	8.76	9.60	8.45	9.68
Ho	2.38	2.40	1.72	1.85	1.00	1.96	1.84	2.02	1.71	2.08
Er	6.35	6.33	4.29	4.73	2.39	5.03	4.67	4.95	4.22	5.25
Tm	1.03	1.00	0.61	0.70	0.34	0.83	0.68	0.73	0.59	0.75
Yb	6.89	6.67	3.82	4.48	2.15	5.45	4.06	4.62	3.51	4.40
Lu	0.97	0.93	0.56	0.66	0.32	0.79	0.60	0.66	0.51	0.66
Hf	5.85	6.13	7.95	8.72	4.41	5.15	5.52	6.29	7.02	6.42
Ta	4.46	3.85	1.77	2.26	1.42	5.70	1.75	2.10	1.67	1.82
Th	28.3	29.0	37.7	38.2	34.1	26.5	34.1	38.7	35.3	37.2
U	11.4	9.56	4.36	5.62	3.53	6.23	9.46	8.84	5.23	6.36
T_{Zr}	807	814	843	850	777	794	817	828	841	821
10^4*Ga/Al	3.5	3.4	3.0	2.9	2.9	3.6	2.7	3.2	2.9	3.1

	GD 23-2	GD 24-2	GD 24-3	GD 25-1	GD 26-1	GD 26-2	XY 17-1	XY 17-4	XY 17-5	XY 17-6
					Jiuyishan					
Major elements (wt%)										
SiO_2	75.03	66.99	72.47	70.02	72.13	72.10	69.62	65.94	64.07	64.85
TiO_2	0.21	0.71	0.29	0.53	0.34	0.29	0.58	0.96	1.14	0.98
Al_2O_3	12.55	14.62	13.55	13.99	13.87	13.52	13.92	14.01	13.76	14.24
Fe_2O_3t	2.16	6.32	3.20	5.68	2.68	3.50	4.89	6.93	7.05	6.08
MnO	0.03	0.08	0.04	0.06	0.04	0.06	0.07	0.09	0.08	0.07
MgO	0.20	0.74	0.23	0.16	0.47	0.24	0.59	1.31	1.54	1.25
CaO	1.09	3.01	1.30	2.36	1.78	1.50	2.24	2.88	3.02	3.21
Na_2O	2.50	3.01	2.62	2.42	2.96	3.01	2.80	2.78	2.43	2.69
K_2O	5.48	4.08	5.56	4.15	5.06	4.85	4.79	4.21	3.78	4.18
P_2O_5	0.07	0.25	0.10	0.24	0.10	0.10	0.18	0.28	0.35	0.30
LOI	0.56	0.07	0.51	0.32	0.39	0.68	0.02	0.61	2.21	1.68
Total	99.88	99.89	99.86	99.92	99.83	99.85	99.69	100.01	99.43	99.52
A/CNK	1.04	0.98	1.07	1.10	1.02	1.04	1.00	0.97	1.01	0.96
MALI	6.89	4.07	6.87	4.21	6.24	6.37	5.35	4.11	3.19	3.65
Fe*	0.91	0.88	0.93	0.97	0.84	0.93	0.88	0.83	0.80	0.81
Trace elements (ppm)										
Ga	19.7	22.3	21.2	21.6	17.7	23.7	21.4	21.3	22.5	22.1
Rb	245	160	236	171	267	473	207	176	180	170
Sr	72.0	174	103	160	148	75.1	134	163	163	187
Y	53.6	42.7	52.0	55.1	32.2	54.3	48.6	44.8	44.7	43.0
Zr	226	505	267	568	167	244	392	321	399	378
Nb	21.6	30.2	23.9	32.9	16.6	30.4	29.2	27.0	31.9	28.4
Ba	619	1290	900	1422	576	784	1152	985	784	1170
La	71.2	72.2	65.4	76.3	50.8	65.4	74.6	44.7	73.6	63.3
Ce	147	143	132	153	101	134	146	90.7	152	131
Pr	18.2	17.7	16.5	19.4	12.2	16.8	18.4	11.6	19.0	16.5
Nd	64.5	63.0	58.1	70.4	41.1	60.5	66.1	43.0	67.7	58.4
Sm	12.9	12.1	11.7	13.4	7.95	12.5	12.6	9.25	12.6	11.2
Eu	1.13	2.78	1.48	2.66	0.98	1.23	2.22	2.29	2.23	2.51
Gd	10.9	10.3	10.1	11.5	6.54	10.7	11.0	8.73	10.7	9.68
Tb	1.65	1.40	1.54	1.67	0.96	1.74	1.53	1.31	1.48	1.39
Dy	9.63	7.50	9.14	9.62	5.47	10.1	8.89	7.71	8.49	7.95
Ho	2.01	1.63	1.96	2.23	1.16	2.04	1.83	1.68	1.75	1.68
Er	5.11	4.09	5.02	5.86	3.00	5.05	4.75	4.40	4.53	4.39
Tm	0.74	0.61	0.75	0.90	0.46	0.78	0.72	0.68	0.68	0.66
Yb	4.46	3.65	4.54	5.73	2.96	5.06	4.47	4.18	4.39	4.22
Lu	0.67	0.59	0.69	0.93	0.46	0.74	0.69	0.64	0.66	0.65
Hf	6.52	12.1	7.15	13.7	4.83	6.81	10.1	8.23	10.1	9.52
Ta	1.94	1.85	2.03	2.40	2.00	4.12	2.35	2.28	2.44	2.27
Th	36.6	24.7	31.5	26.7	35.4	33.0	29.6	19.5	30.4	26.4
U	6.44	2.29	6.93	5.43	8.96	9.90	4.47	4.85	5.30	4.34
T_{Zr}	821	879	836	913	787	824	861	832	858	845
10^4*Ga/Al	3.0	2.9	3.0	2.9	2.4	3.3	2.9	2.9	3.1	2.9

	XY 18-1	XY 18-4	XY 16-1	XY 16-2	GD 28-1	GD 28-2	GD 29-2	GD 29-4	GD 29-6
					Jiuyishan				
Major elements (wt%)									
SiO_2	69.44	69.69	74.98	74.37	70.89	73.91	75.61	73.95	74.45
TiO_2	0.52	0.51	0.22	0.27	0.29	0.23	0.12	0.25	0.15
Al_2O_3	14.15	14.02	12.43	13.10	14.48	13.15	13.09	12.63	13.28
Fe_2O_3t	4.48	4.45	2.20	2.53	2.88	2.33	1.90	3.02	1.83
MnO	0.06	0.06	0.03	0.03	0.03	0.02	0.02	0.03	0.02
MgO	0.56	0.56	0.19	0.24	0.18	0.13	0.05	0.12	0.07
CaO	2.21	2.25	1.27	1.45	1.37	1.33	0.81	1.05	1.30
Na_2O	2.73	2.73	2.99	2.98	3.13	2.88	3.00	2.88	3.45
K_2O	5.32	5.19	4.82	4.60	6.15	5.50	4.88	5.46	4.95
P_2O_5	0.16	0.17	0.04	0.05	0.07	0.05	0.02	0.04	0.03
LOI	0.16	0.15	0.45	0.44	0.34	0.33	0.40	0.46	0.28
Total	99.80	99.77	99.62	100.05	99.80	99.86	99.91	99.88	99.81
A/CNK	0.99	0.99	1.00	1.05	1.01	1.00	1.12	1.01	0.99
MALI	5.84	5.67	6.54	6.14	7.90	7.05	7.06	7.29	7.10
Fe*	0.88	0.88	0.91	0.91	0.94	0.94	0.97	0.96	0.96
Trace elements (ppm)									
Ga	21.9	19.8	21.7	21.7	22.8	19.8	22.4	23.1	23.0
Rb	199	183	300	288	282	253	445	365	285
Sr	139	141	53.5	64.2	90.3	76.1	29.2	43.1	51.0
Y	45.4	40.7	71.1	67.8	67.7	45.9	90.1	83.4	53.1
Zr	421	399	278	302	317	247	201	288	241
Nb	26.8	25.8	24.1	26.2	22.1	17.7	29.9	30.5	15.5
Ba	1286	1266	321	452	671	542	111	267	287
La	75.3	70.8	89.3	82.1	92.8	65.3	60.0	95.3	100
Ce	145	139	181	164	174	127	123	194	208
Pr	18.6	17.1	22.5	20.3	22.0	15.3	14.8	22.6	24.6
Nd	66.7	61.7	79.4	72.5	78.5	53.7	51.8	82.3	84.3
Sm	12.4	11.3	15.0	14.0	16.4	11.1	12.2	17.8	16.0
Eu	2.35	2.30	0.88	1.04	1.31	1.19	0.45	0.71	0.86
Gd	10.5	9.56	13.1	12.7	14.8	9.98	12.0	15.9	12.2
Tb	1.49	1.30	2.00	1.97	2.31	1.52	2.17	2.53	1.75
Dy	8.20	7.47	12.6	12.2	13.8	9.25	14.6	15.8	9.82
Ho	1.78	1.53	2.62	2.53	2.66	1.80	3.09	3.13	1.88
Er	4.43	3.94	6.99	6.67	6.73	4.64	8.88	8.41	4.98
Tm	0.65	0.58	1.09	1.00	0.93	0.65	1.39	1.19	0.72
Yb	4.03	3.73	6.88	6.31	5.22	3.88	8.37	7.30	4.41
Lu	0.63	0.55	0.98	0.90	0.75	0.56	1.24	1.04	0.65
Hf	10.5	10.2	8.73	9.03	9.60	7.38	7.75	9.35	8.03
Ta	2.17	2.02	2.62	2.84	1.68	1.47	4.11	2.87	1.30
Th	30.6	26.7	50.2	44.1	31.6	22.7	50.8	58.3	87.0
U	5.47	3.31	9.35	8.58	5.32	3.90	15.5	9.26	13.6
T_{Zr}	866	861	836	848	843	823	818	839	820
10^4*Ga/Al	2.9	2.7	3.3	3.1	3.0	2.8	3.2	3.5	3.3

	XY 2-1	XY 2-2	XY 2-4	XY 3-1	XY 3-3	XY 3-6	XY 3-7	XY 4-3	XY 4-4	XY 4-5
						Jiufeng				
Major elements (wt.%)										
SiO_2	77.59	76.74	77.74	73.70	73.72	74.06	74.24	73.56	73.09	73.38
TiO_2	0.02	0.04	0.03	0.19	0.19	0.23	0.19	0.27	0.31	0.28
Al_2O_3	12.61	12.83	12.40	14.09	14.25	13.93	13.92	13.96	13.95	14.46
Fe_2O_3t	0.33	0.53	0.46	1.32	1.26	1.57	1.28	1.48	1.57	1.22
MnO	0.03	0.04	0.04	0.03	0.03	0.05	0.04	0.02	0.02	0.02
MgO	0.08	0.09	0.08	0.34	0.35	0.40	0.35	0.48	0.50	0.41
CaO	0.67	0.69	0.75	0.94	0.73	0.95	0.78	0.76	0.51	0.60
Na_2O	3.31	3.18	3.54	2.99	2.96	3.05	2.87	2.65	2.42	2.52
K_2O	4.64	5.29	4.46	5.59	5.57	5.07	5.68	5.75	5.70	5.90
P_2O_5	0.01	0.01	0.01	0.15	0.15	0.16	0.16	0.16	0.17	0.17
LOI	0.41	0.44	0.39	0.55	0.73	0.63	0.59	0.90	1.30	0.83
Total	99.70	99.88	99.88	99.90	99.92	100.10	100.10	99.97	99.54	99.78
A/CNK	1.08	1.05	1.03	1.11	1.17	1.14	1.13	1.17	1.26	1.24
MALI	7.29	7.79	7.26	7.64	7.80	7.17	7.77	7.63	7.61	7.81
Fe*	0.80	0.84	0.85	0.78	0.76	0.78	0.77	0.74	0.74	0.73
Trace elements (ppm)										
Ga	15.7	15.7	16.0	18.9	18.1	20.4	21.8	19.3	23.3	22.8
Rb	480	499	416	458	469	517	498	408	485	428
Sr	20.6	21.0	17.4	53.7	78.5	57.9	49.6	62.5	41.4	56.6
Y	54.0	51.3	46.8	26.7	27.0	26.5	32.5	26.1	21.9	16.0
Zr	54.5	41.3	47.9	119	117	130	135	141	179	163
Nb	20.0	15.4	16.6	25.0	23.6	25.7	31.4	22.9	23.1	21.1
Ba	27.3	25.5	12.4	234	239	234	189	314	314	330
La	11.3	15.3	12.6	35.9	35.8	35.1	40.2	54.1	56.5	54.7
Ce	26.6	36.7	28.3	76.9	76.3	74.8	86.5	111	118	113
Pr	3.59	5.05	3.81	9.43	9.35	9.25	10.8	14.2	15.4	15.2
Nd	13.8	19.4	14.2	32.7	32.2	31.9	36.9	50.0	54.1	52.7
Sm	4.88	6.03	4.59	7.05	6.92	6.98	8.13	9.80	10.5	10.3
Eu	0.18	0.16	0.14	0.51	0.51	0.48	0.48	0.65	0.68	0.68
Gd	5.57	6.05	5.12	5.67	5.63	5.65	6.66	7.21	7.22	6.64
Tb	1.18	1.16	1.05	0.87	0.85	0.85	1.02	0.96	0.88	0.77
Dy	8.35	7.99	7.14	4.85	4.88	4.79	5.79	5.19	4.36	3.33
Ho	1.92	1.77	1.74	0.92	0.93	0.91	1.12	0.92	0.75	0.57
Er	5.34	4.91	4.65	2.30	2.41	2.29	2.84	2.27	1.80	1.29
Tm	0.86	0.79	0.73	0.35	0.36	0.35	0.43	0.33	0.25	0.17
Yb	5.46	5.12	4.62	2.19	2.26	2.20	2.70	2.06	1.42	0.98
Lu	0.81	0.76	0.68	0.32	0.33	0.32	0.40	0.30	0.21	0.14
Hf	2.85	1.95	2.55	3.80	3.78	4.09	4.38	4.31	5.38	4.74
Ta	3.96	4.14	3.50	4.66	4.55	6.25	7.60	3.67	2.84	2.58
Th	22.8	27.8	25.1	32.3	31.8	32.0	35.6	44.0	46.3	43.9
U	14.0	12.0	10.4	14.0	17.5	27.3	26.9	11.2	8.99	7.79
T_{Zr}	709	685	695	769	772	779	781	788	816	806
10^4*Ga/Al	2.4	2.3	2.4	2.5	2.4	2.8	3.0	2.6	3.1	3.0

	XY 4-7	XY 5-1	XY 5-3	XY 6-1	XY 6-2	XY 7-1	XY 7-2	XY 7-3	XY 7-4	XY 8-1
					Jiufeng					
Major elements (wt.%)										
SiO_2	75.41	76.94	76.04	80.21	77.04	76.02	76.15	76.25	75.83	69.96
TiO_2	0.17	0.06	0.05	0.06	0.05	0.01	0.01	0.01	0.01	0.47
Al_2O_3	13.67	12.59	13.22	10.95	12.72	13.86	14.04	13.96	13.79	14.67
Fe_2O_3t	1.11	0.89	0.76	0.68	0.70	0.32	0.36	0.35	0.33	2.95
MnO	0.04	0.07	0.06	0.04	0.04	0.14	0.14	0.14	0.13	0.05
MgO	0.28	0.11	0.15	0.16	0.19	0.07	0.08	0.06	0.06	0.96
CaO	0.86	0.71	0.65	0.40	0.44	0.33	0.34	0.39	0.47	1.83
Na_2O	2.83	3.46	3.39	2.71	2.89	4.03	3.82	4.34	4.08	2.80
K_2O	4.98	4.45	5.02	4.09	4.79	4.30	4.23	3.88	4.26	5.17
P_2O_5	0.09	0.02	0.02	0.03	0.02	0.02	0.02	0.02	0.02	0.20
LOI	0.62	0.59	0.60	0.62	0.65	0.72	0.72	0.65	0.73	0.68
Total	100.04	99.91	99.94	99.94	99.54	99.82	99.91	100.06	99.70	99.74
A/CNK	1.18	1.07	1.08	1.14	1.18	1.17	1.22	1.16	1.13	1.09
MALI	6.95	7.20	7.76	6.40	7.24	8.00	7.70	7.84	7.87	6.14
Fe*	0.78	0.88	0.82	0.79	0.77	0.81	0.81	0.84	0.82	0.73
Trace elements (ppm)										
Ga	18.0	19.7	18.4	14.5	17.5	27.5	24.3	26.3	27.3	19.3
Rb	475	628	646	451	547	1231	1241	1137	1207	369
Sr	60.6	15.4	18.1	18.4	19.6	1.70	1.87	1.74	2.11	131
Y	38.6	91.9	82.2	97.5	78.8	71.2	59.5	69.4	76.4	30.7
Zr	138	74.9	69.3	99.2	76.7	38.7	35.3	34.3	30.0	154
Nb	22.2	37.8	27.1	35.7	21.3	54.7	56.7	52.1	55.9	24.3
Ba	243	31.2	51.6	44.6	49.3	5.09	5.56	3.53	4.35	463
La	34.4	23.8	24.2	25.4	20.3	12.8	11.1	13.1	13.0	42.4
Ce	72.8	55.0	52.5	58.7	44.9	35.4	32.4	36.6	36.5	86.3
Pr	8.80	7.45	7.43	7.79	5.98	5.21	4.50	5.41	5.43	10.6
Nd	31.2	28.5	28.6	30.6	23.1	20.4	17.9	21.2	21.3	36.5
Sm	6.84	9.63	9.17	9.45	7.12	9.07	7.84	9.27	9.66	7.44
Eu	0.53	0.14	0.20	0.17	0.16	0.02	0.02	0.02	0.02	0.93
Gd	6.03	10.0	9.44	10.6	8.08	8.12	7.18	8.24	8.93	6.04
Tb	1.00	2.08	1.88	2.24	1.69	1.71	1.51	1.72	1.91	0.91
Dy	6.40	14.4	12.9	16.0	12.2	10.7	9.58	10.8	11.9	5.19
Ho	1.34	3.18	2.80	3.49	2.74	2.01	1.77	2.03	2.29	1.09
Er	3.64	8.92	7.77	9.60	7.61	5.60	4.75	5.66	6.42	2.85
Tm	0.60	1.52	1.30	1.58	1.26	1.09	0.90	1.10	1.24	0.45
Yb	4.09	10.4	8.87	10.6	8.37	8.39	6.81	8.50	9.51	2.82
Lu	0.60	1.56	1.32	1.51	1.21	1.29	1.01	1.30	1.49	0.44
Hf	4.65	3.97	3.78	4.93	3.76	3.70	3.41	3.48	3.24	4.60
Ta	5.61	9.80	7.26	10.4	4.57	21.3	21.1	18.6	23.0	4.07
Th	34.0	34.7	32.9	37.6	29.6	11.5	10.1	10.0	10.5	34.7
U	11.2	27.6	20.6	28.2	15.0	6.91	7.39	7.76	12.8	7.76
T_{Zr}	789	731	725	764	742	687	685	678	667	783
10^4*Ga/Al	2.5	3.0	2.6	2.5	2.6	3.8	3.3	3.6	3.7	2.5

	XY 9-1	XY 9-3	XY 9-5	XY 9-6	XY 9-9	XY 10-1	XY 10-2	XY 10-3
					Jiufeng			
Major elements (wt.%)								
SiO_2	70.01	69.06	70.02	70.67	71.73	70.18	68.85	70.01
TiO_2	0.54	0.57	0.53	0.44	0.34	0.55	0.57	0.50
Al_2O_3	13.74	14.30	14.11	13.96	14.22	14.05	14.39	14.14
Fe_2O_3t	3.64	3.75	3.47	2.93	2.42	3.53	3.57	3.08
MnO	0.07	0.07	0.08	0.08	0.05	0.06	0.06	0.06
MgO	1.15	1.22	1.08	0.94	0.76	1.17	1.20	1.02
CaO	2.43	2.60	2.41	2.27	2.09	2.91	2.83	2.43
Na_2O	2.48	2.79	2.70	2.65	3.07	2.89	2.90	2.75
K_2O	4.42	4.54	4.66	4.90	4.73	4.19	4.52	5.00
P_2O_5	0.15	0.16	0.13	0.12	0.11	0.15	0.16	0.13
LOI	1.24	0.58	0.80	0.75	0.38	0.47	0.69	0.66
Total	99.87	99.65	100.00	99.70	99.91	100.16	99.74	99.78
A/CNK	1.03	1.01	1.02	1.01	1.02	0.96	0.97	0.98
MALI	4.48	4.73	4.96	5.27	5.71	4.18	4.59	5.32
Fe*	0.74	0.73	0.74	0.74	0.74	0.73	0.73	0.73
Trace elements (ppm)								
Ga	19.1	19.2	18.0	17.4	16.7	17.1	18.0	16.4
Rb	376	333	386	394	270	276	311	315
Sr	146	172	169	158	185	185	189	178
Y	41.5	44.0	38.6	29.3	17.8	32.9	31.7	29.5
Zr	198	196	176	170	156	202	187	146
Nb	25.4	26.8	24.3	19.7	18.9	20.0	21.1	19.3
Ba	492	484	463	580	730	446	608	638
La	56.1	46.1	49.5	43.5	45.1	30.6	47.5	26.4
Ce	113	95.4	100	87.7	86.4	63.7	93.8	55.7
Pr	13.5	11.9	12.2	10.4	10.1	8.07	11.2	6.95
Nd	46.0	41.3	41.4	35.2	33.8	28.6	38.2	25.4
Sm	9.12	9.09	8.38	6.72	5.91	6.37	7.05	5.49
Eu	1.06	1.11	1.05	1.00	0.96	1.06	1.12	1.01
Gd	7.60	7.73	6.95	5.41	4.42	5.62	5.82	4.79
Tb	1.17	1.22	1.05	0.80	0.56	0.88	0.87	0.76
Dy	6.84	7.17	6.21	4.61	3.11	5.22	5.20	4.74
Ho	1.48	1.57	1.36	0.99	0.61	1.17	1.11	1.04
Er	3.97	4.18	3.68	2.70	1.62	3.18	3.03	2.80
Tm	0.62	0.65	0.60	0.43	0.25	0.51	0.48	0.45
Yb	3.97	3.90	3.85	2.83	1.71	3.18	3.15	3.00
Lu	0.61	0.62	0.64	0.46	0.28	0.52	0.49	0.46
Hf	5.99	5.67	5.34	5.06	4.61	5.63	5.24	4.30
Ta	4.63	4.64	5.19	3.66	3.81	3.36	3.29	3.57
Th	42.3	38.0	37.2	34.3	27.1	31.8	30.7	36.2
U	14.8	17.1	16.5	13.8	10.8	15.5	12.0	14.7
T_{Zr}	802	795	789	786	780	794	787	769
10^4*Ga/Al	2.6	2.5	2.4	2.4	2.2	2.3	2.4	2.2

	GD 08-3	GD 08-4	GD 08-5	GD 10-1	GD 10-2	GD 10-3	GD 11-1	GD 11-2	GD 13	GD 14-1
						Dadongshan				
Major elements (%)										
SiO2	73.63	72.06	73.88	73.75	72.64	76.50	74.78	73.82	76.35	76.99
TiO2	0.25	0.29	0.27	0.18	0.19	0.18	0.18	0.18	0.12	0.14
Al2O3	13.29	13.74	13.32	13.25	14.10	12.28	13.58	13.40	12.47	11.75
Fe2O3t	2.31	2.45	2.40	1.86	2.15	1.97	1.93	1.90	1.61	1.62
MnO	0.04	0.04	0.04	0.04	0.04	0.04	0.10	0.10	0.06	0.04
MgO	0.31	0.36	0.27	0.15	0.16	0.18	0.15	0.14	0.03	0.08
CaO	1.07	0.52	1.09	0.78	0.40	0.57	0.71	0.70	0.31	0.73
Na2O	2.73	2.46	2.58	2.73	3.03	2.50	2.17	2.14	3.18	2.62
K2O	5.12	6.85	5.55	5.97	5.89	5.17	5.29	5.22	4.99	5.02
P2O5	0.05	0.14	0.07	0.05	0.05	0.04	0.07	0.07	0.01	0.03
LOI	0.61	0.92	0.48	1.01	0.54	0.72	1.14	1.34	0.51	0.87
Total	99.40	99.82	99.96	99.75	99.20	100.16	100.09	99.02	99.64	99.89
A/CNK	1.11	1.11	1.09	1.07	1.17	1.14	1.28	1.28	1.11	1.06
MALI	6.78	8.78	7.04	7.93	8.51	7.11	6.75	6.67	7.86	6.90
Fe*	0.87	0.86	0.89	0.92	0.92	0.91	0.92	0.92	0.98	0.95
Trace elements (ppm)										
Ga	20.1	19.4	19.3	18.8	19.3	21.1	18.3	20.9	21.4	19.0
Rb	383	487	525	412	506	474	482	628	647	436
Sr	93.7	73.7	92.4	93.0	109	95.2	111	45.9	67.6	42.7
Y	38.3	33.9	40.2	39.5	54.7	53.8	60.7	37.4	42.4	117
Zr	201	147	179	160	127	129	149	113	121	121
Nb	21.9	17.3	21.6	21.8	20.9	23.4	19.1	26.7	29.9	34.9
Ba	444	260	333	313	234	201	181	252	239	93.1
La	51.5	53.4	53.9	46.8	40.0	47.0	38.8	35.9	39.8	40.2
Ce	105	103	114	96.3	85.3	98.9	83.0	74.4	81.9	59.5
Pr	12.5	11.5	13.9	10.9	10.2	12.2	10.0	8.59	9.34	10.8
Nd	46.2	40.6	51.6	39.7	37.5	43.4	36.4	30.9	33.4	41.3
Sm	8.43	7.58	9.93	7.64	8.67	9.95	8.17	6.51	7.16	12.1
Eu	0.79	0.60	0.74	0.58	0.47	0.47	0.38	0.35	0.40	0.25
Gd	6.81	6.43	8.10	6.80	8.01	8.87	7.96	5.57	6.36	13.8
Tb	1.06	1.04	1.18	1.13	1.44	1.54	1.47	1.01	1.11	2.74
Dy	6.29	5.94	6.73	6.69	8.80	8.62	8.81	5.89	6.56	17.0
Ho	1.25	1.13	1.34	1.29	1.71	1.70	1.90	1.17	1.28	3.54
Er	3.76	3.34	3.84	3.82	5.40	5.04	5.83	3.51	3.79	10.6
Tm	0.61	0.52	0.58	0.59	0.94	0.86	0.99	0.59	0.64	1.71
Yb	3.87	3.20	3.76	3.73	6.53	6.10	6.50	3.91	4.07	10.9
Lu	0.60	0.48	0.56	0.58	0.98	0.91	0.99	0.58	0.62	1.62
Hf	6.39	4.93	5.61	5.23	4.69	4.53	5.52	4.09	4.24	5.50
Ta	4.14	2.61	2.79	4.10	4.40	5.00	4.76	5.68	7.13	6.27
Th	49.1	52.9	49.4	45.7	45.4	49.1	49.2	37.3	39.7	45.7
U	24.1	17.5	12.3	19.3	17.7	19.2	17.2	16.1	13.9	29.4
T_{Zr}	815	785	803	791	778	782	803	779	774	771
10^4*Ga/Al	2.9	2.7	2.7	2.7	2.6	3.2	2.5	2.9	3.2	3.1

	GD 14-2	GD 14-3	GD 15-1	GD 15-2	GD 15-3	GD 16-2	GD 16-3	GD 17-2	GD 17-3	GD 18-1
					Dadongshan					
Major elements (%)										
SiO2	75.03	76.18	73.93	72.73	73.37	73.35	74.62	75.68	75.89	74.91
TiO2	0.12	0.15	0.30	0.35	0.30	0.16	0.14	0.11	0.10	0.11
Al2O3	12.64	12.05	13.33	13.24	13.20	13.51	13.21	12.31	12.21	13.33
Fe2O3t	1.60	1.90	2.41	2.89	2.59	1.91	1.66	1.90	1.63	1.65
MnO	0.04	0.05	0.03	0.04	0.05	0.04	0.04	0.06	0.04	0.04
MgO	0.08	0.12	0.30	0.38	0.30	0.09	0.06	0.01	0.01	0.01
CaO	0.94	0.50	1.49	1.43	1.17	1.04	1.03	0.74	0.76	0.56
Na2O	2.98	2.62	2.70	2.71	2.74	2.85	2.82	2.93	2.96	3.01
K2O	5.15	4.97	5.22	5.44	6.06	5.82	5.48	5.29	5.05	5.56
P2O5	0.03	0.05	0.05	0.06	0.05	0.02	0.01	0.01	0.00	0.01
LOI	1.03	0.81	0.60	0.73	0.52	0.45	0.11	0.34	0.45	0.36
Total	99.64	99.40	100.35	99.98	100.35	99.24	99.17	99.36	99.10	99.55
A/CNK	1.04	1.14	1.04	1.02	1.00	1.05	1.06	1.03	1.04	1.11
MALI	7.19	7.09	6.43	6.71	7.63	7.63	7.26	7.48	7.25	8.00
Fe*	0.95	0.94	0.88	0.87	0.88	0.95	0.96	0.99	0.99	1.00
Trace elements (ppm)										
Ga	16.9	16.3	17.2	18.5	18.9	16.4	16.3	16.4	16.8	16.8
Rb	464	429	451	295	327	327	403	459	462	417
Sr	65.9	42.9	65.6	117	84.6	100	48.6	12.1	13.6	34.3
Y	45.5	20.6	50.0	38.4	43.3	33.9	37.0	51.8	56.1	40.2
Zr	103	86.6	120	197	175	178	97.4	126	110	113
Nb	26.3	22.6	28.8	16.2	17.4	15.1	17.5	21.4	21.6	14.5
Ba	144	174	148	485	562	590	166	41.0	37.9	95.1
La	29.2	18.8	38.9	70.4	75.9	67.7	36.3	29.7	25.2	32.9
Ce	61.5	39.7	83.3	132	144	123	77.8	65.2	57.4	67.1
Pr	7.23	4.48	10.4	14.8	16.0	13.6	8.85	7.76	7.28	8.63
Nd	27.5	18.4	39.2	50.8	55.0	47.7	33.0	29.3	28.8	33.3
Sm	6.71	4.70	9.70	8.71	9.52	7.76	6.71	7.26	7.45	7.46
Eu	0.31	0.26	0.34	0.84	0.85	0.81	0.51	0.23	0.21	0.36
Gd	6.61	4.06	8.74	6.98	7.65	6.61	5.99	6.99	7.18	7.17
Tb	1.23	0.65	1.47	1.12	1.25	1.04	0.98	1.31	1.31	1.13
Dy	7.64	3.66	8.45	6.56	6.97	5.85	6.03	8.40	8.62	6.71
Ho	1.55	0.66	1.59	1.25	1.42	1.16	1.30	1.78	1.86	1.35
Er	4.50	1.75	4.77	3.82	4.25	3.46	3.64	5.19	5.45	3.79
Tm	0.70	0.32	0.77	0.59	0.69	0.56	0.60	0.86	0.89	0.59
Yb	4.62	1.99	4.95	3.90	4.41	4.43	3.97	6.70	6.05	4.00
Lu	0.70	0.31	0.75	0.58	0.69	0.53	0.59	0.89	0.92	0.57
Hf	3.77	3.19	4.52	6.02	5.22	5.40	3.79	5.63	4.60	4.24
Ta	3.62	4.37	4.26	1.99	2.52	2.14	6.69	4.72	4.82	2.71
Th	47.0	34.1	55.4	46.8	50.4	44.9	55.6	49.1	51.3	51.3
U	16.9	9.84	17.7	9.41	9.70	8.86	12.7	14.8	14.8	10.1
T_{Zr}	753	749	764	804	791	798	750	770	760	766
10^4*Ga/Al	2.5	2.6	2.4	2.6	2.7	2.3	2.3	2.5	2.6	2.4

	GD 47-1	GD 47-2	GD 47-3	GD 47-4	GD 47-5	GD 51-1	GD 51-2
			Xiaoliang			Gangwei	
Major elements (wt.%)							
SiO_2	64.61	68.04	67.44	70.08	67.16	65.83	64.11
TiO_2	0.61	0.43	0.54	0.48	0.49	0.51	0.70
Al_2O_3	15.57	13.99	14.87	13.62	14.79	14.92	13.08
Fe_2O_3t	4.50	2.79	3.63	3.07	3.38	4.53	7.20
MnO	0.06	0.05	0.07	0.05	0.06	0.09	0.15
MgO	0.62	0.44	0.83	0.60	0.64	1.59	2.83
CaO	1.02	1.57	2.62	1.37	1.62	3.49	3.74
Na_2O	3.37	3.81	3.57	3.06	3.12	3.05	2.60
K_2O	6.87	5.52	4.37	4.51	5.94	3.96	3.93
P_2O_5	0.18	0.13	0.14	0.13	0.13	0.17	0.20
LOI	2.21	2.84	1.60	2.71	2.31	1.57	1.27
Total	99.63	99.61	99.67	99.69	99.64	99.70	99.81
A/CNK	1.05	0.93	0.97	1.10	1.02	0.95	0.85
MALI	9.22	7.76	5.32	6.20	7.43	3.52	2.79
Fe*	0.87	0.85	0.80	0.82	0.83	0.72	0.70
Trace elements (ppm)							
Ga	16.9	13.0	17.5	14.4	15.3	17.2	17.2
Rb	227	175	146	157	176	233	240
Sr	225	154	225	213	246	471	302
Y	18.4	25.9	29.1	21.8	26.3	21.1	34.9
Zr	296	255	213	195	174	131	158
Nb	14.0	16.3	18.9	17.3	16.4	12.4	17.7
Ba	697	592	604	438	807	605	288
La	70.4	54.1	54.4	41.2	42.3	33.5	43.2
Ce	127	98.9	102	77.7	79.5	61.7	83.9
Pr	13.6	11.2	11.5	8.89	9.10	6.96	9.82
Nd	42.8	36.8	38.1	29.9	31.3	23.9	34.7
Sm	6.55	6.74	7.17	5.64	6.26	4.55	7.11
Eu	1.09	1.14	1.19	0.98	1.12	1.06	1.26
Gd	5.14	5.69	6.10	4.73	5.50	4.02	6.31
Tb	0.62	0.82	0.89	0.68	0.81	0.59	0.97
Dy	3.35	4.68	5.34	3.99	4.87	3.51	5.90
Ho	0.64	0.92	1.04	0.78	0.94	0.71	1.21
Er	1.75	2.51	2.87	2.14	2.55	2.00	3.34
Tm	0.26	0.36	0.41	0.30	0.36	0.30	0.50
Yb	1.60	2.32	2.50	1.94	2.22	1.99	3.33
Lu	0.27	0.37	0.38	0.29	0.34	0.32	0.53
Hf	8.01	6.69	5.80	5.44	4.73	3.69	4.57
Ta	0.72	1.33	1.26	1.34	1.08	1.10	1.45
Th	28.8	20.2	23.7	19.0	21.7	27.1	34.8
U	4.21	3.82	4.04	3.32	3.77	9.44	11.6
T_{Zr}	831	809	796	808	784	750	749
10^4*Ga/Al	2.05	1.75	2.22	2.00	1.96	2.18	2.49

	GD 51-3	GD 51-4	GD 51-5	GD 52-1	GD 52-2	GD 52-3	GD 52-4	GD 60-1
	Gangwei				Lunshui			Gudoushan
Major elements (wt.%)								
SiO_2	66.83	66.71	66.38	70.56	72.03	70.71	69.59	72.94
TiO_2	0.48	0.45	0.51	0.26	0.25	0.25	0.27	0.30
Al_2O_3	14.85	15.35	15.00	14.79	14.07	14.84	15.22	13.33
Fe_2O_3t	4.24	3.65	3.95	2.77	2.71	2.54	2.76	2.66
MnO	0.08	0.11	0.07	0.08	0.08	0.08	0.08	0.06
MgO	1.53	1.38	1.43	0.57	0.57	0.55	0.57	0.42
CaO	3.46	2.98	3.37	2.32	2.31	2.25	2.30	1.90
Na_2O	2.97	3.05	3.08	3.50	3.39	3.49	3.54	3.52
K_2O	4.12	4.32	4.37	4.54	4.08	4.74	4.93	3.78
P_2O_5	0.16	0.14	0.15	0.09	0.09	0.09	0.10	0.08
LOI	1.03	1.54	1.37	0.29	0.24	0.27	0.40	0.80
Total	99.73	99.67	99.68	99.79	99.83	99.78	99.75	99.81
A/CNK	0.95	1.02	0.94	0.99	0.99	0.99	0.99	1.00
MALI	3.63	4.39	4.08	5.72	5.15	5.97	6.18	5.40
Fe*	0.71	0.70	0.71	0.81	0.81	0.81	0.81	0.85
Trace elements (ppm)								
Ga	16.1	17.2	16.0	15.2	14.6	15.0	14.7	16.4
Rb	213	258	243	137	125	141	145	268
Sr	427	419	432	427	409	432	443	160
Y	19.5	18.5	22.8	31.1	25.6	22.4	26.0	46.9
Zr	165	148	139	167	139	171	156	183
Nb	11.6	11.9	13.0	13.7	14.2	13.7	15.2	16.6
Ba	619	536	613	574	527	621	662	290
La	30.9	37.9	34.2	36.0	32.6	28.2	28.0	34.0
Ce	57.3	60.5	65.6	58.1	56.9	49.9	49.2	68.4
Pr	6.43	6.32	7.56	6.94	6.42	5.71	6.04	8.27
Nd	22.1	21.1	26.2	24.0	21.9	19.7	21.5	29.7
Sm	4.16	3.90	5.00	4.88	4.46	4.16	4.75	6.96
Eu	1.00	0.91	1.11	1.11	0.97	0.96	1.09	0.89
Gd	3.64	3.41	4.39	4.74	4.05	3.66	4.34	6.49
Tb	0.53	0.49	0.65	0.73	0.64	0.58	0.69	1.10
Dy	3.24	3.02	3.93	4.70	4.01	3.58	4.39	7.22
Ho	0.67	0.62	0.80	1.00	0.84	0.74	0.90	1.47
Er	1.88	1.74	2.20	2.86	2.34	2.08	2.52	4.37
Tm	0.30	0.28	0.35	0.43	0.36	0.31	0.39	0.69
Yb	1.97	1.82	2.26	2.76	2.27	2.01	2.41	4.54
Lu	0.32	0.30	0.35	0.42	0.34	0.31	0.36	0.71
Hf	4.81	4.41	4.19	4.25	3.55	4.29	4.25	5.83
Ta	1.04	1.11	1.26	1.16	1.25	1.17	1.42	3.81
Th	24.9	28.8	31.5	9.11	9.78	9.59	10.0	25.2
U	9.05	13.9	14.0	2.28	2.30	2.52	2.75	9.77
T_{Zr}	771	769	754	781	768	783	774	795
10^4*Ga/Al	2.05	2.11	2.01	1.94	1.96	1.90	1.83	2.32

	GD 60-4	GD 61-1	GD 61-3	GD 61-5	GD 62-3	GD 63-1	GD 63-2	GD 63-4	GD 63-7	GD 64-1	GD 64-3
	Gudoushan					Wuguishan					
Major elements (wt.%)											
SiO_2	71.07	70.63	73.69	71.94	72.54	76.06	76.77	75.62	76.07	76.18	76.04
TiO_2	0.24	0.46	0.31	0.29	0.22	0.09	0.10	0.09	0.11	0.09	0.09
Al_2O_3	14.26	14.04	13.09	14.18	14.28	12.20	12.16	12.95	12.36	12.50	13.13
Fe_2O_3t	2.40	3.86	2.94	2.32	2.40	1.56	1.55	1.42	1.63	1.62	1.55
MnO	0.06	0.10	0.08	0.04	0.06	0.05	0.05	0.05	0.05	0.05	0.05
MgO	0.36	0.66	0.50	0.39	0.29	0.05	0.07	0.05	0.07	0.06	0.06
CaO	1.48	2.39	2.07	1.30	1.66	0.81	0.80	0.95	0.84	0.66	0.61
Na_2O	3.49	3.22	3.28	2.81	3.67	3.31	3.07	3.44	3.26	3.20	2.90
K_2O	5.43	4.05	3.50	6.15	4.35	4.86	4.91	4.89	4.75	5.14	5.13
P_2O_5	0.07	0.13	0.09	0.08	0.06	0.02	0.02	0.02	0.02	0.01	0.01
LOI	0.89	0.31	0.33	0.31	0.29	0.81	0.41	0.36	0.69	0.37	0.33
Total	99.74	99.84	99.87	99.82	99.81	99.84	99.89	99.85	99.85	99.87	99.91
A/CNK	1.00	1.00	1.01	1.04	1.04	1.00	1.03	1.02	1.03	1.04	1.15
MALI	7.44	4.88	4.71	7.67	6.37	7.36	7.18	7.39	7.18	7.68	7.43
Fe*	0.86	0.84	0.84	0.84	0.88	0.96	0.95	0.96	0.95	0.96	0.96
Trace elements (ppm)											
Ga	15.7	17.7	18.0	16.9	16.6	15.0	13.2	16.5	15.7	15.8	16.3
Rb	288	281	226	203	293	358	315	379	347	388	419
Sr	176	115	198	153	161	48.9	23.8	37.7	37.7	26.3	30.6
Y	27.0	73.9	35.2	32.6	28.7	53.8	40.4	55.5	58.7	78.3	74.2
Zr	116	106	178	168	193	96.5	82.0	95.6	103	101	78.8
Nb	11.6	17.0	16.3	17.5	14.6	19.0	10.9	19.6	21.0	29.2	21.5
Ba	471	168	479	259	1141	64.6	44.6	61.7	56.1	58.0	106
La	25.5	30.6	54.6	42.7	40.6	21.9	16.4	27.2	22.9	22.1	21.9
Ce	49.8	51.2	105	85.4	79.8	48.1	32.9	59.6	51.3	49.5	49.8
Pr	5.97	7.61	12.4	10.4	9.48	6.32	4.78	7.53	6.69	6.56	6.61
Nd	21.3	29.8	42.6	36.7	32.6	23.5	18.0	27.1	24.9	25.0	25.2
Sm	4.77	7.87	8.28	7.58	6.81	6.99	5.32	7.42	7.40	8.16	8.19
Eu	0.89	1.00	1.24	0.89	1.09	0.29	0.22	0.32	0.28	0.27	0.30
Gd	4.46	9.06	6.89	6.38	5.60	6.96	5.39	7.13	7.50	9.13	9.00
Tb	0.72	1.58	0.99	0.95	0.85	1.30	1.02	1.34	1.41	1.78	1.81
Dy	4.64	11.0	5.90	5.67	4.96	8.88	7.03	8.85	9.52	12.6	12.6
Ho	0.95	2.37	1.20	1.13	0.96	1.86	1.49	1.84	2.00	2.72	2.73
Er	2.63	7.12	3.30	3.09	2.63	5.43	4.30	5.38	5.78	7.92	7.97
Tm	0.41	1.12	0.49	0.46	0.39	0.89	0.67	0.83	0.90	1.23	1.22
Yb	2.55	7.32	3.06	2.88	2.47	5.79	4.36	5.45	5.67	7.59	7.37
Lu	0.40	1.16	0.50	0.44	0.37	0.86	0.65	0.82	0.85	1.14	1.08
Hf	3.93	3.53	5.28	5.17	5.50	4.18	3.45	3.84	4.28	4.37	3.28
Ta	1.48	3.34	1.26	2.28	1.48	3.59	1.63	3.39	3.17	3.30	2.98
Th	25.8	25.1	25.9	31.3	31.4	40.3	31.4	43.2	43.7	42.5	41.5
U	10.5	10.9	5.98	8.28	7.32	14.3	11.5	17.7	21.3	19.2	20.7
T_{Zr}	752	745	794	789	802	745	735	745	753	752	741
10^4*Ga/ Al	2.08	2.38	2.60	2.26	2.20	2.33	2.04	2.41	2.41	2.39	2.35

Note: LOI stands for loss on ignition; A/CNK = mole $Al_2O_3/(CaO + K_2O + Na_2O)$;
Fe* = $(FeO + Fe_2O_3 \times 0.9)/ (FeO + Fe_2O_3 \times 0.9 + MgO)$;
$T_{Zr} = 12{,}900/[2.95 + 0.85M + \ln(496{,}000/Zr_{melt})]$, $M = [(Na + K + 2\cdot Ca)/(Al\cdot Si)$.

Appendix Table 9 Whole-rock Sr-Nd isotope compositions

Sample	$^{87}Rb/^{86}Sr$	$^{87}Sr/^{86}Sr$ (2σ)	I_{Sr}	$^{147}Sm/^{144}Nd$	$^{143}Nd/^{144}Nd$ (2σ)	T_{DM} (Ga)	T_{2DM} (Ga)	εNd(T)
Jiuyishan								
XY13-1	4.00	0.726065 ± 10	0.7170	0.115	0.512175 ± 6	1.50	1.55	-7.42
XY13-4	4.55	0.726694 ± 7	0.7164	0.114	0.512176 ± 6	1.49	1.54	-7.40
XY13-7				0.196	0.512269 ± 6		1.50	-7.18
XY15-2				0.129	0.512170 ± 7	1.72	1.55	-7.42
XY15-6				0.119	0.512132 ± 10	1.64	1.62	-8.35
XY16-2				0.117	0.512229 ± 6	1.45	1.46	-6.41
XY17-4	3.11	0.724038 ± 9	0.7169	0.130	0.512212 ± 7	1.71	1.51	-7.00
XY17-5	3.20	0.724336 ± 9	0.7170	0.113	0.512211 ± 7	1.41	1.49	-6.68
XY17-6	2.63	0.722963 ± 11	0.7170	0.116	0.512207 ± 7	1.47	1.50	-6.83
XY18-1	4.15	0.726364 ± 10	0.7169	0.112	0.512194 ± 7	1.44	1.51	-7.00
XY18-4	3.76	0.725596 ± 11	0.7170	0.110	0.512200 ± 7	1.40	1.50	-6.85
XY19-1				0.139	0.512205 ± 7	1.93	1.54	-7.32
XY20-1				0.111	0.512191 ± 7	1.42	1.52	-7.03
XY21-1	4.69	0.725766 ± 11	0.7151	0.104	0.512200 ± 6	1.32	1.49	-6.72
XY22-2				0.138	0.512216 ± 7	1.88	1.52	-7.08
GD21-2				0.117	0.512193 ± 6	1.51	1.52	-7.11
GD23-1				0.120	0.512194 ± 6	1.56	1.53	-7.16
GD23-2				0.120	0.512192 ± 7	1.55	1.53	-7.19
GD24-2	2.66	0.722745 ± 8	0.7167	0.116	0.512205 ± 6	1.48	1.50	-6.87
GD25-1	3.10	0.725162 ± 8	0.7181	0.115	0.512175 ± 7	1.50	1.55	-7.42
GD26-1				0.117	0.512083 ± 8	1.68	1.70	-9.26
GD28-1				0.126	0.512237 ± 6	1.59	1.47	-6.44
GD28-2				0.125	0.512223 ± 7	1.59	1.49	-6.69
GD29-4				0.131	0.512226 ± 7	1.69	1.49	-6.74
Jiufeng								
XY2-1	68.5			0.214	0.512054 ± 10			-11.8
XY3-1	24.9			0.130	0.511968 ± 9	2.15	1.90	-11.7
XY3-3	17.4			0.130	0.512006 ± 6	2.08	1.84	-11.0
XY4-3	18.9			0.118	0.511967 ± 8	1.89	1.88	-11.5
XY4-5	22.5			0.114	0.511907 ± 8	1.89	1.97	-12.6
XY7-1				0.269	0.512148 ± 8		1.87	-11.0
XY8-1	8.17			0.123	0.511979 ± 3	1.97	1.87	-11.4
XY9-1	7.47	0.730871 ± 5	0.7139	0.120	0.511994 ± 14	1.87	1.84	-11.0
XY9-3	5.61	0.727116 ± 4	0.7143	0.133	0.512022 ± 6	2.13	1.82	-10.7
XY9-9	4.23	0.722141 ± 6	0.7125	0.106	0.512054 ± 7	1.54	1.72	-9.5
XY10-1	4.32	0.722972 ± 6	0.7131	0.135	0.512069 ± 7	2.08	1.74	-9.8
XY10-2	4.77	0.724197 ± 6	0.7134	0.112	0.512055 ± 7	1.63	1.73	-9.6
Dadongshan								
GD08-3	11.9	0.744172 ± 11	0.7172	0.110	0.512071 ± 14	1.59	1.70	-9.3

GD08-4	19.2	0.762951 ± 9	0.7193	0.113	0.511959 ± 13	1.80	1.89	-11.5
GD10-3	14.5	0.745238 ± 12	0.7123	0.139	0.512053 ± 12	2.22	1.78	-10.2
GD11-2	39.9	0.805252 ± 13	0.7144	0.127	0.512001 ± 13	2.02	1.84	-11.0
GD14-1	29.8	0.783908 ± 10	0.7162	0.177	0.512080 ± 15	4.42	1.78	-10.5
GD14-3	29.1	0.779869 ± 9	0.7136	0.154	0.512057 ± 13	2.77	1.79	-10.5
GD15-3	11.2	0.740378 ± 11	0.7149	0.105	0.512065 ± 13	1.51	1.70	-9.3
GD16-3	24.1	0.769539 ± 10	0.7146	0.123	0.512078 ± 12	1.80	1.71	-9.4
Coastal granites								
GD47-1	2.92	0.712790 ± 5	0.7061	0.093	0.512275 ± 7	1.10	1.35	-5.0
GD47-3				0.114	0.512220 ± 8	1.42	1.47	-6.5
GD51-1	1.43	0.710035 ± 5	0.7068	0.115	0.512369 ± 8	1.21	1.24	-3.6
GD51-4	1.78	0.710671 ± 4	0.7066	0.112	0.512389 ± 8	1.14	1.20	-3.1
GD52-1	0.93	0.709767 ± 7	0.7077	0.123	0.512393 ± 11	1.27	1.21	-3.3
GD52-2	0.93	0.707722± 5	0.7057	0.123	0.512275 ± 11	1.36	1.30	-4.3

Note: $^{87}Rb/^{86}Sr$ and $^{147}Sm/^{144}Nd$ are calculated using trace element contents determined by TIMS (Dadongshan) and ICP-MS (all of the others).

$\varepsilon Nd(t) = [(^{143}Nd/^{144}Nd - {}^{147}Sm/^{144}Nd \times (e^{\lambda t} - 1)]/[(^{143}Nd/^{144}Nd)_{CHUR(0)} - (^{147}Sm/^{144}Nd)_{CHUR(0)} \times (e^{\lambda t} - 1)] - 1 \times 10{,}000;$

$T_{DM} = (1/\lambda) \times \ln[1 + (^{143}Nd/^{144}Nd - 0.51315)/(^{147}Sm/^{144}Nd - 0.2137)];$

$T_{2DM} = T_{DM} - (T_{DM} - t)(f_{CC} - f)/(f_{CC} - f_{DM})$, $f_{Sm/Nd} = (^{147}Sm/^{144}Nd)/(^{147}Sm/^{144}Nd)_{CHUR(0)} - 1;$

$(^{143}Nd/^{144}Nd)_{CHUR(0)} = 0.512638$, $(^{147}Sm/^{144}Nd)_{CHUR(0)} = 0.1967$, $(^{147}Sm/^{144}Nd)_{DM} = 0.2137$, $(^{147}Sm/^{144}Nd)_{CC} = 0.118$, t = 154 Ma, $\lambda = 6.54 \times 10^{-12}$ year^{-1}, DM: depleted mantle, CC: continental crust.

Appendix Table 10 In-situ zircon U-Th-Pb isotope compositions

	U (ppm)	Th (ppm)	Th/U	f_{206}[a] (%)	$^{207}Pb^*/^{206}Pb^*$	± σ	$^{207}Pb^*/^{235}U$	± σ (%)	$^{206}Pb^*/^{238}U$	± σ (%)	$t_{207/206}$ (Ma)	± σ	$t_{207/235}$ (Ma)	± σ	$t_{206/238}$ (Ma)	± σ
GD23-1 (25°08'52.8"N, 112°13'07.4"E):																
@1	272	182	0.67	0.08	0.04803	3.08	0.16093	3.45	0.0243	1.56	100.8	71.2	151.5	4.9	154.8	2.4
@2	138	100	0.72	0.16	0.04824	3.25	0.16689	3.61	0.0251	1.56	111.1	75.0	156.7	5.3	159.7	2.5
@3	715	190	0.27	0.00	0.04931	1.39	0.16791	2.14	0.0247	1.63	162.4	32.1	157.6	3.1	157.3	2.5
@4	241	168	0.70	0.00	0.04967	2.46	0.16397	3.03	0.0239	1.76	179.8	56.4	154.2	4.3	152.5	2.7
@5	191	135	0.71	0.12	0.05044	2.73	0.16694	3.15	0.0240	1.57	215.5	62.0	156.8	4.6	152.9	2.4
@6	1053	99	0.09	0.02	0.04933	1.17	0.16778	1.90	0.0247	1.50	163.5	27.1	157.5	2.8	157.1	2.3
@7	199	133	0.67	0.00	0.04998	2.82	0.16457	3.22	0.0239	1.56	193.9	64.3	154.7	4.6	152.1	2.3
@8	354	159	0.45	0.00	0.04793	2.48	0.15846	2.97	0.0240	1.62	96.0	57.8	149.4	4.1	152.7	2.4
@9	614	177	0.29	0.04	0.05054	1.56	0.17169	2.21	0.0246	1.57	220.0	35.7	160.9	3.3	156.9	2.4
@10	187	120	0.64	0.12	0.04861	2.81	0.16025	3.28	0.0239	1.69	129.1	64.8	150.9	4.6	152.3	2.5
@11	249	173	0.69	0.00	0.05091	2.73	0.16980	3.13	0.0242	1.53	236.9	61.9	159.2	4.6	154.1	2.3
@12	312	195	0.62	0.00	0.05069	2.03	0.16817	2.61	0.0241	1.63	226.8	46.4	157.8	3.8	153.3	2.5
@13	215	135	0.63	0.12	0.04677	3.34	0.15678	3.69	0.0243	1.56	37.3	78.1	147.9	5.1	154.9	2.4
@14	167	114	0.68	0.13	0.04872	2.91	0.16048	3.30	0.0239	1.55	134.3	67.0	151.1	4.6	152.2	2.3
@15	139	69	0.50	0.18	0.04711	4.15	0.15482	4.47	0.0238	1.66	54.6	96.1	146.2	6.1	151.9	2.5
@16	200	126	0.63	0.30	0.04696	3.51	0.15624	3.89	0.0241	1.67	47.4	81.9	147.4	5.4	153.7	2.5
Weighted mean (2σ) (n = 16)															**154.3**	**1.2**
XY20-1 (25°13'09"N, 112°10'59"E):																
@1	158	101	0.64	0.00	0.05065	3.45	0.16925	3.82	0.0242	1.65	224.7	77.8	158.8	5.6	154.4	2.5
@2	227	177	0.78	0.07	0.04746	2.79	0.16369	3.19	0.0250	1.53	72.6	65.1	153.9	4.6	159.3	2.4
@3	171	108	0.63	0.00	0.04951	3.30	0.16560	3.69	0.0243	1.66	171.9	75.3	155.6	5.3	154.5	2.5
@4	127	85	0.67	0.00	0.04616	4.72	0.15115	5.00	0.0238	1.66	0.0	116	142.9	6.7	151.3	2.5
@5	196	131	0.67	0.13	0.05120	2.80	0.16573	3.25	0.0235	1.64	249.8	63.1	155.7	4.7	149.6	2.4
@6	203	138	0.68	0.00	0.04883	2.75	0.16237	3.18	0.0241	1.59	139.6	63.3	152.8	4.5	153.6	2.4

@7	198	140	0.71	0.00	0.04955	3.03	0.16362	3.45	0.0240	1.64	173.8	69.3	153.9	4.9	152.6	2.5
@8	175	110	0.63	0.00	0.05124	3.18	0.16697	3.60	0.0236	1.67	251.8	71.6	156.8	5.2	150.6	2.5
@9	218	148	0.68	0.11	0.04930	2.69	0.16664	3.21	0.0245	1.75	161.9	61.7	156.5	4.7	156.1	2.7
@10	194	151	0.78	0.00	0.04745	3.91	0.15836	4.22	0.0242	1.61	72.0	90.4	149.3	5.9	154.2	2.4
@11	193	109	0.57	0.08	0.04760	3.28	0.16297	3.73	0.0248	1.77	79.3	76.1	153.3	5.3	158.1	2.8
@12	180	111	0.62	0.00	0.04523	3.10	0.15230	3.49	0.0244	1.61	-43.3	73.7	143.9	4.7	155.6	2.5
@13	172	95	0.56	0.00	0.04798	3.11	0.15667	3.63	0.0237	1.87	98.4	72.0	147.8	5.0	150.9	2.8
@14	129	66	0.51	0.00	0.05080	4.90	0.16950	5.16	0.0242	1.64	231.9	109	159.0	7.6	154.1	2.5
@15	166	99	0.59	0.00	0.04783	3.06	0.15662	3.51	0.0237	1.72	91.0	71.0	147.7	4.8	151.3	2.6
@16	118	96	0.81	0.19	0.05003	3.58	0.16827	3.98	0.0244	1.73	196.4	81.2	157.9	5.8	155.4	2.7
Weighted mean (2σ) (n = 16)															**153.8**	**1.2**
XY17-6(25°06'02"N, 112°07'19"E):																
@1	143	88	0.61	0.00	0.04862	3.00	0.16205	3.36	0.0242	1.52	129.7	69.0	152.5	4.8	154.0	2.3
@2	160	94	0.59	0.04	0.04800	3.37	0.16219	3.87	0.0245	1.91	99.4	77.7	152.6	5.5	156.1	2.9
@3	165	88	0.53	0.00	0.04991	4.23	0.16709	4.51	0.0243	1.58	190.8	95.4	156.9	6.6	154.6	2.4
@4	218	109	0.50	0.00	0.05077	2.34	0.17061	2.86	0.0244	1.64	230.4	53.2	159.9	4.2	155.2	2.5
@5	100	81	0.81	0.00	0.04904	4.19	0.16309	4.53	0.0241	1.71	149.8	95.4	153.4	6.5	153.6	2.6
@6	145	144	0.99	0.21	0.04967	2.96	0.16590	3.34	0.0242	1.55	179.8	67.6	155.9	4.8	154.3	2.4
@7	132	61	0.46	0.00	0.04877	3.06	0.16484	3.61	0.0245	1.91	136.9	70.4	154.9	5.2	156.1	3.0
@8	179	101	0.56	0.00	0.04646	5.82	0.15593	6.01	0.0243	1.50	21.7	134	147.1	8.3	155.0	2.3
@9	146	86	0.59	0.13	0.05219	2.84	0.17416	3.22	0.0242	1.50	293.6	63.7	163.0	4.9	154.2	2.3
@10	202	112	0.56	0.00	0.04876	2.87	0.16295	3.34	0.0242	1.71	136.3	66.2	153.3	4.8	154.4	2.6
@11	143	81	0.56	0.00	0.04852	2.98	0.16032	3.48	0.0240	1.81	124.7	68.6	151.0	4.9	152.7	2.7
@12	157	98	0.62	0.16	0.04976	2.86	0.16532	3.28	0.0241	1.61	183.6	65.4	155.3	4.7	153.5	2.4
@13	246	168	0.68	0.00	0.04908	2.25	0.16637	2.82	0.0246	1.69	151.5	52.0	156.3	4.1	156.6	2.6
@14	192	104	0.54	0.10	0.04886	2.56	0.16272	3.03	0.0242	1.61	140.9	59.1	153.1	4.3	153.9	2.5
@15	144	84	0.59	0.00	0.04847	3.67	0.15843	3.99	0.0237	1.56	122.4	84.3	149.3	5.6	151.0	2.3
@16	143	68	0.47	0.00	0.04944	3.56	0.16577	3.88	0.0243	1.54	168.8	81.1	155.7	5.6	154.9	2.4
Weighted mean (2σ) (n = 16)															**154.3**	**1.2**

XY18-1 (25°08'32"N, 112°08'45"E):

@1	152	108	0.71	0.18	0.04809	3.09	0.15861	3.44	0.0239	1.52	103.8	71.4	149.5	4.8	152.4	2.3
@2	207	129	0.62	0.21	0.04768	3.06	0.16213	3.55	0.0247	1.81	83.2	71.0	152.6	5.0	157.1	2.8
@3	114	68	0.59	0.00	0.05112	3.34	0.17218	3.78	0.0244	1.78	246.2	75.1	161.3	5.7	155.6	2.7
@4	745	229	0.31	0.00	0.05009	1.37	0.17186	2.24	0.0249	1.78	199.2	31.4	161.0	3.3	158.5	2.8
@5	309	271	0.88	0.00	0.04967	2.11	0.16624	2.59	0.0243	1.50	179.6	48.5	156.2	3.8	154.6	2.3
@6	228	106	0.47	0.22	0.05082	2.62	0.17156	3.08	0.0245	1.60	232.6	59.5	160.8	4.6	155.9	2.5
@7	115	87	0.75	0.00	0.05027	3.38	0.16105	3.72	0.0232	1.55	207.4	76.6	151.6	5.3	148.1	2.3
@8	142	102	0.72	0.11	0.04971	3.13	0.16262	3.64	0.0237	1.87	181.6	71.3	153.0	5.2	151.2	2.8
@9	215	160	0.74	0.00	0.04988	2.46	0.16648	2.95	0.0242	1.63	189.3	56.3	156.4	4.3	154.2	2.5
@10	268	202	0.75	0.00	0.04582	3.31	0.15396	3.64	0.0244	1.52	-11.7	78.0	145.4	4.9	155.2	2.3
@11	276	242	0.88	0.00	0.04787	2.22	0.16176	2.71	0.0245	1.56	92.9	51.8	152.2	3.8	156.1	2.4
@12	227	159	0.70	0.00	0.04938	2.41	0.16644	2.87	0.0244	1.56	165.9	55.3	156.3	4.2	155.7	2.4
@13	199	137	0.69	0.09	0.05056	2.55	0.16559	2.98	0.0238	1.54	221.0	58.0	155.6	4.3	151.3	2.3
@14	200	133	0.67	0.00	0.04692	2.71	0.15654	3.14	0.0242	1.59	45.0	63.6	147.7	4.3	154.1	2.4
@15	198	140	0.71	0.00	0.04949	2.56	0.16336	3.02	0.0239	1.61	171.0	58.7	153.6	4.3	152.5	2.4
@16	239	160	0.67	0.00	0.04758	4.65	0.15803	4.91	0.0241	1.57	78.6	107	149.0	6.8	153.4	2.4
@17	234	168	0.72	0.00	0.04901	2.47	0.16251	2.91	0.0240	1.54	148.5	57.0	152.9	4.1	153.2	2.3
Weighted mean (2σ) (n = 17)															**153.9**	**1.2**
XY13-1 (25°13'41"N, 112°23'13"E):																
@1	172	93	0.54	0.00	0.04920	4.17	0.16810	4.5	0.0248	1.7	157.4	94.9	157.8	6.6	157.8	2.7
@2	24	12	0.52	0.96	0.05246	7.73	0.17745	7.9	0.0245	1.6	305.6	167	165.9	12	156.2	2.5
@3	190	158	0.84	0.00	0.05146	2.91	0.17189	3.3	0.0242	1.6	261.5	65.4	161.1	5.0	154.3	2.5
@4	141	79	0.56	0.00	0.05063	3.25	0.16607	3.6	0.0238	1.6	224.1	73.6	156.0	5.3	151.6	2.4
@5	117	60	0.51	0.00	0.04722	4.87	0.15755	5.1	0.0242	1.6	60.5	112	148.6	7.1	154.1	2.4
@6	38	25	0.68	0.00	0.04791	7.76	0.15999	8.0	0.0242	1.7	94.6	174	150.7	11	154.3	2.7
@7	110	55	0.50	0.10	0.04597	4.93	0.15420	5.3	0.0243	1.8	-3.9	115	145.6	7.2	155.0	2.8
@8	60	32	0.54	0.37	0.05156	4.79	0.17472	5.1	0.0246	1.6	266.1	106	163.5	7.7	156.5	2.5
@9	135	71	0.53	0.00	0.04944	3.86	0.16993	4.1	0.0249	1.5	169.0	87.7	159.4	6.1	158.7	2.4
@10	261	95	0.36	0.00	0.04957	3.27	0.16264	3.6	0.0238	1.6	174.9	74.5	153.0	5.1	151.6	2.3
@11	237	161	0.68	0.00	0.04919	2.56	0.16278	3.0	0.0240	1.5	157.1	58.7	153.1	4.2	152.9	2.3
@12	162	114	0.70	0.20	0.04512	4.07	0.14839	4.4	0.0239	1.6	-49.2	96.3	140.5	5.7	152.0	2.3

@13	124	75	0.61	0.19	0.05187	3.73	0.17079	4.2	0.0239	1.9	279.9	83.1	160.1	6.2	152.1	2.9
@14	89	48	0.53	0.08	0.04529	7.82	0.15006	8.0	0.0240	1.5	-40.0	180	142.0	11	153.1	2.3
@15	144	86	0.59	0.00	0.05323	3.11	0.18057	3.5	0.0246	1.6	338.5	69.0	168.6	5.5	156.7	2.5
@16	221	160	0.73	0.00	0.04550	3.59	0.15411	3.9	0.0246	1.5	-28.7	84.9	145.5	5.3	156.4	2.4
Weighted mean (2σ) (n = 16)															**154.5**	**1.2**
XY2-1 (25°17'04"N, 113°44'28"E):																
@1	582	259	0.45	0.13	0.04882	2.62	0.16836	3.04	0.0250	1.55	139.3	60.4	158.0	4.5	159.2	2.4
@2	1013	462	0.46	0.00	0.04882	1.99	0.16787	2.52	0.0249	1.55	139.2	46.0	157.6	3.7	158.8	2.4
@3	639	290	0.45	0.09	0.04851	2.44	0.17040	2.87	0.0255	1.51	124.4	56.4	159.8	4.3	162.2	2.4
@4	1327	544	0.41	0.08	0.04913	1.67	0.17114	2.28	0.0253	1.55	153.9	38.6	160.4	3.4	160.8	2.5
@5	344	164	0.48	0.00	0.05049	3.46	0.17497	3.79	0.0251	1.54	217.4	78.2	163.7	5.7	160.0	2.4
@6	1779	421	0.24	0.12	0.04890	1.74	0.17352	2.34	0.0257	1.56	143.1	40.3	162.5	3.5	163.8	2.5
@7	2197	865	0.39	1.51	0.04869	4.07	0.16879	4.33	0.0251	1.50	132.8	92.9	158.4	6.4	160.1	2.4
@8	2361	655	0.28	0.06	0.04972	1.38	0.17449	2.05	0.0255	1.51	181.8	31.9	163.3	3.1	162.0	2.4
@9	376	161	0.43	1.55	0.05247	6.20	0.17689	6.41	0.0244	1.63	306.1	135.4	165.4	9.8	155.7	2.5
@10	394	207	0.53	0.00	0.05080	3.64	0.17204	3.96	0.0246	1.57	231.6	81.9	161.2	5.9	156.4	2.4
@11	653	431	0.66	0.00	0.04890	2.20	0.16986	2.73	0.0252	1.60	143.2	50.9	159.3	4.0	160.4	2.5
@12	411	241	0.59	0.00	0.05059	3.96	0.17436	4.28	0.0250	1.63	222.0	89.1	163.2	6.5	159.2	2.6
@13	1684	385	0.23	0.02	0.04996	1.97	0.17508	2.52	0.0254	1.57	193.0	45.1	163.8	3.8	161.8	2.5
@14	368	233	0.63	0.24	0.04869	4.75	0.16409	5.03	0.0244	1.65	132.8	108.1	154.3	7.2	155.7	2.5
@15	1671	630	0.38	1.43	0.04860	3.61	0.16719	3.94	0.0250	1.58	128.6	82.8	157.0	5.7	158.9	2.5
@16	1515	372	0.25	0.04	0.05062	1.81	0.17552	2.40	0.0251	1.58	223.6	41.3	164.2	3.6	160.1	2.5
Weighted mean (2σ) (n = 16)															**159.7**	**1.2**
@17	4923	1004	0.20	0.15	0.04913	1.24	0.17828	1.97	0.0263	1.52	154.2	28.8	166.6	3.0	167.4	2.5
@18	5819	1273	0.22	0.04	0.04917	0.85	0.18150	1.73	0.0268	1.51	156.0	19.7	169.3	2.7	170.3	2.5
@19	5090	1401	0.28	1.54	0.04912	2.92	0.18324	3.32	0.0271	1.58	153.6	67.0	170.8	5.2	172.1	2.7
@20	4618	629	0.14	0.04	0.04903	1.04	0.17922	1.90	0.0265	1.60	149.4	24.1	167.4	2.9	168.7	2.7
@21	4241	1078	0.25	0.42	0.05088	1.50	0.18563	2.17	0.0265	1.57	235.3	34.2	172.9	3.5	168.4	2.6
XY3-1(25°20'28"N, 113°44'51"E):																

@1	560	312	0.56	0.00	0.04889	2.62	0.17120	3.04	0.0254	1.54	142.4	60.3	160.5	4.5	161.7	2.5
@2	549	395	0.72	0.19	0.04824	3.65	0.16463	3.95	0.0248	1.53	111.0	83.9	154.7	5.7	157.6	2.4
@3	2407	1594	0.66	0.03	0.05093	1.33	0.17581	2.01	0.0250	1.50	237.7	30.5	164.4	3.1	159.4	2.4
@4	1859	1622	0.87	0.04	0.04710	1.57	0.16130	2.18	0.0248	1.52	54.1	37.0	151.8	3.1	158.2	2.4
@5	540	268	0.50	0.00	0.05184	2.85	0.17649	3.28	0.0247	1.62	278.3	64.0	165.0	5.0	157.2	2.5
@6	1064	521	0.49	0.03	0.04971	1.93	0.17187	2.47	0.0251	1.54	181.3	44.4	161.0	3.7	159.7	2.4
@7	346	86	0.25	0.00	0.05109	3.15	0.17215	3.50	0.0244	1.53	244.8	71.0	161.3	5.2	155.6	2.4
@8	1225	822	0.67	0.10	0.04786	1.98	0.16321	2.50	0.0247	1.53	92.4	46.1	153.5	3.6	157.5	2.4
@9	1985	895	0.45	0.04	0.04797	1.39	0.16586	2.06	0.0251	1.53	97.9	32.6	155.8	3.0	159.6	2.4
@10	948	342	0.36	0.00	0.05037	2.27	0.17636	2.72	0.0254	1.50	212.0	51.7	164.9	4.1	161.7	2.4
@11	960	539	0.56	1.96	0.04907	4.88	0.16717	5.11	0.0247	1.50	151.2	110.6	157.0	7.5	157.3	2.3
@12	649	270	0.42	0.00	0.04916	2.21	0.17093	2.71	0.0252	1.56	155.6	51.0	160.2	4.0	160.5	2.5
@13	1118	398	0.36	0.08	0.04851	1.92	0.16525	2.45	0.0247	1.52	124.2	44.6	155.3	3.5	157.3	2.4
@14	699	322	0.46	0.08	0.04989	2.81	0.17302	3.20	0.0252	1.53	190.0	64.2	162.0	4.8	160.1	2.4
@15	393	236	0.60	0.13	0.05130	3.30	0.17293	3.70	0.0244	1.68	254.2	74.2	162.0	5.6	155.7	2.6
Weighted mean (2σ) (n = 15)															**158.6**	**1.2**
@16	429	166	0.39	0.02	0.07126	1.00	1.54031	1.80	0.1568	1.50	964.8	20.3	946.6	11.2	938.8	13.1
@17	780	131	0.17	0.00	0.08324	2.67	0.99938	4.91	0.0871	4.13	1275.0	51.1	703.5	25.3	538.2	21.4
XY4-3(25°19'29"N, 113°42'50"E):																
@1	2837	755	0.27	0.00	0.05007	1.50	0.16781	2.12	0.0243	1.50	198.0	34.4	157.5	3.1	154.8	2.3
@2	500	255	0.51	0.09	0.04714	3.39	0.15946	3.83	0.0245	1.77	56.2	79.0	150.2	5.4	156.3	2.7
@3	2034	1013	0.50	0.00	0.04865	1.39	0.16242	2.06	0.0242	1.52	131.1	32.4	152.8	2.9	154.2	2.3
@4	1830	427	0.23	0.03	0.04959	1.37	0.16554	2.04	0.0242	1.50	175.9	31.8	155.5	2.9	154.2	2.3
@5	2034	759	0.37	0.08	0.05000	2.26	0.16595	2.74	0.0241	1.55	195.0	51.7	155.9	4.0	153.3	2.4
@6	3039	788	0.26	0.00	0.04871	1.07	0.16644	1.86	0.0248	1.52	133.7	25.0	156.3	2.7	157.8	2.4
@7	929	523	0.56	0.00	0.04835	1.98	0.16619	2.49	0.0249	1.51	116.2	46.1	156.1	3.6	158.8	2.4
@8	2977	1165	0.39	0.41	0.04793	1.95	0.16783	2.46	0.0254	1.50	95.9	45.6	157.5	3.6	161.7	2.4
@9	2636	240	0.09	0.05	0.04942	1.40	0.17268	2.07	0.0253	1.52	168.0	32.4	161.7	3.1	161.3	2.4
@10	2493	1268	0.51	0.03	0.04971	1.42	0.16966	2.07	0.0248	1.51	181.4	32.8	159.1	3.1	157.6	2.4
@11	741	298	0.40	0.21	0.04833	3.85	0.16127	4.13	0.0242	1.51	115.5	88.3	151.8	5.8	154.1	2.3
@12	718	319	0.45	0.00	0.05121	2.58	0.17342	3.00	0.0246	1.53	250.2	58.2	162.4	4.5	156.4	2.4

@13	1026	506	0.49	0.07	0.04849	2.49	0.16471	2.93	0.0246	1.53	123.2	57.7	154.8	4.2	156.9	2.4
@14	1405	454	0.32	0.00	0.04927	1.79	0.16909	2.34	0.0249	1.50	160.9	41.5	158.6	3.4	158.5	2.4
@15	1162	359	0.31	0.07	0.04933	2.12	0.16739	2.66	0.0246	1.61	163.8	48.7	157.2	3.9	156.7	2.5
@16	1243	469	0.38	0.00	0.04923	1.89	0.16792	2.50	0.0247	1.64	159.0	43.6	157.6	3.7	157.5	2.6
Weighted mean (2σ) (n = 16)															**156.8**	**1.2**
XY7-1(25°19'57"N, 113°37'59"E):																
@1	770	899	1.17	0.07	0.04963	2.51	0.17263	2.99	0.0252	1.63	177.7	57.4	161.7	4.5	160.6	2.6
@2	934	1383	1.48	0.13	0.04981	2.29	0.16673	2.79	0.0243	1.59	186.0	52.5	156.6	4.1	154.6	2.4
@3	2248	1067	0.47	0.00	0.04874	1.58	0.17273	2.23	0.0257	1.58	135.5	36.7	161.8	3.3	163.6	2.6
@4	176	121	0.69	0.32	0.04914	4.52	0.16723	4.82	0.0247	1.67	154.3	102.5	157.0	7.0	157.2	2.6
@5	177	102	0.57	0.00	0.05080	4.33	0.17586	4.70	0.0251	1.83	231.7	97.0	164.5	7.2	159.9	2.9
Weighted mean (2σ) (n = 5)															**159.0**	**4.4**
@6	4624	1369	0.30	0.03	0.04915	1.14	0.17968	1.94	0.0265	1.58	155.1	26.4	167.8	3.0	168.7	2.6
@7	3617	1081	0.30	1.86	0.04883	2.21	0.18436	2.72	0.0274	1.59	139.9	51.1	171.8	4.3	174.1	2.7
@8	4085	2357	0.58	11.78	0.05071	8.15	0.18527	8.30	0.0265	1.58	227.9	178.2	172.6	13.3	168.6	2.6
@9	1323	60	0.05	0.02	0.10607	0.39	3.43410	1.63	0.2348	1.58	1733.0	7.2	1512.2	12.9	1359.6	19.4
@10	328	439	1.34	0.03	0.07177	1.11	1.65938	1.93	0.1677	1.57	979.4	22.5	993.1	12.3	999.4	14.6
@11	913	329	0.36	0.05	0.05161	1.68	0.25001	2.30	0.0351	1.58	268.1	38.0	226.6	4.7	222.6	3.5
@12	174	31	0.18	0.00	0.07718	1.40	1.97229	2.12	0.1853	1.59	1125.8	27.7	1106.1	14.4	1096.1	16.0
@13	161	76	0.47	0.05	0.07281	1.52	1.67339	2.18	0.1667	1.57	1008.6	30.4	998.5	14.0	993.9	14.5
@14	3448	609	0.18	0.72	0.05346	1.51	0.34977	2.18	0.0475	1.57	348.2	33.8	304.5	5.7	298.9	4.6
@15	1049	157	0.15	0.21	0.09151	0.91	1.75209	1.90	0.1389	1.67	1457.2	17.2	1027.9	12.4	838.3	13.2
XY10-1(25°21'56"N, 113°15'09"E):																
@1	857	345	0.40	0.04	0.04924	0.99	0.17487	1.80	0.0258	1.50	159.5	23.0	163.6	2.7	163.9	2.4
@2	1379	410	0.30	0.04	0.04873	0.78	0.16767	1.71	0.0250	1.52	134.9	18.2	157.4	2.5	158.9	2.4
@3	1504	611	0.41	0.01	0.04989	1.02	0.17250	1.86	0.0251	1.56	189.9	23.5	161.6	2.8	159.7	2.5
@4	2162	709	0.33	3.43	0.04932	0.86	0.17324	1.76	0.0255	1.54	163.1	19.9	162.2	2.6	162.2	2.5
@5	2477	857	0.35	0.07	0.04940	0.68	0.16966	1.71	0.0249	1.57	166.7	15.9	159.1	2.5	158.6	2.5
@6	1056	355	0.34	0.00	0.04818	1.68	0.16555	2.30	0.0249	1.57	107.9	39.1	155.5	3.3	158.7	2.5
@7	679	308	0.45	0.00	0.04966	3.49	0.17169	3.85	0.0251	1.62	178.9	79.4	160.9	5.7	159.7	2.6

@8	2176	746	0.34	0.03	0.05058	1.35	0.17449	2.17	0.0250	1.69	221.9	31.0	163.3	3.3	159.3	2.7
@9	1787	483	0.27	0.06	0.05012	1.55	0.17069	2.25	0.0247	1.63	200.8	35.6	160.0	3.3	157.3	2.5
@10	1264	368	0.29	0.76	0.04975	3.11	0.16860	3.48	0.0246	1.57	183.4	70.8	158.2	5.1	156.5	2.4
@11	1162	241	0.21	0.00	0.05129	1.71	0.17617	2.38	0.0249	1.65	253.7	38.9	164.8	3.6	158.6	2.6
@12	1717	457	0.27	0.03	0.04883	1.53	0.16668	2.16	0.0248	1.52	139.6	35.5	156.5	3.1	157.7	2.4
@13	2472	680	0.28	0.23	0.05026	1.49	0.17216	2.14	0.0248	1.54	206.9	34.1	161.3	3.2	158.2	2.4
@14	1463	465	0.32	0.04	0.04957	2.26	0.16773	2.71	0.0245	1.51	175.1	51.9	157.5	4.0	156.3	2.3
Weighted mean (2σ) (n = 14)															**158.9**	**1.3**

Dadongshan

GD08-5 (24°37’46’’N, 113°13’38’’E):

@1	1381	558	0.42	0.24	0.04857	1.67	0.17222	1.77	0.026	0.59	127.2	39.2	163.7	1.0
@2	1533	392	0.26	0.18	0.04875	2.28	0.17383	2.42	0.026	0.83	135.7	53.5	164.6	1.4
@3	460	235	0.53	1.82	0.04852	7.11	0.17614	7.20	0.026	1.17	124.9	167.4	167.5	1.9
@4	781	409	0.54	0.28	0.04949	2.69	0.17490	2.86	0.026	0.96	171.2	62.8	163.1	1.6
@5	226	160	0.73	1.18	0.04976	7.88	0.17389	8.02	0.025	1.51	183.9	183.5	161.3	2.4
@6	599	231	0.40	0.32	0.04969	3.32	0.17522	3.48	0.026	1.04	180.5	77.5	162.8	1.7
@7	1467	532	0.38	0.22	0.04907	1.86	0.17694	2.09	0.026	0.93	151.0	43.7	166.4	1.5
@8	236	131	0.57	1.14	0.04481	4.70	0.16068	4.90	0.026	1.38	-65.7	114.6	165.5	2.3
@9	378	196	0.54	0.84	0.04709	5.02	0.17331	5.17	0.027	1.23	53.9	119.8	169.8	2.1
@10	125	78	0.65	1.90	0.04908	12.85	0.17561	13.11	0.026	2.59	151.5	301.0	165.2	4.2
@11	333	187	0.58	0.77	0.05119	5.93	0.18423	6.06	0.026	1.24	249.5	136.5	166.1	2.0
Weighted mean (2σ) (n = 11)													**165.0**	**1.0**
@12	4476	3325	0.77	0.42	0.04858	1.76	0.19590	1.82	0.029	0.49	127.4	41.4	185.8	0.9
@13	4893	2618	0.55	0.17	0.04853	0.78	0.18861	0.92	0.028	0.49	125.3	18.3	179.2	0.9
@14	4188	520	0.13	0.38	0.04940	1.09	0.18104	1.21	0.027	0.51	167.0	25.5	169.1	0.9
@15	3006	658	0.23	0.36	0.04874	1.31	0.19065	1.42	0.028	0.54	135.2	30.8	180.3	1.0
@16	1157	752	0.67	7.01	0.04992	8.96	0.17986	9.01	0.026	0.98	191.4	208.4	166.3	1.6
@17	913	312	0.35	0.41	0.04876	2.93	0.18142	3.09	0.027	0.98	136.2	68.9	171.7	1.7
@18	471	168	0.37	0.57	0.05030	4.49	0.17503	4.63	0.025	1.13	208.7	104.1	160.7	1.8
@19	765	349	0.47	0.22	0.04839	2.31	0.17872	2.51	0.027	0.96	118.4	54.6	170.4	1.6
@20	444	111	0.26	1.02	0.05642	3.63	0.42075	3.76	0.054	1.01	468.8	80.3	339.6	3.3

@21	231	190	0.85	0.84	0.04890	7.25	0.21764	7.39	0.032	1.46	143.1	170.1			204.8	2.9
GD15-1 (24°45’11’’N, 112°58’57’’E):																
@1	254	165	0.67	0.58	0.04747	4.01	0.16042	4.13	0.025	0.98	72.9	95.3			156.1	1.5
@2	271	157	0.60	0.82	0.04820	5.41	0.16537	5.50	0.025	0.97	109.1	127.8			158.4	1.5
@3	295	161	0.57	0.62	0.04981	3.40	0.17044	3.52	0.025	0.91	186.1	79.1			158.0	1.4
@4	309	164	0.55	1.13	0.04408	7.62	0.15045	7.69	0.025	0.98	-106.1	187.5			157.6	1.5
@5	306	195	0.66	0.81	0.05355	5.01	0.18974	10.00	0.026	0.94	352.0	113.3			163.6	1.5
@6	313	212	0.70	0.91	0.04974	5.41	0.17068	5.49	0.025	0.93	182.7	126.0			158.5	1.5
@7	188	101	0.55	1.06	0.04588	6.74	0.16037	6.83	0.025	1.13	-8.4	162.6			161.4	1.8
@8	286	149	0.54	0.60	0.05020	4.79	0.17889	10.00	0.026	0.97	204.3	111.2			164.5	1.6
@9	189	118	0.64	0.33	0.05534	3.72	0.19294	10.00	0.025	1.09	425.8	82.9			161.0	1.7
@10	273	173	0.65	1.67	0.04676	8.48	0.15917	8.54	0.025	1.05	36.8	202.9			157.2	1.6
@11	305	213	0.72	1.16	0.04453	6.63	0.15614	6.70	0.025	0.97	-81.3	162.4			161.9	1.5
@12	603	270	0.46	0.62	0.04774	3.75	0.16065	3.83	0.024	0.76	86.2	89.0			155.5	1.2
Weighted mean (2σ) (n = 12)															**159.0**	**2.0**
@13	611	302	0.51	0.44	0.04653	3.63	0.15161	3.71	0.024	0.80	25.2	87.0			150.6	1.2
@14	268	151	0.58	0.78	0.04743	6.18	0.17264	6.26	0.026	1.01	71.2	146.9			168.0	1.7
@15	462	394	0.88	0.23	0.05123	2.78	0.16541	2.90	0.023	0.83	251.3	64.0			149.2	1.2

Xiaoliang

GD47-1 (21°31’10”N, 110°59’14”E):																
@1	199	75	0.376	0.11	0.05005	4.39	0.1703	4.68	0.02469	1.64	197.2	98.9	159.7	6.9	157.2	2.5
@2	470	350	0.743	0.08	0.04834	2.47	0.1668	2.91	0.02503	1.54	116.0	57.3	156.7	4.2	159.4	2.4
@3	976	475	0.487	0.04	0.05052	1.60	0.1762	2.20	0.02529	1.51	218.8	36.6	164.8	3.4	161.0	2.4
@4	389	199	0.512	0.00	0.05141	2.45	0.1744	2.89	0.02460	1.53	259.3	55.3	163.2	4.4	156.7	2.4
@5	248	123	0.495	0.00	0.04772	3.43	0.1629	3.76	0.02476	1.54	85.5	79.4	153.2	5.4	157.7	2.4
@6	322	231	0.718	0.00	0.06170	2.98	1.0753	6.41	0.12639	5.67	663.7	62.7	741.3	34.3	767.3	41.2
@7	553	217	0.393	0.11	0.04900	3.28	0.1675	3.61	0.02479	1.52	147.7	75.0	157.2	5.3	157.9	2.4
@8	129	58	0.451	0.49	0.04600	7.38	0.1589	7.55	0.02506	1.59	-2.2	169.1	149.8	10.6	159.5	2.5
@9	226	114	0.503	0.00	0.04765	3.24	0.1662	3.58	0.02531	1.54	81.7	75.0	156.1	5.2	161.1	2.5
@10	730	318	0.436	0.00	0.04834	1.79	0.1687	2.34	0.02531	1.51	116.2	41.6	158.3	3.4	161.1	2.4

@11	209	126	0.605	0.00	0.06509	1.29	1.1690	1.98	0.13025	1.50	777.3	26.9	786.2	10.9	789.3	11.2
@12	303	111	0.367	0.21	0.04769	3.81	0.1598	4.21	0.02430	1.79	84.0	87.9	150.5	5.9	154.8	2.7
@13	517	290	0.560	0.15	0.04782	2.49	0.1678	2.92	0.02544	1.52	90.3	58.0	157.5	4.3	162.0	2.4
@14	503	403	0.802	0.08	0.04679	2.32	0.1639	2.78	0.02541	1.53	38.5	54.5	154.1	4.0	161.7	2.4
@15	944	430	0.456	0.00	0.04979	2.21	0.1738	2.69	0.02532	1.54	185.2	50.6	162.7	4.1	161.2	2.5
Weighted mean (2σ) (n = 13)															**159.4**	**1.3**
Gangwei																
GD51-1 (22°04'07"N, 111°45'07"E):																
@1	1053	652	0.619	0.09	0.04886	1.51	0.1750	2.13	0.02598	1.51	141.1	35.0	163.8	3.2	165.3	2.5
@2	954	496	0.520	0.04	0.04847	1.51	0.1749	2.13	0.02617	1.51	122.2	35.1	163.7	3.2	166.5	2.5
@3	1139	876	0.769	0.00	0.04931	1.41	0.1792	2.07	0.02635	1.51	162.8	32.6	167.3	3.2	167.7	2.5
@4	940	463	0.493	0.14	0.04927	2.11	0.1810	2.63	0.02665	1.57	160.6	48.6	169.0	4.1	169.6	2.6
@5	1064	675	0.634	0.00	0.04978	1.35	0.1797	2.04	0.02618	1.53	184.9	31.1	167.8	3.2	166.6	2.5
@6	939	551	0.587	0.04	0.04984	1.50	0.1761	2.20	0.02562	1.60	187.7	34.5	164.7	3.3	163.1	2.6
@7	1379	957	0.694	0.02	0.05002	1.21	0.1845	1.96	0.02675	1.54	195.9	27.8	171.9	3.1	170.2	2.6
@8	293	110	0.374	0.22	0.04863	3.18	0.1751	3.53	0.02611	1.52	130.0	73.1	163.8	5.3	166.2	2.5
@9	332	164	0.492	0.00	0.04968	2.45	0.1732	2.89	0.02528	1.53	180.0	56.2	162.2	4.3	161.0	2.4
@10	830	471	0.567	0.00	0.04949	1.51	0.1764	2.15	0.02586	1.53	170.9	34.8	165.0	3.3	164.6	2.5
@11	1186	753	0.635	0.00	0.04862	1.31	0.1770	2.01	0.02640	1.52	129.8	30.6	165.5	3.1	168.0	2.5
@12	932	572	0.613	0.00	0.05010	1.40	0.1802	2.06	0.02609	1.51	199.5	32.3	168.3	3.2	166.0	2.5
@13	1038	499	0.481	0.04	0.04959	1.40	0.1753	2.13	0.02563	1.60	176.0	32.3	164.0	3.2	163.2	2.6
@14	1197	709	0.592	0.03	0.04873	1.82	0.1732	2.39	0.02578	1.54	134.9	42.3	162.2	3.6	164.1	2.5
@15	1275	854	0.670	0.00	0.04928	1.27	0.1761	1.99	0.02592	1.54	161.2	29.4	164.7	3.0	164.9	2.5
Weighted mean (2σ) (n = 15)															**165.7**	**1.3**
Gudoushan																
GD61-1 (22°14'15"N, 112°55'06"E):																
@01	125	99	0.792	0.51	0.15300	4.77	0.0244	1.58	0.04543	4.50	-32.3	105.8	144.6	6.5	155.6	2.4
@02	1174	442	0.377	0.27	0.16749	1.91	0.0247	1.52	0.04917	1.16	156.0	26.8	157.2	2.8	157.3	2.4
@03	176	101	0.574	0.00	0.17243	2.77	0.0252	1.53	0.04963	2.31	177.6	53.0	161.5	4.1	160.4	2.4
@04	427	165	0.387	0.05	0.17191	2.12	0.0253	1.51	0.04927	1.48	160.5	34.3	161.1	3.2	161.1	2.4
@05	266	157	0.591	0.05	0.17576	2.40	0.0257	1.52	0.04965	1.87	178.5	43.0	164.4	3.7	163.4	2.4

@06	691	281	0.406	0.04	0.17360	2.22	0.0256	1.51	0.04922	1.63	158.5	37.7	162.5	3.3	162.8	2.4
@07	152	142	0.935	0.26	0.16704	4.46	0.0252	1.54	0.04815	4.19	106.7	96.1	156.8	6.5	160.2	2.4
@08	513	77	0.150	0.03	0.16914	2.56	0.0253	1.52	0.04854	2.06	125.9	47.7	158.7	3.8	160.9	2.4
@09	372	202	0.544	0.25	0.17333	2.93	0.0251	1.52	0.05003	2.51	196.2	57.2	162.3	4.4	160.0	2.4
@10	172	87	0.502	0.12	0.17440	3.01	0.0254	1.51	0.04985	2.61	187.8	59.5	163.2	4.6	161.5	2.4
@11	776	146	0.188	0.07	0.17322	2.19	0.0254	1.80	0.04939	1.24	166.3	28.8	162.2	3.3	161.9	2.9
@12	357	457	1.281	0.15	0.16684	2.88	0.0252	1.51	0.04808	2.45	103.2	56.9	156.7	4.2	160.2	2.4
@13	760	244	0.321	0.09	0.17888	2.22	0.0256	1.51	0.05068	1.63	226.4	37.1	167.1	3.4	162.9	2.4
@14	539	227	0.421	0.07	0.17496	2.10	0.0254	1.51	0.04996	1.46	193.0	33.6	163.7	3.2	161.7	2.4
Weighted mean (2σ) (n = 14)															**160.7**	**1.3**
Wuguishan																
GD62-1 (22°29'53"N, 113°19'17"E):																
@01	162	112	0.693	0.00	0.17523	2.86	0.0249	1.53	0.05108	2.42	244.4	54.8	163.9	4.3	158.4	2.4
@02	808	428	0.529	0.09	0.17194	1.93	0.0248	1.53	0.05020	1.18	204.2	27.0	161.1	2.9	158.2	2.4
@03	1355	835	0.616	0.06	0.17185	1.83	0.0255	1.52	0.04889	1.02	142.3	23.7	161.0	2.7	162.3	2.4
@04	856	452	0.528	0.00	0.17036	1.84	0.0246	1.50	0.05026	1.07	207.1	24.6	159.7	2.7	156.6	2.3
@05	366	278	0.760	0.00	0.16629	2.23	0.0250	1.51	0.04825	1.64	111.5	38.2	156.2	3.2	159.2	2.4
@06	818	406	0.497	0.05	0.17441	1.87	0.0253	1.50	0.05000	1.12	194.8	25.9	163.2	2.8	161.1	2.4
@07	1106	413	0.373	0.01	0.16971	2.03	0.0251	1.51	0.04897	1.36	146.2	31.5	159.2	3.0	160.0	2.4
@08	145	104	0.721	0.51	0.15867	4.32	0.0247	1.58	0.04655	4.01	26.2	93.6	149.5	6.0	157.4	2.5
@09	468	232	0.496	0.05	0.17723	2.36	0.0258	1.53	0.04987	1.79	189.1	41.1	165.7	3.6	164.0	2.5
@10	288	157	0.546	0.11	0.17026	2.53	0.0250	1.52	0.04948	2.03	170.5	46.8	159.6	3.8	158.9	2.4
@11	194	105	0.544	0.00	0.16441	3.16	0.0245	1.52	0.04870	2.77	133.6	63.8	154.6	4.5	155.9	2.3
@12	306	214	0.700	0.40	0.16172	3.32	0.0245	1.50	0.04795	2.96	97.0	68.5	152.2	4.7	155.8	2.3
@13	1632	737	0.452	0.47	0.17302	1.88	0.0254	1.50	0.04939	1.13	166.4	26.2	162.0	2.8	161.7	2.4
@14	952	484	0.509	0.00	0.17775	1.80	0.0259	1.50	0.04979	0.99	185.3	22.8	166.1	2.8	164.8	2.4
Weighted mean (2σ) (n = 14)															**159.5**	**1.6**

Note: [a] f_{206} stands for percentage of common lead in measured ^{206}Pb. Data showing in grey are not included for the calculation of weighted mean age.
Some of them are results of inherited or xenocrystic zircons, the rest are high either in U or in f_{206}, giving inaccurate results.
Samples GD08-5 and GD15-1 were analysed using SHRIMP II, whereas the rest were analysed using Cameca IMS-1280 SIMS.

Appendix Table 11 In-situ zircon Hf-O isotope compositions

Sample	$^{176}Yb/^{177}Hf$	$^{176}Lu/^{177}Hf$	$^{176}Hf/^{177}Hf$	± 2σ	εHf(T)	± 2σ	T_{DM} (Ga)	T_{DM}^{C} (Ga)	$^{18}O/^{16}O$	$\delta^{18}O_{Meas}$ (‰)	2SE	$\delta^{18}O_{Corr}$ (‰)
Session one: Jiuyishan*												
GD23-1:												
Tem@2									2.0161E-03	5.42		
@1	0.033091	0.000921	0.282495	0.000016	-6.5	0.6	1.07	1.62	2.0183E-03	6.52	0.20	9.31
@2	0.032848	0.000918	0.282523	0.000015	-5.5	0.5	1.03	1.56	2.0187E-03	6.75	0.20	9.54
@3	0.062997	0.001763	0.282517	0.000014	-5.8	0.5	1.06	1.57	2.0184E-03	6.59	0.12	9.38
Tem@3									2.0160E-03	5.36		
@4	0.031921	0.000877	0.282501	0.000016	-6.3	0.6	1.06	1.60	2.0185E-03	6.64	0.20	9.43
@5	0.032354	0.000900	0.282468	0.000019	-7.4	0.7	1.10	1.68	2.0227E-03	8.75	0.24	11.54
@6	0.030464	0.000887	0.282532	0.000038	-5.2	1.3	1.02	1.54	2.0186E-03	6.70	0.19	9.50
Tem@4									2.0160E-03	5.40		
@7	0.024616	0.000719	0.282504	0.000033	-6.2	1.2	1.05	1.60	2.0182E-03	6.48	0.17	9.28
91500@1									2.0196E-03	7.18	0.23	9.99
@8	0.033404	0.000979	0.282520	0.000029	-5.6	1.0	1.04	1.56	2.0187E-03	6.76	0.18	9.57
@9	0.051087	0.001458	0.282526	0.000030	-5.5	1.1	1.04	1.55	2.0188E-03	6.78	0.19	9.60
Tem@5									2.0158E-03	5.30		
@10	0.027948	0.000795	0.282507	0.000029	-6.1	1.0	1.05	1.59	2.0192E-03	6.98	0.18	9.81
@11	0.030433	0.000863	0.282542	0.000026	-4.8	0.9	1.00	1.51	2.0189E-03	6.81	0.17	9.64
@12	0.032260	0.000907	0.282506	0.000030	-6.1	1.0	1.05	1.59	2.0181E-03	6.43	0.18	9.26
Tem@6									2.0163E-03	5.51		
@13	0.029548	0.000846	0.282494	0.000034	-6.5	1.2	1.07	1.62	2.0179E-03	6.35	0.26	9.19
@14	0.025963	0.000746	0.282518	0.000035	-5.7	1.2	1.03	1.56	2.0192E-03	6.98	0.25	9.83
91500@2									2.0187E-03	6.72	0.20	9.58
@15	0.021956	0.000631	0.282538	0.000045	-5.0	1.6	1.00	1.52	2.0185E-03	6.65	0.19	9.52
Tem@7									2.0161E-03	5.44		
@16	0.040027	0.001114	0.282505	0.000035	-6.2	1.2	1.06	1.60	2.0198E-03	7.26	0.24	10.13
XY20-1:												

@1	0.026314	0.000759	0.282496	0.000017	-6.5	0.6	1.06	1.62	2.0181E-03	6.43	0.15	9.30
@2	0.041421	0.001159	0.282541	0.000015	-4.9	0.5	1.01	1.52	2.0187E-03	6.72	0.16	9.61
Tem@8									2.0157E-03	5.22		
@3	0.026472	0.000776	0.282534	0.000024	-5.1	0.9	1.01	1.53	2.0174E-03	6.11	0.20	9.00
@4	0.028284	0.000824	0.282473	0.000023	-7.3	0.8	1.10	1.67	2.0186E-03	6.67	0.13	9.57
@5	0.024332	0.000683	0.282512	0.000016	-5.9	0.6	1.04	1.58	2.0185E-03	6.62	0.15	9.52
91500@3									2.0197E-03	7.24	0.19	10.15
Tem@9									2.0157E-03	5.26		
@6	0.025221	0.000724	0.282483	0.000014	-6.9	0.5	1.08	1.64	2.0183E-03	6.55	0.19	9.47
@7	0.026230	0.000743	0.282511	0.000015	-5.9	0.5	1.04	1.58	2.0190E-03	6.88	0.18	9.80
@8	0.023886	0.000675	0.282516	0.000017	-5.7	0.6	1.03	1.57	2.0179E-03	6.36	0.24	9.28
Tem@10									2.0158E-03	5.27		
@9	0.028320	0.000798	0.282507	0.000018	-6.1	0.6	1.05	1.59	2.0180E-03	6.37	0.24	9.31
@10	0.055700	0.001583	0.282549	0.000024	-4.7	0.9	1.01	1.50	2.0185E-03	6.63	0.19	9.57
@11	0.028039	0.000787	0.282492	0.000022	-6.6	0.8	1.07	1.63	2.0181E-03	6.43	0.17	9.37
Tem@11									2.0155E-03	5.16		
91500@4									2.0194E-03	7.07	0.23	10.02
@12	0.029039	0.000833	0.282529	0.000022	-5.3	0.8	1.02	1.54	2.0182E-03	6.51	0.14	9.45
@13	0.028971	0.000833	0.282497	0.000017	-6.4	0.6	1.06	1.61	2.0187E-03	6.72	0.18	9.67
@14	0.024963	0.000733	0.282489	0.000020	-6.7	0.7	1.07	1.63	2.0185E-03	6.62	0.22	9.57
Tem@12									2.0158E-03	5.26		
@15	0.030512	0.000887	0.282526	0.000018	-5.4	0.6	1.02	1.55	2.0180E-03	6.37	0.15	9.33
@16	0.027311	0.000793	0.282511	0.000017	-5.9	0.6	1.04	1.58	2.0185E-03	6.64	0.25	9.59
XY17-6:												
@1	0.023821	0.000667	0.282528	0.000033	-5.3	1.2	1.01	1.54	2.0171E-03	5.91	0.20	8.87
Tem@13									2.0159E-03	5.34		
@2	0.025998	0.000765	0.282545	0.000029	-4.7	1.0	0.99	1.50	2.0168E-03	5.77	0.18	8.72
91500@5									2.0198E-03	7.26	0.28	10.22
@3	0.023093	0.000649	0.282546	0.000026	-4.7	0.9	0.99	1.50	2.0163E-03	5.54	0.24	8.50
@4	0.023165	0.000650	0.282540	0.000039	-4.9	1.4	1.00	1.51	2.0174E-03	6.08	0.14	9.03
Tem@14									2.0151E-03	4.95		
@5	0.037294	0.001030	0.282537	0.000024	-5.0	0.8	1.01	1.52	2.0170E-03	5.89	0.23	8.84

@6	0.041416	0.001130	0.282569	0.000040	-3.9	1.4	0.97	1.45	2.0179E-03	6.31	0.25	9.26
@7	0.021735	0.000614	0.282556	0.000038	-4.3	1.3	0.97	1.48	2.0172E-03	5.97	0.18	8.91
Tem@15									2.0162E-03	5.51		
@8	0.024797	0.000703	0.282549	0.000032	-4.6	1.1	0.99	1.50	2.0174E-03	6.08	0.22	9.02
@9	0.028043	0.000783	0.282549	0.000049	-4.6	1.7	0.99	1.50	2.0169E-03	5.83	0.22	8.77
91500@6									2.0196E-03	7.21	0.13	10.14
@10	0.023736	0.000676	0.282613	0.000053	-2.3	1.9	0.90	1.35	2.0177E-03	6.23	0.19	9.16
Tem@16									2.0159E-03	5.36		
@11	0.022487	0.000643	0.282554	0.000040	-4.4	1.4	0.98	1.48	2.0182E-03	6.47	0.20	9.39
@12	0.030197	0.000856	0.282517	0.000030	-5.7	1.1	1.04	1.57	2.0183E-03	6.54	0.15	9.46
@13	0.028835	0.000805	0.282529	0.000038	-5.3	1.4	1.02	1.54	2.0186E-03	6.67	0.20	9.58
Tem@17									2.0152E-03	4.99		
@14	0.024946	0.000702	0.282554	0.000044	-4.4	1.6	0.98	1.48	2.0179E-03	6.35	0.23	9.25
@15	0.020946	0.000592	0.282563	0.000032	-4.1	1.1	0.96	1.46	2.0174E-03	6.06	0.17	8.96
@16	0.023031	0.000654	0.282518	0.000028	-5.7	1.0	1.03	1.56	2.0155E-03	5.14	0.26	8.03
91500@7									2.0193E-03	7.03	0.25	9.91
XY18-1:												
Tem@18									2.0164E-03	5.57		
@1	0.028938	0.000860	0.282535	0.000041	-5.1	1.4	1.01	1.53	2.0175E-03	6.13	0.21	9.00
@2	0.027824	0.000763	0.282508	0.000022	-6.0	0.8	1.05	1.59	2.0191E-03	6.95	0.18	9.81
@3	0.032289	0.000952	0.282577	0.000031	-3.6	1.1	0.95	1.43	2.0182E-03	6.49	0.25	9.35
Tem@19									2.0158E-03	5.29		
@4	0.053285	0.001493	0.282551	0.000038	-4.6	1.4	1.01	1.50	2.0178E-03	6.29	0.19	9.13
@5	0.037392	0.001018	0.282528	0.000039	-5.4	1.4	1.02	1.54	2.0180E-03	6.36	0.24	9.20
@6	0.038734	0.001159	0.282535	0.000032	-5.1	1.1	1.02	1.53	2.0185E-03	6.62	0.24	9.45
Tem@20									2.0167E-03	5.72		
91500@8									2.0197E-03	7.25	0.23	10.06
@7	0.029984	0.000891	0.282600	0.000036	-2.8	1.3	0.92	1.38	2.0184E-03	6.61	0.23	9.41
@8	0.024016	0.000670	0.282543	0.000043	-4.8	1.5	0.99	1.51	2.0180E-03	6.37	0.19	9.17
@9	0.029323	0.000852	0.282505	0.000036	-6.2	1.3	1.05	1.60	2.0184E-03	6.58	0.24	9.37
Tem@21									2.0151E-03	4.93		
@10	0.027846	0.000771	0.282520	0.000042	-5.6	1.5	1.03	1.56	2.0183E-03	6.56	0.19	9.33

@11	0.040619	0.001124	0.282540	0.000039	-5.0	1.4	1.01	1.52	2.0182E-03	6.47	0.19	9.23
@12	0.028508	0.000786	0.282517	0.000032	-5.7	1.1	1.03	1.57	2.0183E-03	6.56	0.21	9.31
Tem@22									2.0162E-03	5.47		
@13	0.030051	0.000836	0.282519	0.000029	-5.7	1.0	1.03	1.56	2.0182E-03	6.49	0.18	9.23
@14	0.028848	0.000843	0.282545	0.000030	-4.7	1.1	1.00	1.51	2.0123E-03	3.55	0.19	6.29
@15	0.030781	0.000860	0.282510	0.000027	-6.0	1.0	1.04	1.58	2.0176E-03	6.17	0.21	8.90
Tem@23									2.0161E-03	5.45		
@16	0.028385	0.000796	0.282534	0.000025	-5.1	0.9	1.01	1.53	2.0183E-03	6.51	0.24	9.23
@17	0.029928	0.000825	0.282520	0.000022	-5.6	0.8	1.03	1.56	2.0188E-03	6.79	0.22	9.49
XY13-1:												
@1	0.036229	0.001055	0.282489	0.000044	-6.7	1.5	1.08	1.63	2.0184E-03	6.61	0.19	9.31
Tem@24									2.0170E-03	5.90		
@2	0.034434	0.001054	0.282482	0.000026	-7.0	0.9	1.09	1.65	2.0179E-03	6.35	0.13	9.04
@3	0.054910	0.001525	0.282475	0.000024	-7.3	0.8	1.11	1.67	2.0182E-03	6.50	0.19	9.19
@4	0.035374	0.001002	0.282464	0.000023	-7.6	0.8	1.11	1.69	2.0184E-03	6.59	0.22	9.27
Tem@25									2.0164E-03	5.59		
@5	0.060640	0.001919	0.282460	0.000021	-7.8	0.7	1.15	1.70	2.0184E-03	6.59	0.22	9.27
@6	0.045755	0.001256	0.282464	0.000023	-7.6	0.8	1.12	1.69	2.0188E-03	6.77	0.24	9.44
@7	0.037600	0.001077	0.282494	0.000023	-6.6	0.8	1.07	1.62	2.0185E-03	6.62	0.18	9.29
Tem@26									2.0156E-03	5.20		
@8	0.043189	0.001249	0.282480	0.000027	-7.1	1.0	1.10	1.65	2.0181E-03	6.42	0.17	9.09
@9	0.050469	0.001452	0.282472	0.000023	-7.4	0.8	1.12	1.67	2.0188E-03	6.80	0.16	9.47
@10	0.042034	0.001147	0.282447	0.000024	-8.2	0.8	1.14	1.73	2.0188E-03	6.76	0.20	9.43
Tem@27									2.0160E-03	5.39		
@11	0.059019	0.001646	0.282471	0.000021	-7.4	0.8	1.12	1.68	2.0186E-03	6.67	0.17	9.34
@12	0.045662	0.001296	0.282503	0.000024	-6.3	0.9	1.07	1.60	2.0179E-03	6.34	0.20	9.01
@13	0.064077	0.001840	0.282489	0.000024	-6.8	0.9	1.10	1.64	2.0182E-03	6.47	0.12	9.14
Tem@28									2.0166E-03	5.71		
@14	0.030946	0.000903	0.282504	0.000022	-6.2	0.8	1.06	1.60	2.0182E-03	6.47	0.22	9.15
@15	0.039443	0.001143	0.282481	0.000026	-7.0	0.9	1.09	1.65	2.0177E-03	6.22	0.22	8.91
@16	0.051628	0.001459	0.282496	0.000023	-6.5	0.8	1.08	1.62	2.0180E-03	6.36	0.19	9.06
Tem@29									2.0162E-03	5.49		

91500 avg.									**2.0195E-03**	**7.12**		**9.95**
±1SD									**3.6763E-07**			**0.18**
Tem avg.									**2.0160E-03**	**5.37**		**8.20**
±1SD									**4.4737E-07**			**0.22**
Session two: **Jiufeng***												
Tem@1									2.0184E-3	6.57	0.15	
Tem@2									2.0184E-3	6.57	0.25	
Tem@3									2.0185E-3	6.64	0.32	
91500@1									2.0218E-3	8.29	0.24	9.89
Tem@3-1									2.0184E-3	6.56	0.24	
XY10-1:												
@1	0.088064	0.002380	0.282426	0.000016	-9.0	0.6	1.21	1.78	2.0175E-3	6.16	0.44	7.75
@2	0.038820	0.001054	0.282385	0.000019	-10.3	0.7	1.23	1.86	2.0180E-3	6.39	0.33	7.99
Tem@4									2.0183E-3	6.51	0.22	
@3	0.033123	0.000977	0.282387	0.000018	-10.2	0.6	1.22	1.86	2.0185E-3	6.62	0.28	8.22
@4	0.045043	0.001265	0.282405	0.000017	-9.6	0.6	1.21	1.82	2.0175E-3	6.15	0.36	7.74
@5	0.032403	0.000917	0.282401	0.000014	-9.7	0.5	1.20	1.83	2.0186E-3	6.70	0.47	8.30
@6	0.057591	0.001651	0.282373	0.000016	-10.8	0.6	1.26	1.89	2.0167E-3	5.75	0.31	7.34
Tem@5									2.0185E-3	6.62	0.26	
Tem@6									2.0192E-3	7.00	0.21	
91500@2									2.0216E-3	8.16	0.22	9.69
@7	0.046684	0.001320	0.282417	0.000016	-9.2	0.6	1.19	1.79	2.0192E-3	6.99	0.23	8.59
@8	0.051148	0.001427	0.282386	0.000014	-10.3	0.5	1.24	1.86	2.0177E-3	6.22	0.30	7.81
@9	0.048056	0.001393	0.282410	0.000021	-9.5	0.7	1.20	1.81	2.0193E-3	7.02	0.26	8.61
@10	0.043573	0.001250	0.282409	0.000032	-9.5	1.1	1.20	1.81	2.0192E-3	6.96	0.44	8.56
@11	0.057119	0.001690	0.282440	0.000038	-8.5	1.3	1.17	1.74	2.0188E-3	6.79	0.29	8.38
@12	0.031279	0.000891	0.282406	0.000035	-9.6	1.2	1.19	1.81	2.0196E-3	7.18	0.26	8.78
Tem@7									2.0184E-3	6.60	0.25	
Tem@8									2.0191E-3	6.93	0.36	
@13	0.036743	0.001091	0.282436	0.000045	-8.5	1.6	1.16	1.75	2.0191E-3	6.93	0.32	8.53
91500@3									2.0231E-3	8.91	0.30	10.38

@14	0.067823	0.001926	0.282426	0.000043	-9.0	1.5	1.20	1.78	2.0186E-3	6.70	0.28	8.30
@15	0.031107	0.000946	0.282412	0.000048	-9.4	1.7	1.19	1.80	2.0193E-3	7.02	0.31	8.61
@16	0.039864	0.001168	0.282409	0.000052	-9.5	1.9	1.20	1.81	2.0200E-3	7.37	0.31	8.97
@17	0.030339	0.000927	0.282426	0.000049	-8.9	1.7	1.17	1.77	2.0195E-3	7.12	0.38	8.72
@18	0.055392	0.001618	0.282412	0.000043	-9.4	1.5	1.21	1.81	2.0175E-3	6.13	0.26	7.73
Tem@9									2.0189E-3	6.81	0.15	
Tem@10									2.0189E-3	6.81	0.31	
@19	0.035439	0.001059	0.282448	0.000044	-8.1	1.5	1.14	1.72	2.0197E-3	7.23	0.38	8.83
@20	0.042883	0.001337	0.282428	0.000041	-8.8	1.5	1.18	1.77	2.0156E-3	5.19	0.25	6.79
91500@4									2.0227E-3	8.74	0.32	10.18
XY4-3:												
@1	0.051607	0.001475	0.282384	0.000021	-10.4	0.7	1.24	1.87	2.0204E-3	7.60	0.23	9.19
@2	0.035480	0.001032	0.282402	0.000034	-9.8	1.2	1.20	1.83	2.0202E-3	7.47	0.28	9.06
@3	0.021819	0.000627	0.282347	0.000029	-11.7	1.0	1.27	1.95	2.0210E-3	7.86	0.29	9.46
@4	0.069899	0.001964	0.282451	0.000030	-8.1	1.1	1.16	1.72	2.0194E-3	7.10	0.22	8.69
Tem@11									2.0181E-3	6.45	0.16	
Tem@12									2.0175E-3	6.15	0.28	
@5	0.044973	0.001281	0.282367	0.000032	-11.0	1.1	1.26	1.91	2.0194E-3	7.09	0.37	8.68
@6	0.020625	0.000600	0.282392	0.000039	-10.0	1.4	1.20	1.84	2.0205E-3	7.65	0.20	9.24
@7	0.035403	0.001048	0.282426	0.000051	-8.9	1.8	1.17	1.77	2.0191E-3	6.95	0.30	8.54
@8	0.032791	0.000946	0.282413	0.000047	-9.4	1.7	1.18	1.80	2.0201E-3	7.42	0.27	9.01
91500@5									2.0226E-3	8.68	0.30	10.17
@9	0.045242	0.001271	0.282410	0.000042	-9.5	1.5	1.20	1.81	2.0200E-3	7.39	0.37	8.98
@10	0.025985	0.000739	0.282449	0.000046	-8.1	1.6	1.13	1.72	2.0210E-3	7.86	0.21	9.46
Tem@13									2.0189E-3	6.82	0.29	
Tem@14									2.0190E-3	6.88	0.15	
@11	0.052118	0.001467	0.282429	0.000046	-8.8	1.6	1.18	1.77	2.0186E-3	6.67	0.38	8.27
@12	0.041348	0.001237	0.282441	0.000049	-8.4	1.7	1.15	1.74	2.0183E-3	6.54	0.22	8.14
@13	0.030180	0.000861	0.282378	0.000050	-10.6	1.8	1.23	1.88	2.0194E-3	7.06	0.25	8.65
@14	0.021799	0.000623	0.282399	0.000047	-9.8	1.7	1.19	1.83	2.0208E-3	7.76	0.32	9.35
@15	0.031920	0.000915	0.282412	0.000045	-9.4	1.6	1.18	1.80	2.0195E-3	7.15	0.18	8.75
@16	0.033293	0.000961	0.282401	0.000044	-9.8	1.5	1.20	1.83	2.0178E-3	6.30	0.29	7.89

91500@6									2.0219E-3	8.31	0.31	9.90
Tem@15									2.0188E-3	6.77	0.25	
Tem@16									2.0186E-3	6.68	0.16	
@17	0.033992	0.000987	0.282449	0.000034	-8.1	1.2	1.13	1.72	2.0190E-3	6.88	0.26	8.48
@18	0.043392	0.001250	0.282415	0.000025	-9.3	0.9	1.19	1.80	2.0192E-3	6.98	0.27	8.57
@19	0.025101	0.000738	0.282419	0.000050	-9.1	1.8	1.17	1.79				
XY3-1:												
@1	0.026013	0.000733	0.282450	0.000032	-8.0	1.1	1.13	1.72	2.0189E-3	6.83	0.35	8.42
@2	0.045790	0.001288	0.282389	0.000032	-10.2	1.1	1.23	1.86	2.0194E-3	7.10	0.34	8.70
Tem@17									2.0181E-3	6.43	0.22	
@3	0.043251	0.001186	0.282408	0.000031	-9.5	1.1	1.20	1.81	2.0194E-3	7.09	0.37	8.68
@4	0.018081	0.000534	0.282407	0.000041	-9.5	1.4	1.18	1.81	2.0203E-3	7.54	0.26	9.13
@5	0.024099	0.000688	0.282400	0.000035	-9.7	1.3	1.19	1.83	2.0194E-3	7.10	0.24	8.69
91500@7									2.0226E-3	8.70	0.22	10.43
@6	0.044901	0.001246	0.282441	0.000040	-8.4	1.4	1.15	1.74	2.0196E-3	7.20	0.18	8.79
Tem@18									2.0186E-3	6.67	0.26	
Tem@19									2.0185E-3	6.65	0.33	
@7	0.034200	0.000975	0.282412	0.000050	-9.4	1.8	1.19	1.80	2.0195E-3	7.15	0.23	8.74
@8	0.028610	0.000831	0.282396	0.000041	-9.9	1.4	1.20	1.84	2.0190E-3	6.86	0.22	8.46
@9	0.029301	0.000853	0.282405	0.000044	-9.6	1.6	1.19	1.82	2.0184E-3	6.60	0.29	8.20
@10	0.031732	0.000929	0.282407	0.000044	-9.5	1.5	1.19	1.81	2.0183E-3	6.52	0.32	8.11
@11	0.023526	0.000700	0.282378	0.000044	-10.5	1.6	1.22	1.88	2.0184E-3	6.59	0.28	8.19
@12	0.052232	0.001630	0.282383	0.000039	-10.4	1.4	1.25	1.87	2.0176E-3	6.17	0.27	7.76
Tem@20									2.0177E-3	6.23	0.29	
Tem@21									2.0178E-3	6.26	0.31	
@13	0.047554	0.001369	0.282485	0.000041	-6.8	1.5	1.10	1.64	2.0193E-3	7.05	0.30	8.64
@14	0.037066	0.001103	0.282382	0.000028	-10.4	1.0	1.23	1.87	2.0178E-3	6.30	0.22	7.89
@15	0.019618	0.000582	0.282371	0.000015	-10.7	0.5	1.23	1.89	2.0194E-3	7.08	0.21	8.68
91500@8									2.0222E-3	8.50	0.35	10.31
@16	0.025657	0.000722	0.282384	0.000022	-10.3	0.8	1.22	1.86				
@17	0.027883	0.000794	0.282432	0.000044	-8.6	1.6	1.15	1.76				
@18	0.050552	0.001433	0.282354	0.000043	-11.5	1.5	1.28	1.94				

XY2-1:												
@1	0.027628	0.000790	0.282370	0.000029	-10.8	1.0	1.24	1.89	2.0185E-3	6.61	0.25	8.21
@2	0.036443	0.001028	0.282341	0.000031	-11.9	1.1	1.29	1.96	2.0188E-3	6.80	0.29	8.39
@3	0.067972	0.001920	0.282396	0.000031	-10.0	1.1	1.24	1.84	2.0193E-3	7.03	0.37	8.63
Tem@22									2.0175E-3	6.15	0.39	
Tem@23									2.0182E-3	6.48	0.27	
@4	0.060440	0.001784	0.282357	0.000045	-11.4	1.6	1.29	1.93	2.0181E-3	6.43	0.31	8.02
@5	0.034066	0.001016	0.282364	0.000040	-11.0	1.4	1.25	1.91	2.0193E-3	7.05	0.23	8.64
@6	0.065502	0.001916	0.282392	0.000039	-10.1	1.4	1.24	1.85	2.0179E-3	6.34	0.33	7.94
@7	0.045550	0.001361	0.282353	0.000041	-11.5	1.5	1.28	1.94	2.0191E-3	6.91	0.21	8.50
91500@9									2.0207E-3	7.73	0.33	9.38
@8	0.032391	0.000929	0.282336	0.000036	-12.0	1.3	1.29	1.97	2.0192E-3	6.96	0.25	8.56
@9	0.039359	0.001125	0.282348	0.000032	-11.6	1.1	1.28	1.95	2.0190E-3	6.89	0.31	8.48
Tem@24									2.0183E-3	6.54	0.30	
Tem@25									2.0191E-3	6.94	0.25	
@9	0.053560	0.001502	0.282377	0.000025	-10.6	0.9	1.25	1.88				
@10	0.034521	0.001004	0.282369	0.000034	-10.9	1.2	1.25	1.90				
@11	0.030334	0.000881	0.282347	0.000041	-11.6	1.5	1.27	1.95				
@12	0.067762	0.002001	0.282402	0.000034	-9.8	1.2	1.23	1.83				
@13	0.049823	0.001442	0.282402	0.000041	-9.7	1.4	1.22	1.83				
@14	0.082768	0.002199	0.282414	0.000032	-9.4	1.1	1.22	1.80				
@15	0.046916	0.001401	0.282412	0.000041	-9.4	1.4	1.20	1.80				
@16	0.046792	0.001296	0.282396	0.000044	-9.9	1.6	1.22	1.84				
@17	0.044408	0.001343	0.282369	0.000019	-10.9	0.7	1.26	1.90				
@18	0.052225	0.001544	0.282370	0.000019	-10.9	0.7	1.26	1.90				
@19	0.067294	0.002097	0.282391	0.000020	-10.2	0.7	1.25	1.85				
@20	0.042666	0.001187	0.282414	0.000024	-9.3	0.8	1.19	1.80				
@21	0.051727	0.001460	0.282363	0.000033	-11.1	1.2	1.27	1.91				
@22	0.044644	0.001332	0.282393	0.000024	-10.0	0.8	1.22	1.85				
@23	0.084435	0.002424	0.282395	0.000039	-10.1	1.4	1.26	1.85				

XY7-1:

@1	0.158853	0.004168	0.282508	0.000036	-6.3	1.3	1.15	1.61				
@2	0.132887	0.003955	0.282472	0.000046	-7.5	1.6	1.20	1.69				
@3	0.080112	0.002251	0.282412	0.000048	-9.5	1.7	1.23	1.81				
@4	0.048136	0.001412	0.282410	0.000042	-9.5	1.5	1.20	1.81				
@5	0.085067	0.002459	0.282414	0.000044	-9.4	1.6	1.23	1.81				
@6	0.046452	0.001393	0.282361	0.000042	-11.2	1.5	1.27	1.92				
@7	0.132607	0.004081	0.282357	0.000046	-11.6	1.6	1.38	1.94				
@8	0.032237	0.000976	0.282360	0.000033	-11.2	1.2	1.26	1.92				
91500 avg.									**2.0221E-03**	**8.45**		**10.05**
±1SD									**7.3082E-07**			**0.36**
Tem avg.									**2.0184E-03**	**6.60**		**8.20**
±1SD									**4.7005E-07**			**0.23**
Session three: **Gudoushan***												
TEM@1									2.017E-3	5.69	0.42	
TEM@2									2.016E-3	5.52	0.36	
TEM@3									2.016E-3	5.53	0.40	
GD61-1:												
@1	0.077809	0.001243	0.282395	0.000030	-9.9	1.1	1.22	1.84	2.013E-3	3.72	0.42	6.72
@2	0.123360	0.002341	0.282408	0.000026	-9.6	0.9	1.24	1.82	2.015E-3	4.94	0.21	7.94
TEM@4									2.016E-3	5.22	0.39	
@3	0.094349	0.001531	0.282443	0.000050	-8.2	1.8	1.16	1.73	2.017E-3	6.06	0.27	9.07
@4	0.065013	0.001066	0.282423	0.000044	-8.9	1.6	1.17	1.78	2.016E-3	5.45	0.33	8.45
TEM@5									2.015E-3	5.08	0.21	
@5	0.048552	0.000866	0.282397	0.000035	-9.8	1.2	1.20	1.83	2.015E-3	5.10	0.40	8.10
@6	0.107320	0.001654	0.282407	0.000048	-9.6	1.7	1.22	1.82	2.016E-3	5.38	0.40	8.38
TEM@6									2.016E-3	5.44	0.31	
@7	0.090592	0.001512	0.282429	0.000044	-8.8	1.5	1.18	1.77	2.015E-3	4.84	0.34	7.84
@8	0.082281	0.001512	0.282445	0.000031	-8.2	1.1	1.16	1.73	2.015E-3	4.95	0.26	7.95
TEM@7									2.016E-3	5.20	0.32	
@9	0.065722	0.001285	0.282397	0.000029	-9.9	1.0	1.22	1.84	2.015E-3	5.13	0.21	8.13
@10	0.160552	0.002583	0.282514	0.000032	-5.9	1.1	1.09	1.58	2.015E-3	5.07	0.32	8.07
TEM@8									2.015E-3	5.03	0.33	

@11	0.072048	0.001148	0.282487	0.000031	-6.7	1.1	1.09	1.63	2.016E-3	5.16	0.23	8.16
@12									2.013E-3	4.09	0.27	7.09
TEM@9									2.016E-3	5.18	0.33	
@13									2.015E-3	4.95	0.32	7.95
@14									2.015E-3	4.89	0.28	7.89
TEM@10									2.015E-3	4.87	0.31	
@15									2.015E-3	4.76	0.33	7.76
TEM@11									2.015E-3	5.12	0.34	
TEM@12									2.015E-3	4.94	0.24	
TEM@13									2.015E-3	4.77	0.29	
Tem avg.									**2.0156E-03**	**5.20**		**8.20**
±1SD									**5.5625E-07**			**0.28**
Session four: **Wuguishan***												
TEM@1									2.015E-3	4.95	0.33	
TEM@2									2.017E-3	5.79	0.47	
TEM@3									2.016E-3	5.51	0.33	
GD62-1：												
@1	0.042023	0.000701	0.282438	0.000046	-8.4	1.6	1.14	1.74	2.014E-3	4.42	0.45	7.28
@2	0.043039	0.000780	0.282452	0.000039	-7.9	1.4	1.13	1.71	2.016E-3	5.18	0.34	8.04
@3	0.048053	0.000870	0.282425	0.000027	-8.8	0.9	1.16	1.77	2.014E-3	4.34	0.34	7.20
TEM@4									2.016E-3	5.45	0.30	
TEM@5									2.016E-3	5.56	0.28	
@4	0.060659	0.001074	0.282441	0.000049	-8.3	1.7	1.15	1.74	2.015E-3	5.09	0.33	7.95
@5	0.040776	0.000718	0.282447	0.000038	-8.1	1.3	1.13	1.72	2.016E-3	5.37	0.29	8.23
@6	0.068392	0.001202	0.282457	0.000046	-7.8	1.6	1.13	1.70	2.016E-3	5.47	0.30	8.33
TEM@6									2.016E-3	5.44	0.30	
TEM@7									2.017E-3	5.67	0.26	
@7	0.079558	0.001782	0.282481	0.000034	-7.0	1.2	1.11	1.65	2.015E-3	5.02	0.40	7.88
@8	0.083654	0.002079	0.282356	0.000042	-11.4	1.5	1.30	1.93	2.016E-3	5.61	0.44	8.47
@9	0.082883	0.001432	0.282465	0.000040	-7.5	1.4	1.13	1.69	2.015E-3	4.96	0.37	7.82
TEM@8									2.017E-3	5.67	0.26	

TEM@9									2.016E-3	5.60	0.29	
@10	0.038859	0.000681	0.282436	0.000041	-8.4	1.4	1.14	1.75	2.015E-3	4.89	0.34	7.75
@11	0.049237	0.000869	0.282450	0.000033	-8.0	1.2	1.13	1.72	2.015E-3	5.00	0.25	7.86
@12	0.047975	0.000800	0.282446	0.000034	-8.1	1.2	1.13	1.72	2.015E-3	4.78	0.26	7.64
TEM@10									2.015E-3	5.08	0.26	
@13	0.037648	0.000660	0.282450	0.000056	-8.0	2.0	1.12	1.72	2.014E-3	4.45	0.22	7.31
@14	0.066357	0.001044	0.282407	0.000048	-9.5	1.7	1.20	1.81	2.015E-3	4.77	0.31	7.63
@15	0.048265	0.000950	0.282437	0.000033	-8.5	1.2	1.15	1.75	2.014E-3	4.33	0.29	7.18
TEM@11									2.016E-3	5.16	0.26	
TEM@12									2.015E-3	4.90	0.38	
@16	0.069045	0.001092	0.282456	0.000036	-7.8	1.3	1.13	1.70	2.014E-3	4.28	0.29	7.13
@17	0.039464	0.000695	0.282405	0.000041	-9.6	1.5	1.19	1.82	2.014E-3	4.51	0.23	7.37
TEM@13									2.016E-3	5.17	0.33	
TEM@14									2.015E-3	4.83	0.34	
Tem avg.									**2.0159E-03**	**5.34**		**8.20**
±1SD									**6.3896E-07**			**0.32**

Sample	$^{176}Yb/^{177}Hf$	$^{176}Lu/^{177}Hf$	$^{176}Hf/^{177}Hf$	± 2σ	εHf(T)	± 2σ	T_{DM} (Ga)	T_{DM}^{C} (Ga)	$^{18}O/^{16}O$	$\delta^{18}O_{Meas}$ (‰)	2SE	IMF	$\delta^{18}O_{Corr}$ (‰)
Session five*													
Tem@1									2.0183E-3	6.54	0.35	1.85	8.38
Tem @2									2.0177E-3	6.24	0.24	1.85	8.09
Tem @3									2.0177E-3	6.23	0.37	1.86	8.09
GD51-1: Gangwei													
@1	0.042274	0.001176	0.282634	0.000025	-1.5	0.9	0.88	1.30	2.0141E-3	4.43	0.26	1.88	6.31
@2	0.040706	0.001116	0.282665	0.000018	-0.4	0.7	0.83	1.23	2.0154E-3	5.07	0.40	1.91	6.97
@3	0.035312	0.000977	0.282620	0.000021	-2.0	0.7	0.89	1.33	2.0150E-3	4.88	0.28	1.94	6.83
@4	0.044178	0.001200	0.282642	0.000021	-1.2	0.7	0.87	1.29	2.0145E-3	4.62	0.30	1.98	6.60
@5	0.049002	0.001358	0.282671	0.000019	-0.2	0.7	0.83	1.22	2.0140E-3	4.40	0.15	2.03	6.43
@6	0.047781	0.001331	0.282656	0.000021	-0.7	0.7	0.85	1.26	2.0150E-3	4.88	0.26	2.07	6.96
Tem @4									2.0171E-3	5.96	0.26	2.13	8.08
Tem @5									2.0176E-3	6.20	0.35	2.18	8.38

@7	0.046593	0.001246	0.282655	0.000018	-0.8	0.6	0.85	1.26	2.0145E-3	4.65	0.28	2.23	6.88
@8	0.044711	0.001172	0.282647	0.000021	-1.0	0.7	0.86	1.28	2.0142E-3	4.47	0.41	2.29	6.76
@9	0.036781	0.000973	0.282662	0.000019	-0.5	0.7	0.84	1.24	2.0142E-3	4.48	0.19	2.34	6.83
@10	0.033570	0.000919	0.282622	0.000019	-1.9	0.7	0.89	1.33	2.0132E-3	4.00	0.27	2.40	6.40
@11	0.041238	0.001218	0.282646	0.000022	-1.1	0.8	0.86	1.28	2.0150E-3	4.91	0.27	2.45	7.36
@12	0.047622	0.001277	0.282670	0.000022	-0.2	0.8	0.83	1.22	2.0142E-3	4.49	0.23	2.50	7.00
Tem @6									2.0164E-3	5.59	0.39	2.55	8.14
Tem @7									2.0166E-3	5.67	0.32	2.60	8.27
@13	0.040525	0.001080	0.282645	0.000020	-1.1	0.7	0.86	1.28	2.0135E-3	4.14	0.36	2.64	6.78
@14	0.041254	0.001116	0.282635	0.000018	-1.5	0.6	0.88	1.30	2.0144E-3	4.57	0.35	2.68	7.24
@15	0.042268	0.001166	0.282613	0.000018	-2.2	0.6	0.91	1.35	2.0136E-3	4.21	0.27	2.71	6.92
@16	0.044364	0.001293	0.282672	0.000017	-0.2	0.6	0.83	1.22	2.0131E-3	3.92	0.27	2.74	6.66
@17	0.044263	0.001197	0.282646	0.000023	-1.1	0.8	0.86	1.28	2.0133E-3	4.04	0.19	2.76	6.80
@18	0.044421	0.001161	0.282650	0.000024	-0.9	0.8	0.86	1.27	2.0131E-3	3.96	0.22	2.78	6.74
Tem @8									2.0162E-3	5.50	0.22	2.79	8.30
Tem @9									2.0158E-3	5.27	0.29	2.80	8.08
@18-1									2.0129E-3	3.86	0.41	2.80	6.66
@17-1									2.0134E-3	4.08	0.20	2.80	6.88
@14-1									2.0130E-3	3.91	0.25	2.79	6.70
@4-1									2.0131E-3	3.96	0.35	2.77	6.72
@19-1									2.0137E-3	4.24	0.25	2.74	6.98
GD47-1: Xiaoliang													
@1	0.038936	0.000972	0.282520	0.000024	-5.5	0.8	1.03	1.56	2.0149E-3	4.81	0.17	2.71	7.53
Tem @10									2.0165E-3	5.61	0.40	2.68	8.29
Tem @11									2.0162E-3	5.46	0.45	2.64	8.10
@2	0.044377	0.001022	0.282641	0.000043	-1.2	1.5	0.87	1.29	2.0137E-3	4.25	0.27	2.59	6.83
@3	0.043406	0.001026	0.282508	0.000053	-5.9	1.9	1.05	1.59	2.0146E-3	4.68	0.25	2.53	7.21
@4	0.045555	0.001070	0.282555	0.000041	-4.3	1.5	0.99	1.48	2.0140E-3	4.40	0.25	2.47	6.87
@5	0.046749	0.001062	0.282560	0.000041	-4.1	1.4	0.98	1.47	2.0141E-3	4.45	0.32	2.41	6.85
@6	0.042183	0.001012	0.282599	0.000029	-2.7	1.0	0.93	1.38	2.0152E-3	5.01	0.24	2.33	7.34
@7	0.059301	0.001467	0.282574	0.000029	-3.7	1.0	0.97	1.44	2.0148E-3	4.81	0.29	2.26	7.06

Tem @12									2.0176E-3	6.19	0.26	2.18	8.37
Tem @13									2.0171E-3	5.94	0.28	2.09	8.03
@8	0.033027	0.000863	0.282584	0.000022	-3.2	0.8	0.94	1.41	2.0147E-3	4.74	0.28	2.00	6.75
@9	0.086358	0.002271	0.282592	0.000025	-3.1	0.9	0.97	1.41	2.0174E-3	6.06	0.18	1.91	7.97
@10	0.039711	0.000901	0.282546	0.000020	-4.6	0.7	1.00	1.50	2.0165E-3	5.65	0.36	1.82	7.46
@11	0.036331	0.000875	0.282535	0.000021	-5.0	0.8	1.01	1.53	2.0165E-3	5.64	0.20	1.72	7.36
@12	0.037974	0.000936	0.282571	0.000019	-3.7	0.7	0.96	1.44	2.0163E-3	5.55	0.24	1.62	7.17
@13	0.043380	0.001170	0.282606	0.000023	-2.5	0.8	0.92	1.37	2.0160E-3	5.41	0.23	1.52	6.93
Tem @14									2.0189E-3	6.83	0.23	1.42	8.25
Tem @15									2.0188E-3	6.80	0.29	1.32	8.12
@14	0.050127	0.001119	0.282539	0.000019	-4.9	0.7	1.01	1.52	2.0168E-3	5.79	0.38	1.22	7.01
@15	0.039503	0.000827	0.282527	0.000022	-5.3	0.8	1.02	1.54	2.0169E-3	5.85	0.34	1.12	6.97
@16	0.045545	0.000962	0.282511	0.000021	-5.8	0.7	1.05	1.58	2.0170E-3	5.87	0.28	1.02	6.89
@17	0.037365	0.000816	0.282584	0.000019	-3.2	0.7	0.94	1.41	2.0180E-3	6.39	0.29	0.93	7.32
@18	0.045792	0.000956	0.282508	0.000023	-5.9	0.8	1.05	1.59	2.0193E-3	7.01	0.23	0.84	7.85
Tem @16									2.0204E-3	7.58	0.27	0.75	8.34
Tem @17									2.0204E-3	7.58	0.40	0.67	8.25
Tem @18									2.0202E-3	7.46	0.28	0.60	8.06
Tem avg.									**2.0177E-3**	**6.26**		**1.94**	**8.20**
±1SD									**1.4771E-6**	**0.74**			**0.12**

Analytial results listed in sequence as measured.

Notes: Meas. = Measured; Corr. = Corrected; SE = Standard Error; Tem = Temora 2; avg. = average; SD = standard deviation.

Measured $^{18}O/^{16}O$ ratios were normalized by using Vienna Standard Mean Ocean Water compositions (VSMOW, $^{18}O/^{16}O = 0.0020052$);

$\delta^{18}O_{Measured} = [(^{18}O/^{16}O)_{Measured}/(^{18}O/^{16}O)_{VSMOW} - 1] \times 1000‰$;

$\delta^{18}O_{Corrected} = \delta^{18}O_{Measured} - IMF$, IMF is instrumental mass fractionation factor;

** IMF values for each analysis are estimated using an equation fitted to the variation of $\delta^{18}O$ for TEMORA 2 as time passes.

The equation presents as: $IMF = -2e(-8)t^4 + 7e(-6)t^3 - 0.0006t^2 + 0.0022t + 6.3524 - 8.20$, $R^2 = 0.9717$, t = time (minute) (**Fig. 3.1**).

∗$IMF = \delta^{18}O\ (Tem\ avg.)_{Measured} - 8.20‰$.

Appendix Table 12 Physical-chemical conditions estimated using amphibole compositions

Sample	Gangwei									Lunshui				
Input														
SiO_2 (wt.%)	52.13	51.6	52.29	50.81	49.14	50.52	52.21	53.43	50.16	44.88	44.08	44.56	44.94	45.46
TiO_2 (wt.%)	0.3	0.43	0.17	0.53	0.77	0.57	0.25	0.12	0.58	1.37	1.71	1.25	1.37	1.3
Al_2O_3 (wt.%)	3.48	3.66	3.27	4.12	5.5	4.22	3.11	2.29	4.48	8.06	8.52	8.09	7.97	7.97
Cr_2O_3 (wt.%)	0	0.03	0.01	0	0.02	0	0	0.03	0.03	0.11	0.04	0	0	0
FeO (wt.%)	12.7	12.84	12.55	12.79	13.65	13.19	12.23	11.67	12.97	18.43	17.95	18.72	17.62	17.69
MnO (wt.%)	0.71	0.64	0.76	0.77	0.75	0.73	0.7	0.75	0.72	1.47	1.39	1.66	1.37	1.41
MgO (wt.%)	15.38	15.34	15.27	14.69	13.89	14.69	15.47	15.97	14.59	10.08	10.25	9.81	10.5	10.55
CaO (wt.%)	11.87	11.88	11.84	11.38	11.5	11.67	11.81	11.9	11.44	10.93	11.18	11.01	10.96	10.9
Na_2O (wt.%)	0.59	0.74	0.59	0.9	1.15	0.66	0.44	0.3	0.78	1.64	1.81	1.68	1.75	1.62
K_2O (wt.%)	0.23	0.31	0.21	0.38	0.53	0.38	0.24	0.16	0.41	1.03	1.01	1.03	0.94	0.93
F (wt.%)	-	-	-	-	-	-	-	-	-	-	-	-	-	-
Cl (wt.%)	-	-	-	-	-	-	-	-	-	-	-	-	-	-
Output														
Al#	**0.12**	**0.06**	**0.17**	**0.15**	**0.13**	**0.09**	**0.14**	**0.17**	**0.11**	**0.08**	**0.06**	**0.08**	**0.09**	**0.10**
						Physical-chemical conditions								
T (°C)	**699**	**709**	**690**	**713**	**754**	**720**	**696**	**680**	**725**	**819**	**845**	**822**	**821**	**812**
uncertanty (σ_{est})	22	22	22	22	22	22	22	22	22	22	22	22	22	22
P (MPa)	**45**	**47**	**43**	**53**	**75**	**54**	**41**	**34**	**58**	**147**	**167**	**150**	**145**	**143**
uncertanty (Max error)	5	5	5	6	8	6	5	8	6	16	18	17	16	16
continental depth (km)	1.7	1.8	1.6	2.0	2.8	2.1	1.6	1.3	2.2	5.6	6.3	5.7	5.5	5.4

ΔNNO	**2.1**	**2.1**	**2.1**	**1.9**	**1.5**	**1.9**	**2.2**	**2.4**	**1.9**	**0.2**	**0.1**	**0.1**	**0.3**	**0.4**
logfO_2	**-14.1**	**-13.9**	**-14.3**	**-14.0**	**-13.4**	**-13.8**	**-14.1**	**-14.4**	**-13.7**	**-13.2**	**-12.8**	**-13.2**	**-13.1**	**-13.2**
uncertanty (σ_{est})	0.4	0.4	0.4	0.4	0.4	0.4	0.4	0.4	0.4	0.4	0.4	0.4	0.4	0.4
H_2O_{melt} (wt.%)	**4.6**	**4.2**	**4.7**	**4.4**	**4.6**	**4.6**	**4.4**	**4.2**	**4.6**	**5.0**	**4.9**	**5.1**	**5.0**	**5.3**
uncertanty*	0.4	0.4	0.4	0.4	0.4	0.4	0.4	0.4	0.4	0.4	0.4	0.4	0.4	0.4

Note: "-" means no input

References

Anderson, J.L., 1983, Proterozoic anorogenic granite plutonism of North America: Geological Society of America Memoir, v. 161, p. 133-154.

Anderson, J.L., and Smith, D.R., 1995, The effects of temperature and fO_2 on the Al-in-hornblende barometer: American Mineralogist, v. 80, p. 549-559.

Bai, D.Y., Chen, J.C., Ma, T.Q., and Wang, X.H., 2005, Geochemical characteristics and tectonic setting of Qitianling A-type granitic pluton in southeas Hunan: Acta Petrologica Et Mineralogica, v. 24, p. 255-272 (in Chinese with English abstract).

Barbarin, B., 1999, A review of the relationships between granitoid types, their origins and their geodynamic environments: Lithos, v. 46, p. 605-626.

Barboza, S.A., and Bergantz, G.W., 2000, Metamorphism and anatexis in the mafic complex contact aureole, Ivrea zone, northern Italy: Journal of Petrology, v. 41, p. 1307-1327.

Barboza, S.A., Bergantz, G.W., and Brown, M., 1999, Regional granulite facies metamorphism in the Ivrea zone: Is the Mafic Complex the smoking gun or a red herring?: Geology, v. 27, p. 447-450.

Barker, F., Wones, D.R., Sharp, W.N., and Desborough, G.A., 1975, Pikes Peak Batholith, Colorado Front Range, and model for origin of "gabbro-anorthosite-syenite-potassic" granite suite: Precambrian Research, v. 2, p. 97-160.

Bea, F., Fershtater, G., and Corretge, L.G., 1992, The geochemistry of phosphorus in granite rocks and the effect of aluminum: Lithos, v. 29, p. 43-56.

Bea, F., and Montero, P., 1999, Behavior of accessory phases and redistribution of Zr, REE, Y, Th, and U during metamorphism and partial melting of metapelites in the lower crust: An example from the Kinzigite Formation of Ivrea-Verbano, NW Italy: Geochimica Et Cosmochimica Acta, v. 63, p. 1133-1153.

Benzerara, K., Menguy, N., Banerjee, N.R., Tyliszczak, T., Brown, G.E., and Guyot, F., 2007, Alteration of submarine basaltic glass from the Ontong Java Plateau: A STXM and TEM study: Earth and Planetary Science Letters, v. 260, p. 187-200.

Black, L.P., Kamo, S.L., Allen, C.M., Davis, D.W., Aleinikoff, J.N., Valley, J.W.,

Mundil, R., Campbell, I.H., Korsch, R.J., Williams, I.S., and Foudoulis, C., 2004, Improved $^{206}Pb/^{238}U$ microprobe geochronology by the monitoring of a trace-element-related matrix effect: SHRIMP, ID-TIMS, ELA-ICP-MS and oxygen isotope documentation for a series of zircon standards: Chemical Geology, v. 205, p. 115-140.

Blevin, P.L., and Chappell, B.W., 1992, The role of magma sources, oxidation-states and fractionation in determining the granite metallogeny of eastern Australia: Transactions of the Royal Society of Edinburgh-Earth Sciences, v. 83, p. 305-316.

Blevin, P.L., and Chappell, B.W., 1995, Chemistry, origin, and evolution of mineralized granites in the Lachlan Fold Belt, Australia: The metallogeny of I- and S-type granites: Economic Geology and the Bulletin of the Society of Economic Geologists, v. 90, p. 1604-1619.

Bonin, B., 2007, A-type granites and related rocks: Evolution of a concept, problems and prospects: Lithos, v. 97, p. 1-29.

Bonin, B.L., Azzouni-Sekkal, A., Bussy, F., and Ferrag, S., 1998, Alkali-calcic and alkaline post-orogenic (PO) granite magmatism: petrologic constraints and geodynamic settings: Lithos, v. 45, p. 45-70.

Carroll, M.R., and Wyllie, P.J., 1990, The system tonalite-H_2O at 15 Kbar and the genesis of calc-alkaline magmas: American Mineralogist, v. 75, p. 345-357.

Carter, A., and Clift, P.D., 2008, Was the Indosinian orogeny a Triassic mountain building or a thermotectonic reactivation event?: Comptes Rendus Geoscience, v. 340, p. 83-93.

Castro, A., Douce, A.E.P., Corretge, L.G., de la Rosa, J.D., El-Biad, M., and El-Hmidi, H., 1999, Origin of peraluminous granites and granodiorites, Iberian massif, Spain: an experimental test of granite petrogenesis: Contributions to Mineralogy and Petrology, v. 135, p. 255-276.

Castro, A., Garcia-Casco, A., Fernandez, C., Corretge, L.G., Moreno-Ventas, I., Gerya, T., and Low, I., 2009, Ordovician ferrosilicic magmas: Experimental evidence for ultrahigh temperatures affecting a metagreywacke source: Gondwana Research, v. 16, p. 622-632.

Cavosie, A.J., Kita, N.T., and Valley, J.W., 2009, Primitive oxygen-isotope ratio recorded in magmatic zircon from the Mid-Atlantic Ridge: American Mineralogist, v. 94, p. 926-934.

Chappell, B.W., 1996, Magma mixing and the production of compositional variation within granite suites: Evidence from the granites of southeastern Australia: Journal of Petrology, v. 37, p. 449-470.

Chappell, B.W., 1999, Aluminium saturation in I- and S-type granites and the characterization of fractionated haplogranites: Lithos, v. 46, p. 535-551.

Chappell, B.W., 2004, Towards a unified model for granite genesis: Transactions of the Royal Society of Edinburgh-Earth Sciences, v. 95, p. 1-10.

Chappell, B.W., Bryant, C.J., Wyborn, D., White, A.J.R., and Williams, I.S., 1998, High- and low-temperature I-type granites: Resource Geology, v. 48, p. 225-235.

Chappell, B.W., and White, A.J.R., 1974, Two contrasting granite types: Pacific Geology, v. 8, p. 173-174.

Chappell, B.W., and White, A.J.R., 1992, I-Type and S-Type granites in the Lachlan Fold Belt: Transactions of the Royal Society of Edinburgh-Earth Sciences, v. 83, p. 1-26.

Chappell, B.W., and White, A.J.R., 2001, Two contrasting granite types: 25 years later: Australian Journal of Earth Sciences, v. 48, p. 489-499.

Chappell, B.W., White, A.J.R., and Hine, R., 1988, Granite provinces and basement terranes in the Lachlan Fold Belt, southeastern Australia: Australian Journal of Earth Sciences, v. 35, p. 505-521.

Chappell, B.W., White, A.J.R., Williams, I.S., and Wyborn, D., 2004, Low- and high-temperature granites: Transactions of the Royal Society of Edinburgh-Earth Sciences, v. 95, p. 125-140.

Chappell, B.W., White, A.J.R., and Wyborn, D., 1987, The importance of residual source material (restite) in granite petrogenesis: Journal of Petrology, v. 28, p. 1111-1138.

Chen, C.H., Lee, C.Y., and Shinjo, R.I., 2008, Was there Jurassic paleo-Pacific subduction in South China?: Constraints from Ar-40/Ar-39 dating, elemental and Sr-Nd-Pb isotopic geochemistry of the Mesozoic basalts: Lithos, v. 106, p. 83-92.

Chen, J.F., Foland, K.A., Xing, F.M., Xu, X.A., and Zhou, T.X., 1991, Magmatism along the southeast margin of the Yangtze Block: Precambrian collision of the Yangtze and Cathysia Blocks of China: Geology, v. 19, p. 815-818.

Chen, J.F., and Jahn, B.M., 1998, Crustal evolution of southeastern China: Nd and Sr

isotopic evidence: Tectonophysics, v. 284, p. 101-133.

Chen, J.L., Xu, J.F., Wang, B.D., Kang, Z.Q., and Jie, L., 2010, Origin of Cenozoic alkaline potassic volcanic rocks at KonglongXiang, Lhasa terrane, Tibetan Plateau: Products of partial melting of a mafic lower-crustal source?: Chemical Geology, v. 273, p. 286-299.

Chen, P.R., Hua, R.M., Zhang, B.T., Lu, J.J., and Fan, C.F., 2002, Early Yanshanian post-orogenic granitoids in the Nanling region: Petrological constraints and geodynamic settings: Science in China Series D-Earth Sciences, v. 45, p. 755-768.

Chen, P.R., Zhang, M., and Chen, W.F., 2007a, Granites of the Jiufeng-Zhuguangshan, *in* Zhou, X.M., ed., The petrogenesis of late Mesozoic granites and the geodynamic evolution of lithosphere in the Nanling Range, Volume 2: Beijing, Science Press, p. 691 (in Chinese).

Chen, P.R., Zhou, X.M., Zhang, W.L., Li, H.M., Fan, C.F., Sun, T., Chen, W.F., and Zhang, M., 2005, Petrogenesis and significance of early Yanshanian syenite-granite complex in eastern Nanling Range: Science in China Series D-Earth Sciences, v. 48, p. 912-924.

Chen, R., Xing, G.F., Yang, Z., Zhou, Y., Yu, M.T., and Li, L., 2007b, Early Jurassic zircon SHRIMP U-Pb age of the dacitic volcanic rocks in the southeastern Zhejiang Province determined firstly and its geological significances: Geological Review, v. 53, p. 31-35.

Chen, T.Y., Wang, X.Y., Ren, J.S., and Liu, Z.G., 1986, Isotopic geochronology of the Jiuyishan and Baimashan composite granitic intrusions, Hunan: Geological Review, v. 32, p. 433-439 (in Chinese with English abstract).

Chen, W.F., Chen, P.R., Huang, H.Y., Ding, X., and Sun, T., 2007c, Chronological and geochemical studies of granite and enclave in Baimashan pluton, Hunan, South China: Science in China Series D-Earth Sciences, v. 50, p. 1606-1627.

Cho, D.L., Lee, S.R., and Armstrong, R., 2008, Termination of the Permo-Triassic Songrim (Indosinian) orogeny in the Ogcheon belt, South Korea: Occurrence of ca. 220 Ma post-orogenic alkali granites and their tectonic implications: Lithos, v. 105, p. 191-200.

Christie, D.M., Carmichael, I.S.E., and Langmuir, C.H., 1986, Oxidation states of mid-ocean ridge basalt glasses: Earth and Planetary Science Letters, v. 79, p. 397-411.

Chung, S.L., Wang, K.L., Crawford, A.J., Kamenetsky, V.S., Chen, C.H., Lan, C.Y., and Chen, C.H., 2001, High-Mg potassic rocks from Taiwan: implications for the genesis of orogenic potassic lavas: Lithos, v. 59, p. 153-170.

Clemens, J.D., Birch, W.D., and Dudley, R.A., 2011a, S-type ignimbrites with polybaric crystallisation histories: the Tolmie Igneous Complex, Central Victoria, Australia: Contributions to Mineralogy and Petrology, v. 162, p. 1315-1337.

Clemens, J.D., Helps, P.A., and Stevens, G., 2010, Chemical structure in granitic magmas: A signal from the source?: Earth and Environmental Science Transactions of the Royal Society of Edinburgh, v. 100, p. 159-172.

Clemens, J.D., Holloway, J.R., and White, A.J.R., 1986, Origin of an A-type granite: Experimental constraints: American Mineralogist, v. 71, p. 317-324.

Clemens, J.D., and Petford, N., 1999, Granitic melt viscosity and silicic magma dynamics in contrasting tectonic settings: Journal of the Geological Society, v. 156, p. 1057-1060.

Clemens, J.D., and Stevens, G., 2012, What controls chemical variation in granitic magmas?: Lithos, v. 134, p. 317-329.

Clemens, J.D., Stevens, G., and Farina, F., 2011b, The enigmatic sources of I-type granites: The peritectic connexion: Lithos, v. 126, p. 174-181.

Clemens, J.D., and Watkins, J.M., 2001, The fluid regime of high-temperature metamorphism during granitoid magma genesis: Contributions to Mineralogy and Petrology, v. 140, p. 600-606.

Coleman, D.S., Gray, W., and Glazner, A.F., 2004, Rethinking the emplacement and evolution of zoned plutons: Geochronologic evidence for incremental assembly of the Tuolumne Intrusive Suite, California: Geology, v. 32, p. 433-436.

Collins, W.J., 1996, Lachlan Fold Belt granitoids: Products of three-component mixing: Transactions of the Royal Society of Edinburgh-Earth Sciences, v. 87, p. 171-181.

Collins, W.J., 1998, Evaluation of petrogenetic models for Lachlan Fold Belt granitoids: implications for crustal architecture and tectonic models: Australian Journal of Earth Sciences, v. 45, p. 483-500.

Collins, W.J., 1999, Evaluation of petrogenetic models for Lachlan Fold Belt granitoids: implications for crustal architecture and tectonic models - Reply:

Australian Journal of Earth Sciences, v. 46, p. 831-836.

Collins, W.J., Beams, S.D., White, A.J.R., and Chappell, B.W., 1982, Nature and origin of A-type granites with particular reference to southeastern Australia: Contributions to Mineralogy and Petrology, v. 80, p. 189-200.

Creaser, R.A., Price, R.C., and Wormald, R.J., 1991, A-type granites revisited: Assessment of a residual-source model: Geology, v. 19, p. 163-166.

Cui, S., and Li, J., 1983, On the Indosinian orogeny along the Chinese Western Pacific belt: Acta Geologica Sinica, v. 57, p. 51-61 (in Chinese with English abstract).

Dall'Agnol, R., and de Oliveira, D.C., 2007, Oxidized, magnetite-series, rapakivi-type granites of Carajas, Brazil: Implications for classification and petrogenesis of A-type granites: Lithos, v. 93, p. 215-233.

Dall'Agnol, R., Scaillet, B., and Pichavant, M., 1999, An experimental study of a Lower Proterozoic A-type granite from the eastern Amazonian Craton, Brazil: Journal of Petrology, v. 40, p. 1673-1698.

Davidson, J.P., and Tepley, F.J., 1997, Recharge in volcanic systems: Evidence from isotope profiles of phenocrysts: Science, v. 275, p. 826-829.

Deng, X.G., Li, X.H., Liu, Y.M., Huang, G.F., and Hou, M.S., 2005, Geochemical characteristics of Qitianling granites and their implications for mineralization: Acta Petrologica Et Mineralogica, v. 24, p. 93-102 (in Chinese with English abstract).

Depaolo, D.J., 1981, Trace-element and isotopic effects of combined wallrock assimilation and fractional crystallization: Earth and Planetary Science Letters, v. 53, p. 189-202.

Depaolo, D.J., and Wasserburg, G.J., 1979, Petrogenetic mixing models and Nd-Sr isotopic patterns: Geochimica Et Cosmochimica Acta, v. 43, p. 615-627.

Dickinson, W.R., 1975, Potash-depth (K-h) relations in continental-margin and intra-oceanic magmatic arcs: Geology, v. 3, p. 53-56.

Ebadi, A., and Johannes, W., 1991, Beginning of melting and composition of first melts in the system Qz-Ab-Or-H_2O-CO_2: Contributions to Mineralogy and Petrology, v. 106, p. 286-295.

Eby, G.N., 1992, Chemical subdivision of the A-type granitoids: Petrogenetic and tectonic implications: Geology, v. 20, p. 641-644.

Eiler, J.M., 2001, Oxygen isotope variations of basaltic lavas and upper mantle rocks,

Stable Isotope Geochemistry, Volume 43: Reviews in Mineralogy & Geochemistry: Washington, Mineralogical Soc America, p. 319-364.

Fernandez, C., Becchio, R., Castro, A., Viramonte, J.M., Moreno-Ventas, I., and Corretge, L.G., 2008, Massive generation of atypical ferrosilicic magmas along the Gondwana active margin: Implications for cold plumes and back-arc magma generation: Gondwana Research, v. 14, p. 451-473.

Flood, R.H., and Shaw, S.E., 1975, Cordierite-bearing granite suite from New England Batholith, NSW, Australia: Contributions to Mineralogy and Petrology, v. 52, p. 157-164.

Foster, M.D., 1960, Interpretation of the composition of trioctahedral mica: U.S. Geological Survey Professional Paper, v. 354-B, p. 11-48.

Frost, B.R., Barnes, C.G., Collins, W.J., Arculus, R.J., Ellis, D.J., and Frost, C.D., 2001, A geochemical classification for granitic rocks: Journal of Petrology, v. 42, p. 2033-2048.

Frost, C.D., and Frost, B.R., 1997, Reduced rapakivi-type granites: The tholeiite connection: Geology, v. 25, p. 647-650.

Frost, C.D., and Frost, B.R., 2011, On ferroan (A-type) granitoids: Their compositional variability and modes of origin: Journal of Petrology, v. 52, p. 39-53.

Fu, J.M., Ma, C.Q., Xie, C.F., Zhang, Y.M., and Peng, S.B., 2004a, Geochemistry and tectonic setting of Xishan aluminous A-type granitic volcanic-intrusive complex, southern Hunan: Journal of Earth Sciences and Environment, v. 26, p. 15-23 (in Chinese with English abstract).

Fu, J.M., Ma, C.Q., Xie, C.F., Zhang, Y.M., and Peng, S.B., 2004b, SHRIMP U-Pb zircon dating of the Jiuyishan composite granite in Hunan and its geological significance: Geotectonica et Metallogenia, v. 28, p. 370-378 (in Chinese with English abstract).

Fu, J.M., Ma, C.Q., Xie, C.F., Zhang, Y.M., and Peng, S.B., 2005, Ascertainment of the Jinjiling aluminous A-type granite, Hunan Province: Geochemica, v. 34, p. 215-226 (in Chinese with English abstract).

Fu, J.M., Ma, C.Q., Xie, C.F., Zhang, Y.M., Peng, S.B., and Liu, Y.H., 2003a, The discovery of ultramafic enclaves in Xishan granitic volcanic-intrusive complex rocks in southern Hunan: Journal of Mineralogy and Petrology, v. 23, p. 13-15 (in Chinese with English abstract).

Fu, J.M., Xie, C.F., Zhang, Y.M., Peng, S.B., and Liu, Y.H., 2003b, Genesis of the Xishan high-K calc-alkaline volcanic rocks in southern Hunan Province: Geology and Mineral Resources of South China, p. 16-22.

Fujian, B.o.G.a.M.R., 1985, Regional geology of Fujian Province: Beijing, Geological Publishing House, 671 p.

Gao, S., Yang, J., Zhou, L., Li, M., Hu, Z.C., Guo, J.L., Yuan, H.L., Gong, H.J., Xiao, G.Q., and Wei, J.Q., 2011, Age and growth of the Archean Kongling Terrain, south China, with emphasis on 3.3 Ga granitoid gneisses: American Journal of Science, v. 311, p. 153-182.

Gilder, S.A., Keller, G.R., Luo, M., and Goodell, P.C., 1991, Timing and spatial-distribution of rifting in China: Tectonophysics, v. 197, p. 225-243.

Gray, C.M., 1984, An isotopic mixing model for the origin of granitic-rocks in southeastern Australia: Earth and Planetary Science Letters, v. 70, p. 47-60.

Gregory, C.J., McFarlane, C.R.M., Hermann, J., and Rubatto, D., 2009, Tracing the evolution of calc-alkaline magmas: In-situ Sm-Nd isotope studies of accessory minerals in the Bergell Igneous Complex, Italy: Chemical Geology, v. 260, p. 73-86.

Griffin, W.L., Wang, X., Jackson, S.E., Pearson, N.J., O'Reilly, S.Y., Xu, X.S., and Zhou, X.M., 2002, Zircon chemistry and magma mixing, SE China: In-situ analysis of Hf isotopes, Tonglu and Pingtan igneous complexes: Lithos, v. 61, p. 237-269.

Grimes, C., Ushikubo, T., John, B., and Valley, J., 2011, Uniformly mantle-like $\delta^{18}O$ in zircons from oceanic plagiogranites and gabbros: Contributions to Mineralogy and Petrology, v. 161, p. 13-33.

Gu, C.Y., Hua, R.M., and Qi, H.W., 2006, Geochemistry and petrogenesis of the Yanshanian Huashan-Guposhan granites in Guangxi: Acta Petrologica Et Mineralogica, v. 25, p. 97-109 (in Chinese with English abstract).

Guangdong, B.o.G.a.M.R., 1988, Regional geology of the Guangdong Province: Beijing, Geological Publishing House, 941 p.

Hawkesworth, C.J., and Kemp, A.I.S., 2006, Evolution of the continental crust: Nature, v. 443, p. 811-817.

Hawthorne, F.C., 1981, Crystal chemistry of the amphiboles: Reviews in Mineralogy and Geochemistry, v. 9A, p. 1-102.

He, B., Xu, Y.G., and Campbell, I., 2009, Pre-eruptive uplift in the Emeishan?:

Nature Geoscience, v. 2, p. 530-531.

He, B., Xu, Y.G., Chung, S.L., Xiao, L., and Wang, Y., 2003, Sedimentary evidence for a rapid, kilometer-scale crustal doming prior to the eruption of the Emeishan flood basalts: Earth and Planetary Science Letters, v. 213, p. 391-405.

He, Z.Y., Xu, X.S., and Niu, Y.L., 2010, Petrogenesis and tectonic significance of a Mesozoic granite-syenite-gabbro association from inland South China: Lithos, v. 119, p. 621-641.

Hildreth, W., and Moorbath, S., 1988, Crustal contributions to arc magmatism in the Andes of central Chile: Contributions to Mineralogy and Petrology, v. 98, p. 455-489.

Hsü, K.J., Sun, S., Li, J.L., Chen, H.H., Pen, H.P., and Sengor, A.M.C., 1988, Mesozoic overthrust tectonics in South China: Geology, v. 16, p. 418-421.

Huang, H.-Q., Li, X.-H., Li, W.-X., and Li, Z.-X., 2011, Formation of high $\delta^{18}O$ fayalite-bearing A-type granite by high-temperature melting of granulitic metasedimentary rocks, southern China: Geology, v. 39, p. 903-906.

Huang, H.Q., Li, X.H., Li, W.X., and Liu, Y., 2008, Age and origin of the Dadongshan granite from the Nanling Range: SHRIMP U-Pb zircon age, geochemistry and Sr-Nd-Hf isotopes: Geological Journal of China Universities, v. 14, p. 317-333.

Huang, X.L., Niu, Y.L., Xu, Y.G., Chen, L.L., and Yang, Q.J., 2010, Mineralogical and geochemical constraints on the petrogenesis of post-collisional potassic and ultrapotassic rocks from western Yunnan, SW China: Journal of Petrology, v. 51, p. 1617-1654.

Hunan, B.o.G.a.M.R., 1987, Regional geology of the Hunan Province: Beijing, Geological Publishing House, 718 p.

Jahn, B.M., 1974, Mesozoic thermal events in southeast China: Nature, v. 248, p. 480-483.

Jahn, B.M., Wu, F.Y., Capdevila, R., Martineau, F., Zhao, Z.H., and Wang, Y.X., 2001, Highly evolved juvenile granites with tetrad REE patterns: the Woduhe and Baerzhe granites from the Great Xing'an Mountains in NE China: Lithos, v. 59, p. 171-198.

Jahn, B.M., Zhou, X.H., and Li, J.L., 1990, Formation and tectonic evolution of southeastern China and Taiwan: Isotopic and geochemical constraints:

Tectonophysics, v. 183, p. 145-160.

Janousek, V., Finger, F., Roberts, M., Fryda, J., Pin, C., and Dolejs, D., 2004, Deciphering the petrogenesis of deeply buried granites: whole-rock geochemical constraints on the origin of largely undepleted felsic granulites from the Moldanubian Zone of the Bohemian Massif: Transactions of the Royal Society of Edinburgh-Earth Sciences, v. 95, p. 141-159.

Jenkin, G.R.T., Ellam, R.M., Rogers, G., and Stuart, F.M., 2001, An investigation of closure temperature of the biotite Rb-Sr system: The importance of cation exchange: Geochimica Et Cosmochimica Acta, v. 65, p. 1141-1160.

Jiang, G.Q., Sohl, L.E., and Christie-Blick, N., 2003, Neoproterozoic stratigraphic comparison of the Lesser Himalaya (India) and Yangtze block (south China): Paleogeographic implications: Geology, v. 31, p. 917-920.

Jiang, Y.H., Jiang, S.Y., Dai, B.Z., Liao, S.Y., Zhao, K.D., and Ling, H.F., 2009, Middle to late Jurassic felsic and mafic magmatism in southern Hunan province, southeast China: Implications for a continental arc to rifting: Lithos, v. 107, p. 185-204.

Jiang, Y.H., Jiang, S.Y., Zhao, K.D., and Ling, H.F., 2006, Petrogenesis of Late Jurassic Qianlishan granites and mafic dykes, Southeast China: implications for a back-arc extension setting: Geological Magazine, v. 143, p. 457-474.

Jiao, W.F., Wu, Y.B., Yang, S.H., Peng, M., and Wang, J., 2009, The oldest basement rock in the Yangtze Craton revealed by zircon U-Pb age and Hf isotope composition: Science in China Series D-Earth Sciences, v. 52, p. 1393-1399.

Kemp, A.I.S., Hawkesworth, C.J., Foster, G.L., Paterson, B.A., Woodhead, J.D., Hergt, J.M., Gray, C.M., and Whitehouse, M.J., 2007, Magmatic and crustal differentiation history of granitic rocks from Hf-O isotopes in zircon: Science, v. 315, p. 980-983.

Kemp, A.I.S., Hawkesworth, C.J., Paterson, B.A., Foster, G.L., Kinny, P.D., Whitehouse, M.J., Maas, R., and Eimf, 2008, Exploring the plutonic-volcanic link: a zircon U-Pb, Lu-Hf and O isotope study of paired volcanic and granitic units from southeastern Australia: Transactions of the Royal Society of Edinburgh-Earth Sciences, v. 97, p. 337-355.

Kerr, A., and Fryer, B.J., 1993, Nd isotope evidence for crust mantle interaction in the generation of A-Type granitoid suites in Labrador, Canada: Chemical Geology, v. 104, p. 39-60.

King, P.L., Chappell, B.W., Allen, C.M., and White, A.J.R., 2001, Are A-type granites the high-temperature felsic granites? Evidence from fractionated granites of the Wangrah Suite: Australian Journal of Earth Sciences, v. 48, p. 501-514.

Landenberger, B., and Collins, W.J., 1996, Derivation of A-type granites from a dehydrated charnockitic lower crust: Evidence from the Chaelundi complex, eastern Australia: Journal of Petrology, v. 37, p. 145-170.

Lee, J.K.W., Williams, I.S., and Ellis, D.J., 1997, Pb, U and Th diffusion in natural zircon: Nature, v. 390, p. 159-162.

Li, L.M., Sun, M., Wang, Y.J., Xing, G.F., Zhao, G.C., Cai, K.D., and Zhang, Y.Z., 2011, Geochronological and geochemical study of Palaeoproterozoic gneissic granites and clinopyroxenite xenoliths from NW Fujian, SE China: Implications for the crustal evolution of the Cathaysia Block: Journal of Asian Earth Sciences, v. 41, p. 204-212.

Li, Q.L., Li, X.H., Liu, Y., Tang, G.Q., Yang, J.H., and Zhu, W.G., 2010a, Precise U-Pb and Pb-Pb dating of Phanerozoic baddeleyite by SIMS with oxygen flooding technique: Journal of Analytical Atomic Spectrometry, v. 25, p. 1107-1113.

Li, S.Y., Zhu, J.C., Zheng, M.G., Wu, Y.Y., Hu, Z.D., and Zhang, G.C., 1986, Rb-Sr chronology and genesis of Jiuyishan granite complex: Uranium Geology, v. 2, p. 257-264 (in Chinese with English abstract).

Li, W.X., Li, X.H., and Li, Z.X., 2005a, Neoproterozoic bimodal magmatism in the Cathaysia Block of South China and its tectonic significance: Precambrian Research, v. 136, p. 51-66.

Li, W.X., Li, X.H., and Li, Z.X., 2010b, Ca. 850 Ma bimodal volcanic rocks in northeastern Jiangxi Province, South China: Initial extension during the breakup of Rodinia?: American Journal of Science, v. 310, p. 951-980.

Li, W.X., Li, X.H., Li, Z.X., and Lou, F.S., 2008a, Obduction-type granites within the NE Jiangxi Ophiolite: Implications for the final amalgamation between the Yangtze and Cathaysia Blocks: Gondwana Research, v. 13, p. 288-301.

Li, X.H., 1991, Geochronology of Wanyangshan-Zhuguangshan granitoid batholith: Implication for the crust development: Science in China Series B-Chemistry Life Sciences & Earth Sciences, v. 34, p. 620-629.

Li, X.H., 1992, Petrogenesis of Zhuguangshan Mesozoic granites: Guangdong

Geology, v. 7, p. 1-13 (in Chinese with English abstract).

Li, X.H., 1997, Timing of the Cathaysia block formation: Constraints from SHRIMP U-Pb zircon geochronology: Episodes, v. 20, p. 188-192.

Li, X.H., 2000, Cretaceous magmatism and lithospheric extension in Southeast China: Journal of Asian Earth Sciences, v. 18, p. 293-305.

Li, X.H., Chen, Z., Liu, D.Y., and Li, W.X., 2003a, Jurassic gabbro-granite-syenite suites from Southern Jiangxi province, SE China: Age, origin, and tectonic significance: International Geology Review, v. 45, p. 898-921.

Li, X.H., Chung, S.L., Zhou, H.W., Lo, C.H., Liu, Y., and Chen, C.H., 2004a, Jurassic intraplate magmatism in southern Hunan-eastern Guangxi: 40Ar/39Ar dating, geochemistry, Sr-Nd isotopes and implications for tectonic evolution of SE China. In: Malpas, J., Fletcher, C. J., Aitchison, J. C., Ali, J. (Eds.), Aspects of the Tectonic Evolution of China.: Geological Society, London, Special Publications, v. 226, p. 193-216.

Li, X.H., Li, W.X., Li, Q.L., Wang, X.C., Liu, Y., and Yang, Y.H., 2010c, Petrogenesis and tectonic significance of the similar to 850 Ma Gangbian alkaline complex in South China: Evidence from in situ zircon U-Pb dating, Hf-O isotopes and whole-rock geochemistry: Lithos, v. 114, p. 1-15.

Li, X.H., Li, W.X., and Li, Z.X., 2007a, On the genetic classification and tectonic implications of the Early Yanshanian granitoids in the Nanling Range, South China: Chinese Science Bulletin, v. 52, p. 1873-1885.

Li, X.H., Li, W.X., Li, Z.X., and Liu, Y., 2008b, 850-790 Ma bimodal volcanic and intrusive rocks in northern Zhejiang, South China: A major episode of continental rift magmatism during the breakup of Rodinia: Lithos, v. 102, p. 341-357.

Li, X.H., Li, W.X., Li, Z.X., Lo, C.H., Wang, J., Ye, M.F., and Yang, Y.H., 2009a, Amalgamation between the Yangtze and Cathaysia Blocks in South China: Constraints from SHRIMP U-Pb zircon ages, geochemistry and Nd-Hf isotopes of the Shuangxiwu volcanic rocks: Precambrian Research, v. 174, p. 117-128.

Li, X.H., Li, W.X., Wang, X.C., Li, Q.L., Liu, Y., and Tang, G.Q., 2009b, Role of mantle-derived magma in genesis of early Yanshanian granites in the Nanling Range, South China: in situ zircon Hf-O isotopic constraints: Science in China Series D-Earth Sciences, v. 52, p. 1262-1278.

Li, X.H., Li, Z.X., Ge, W.C., Zhou, H.W., Li, W.X., Liu, Y., and Wingate, M.T.D., 2003b, Neoproterozoic granitoids in South China: crustal melting above a mantle plume at ca. 825 Ma?: Precambrian Research, v. 122, p. 45-83.

Li, X.H., Li, Z.X., Li, W.X., Liu, Y., Yuan, C., Wei, G.J., and Qi, C.S., 2007b, U-Pb zircon, geochemical and Sr-Nd-Hf isotopic constraints on age and origin of Jurassic I- and A-type granites from central Guangdong, SE China: A major igneous event in response to foundering of a subducted flat-slab?: Lithos, v. 96, p. 186-204.

Li, X.H., Li, Z.X., Li, W.X., and Wang, Y.J., 2006, Initiation of the Indosinian Orogeny in South China: Evidence for a Permian magmatic arc on Hainan Island: Journal of Geology, v. 114, p. 341-353.

Li, X.H., Li, Z.X., Zhou, H.W., Liu, Y., and Kinny, P.D., 2002a, U-Pb zircon geochronology, geochemistry and Nd isotopic study of Neoproterozoic bimodal volcanic rocks in the Kangdian Rift of South China: implications for the initial rifting of Rodinia: Precambrian Research, v. 113, p. 135-154.

Li, X.H., Liu, D.Y., Sun, M., Li, W.X., Liang, X.R., and Liu, Y., 2004b, Precise Sm-Nd and U-Pb isotopic dating of the supergiant Shizhuyuan polymetallic deposit and its host granite, SE China: Geological Magazine, v. 141, p. 225-231.

Li, X.H., Liu, Y., Li, Q.L., Guo, C.H., and Chamberlain, K.R., 2009c, Precise determination of Phanerozoic zircon Pb/Pb age by multicollector SIMS without external standardization: Geochemistry Geophysics Geosystems, v. 10, p. -.

Li, X.H., Qi, C.S., Liu, Y., Liang, X.R., Tu, X.L., Xie, L.W., and Yang, Y.H., 2005b, Petrogenesis of the Neoproterozoic bimodal volcanic rocks along the western margin of the Yangtze Block: New constraints from Hf isotopes and Fe/Mn ratios: Chinese Science Bulletin, v. 50, p. 2481-2486.

Li, X.H., Sun, M., Wei, G.J., Liu, Y., Lee, C.Y., and Malpas, J., 2000a, Geochemical and Sm-Nd isotopic study of amphibolites in the Cathaysia Block, southeastern China: evidence for an extremely depleted mantle in the Paleoproterozoic: Precambrian Research, v. 102, p. 251-262.

Li, X.H., Tatsumoto, M., and Gui, X.T., 1989, The discovery of 2.5 Ga-old Archean relict zircon from the Tanghu granite, South China, and its preliminary implication: Chinese Science Bulletin, v. 34, p. 1364-1369.

Li, X.H., Zhou, H.W., Liu, Y., Lee, C., Sun, M., and Chen, C.H., 2000b, Shoshonitic intrusive suite in SE Guangxi: Petrology and geochemistry: Chinese Science Bulletin, v. 45, p. 653-659.

Li, X.H., Zhou, H.W., Liu, Y., Lee, C.Y., Chen, C.H., Yu, J.S., and Gui, X.T., 2001, Mesozoic shoshonitic intrusives in the Yangchun Basin, western Guangdong, and their tectonic significance: II. Trace elements and Sr-Nd isotopes: Geochemica, v. 30, p. 57-65 (in Chinese with English abstract).

Li, X.H., Zhou, H.W., Liu, Y., Lee, C.Y., Chen, Z.H., Yu, J.S., and Gui, X.T., 2000c, Mesozoic shoshonitic intrusives in the Yangchun Basin, western Guangdong, and their tectonic significance: I. Petrology and isotope geochronology: Geochemica, v. 29, p. 513-520 (in Chinese with English abstract).

Li, Z.-X., Li, X.-H., Chung, S.-L., Lo, C.-H., Xu, X., and Li, W.-X., 2012, Magmatic switch-on and switch-off along the South China continental margin since the Permian: Transition from an Andean-type to a Western Pacific-type plate boundary: Tectonophysics, v. 532–535, p. 271-290.

Li, Z.-X., Li, X.-H., Wartho, J.-A., Clark, C., Li, W.-X., Zhang, C.-L., and Bao, C., 2010d, Magmatic and metamorphic events during the early Paleozoic Wuyi-Yunkai orogeny, southeastern South China: New age constraints and pressure-temperature conditions: Geological Society of America Bulletin, v. 122, p. 772-793.

Li, Z.L., Hu, R.Z., Yang, J.S., Peng, J.T., Li, X.M., and Bi, X.W., 2007c, He, Pb and S isotopic constraints on the relationship between the A-type Qitianling granite and the Furong tin deposit, Hunan Province, China: Lithos, v. 97, p. 161-173.

Li, Z.X., 1994, Collision between the North and South China Blocks: A crustal-detachment model for suturing in the region east of the Tanlu Fault: Geology, v. 22, p. 739-742.

Li, Z.X., 1998, Tectonic history of the major East Asian lithospheric blocks since the mid-Proterozoic-A synthesis: American Geophysical Union Geodynamics Series, v. 27, p. 221-243.

Li, Z.X., Bogdanova, S.V., Collins, A.S., Davidson, A., De Waele, B., Ernst, R.E., Fitzsimons, I.C.W., Fuck, R.A., Gladkochub, D.P., Jacobs, J., Karlstrom, K.E., Lu, S., Natapov, L.M., Pease, V., Pisarevsky, S.A., Thrane, K., and Vernikovsky, V., 2008c, Assembly, configuration, and break-up history of

Rodinia: A synthesis: Precambrian Research, v. 160, p. 179-210.

Li, Z.X., and Li, X.H., 2007, Formation of the 1300-km-wide intracontinental orogen and postorogenic magmatic province in Mesozoic South China: A flat-slab subduction model: Geology, v. 35, p. 179-182.

Li, Z.X., Li, X.H., Kinny, P.D., and Wang, J., 1999, The breakup of Rodinia: Did it start with a mantle plume beneath South China?: Earth and Planetary Science Letters, v. 173, p. 171-181.

Li, Z.X., Li, X.H., Kinny, P.D., Wang, J., Zhang, S., and Zhou, H., 2003c, Geochronology of Neoproterozoic syn-rift magmatism in the Yangtze Craton, South China and correlations with other continents: Evidence for a mantle superplume that broke up Rodinia: Precambrian Research, v. 122, p. 85-109.

Li, Z.X., Li, X.H., Li, W.X., and Ding, S.J., 2008d, Was Cathaysia part of Proterozoic Laurentia? new data from Hainan Island, south China: Terra Nova, v. 20, p. 154-164.

Li, Z.X., Li, X.H., Wartho, J.A., Clark, C., Li, W.X., Zhang, C.L., and Bao, C.M., 2010e, Magmatic and metamorphic events during the early Paleozoic Wuyi-Yunkai orogeny, southeastern South China: New age constraints and pressure-temperature conditions: Geological Society of America Bulletin, v. 122, p. 772-793.

Li, Z.X., Li, X.H., Zhou, H.W., and Kinny, P.D., 2002b, Grenvillian continental collision in south China: New SHRIMP U-Pb zircon results and implications for the configuration of Rodinia: Geology, v. 30, p. 163-166.

Li, Z.X., Wartho, J.A., Occhipinti, S., Zhang, C.L., Li, X.H., Wang, J., and Bao, C.M., 2007d, Early history of the eastern Sibao Orogen (South China) during the assembly of Rodinia: New mica Ar-40/Ar-39 dating and SHRIMP U-Pb detrital zircon provenance constraints: Precambrian Research, v. 159, p. 79-94.

Li, Z.X., Zhang, L.H., and Powell, C.M., 1995, South China in Rodinia: Part of the Missing Link between Australia east Antarctica and Laurentia: Geology, v. 23, p. 407-410.

Ling, H.F., Shen, W.Z., Sun, T., Jiang, S.Y., Jiang, Y.H., Ni, P., Gao, J.F., Huang, G.L., Ye, H.M., and Tan, Z.Z., 2006, Genesis and source characteristics of 22 Yanshanian granites in Guangdong province: study of element and Nd-Sr isotopes: Acta Petrologica Sinica, v. 22, p. 2687-2703.

Ling, W., Gao, S., Zhang, B., Zhou, L., and Xu, Q., 2001, The recognizing of ca. 1.95 Ga tectono-thermal eventin Kongling nucleus and its significance for the evolution of Yangtze Block, South China: Chinese Science Bulletin, v. 46, p. 326-329.

Liu, B., and Xu, X., 1994, Atlas of lithofacies and paleogeography of south China: Beijing, Science Press, 188 p.

Liu, R., Zhou, H.W., Zhang, L., Zhong, Z.Q., Zeng, W., Xiang, H., Jin, S., Lu, X.Q., and Li, C.Z., 2010, Zircon U-Pb ages and Hf isotope compositions of the Mayuan migmatite complex, NW Fujian Province, Southeast China: Constraints on the timing and nature of a regional tectonothermal event associated with the Caledonian orogeny: Lithos, v. 119, p. 163-180.

Liu, Y., Liu, H.C., and Li, X.H., 1996, Simultaneous and precise determination of 40 trace elements in rock samples using ICP-MS: Geochemica, v. 25, p. 552-558 (in Chinese with English abstract).

Loiselle, M.C., and Wones, D.R., 1979, Characteristics and origin of anorogenic granites Geological Society of America Abstracts with Programs, v. 11, p. 468.

Ludwig, K.R., 2001, User manual for Isoplot/Ex rev. 2.49, Spec. Publ. LA, Berkeley Geochronol. Cent., Berkeley, Calif.

Ma, L.F., 2002, Geological Altas of China: Beijing, Geological Publishing House.

Ma, T.Q., Bai, D.Y., Kuang, J., Peng, X.J., and Wang, X.H., 2006, 40Ar-39Ar dating and geochemical characteristics of the granites: Geochemica, v. 35, p. 346-358 (in Chinese with English abstract).

Martin, H., and Moyen, J.F., 2002, Secular changes in tonalite-trondhjemite-granodiorite composition as markers of the progressive cooling of Earth: Geology, v. 30, p. 319-322.

McCulloch, M.T., and Chappell, B.W., 1982, Nd Isotopic characteristics of S-type and I-type granites: Earth and Planetary Science Letters, v. 58, p. 51-64.

Meng, L., Li, Z.-X., Chen, H., Li, X.-H., and Wang, X.-C., 2012, Geochronological and geochemical results from Mesozoic basalts in southern South China Block support the flat-slab subduction model: Lithos, v. 132–133, p. 127-140.

Nyman, M.W., Karlstropm, K.E., Kirby, E., and Graubard, C.M., 1994, Mesoproterozoic contractional orogeny in western North-America: Evidence from ca. 1.4 Ga plutons: Geology, v. 22, p. 901-904.

O'Neil, J.R., and Chappell, B.W., 1977, Oxygen and hydrogen isotope relations in the Berridale batholith: Journal of the Geological Society of London, v. 133, p. 559-571.

O'Neil, J.R., Shaw, S.E., and Flood, R.H., 1977, Oxygen and hydrogen isotope compositions as indicators of granite genesis in New England Batholith, Australia: Contributions to Mineralogy and Petrology, v. 62, p. 313-328.

Otamendi, J.E., and Douce, A.E.P., 2001, Partial melting of aluminous metagreywackes in the Northern Sierra de Comechingones, Central Argentina: Journal of Petrology, v. 42, p. 1751-1772.

Page, F.Z., Fu, B., Kita, N.T., Fournelle, J., Spicuzza, M.J., Schulze, D.J., Viljoen, F., Basei, M.A.S., and Valley, J.W., 2007, Zircons from kimberlite: New insights from oxygen isotopes, trace elements, and Ti in zircon thermometry: Geochimica Et Cosmochimica Acta, v. 71, p. 3887-3903.

Patiño Douce, A.E., 1996, Effects of pressure and H_2O content on the compositions of primary crustal melts: Transactions of the Royal Society of Edinburgh-Earth Sciences, v. 87, p. 11-21.

Patiño Douce, A.E., 1997, Generation of metaluminous A-type granites by low-pressure melting of calc-alkaline granitoids: Geology, v. 25, p. 743-746.

Patiño Douce, A.E., 1999, What do experiments tell us about the relative contributions of crust and mantle to the origin of granitic magmas? In: Castro, A., Fernandez, C. & Vigneresse, J. L. (Eds.) Understanding granites: Integrating new and classical techniques.: Geological Society, London, Special Publications, v. 168, p. 55-75.

Patiño Douce, A.E., and Beard, J.S., 1996, Effects of P, $f(O_2)$ and Mg/Fe ratio on dehydration melting of model metagreywackes: Journal of Petrology, v. 37, p. 999-1024.

Patiño Douce, A.E., and Harris, N., 1998, Experimental constraints on Himalayan anatexis: Journal of Petrology, v. 39, p. 689-710.

Pearce, J.A., Harris, N.B.W., and Tindle, A.G., 1984, Trace-element discrimination diagrams for the tectonic interpretation of granitic-rocks: Journal of Petrology, v. 25, p. 956-983.

Peccerillo, A., and Taylor, S.R., 1976, Geochemistry of Eocene calc-alkaline volcanic-rocks from Kastamonu area, northern Turkey: Contributions to Mineralogy and Petrology, v. 58, p. 63-81.

Peck, W.H., Valley, J.W., and Graham, C.M., 2003, Slow oxygen diffusion rates in igneous zircons from metamorphic rocks: American Mineralogist, v. 88, p. 1003-1014.

Petford, N., Cruden, A.R., McCaffrey, K.J.W., and Vigneresse, J.L., 2000, Granite magma formation, transport and emplacement in the Earth's crust: Nature, v. 408, p. 669-673.

Pitcher, W.S., 1987, Granites and yet more granites forty years on: Geologische Rundschau, v. 76, p. 51-79.

Qi, C.S., Deng, X.G., Li, W.X., Li, X.H., Yang, Y.H., and Xie, L.W., 2007, Origin of the Darongshan-Shiwandashan S-type granitoid belt from southeastern Guangxi: Geochemical and Sr-Nd-Hf isotopic constraints: Acta Petrologica Sinica, v. 23, p. 403-412.

Qiu, Y.M., and Gao, S., 2000, First evidence of > 3.2 Ga continental crust in the Yangtze craton of South China and its implications for Archean crustal evolution and Phanerozoic tectonics: Geology, v. 28, p. 11-14.

Ratschbacher, L., Hacker, B.R., Calvert, A., Webb, L.E., Grimmer, J.C., McWilliams, M.O., Ireland, T., Dong, S.W., and Hu, J.M., 2003, Tectonics of the Qinling (central China): Tectonostratigraphy, geochronology, and deformation history: Tectonophysics, v. 366, p. 1-53.

Ren, J.S., 1984, The Indosinian orogeny and its significance in the tectonic evolution of China: Bulletin of the Chinese Academy of Geological Sciences, v. 9, p. 31-44 (in Chinese with English abstract).

Ren, J.S., 1991, On the geotectonics of southern China: Acta geologica Sinica, v. 4, p. 111-130.

Rickwood, P.C., 1989, Boundary lines within petrologic diagrams which use oxides of major and minor elements: Lithos, v. 22, p. 247-263.

Ridolfi, F., Renzulli, A., and Puerini, M., 2010, Stability and chemical equilibrium of amphibole in calc-alkaline magmas: an overview, new thermobarometric formulations and application to subduction-related volcanoes: Contributions to Mineralogy and Petrology, v. 160, p. 45-66.

Roberts, M.P., and Clemens, J.D., 1993, Origin of high-potassium, calc-alkaline, I-type granitoids: Geology, v. 21, p. 825-828.

Rudnick, R.L., 1995, Making continental crust: Nature, v. 378, p. 571-578.

Shaw, S.E., and Flood, R.H., 1981, The New England Batholith, eastern Australia:

Geochemical variations in time and space: Journal of Geophysical Research, v. 86, p. 530-544.

Shui, T., 1988, Tectonic framework of the continental basement of southeast China: Scientia Sinica Series B, v. 30.

Sisson, T.W., Ratajeski, K., Hankins, W.B., and Glazner, A.F., 2005, Voluminous granitic magmas from common basaltic sources: Contributions to Mineralogy and Petrology, v. 148, p. 635-661.

Skjerlie, K.P., and Johnston, A.D., 1992, Vapor-absent melting at 10-kbar of a biotite-bearing and amphibole-bearing tonalitic gneiss: Implications for the generation of A-type granites: Geology, v. 20, p. 263-266.

Skjerlie, K.P., and Johnston, A.D., 1993, Fluid-absent melting behavior of an F-rich tonalitic gneiss at midcrustal pressures: Implications for the generation of anorogenic granites: Journal of Petrology, v. 34, p. 785-815.

Stacey, J.S., and Kramers, J.D., 1975, Approximation of terrestrial lead isotope evolution by a two-stage model: Earth and Planetary Science Letters, v. 26, p. 207-221.

Steinitz, A., Katzir, Y., Valley, J.W., Be'eri-Shlevin, Y., and Spicuzza, M.J., 2009, The origin, cooling and alteration of A-type granites in southern Israel (northernmost Arabian-Nubian shield): a multi-mineral oxygen isotope study: Geological Magazine, v. 146, p. 276-290.

Stevens, G., Clemens, J.D., and Droop, G.T.R., 1995, Hydrous cordierite in granulites and crustal magma production: Geology, v. 23, p. 925-928.

Stevens, G., Villaros, A., and Moyen, J.F., 2007, Selective peritectic garnet entrainment as the origin of geochemical diversity in S-type granites: Geology, v. 35, p. 9-12.

Streckeisen, A., 1974, Classification and nomenclature of plutonic rocks recommendations of the IUGS subcommission on the systematics of Igneous Rocks: Geologische Rundschau, v. 63, p. 773-786.

Streckeisen, A., and Le Maitre, R.W., 1979, A chemical approximation to the modal QAPF classification of the igneous rocks: Neues Jahrbuch fur Mineralogie, Abhandlungen, v. 136, p. 169-206.

Sun, S.S., and McDonough, W.F., 1989, Chemical and isotopic systematics of oceanic basalt: implications for mantle composition and processes. In: Saunders, A. D., Norry, M. J. (Eds.), Magmatism in the Ocean Basins:

Geological Society, London, Special Publications, v. 42, p. 528-548.

Sun, T., 2006, A new map showing the distribution of the granites in South China and its explanatory notes: Geological Bulletin of China, v. 25, p. 332-335 (in Chinese with English abstract).

Sun, T., Zhou, X.M., Chen, P.R., Li, H.M., Zhou, H.Y., Wang, Z.C., and Shen, W.Z., 2005, Strongly peraluminous granites of mesozoic in eastern Nanling Range, southern China: Petrogenesis and implications for tectonics: Science in China Series D-Earth Sciences, v. 48, p. 165-174.

Trumbull, R.B., Harris, C., Frindt, S., and Wigand, A., 2004, Oxygen and neodymium isotope evidence for source diversity in Cretaceous anorogenic granites from Namibia and implications for A-type granite genesis: Lithos, v. 73, p. 21-40.

Turner, S., Arnaud, N., Liu, J., Rogers, N., Hawkesworth, C., Harris, N., Kelley, S., VanCalsteren, P., and Deng, W., 1996, Post-collision, shoshonitic volcanism on the Tibetan plateau: Implications for convective thinning of the lithosphere and the source of ocean island basalts: Journal of Petrology, v. 37, p. 45-71.

Turner, S.P., Foden, J.D., and Morrison, R.S., 1992, Derivation of some A-type magmas by fractionation of basaltic magma: An example from the Padthaway Ridge, south Australia: Lithos, v. 28, p. 151-179.

Valley, J.W., Chiarenzelli, J.R., and Mclelland, J.M., 1994, Oxygen isotope geochemistry of zircon: Earth and Planetary Science Letters, v. 126, p. 187-206.

Valley, J.W., Kinny, P.D., Schulze, D.J., and Spicuzza, M.J., 1998, Zircon megacrysts from kimberlite: oxygen isotope variability among mantle melts: Contributions to Mineralogy and Petrology, v. 133, p. 1-11.

Valley, J.W., Lackey, J.S., Cavosie, A.J., Clechenko, C.C., Spicuzza, M.J., Basei, M.A.S., Bindeman, I.N., Ferreira, V.P., Sial, A.N., King, E.M., Peck, W.H., Sinha, A.K., and Wei, C.S., 2005, 4.4 billion years of crustal maturation: Oxygen isotope ratios of magmatic zircon: Contributions to Mineralogy and Petrology, v. 150, p. 561-580.

Vasquez, P., Glodny, J., Franz, G., Romer, R.L., and Gerdes, A., 2009, Origin of fayalite granitoids: New insights from the Cobquecura Pluton, Chile, and its metapelitic xenoliths: Lithos, v. 110, p. 181-198.

Vazquez, J.A., and Reid, M.R., 2004, Probing the accumulation history of the

voluminous Toba magma: Science, v. 305, p. 991-994.

Vielzeuf, D., and Montel, J.M., 1994, Partial melting of metagreywackes .1. fluid-absent experiments and phase-relationships: Contributions to Mineralogy and Petrology, v. 117, p. 375-393.

Villaros, A., 2010, Petrogenesis of S-type granite with particular emphasis on source processes: The example of the S-type granite of the Cape Granite Suite: South Africa, University of Stellenbosch.

Villaros, A., Stevens, G., and Buick, I.S., 2009, Tracking S-type granite from source to emplacement: Clues from garnet in the Cape Granite Suite: Lithos, v. 112, p. 217-235.

Waight, T.E., Maas, R., and Nicholls, I.A., 2000, Fingerprinting feldspar phenocrysts using crystal isotopic composition stratigraphy: implications for crystal transfer and magma mingling in S-type granites: Contributions to Mineralogy and Petrology, v. 139, p. 227-239.

Wall, V.J., Clemens, J.D., and Clarke, D.B., 1987, Models for granitoid evolution and source compositions: Journal of Geology, v. 95, p. 731-749.

Wan, Y.S., Liu, D.Y., Wilde, S.A., Cao, J.J., Chen, B., Dong, C.Y., Song, B.A., and Du, L.L., 2010, Evolution of the Yunkai Terrane, South China: Evidence from SHRIMP zircon U-Pb dating, geochemistry and Nd isotope: Journal of Asian Earth Sciences, v. 37, p. 140-153.

Wan, Y.S., Liu, D.Y., Xu, M.H., Zhuang, J.M., Song, B., Shi, Y.R., and Du, L.L., 2007, SHRIMP U-Pb zircon geochronology and geochemistry of metavolcanic and metasedimentary rocks in Northwestern Fujian, Cathaysia block, China: Tectonic implications and the need to redefine lithostratigraphic units: Gondwana Research, v. 12, p. 166-183.

Wang, F.Y., Ling, M.X., Ding, X., Hu, Y.H., Zhou, J.B., Yang, X.Y., Liang, H.Y., Fan, W.M., and Sun, W.D., 2011a, Mesozoic large magmatic events and mineralization in SE China: oblique subduction of the Pacific plate: International Geology Review, v. 53, p. 704-726.

Wang, J., and Li, Z.X., 2003, History of Neoproterozoic rift basins in South China: Implications for Rodinia break-up: Precambrian Research, v. 122, p. 141-158.

Wang, L.K., Zhang, S.L., Yang, W.J., and Xu, W.X., 1989, Granites of different series and types in south China: Their Sr, O, Pb and Nd isotopic compositions and formation environment: Geology and Prospecting, v. 25, p. 29-33 (in

Chinese with English Abstract).

Wang, Q., Wyman, D.A., Li, Z.X., Bao, Z.W., Zhao, Z.H., Wang, Y.X., Jian, P., Yang, Y.H., and Chen, L.L., 2010a, Petrology, geochronology and geochemistry of ca. 780 Ma A-type granites in South China: Petrogenesis and implications for crustal growth during the breakup of the supercontinent Rodinia: Precambrian Research, v. 178, p. 185-208.

Wang, X.C., Li, X.H., Li, W.X., and Li, Z.X., 2007a, Ca. 825 Ma komatiitic basalts in South China: First evidence for >1500 ^{o}C mantle melts by a Rodinian mantle plume: Geology, v. 35, p. 1103-1106.

Wang, X.C., Li, X.H., Li, W.X., and Li, Z.X., 2009, Variable involvements of mantle plumes in the genesis of mid-Neoproterozoic basaltic rocks in South China: A review: Gondwana Research, v. 15, p. 381-395.

Wang, Y., Fan, W., Cawood, P.A., Ji, S., Peng, T., and Chen, X., 2007b, Indosinian high-strain deformation for the Yunkaidashan tectonic belt, south China: Kinematics and Ar-40/Ar-39 geochronological constraints: Tectonics, v. 26, p. -.

Wang, Y., Zhang, F., Fan, W., Zhang, G., Chen, S., Cawood, P.A., and Zhang, A., 2010b, Tectonic setting of the South China Block in the early Paleozoic: Resolving intracontinental and ocean closure models from detrital zircon U-Pb geochronology: Tectonics, v. 29, p. TC6020.

Wang, Y.J., Fan, W.M., and Guo, F., 2003a, Geochemistry of early Mesozoic potassium-rich diorites-granodiorites in southeastern Hunan Province, South China: Petrogenesis and tectonic implications: Geochemical Journal, v. 37, p. 427-448.

Wang, Y.J., Fan, W.M., Guo, F., Peng, T.P., and Li, C.W., 2003b, Geochemistry of Mesozoic mafic rocks adjacent to the Chenzhou-Linwu fault, South China: Implications for the lithospheric boundary between the Yangtze and Cathaysia blocks: International Geology Review, v. 45, p. 263-286.

Wang, Y.J., Fan, W.M., Peng, T.P., and Guo, F., 2004, Early Mesozoic OIB-type alkaline basalts in central Jiagnxi Province and its tectonic implication: Geochemica, v. 33, p. 109-117 (in Chinese with English abstract).

Wang, Y.J., Fan, W.M., Sun, M., Liang, X.Q., Zhang, Y.H., and Peng, T.P., 2007c, Geochronological, geochemical and geothermal constraints on petrogenesis of the Indosinian peraluminous granites in the South China Block: A case

study in the Hunan Province: Lithos, v. 96, p. 475-502.

Wang, Y.J., Fan, W.M., Zhao, G.C., Ji, S.C., and Peng, T.P., 2007d, Zircon U-Pb geochronology of gneissic rocks in the Yunkai massif and its implications on the Caledonian event in the South China Block: Gondwana Research, v. 12, p. 404-416.

Wang, Y.J., Zhang, A.M., Fan, W.M., Zhao, G.C., Zhang, G.W., Zhang, Y.Z., Zhang, F.F., and Li, S.Z., 2011b, Kwangsian crustal anatexis within the eastern South China Block: Geochemical, zircon U-Pb geochronological and Hf isotopic fingerprints from the gneissoid granites of Wugong and Wuyi-Yunkai Domains: Lithos, v. 127, p. 239-260.

Wang, Y.J., Zhang, Y.H., Fan, W.M., and Peng, T.P., 2005, Structural signatures and $^{40}Ar/^{39}Ar$ geochronology of the Indosinian Xuefengshan tectonic belt, South China Block: Journal of Structural Geology, v. 27, p. 985-998.

Watson, E.B., and Harrison, T.M., 1984, Accessory minerals and the geochemical evolution of crustal magmatic systems: A summary and prospectus of experimental approaches: Physics of the Earth and Planetary Interiors, v. 35, p. 19-30.

Wei, C.S., Zhao, Z.F., and Spicuzza, M.J., 2008, Zircon oxygen isotopic constraint on the sources of late Mesozoic A-type granites in eastern China: Chemical Geology, v. 250, p. 1-15.

Whalen, J.B., Currie, K.L., and Chappell, B.W., 1987, A-Type granites: Geochemical characteristics, discrimination and petrogenesis: Contributions to Mineralogy and Petrology, v. 95, p. 407-419.

Whalen, J.B., Jenner, G.A., Longstaffe, F.J., Robert, F., and Gariepy, C., 1996, Geochemical and isotopic (O Nd, Pb and Sr) constraints on A-type granite petrogenesis based on the topsails igneous suite, Newfoundland Appalachians: Journal of Petrology, v. 37, p. 1463-1489.

White, A.J.R., and Chappell, B.W., 1977, Ultrametamorphism and granitoid genesis: Tectonophysics, v. 43, p. 7-22.

White, A.J.R., Clemens, J.D., Holloway, J.R., Silver, L.T., Chappell, B.W., and Wall, V.J., 1986, S-Type granites and their probable absence in southwestern North-America: Geology, v. 14, p. 115-118.

Wiedenbeck, M., Alle, P., Corfu, F., Griffin, W.L., Meier, M., Oberli, F., Vonquadt, A., Roddick, J.C., and Speigel, W., 1995, Three natural zircon standards for

U-Th-Pb, Lu-Hf, trace-element and REE analyses: Geostandards Newsletter, v. 19, p. 1-23.

Wiedenbeck, M., Hanchar, J.M., Peck, W.H., Sylvester, P., Valley, J., Whitehouse, M., Kronz, A., Morishita, Y., Nasdala, L., Fiebig, J., Franchi, I., Girard, J.P., Greenwood, R.C., Hinton, R., Kita, N., Mason, P.R.D., Norman, M., Ogasawara, M., Piccoli, R., Rhede, D., Satoh, H., Schulz-Dobrick, B., Skar, O., Spicuzza, M.J., Terada, K., Tindle, A., Togashi, S., Vennemann, T., Xie, Q., and Zheng, Y.F., 2004, Further characterisation of the 91500 zircon crystal: Geostandards and Geoanalytical Research, v. 28, p. 9-39.

Williams, I.S., 1998, U-Th-Pb geochronology by ion microprobe. In Applications of microanalytical techniques to understand mineralizing process: Review in Economic Geology, v. 7, p. 1-35.

Williams, I.S., Buick, I.S., and Cartwright, I., 1996, An extended episode of early Mesoproterozoic metamorphic fluid flow in the Reynolds Range, central Australia: Journal of Metamorphic Geology, v. 14, p. 29-47.

Wolf, M.B., and London, D., 1994, Apatite dissolution into peraluminous haplogranitic melts: An experimental study of solubilities and mechanisms: Geochimica Et Cosmochimica Acta, v. 58, p. 4127-4145.

Wones, D.R., 1989, Significance of the assemblage titanite + magnetite + quartz in granitic rocks: American Mineralogist, v. 74, p. 744-749.

Woodhead, J.D., and Hergt, J.M., 2005, A preliminary appraisal of seven natural zircon reference materials for in situ Hf isotope determination: Geostandards and Geoanalytical Research, v. 29, p. 183-195.

Wu, F.Y., Yang, Y.H., Xie, L.W., Yang, J.H., and Xu, P., 2006, Hf isotopic compositions of the standard zircons and baddeleyites used in U-Pb geochronology: Chemical Geology, v. 234, p. 105-126.

Wu, Y.B., Gao, S., Gong, H.J., Xiang, H., Jiao, W.F., Yang, S.H., Liu, Y.S., and Yuan, H.L., 2009, Zircon U-Pb age, trace element and Hf isotope composition of Kongling terrane in the Yangtze Craton: refining the timing of Palaeoproterozoic high-grade metamorphism: Journal of Metamorphic Geology, v. 27, p. 461-477.

Xu, K.Q., Sun, N., Wang, D.Z., Hu, S.X., Liu, Y.J., and Ji, S.Y., 1984, On the origin and metallogeny of the granites in South China, *in* Xu, K.Q., and Tu, G.C., eds., Geology of granites and their metallogic relations: Nanjing, Science and

Technology Publication of Jiangsu Province, p. 1-20 (in Chinese with English abstract).

Xu, S.T., Okay, A.I., Ji, S.Y., Sengor, A.M.C., Wen, S., Liu, Y.C., and Jiang, L.L., 1992, Diamond from the Dabie-Shan metamorphic rocks and its implication for tectonic setting: Science, v. 256, p. 80-82.

Xu, X.S., Deng, P., O'Reilly, S.Y., Griffin, W.L., Zhou, X.M., and Tan, Z.Z., 2003, Single zircon LAM-ICPMS U-Pb dating of Guidong complex (SE China) and its petrogenetic significance: Chinese Science Bulletin, v. 48, p. 1892-1899.

Xu, X.S., Lu, W.M., and He, Z.Y., 2007, Age and generation of Fogang granite batholith and Wushi diorite-hornblende gabbro body: Science in China Series D-Earth Sciences, v. 50, p. 209-220.

Xu, X.S., O'Reilly, S.Y., Griffin, W.L., Deng, P., and Pearson, N.J., 2005, Relict proterozoic basement in the Nanling Mountains (SE China) and its tectonothermal overprinting: Tectonics, v. 24, p. -.

Xu, Y.G., Menzies, M.A., Thirlwall, M.F., and Xie, G.H., 2001, Exotic lithosphere mantle beneath the western Yangtze craton: Petrogenetic links to Tibet using highly magnesian ultrapotassic rocks: Geology, v. 29, p. 863-866.

Yang, C., Zhu, J.C., Zhang, P.H., and Xie, C.F., 2006a, Geochemical characteristics and genesis of dioritic enclaves in Lisong Granite, NE Guangxi Province: Geological Journal of China Universities, v. 12, p. 310-318 (in Chinese with English abstract).

Yang, J.H., Wu, F.Y., Chung, S.L., Wilde, S.A., and Chu, M.F., 2004, Multiple sources for the origin of granites: Geochemical and Nd/Sr isotopic evidence from the Gudaoling granite and its mafic enclaves, northeast China: Geochimica Et Cosmochimica Acta, v. 68, p. 4469-4483.

Yang, J.H., Wu, F.Y., Chung, S.L., Wilde, S.A., and Chu, M.F., 2006b, A hybrid origin for the Qianshan A-type granite, northeast China: Geochemical and Sr-Nd-Hf isotopic evidence: Lithos, v. 89, p. 89-106.

Yao, J.M., Hua, R.M., and Lin, J.F., 2005, Zircon LA-ICPMS U-Pb dating and geochemical characteristics of Huangshaping granite in southeast Hunan province, China.: Acta Petrologica Sinica, v. 21, p. 688-696.

Ye, M.F., Li, X.H., Li, W.X., Liu, Y., and Li, Z.X., 2007, SHRIMP zircon U-Pb geochronological and whole-rock geochemical evidence for an early Neoproterozoic Sibaoan magmatic arc along the southeastern margin of the

Yangtze Block: Gondwana Research, v. 12, p. 144-156.

Yin, A., and Nie, S.Y., 1993, An indentation model for the North and South China collision and the development of the Tan-Lu and Honam fault systems, eastern Asia: Tectonics, v. 12, p. 801-813.

Yin, Z.P., Ling, H.F., Huang, G.L., Shen, W.Z., and Wang, L., 2010, The geochemical characteristics and genesis of the Jiufeng granitoids in northern Guangdong Province: Journal of East China Institute of Technology, v. 33, p. 15-21.

Yu, J.H., O'Reilly, S.Y., Wang, L.J., Griffin, W.L., Zhang, M., Wang, R.C., Jiang, S.Y., and Shu, L.S., 2008, Where was South China in the Rodinia supercontinent? Evidence from U-Pb geochronology and Hf isotopes of detrital zircons: Precambrian Research, v. 164, p. 1-15.

Yu, J.H., O'Reilly, S.Y., Wang, L.J., Griffin, W.L., Zhou, M.F., Zhang, M., and Shu, L.S., 2010a, Components and episodic growth of Precambrian crust in the Cathaysia Block, South China: Evidence from U-Pb ages and Hf isotopes of zircons in Neoproterozoic sediments: Precambrian Research, v. 181, p. 97-114.

Yu, J.H., Wang, L.J., O'Reilly, S.Y., Griffin, W.L., Zhang, M., Li, C.Z., and Shu, L.S., 2009a, A Paleoproterozoic orogeny recorded in a long-lived cratonic remnant (Wuyishan terrane), eastern Cathaysia Block, China: Precambrian Research, v. 174, p. 347-363.

Yu, J.H., Zhou, X.M., O'Reilly, Y.S., Zhao, L., Griffin, W.L., Wang, R.C., Wang, L.J., and Chen, X.M., 2005, Formation history and protolith characteristics of granulite facies metamorphic rock in Central Cathaysia deduced from U-Pb and Lu-Hf isotopic studies of single zircon grains: Chinese Science Bulletin, v. 50, p. 2080-2089.

Yu, J.S., Gui, X.T., Li, P.Z., and Yuan, C., 1998, Isotope and trace element geochemistry of granitoid plutons in Yangchun basin, Guangdong: Guangdong Geology, v. 13, p. 1-10 (in Chinese with English abstract).

Yu, X.Q., Di, Y.J., Wu, G.G., Zhang, D., Zheng, Y., and Dai, Y.P., 2009b, The Early Jurassic magmatism in northern Guangdong Province, southeastern China: Constraints from SHRIMP zircon U-Pb dating of Xialan complex: Science in China Series D-Earth Sciences, v. 52, p. 471-483.

Yu, X.Q., Wu, G.G., Zhao, X.X., Gao, J.F., Di, Y.J., Zheng, Y., Dai, Y.P., Li, C.L., and Qiu, J.T., 2010b, The Early Jurassic tectono-magmatic events in southern

Jiangxi and northern Guangdong provinces, SE China: Constraints from the SHRIMP zircon U-Pb dating: Journal of Asian Earth Sciences, v. 39, p. 408-422.

Yui, T.F., Okamoto, K., Usuki, T., Lan, C.Y., Chu, H.T., and Liou, J.G., 2009, Late Triassic-Late Cretaceous accretion/subduction in the Taiwan region along the eastern margin of South China - evidence from zircon SHRIMP dating: International Geology Review, v. 51, p. 304-328.

Zeng, W., Zhang, L., Zhou, H.W., Zhong, Z.Q., Xiang, H., Liu, R., Jin, S., Lu, X.Q., and Li, C.Z., 2008, Caledonian reworking of Paleoproterozoic basement in the Cathaysia Block: Constraints from zircon U-Pb dating, Hf isotopes and trace elements: Chinese Science Bulletin, v. 53, p. 895-904.

Zhang, B.T., Dai, Y.S., Wang, J., Bai, C.Y., and Liu, H.L., 2001, Geology and magma-dynamical features of Jinjiling composite granitic batholith in the western Nanling region: Geological Journal of China Universities, v. 7, p. 50-61.

Zhang, M., Chen, P.R., Zhang, W.L., Chen, W.F., Li, H.M., and Zhang, M.Q., 2003, Geochemical characteristics and petrogenesis of Dadongshan granite pluton in mid Nanling Range: Geochemica, v. 32, p. 529-539.

Zhang, Z.J., Zhang, X., and Badal, J., 2008, Composition of the crust beneath southeastern China derived from an integrated geophysical data set: Journal of Geophysical Research-Solid Earth, v. 113, p. -.

Zhao, J.H., Zhou, M.F., Yan, D.P., Zheng, J.P., and Li, J.W., 2011a, Reappraisal of the ages of Neoproterozoic strata in South China: No connection with the Grenvillian orogeny: Geology, v. 39, p. 299-302.

Zhao, K.D., Jiang, S.Y., Dong, C.Y., Chen, W.F., Chen, P.R., Ling, H.F., Zhang, J., and Wang, K.X., 2011b, Uranium-bearing and barren granites from the Taoshan Complex, Jiangxi Province, South China: Geochemical and petrogenetic discrimination and exploration significance: Journal of Geochemical Exploration, v. 110, p. 126-135.

Zhao, L.A., Guo, F., Fan, W.M., Li, C.W., Qin, X.F., and Li, H.X., 2010, Crustal evolution of the Shiwandashan area in South China: Zircon U-Pb-Hf isotopic records from granulite enclaves in Indo-Sinian granites: Chinese Science Bulletin, v. 55, p. 2028-2038.

Zhao, X.X., and Coe, R.S., 1987, Paleomagnetic constraints on the collision and

rotation of North and South China: Nature, v. 327, p. 141-144.

Zhao, Z.H., Xiong, X.L., Hen, X.D., Wang, Y.X., Qiang, W., Bao, Z.W., and Jahn, B., 2002, Controls on the REE tetrad effect in granites: Evidence from the Qianlishan and Baerzhe granites, China: Geochemical Journal, v. 36, p. 527-543.

Zheng, J.P., Griffin, W.L., Li, L.S., O'Reilly, S.Y., Pearson, N.J., Tang, H.Y., Liu, G.L., Zhao, J.H., Yu, C.M., and Su, Y.P., 2011, Highly evolved Archean basement beneath the western Cathaysia Block, South China: Geochimica Et Cosmochimica Acta, v. 75, p. 242-255.

Zheng, J.P., O'Reilly, S.Y., Griffin, W.L., Zhang, M., Lu, F.X., and Liu, G.L., 2004a, Nature and evolution of Mesozoic-Cenozoic lithospheric mantle beneath the Cathaysia block, SE China: Lithos, v. 74, p. 41-65.

Zheng, Y.F., Wu, Y.B., Chen, F.K., Gong, B., Li, L., and Zhao, Z.F., 2004b, Zircon U-Pb and oxygen isotope evidence for a large-scale ^{18}O depletion event in igneous rocks during the Neoproterozoic: Geochimica Et Cosmochimica Acta, v. 68, p. 4145-4165.

Zhou, X.M., and Li, W.X., 2000, Origin of Late Mesozoic igneous rocks in Southeastern China: Implications for lithosphere subduction and underplating of mafic magmas: Tectonophysics, v. 326, p. 269-287.

Zhou, X.M., Sun, T., Shen, W.Z., Shu, L.S., and Niu, Y.L., 2006, Petrogenesis of Mesozoic granitoids and volcanic rocks in South China: A response to tectonic evolution: Episodes, v. 29, p. 26-33.

Zhu, J.C., 1998, Mesozoic granitoid types and metallogeny of the East China Circum-Pacific continental margin: Resource Geology, v. 48, p. 265-272.

Zhu, J.C., Huang, G.F., Zhang, P.H., Li, F.C., and Rao, B., 2003, On the emplacement age and material sources for the granites of Cailing superunit, Qitianling pluton, south Hunan Province: Geological Review, v. 49, p. 245-252 (in Chinese with English abstract).

Zhu, J.C., Xie, C.F., Zhang, P.H., Yang, C., and Gu, C.Y., 2005a, Niumiao and Tong' an intrusive bodies of NE Guangxi: Petrology, zircon SHRIMP U-Pb geochronology and geochemistry: Acta Petrologica Sinica, v. 21, p. 665-676.

Zhu, J.C., Zhang, H., Xie, C.F., Zhang, P.H., and Yang, C., 2005b, Zircon SHRIMP U-Pb geochronology, petrology and geochemistry of the Zhujianshui granite, Qitianling pluton, southern Hunan Province: Geological Journal of China

Universities, v. 11, p. 335-342 (in Chinese with English abstract).

Zhu, W.G., Zhong, H., Li, X.H., He, D.F., Song, X.Y., Ren, T., Chen, Z.Q., Sun, H.S., and Liao, J.Q., 2010, The early Jurassic mafic-ultramafic intrusion and A-type granite from northeastern Guangdong, SE China: Age, origin, and tectonic significance: Lithos, v. 119, p. 313-329.

Statement:

Every reasonable effort has been made to acknowledge the owners of copyright material. I would be pleased to hear from any copyright owner who has been omitted or incorrectly acknowledged.

Signature: _____

Huiqing Huang

Date: 9 July 2012